DAMAGE AND FRACTURE MECHANICS OF COMPOSITE MATERIALS

by

Saleh R. Abdussalam

A thesis
presented to the University of Manitoba
in fulfilment of the
thesis requirement for the degree of
Doctor of Philosophy
in
Mechanical Engineering

Winnipeg, Manitoba, Canada 1999

THE UNIVERSITY OF MANITOBA

FACULTY OF GRADUATE STUDIES

*****

COPYRIGHT PERMISSION PAGE

DAMAGE AND FRACTURE MECHANICS OF COMPOSITE MATERIALS

BY

SALEH R. ABDUSSALAM

A Thesis/Practicum submitted to the Faculty of Graduate Studies of The University of Manitoba in partial fulfillment of the requirements of the degree of DOCTOR OF PHILOSOPHY

Abstract

The design of structural systems in the aerospace industry has been characterized by a continuing search for strong, yet lightweight, materials to achieve maximum payload capability for minimum weight. In recent years, this search has led to a wide use of fiber reinforced composites, such as carbon, glass and kevelar based composites. Comparison of these new materials with the traditional ones (metals) according to the basic properties, such as density, elastic modulus and also long-time and short-time strength, shows their superiority over traditional materials, when weight is a major design factor, like in the aerospace industry.

Most composite materials of interest to aerospace applications have been adequately characterized under static loading conditions. Related work to study their fracture behaviour has been limited. Since most failure mechanisms involve crack growth and/or delamination, design of such components requires knowledge and understanding of their fracture properties. This thesis includes an experimental and analytical investigation of fracture characteristics of composite materials. The post-peak response of notched specimens subjected to uniaxial cyclic loading is established to evaluate the fracture energy associated with progressive matrix damage and subsequent crack growth. A total of 75 uniaxial tension specimens were tested. The experimental work consisted of first testing several un-notched specimens with different thickness (number of layers) to determine the initial and secondary elastic modulus as well as the tensile strength. The investigation studied the effect of the various fracture parameters, including thickness, fiber orientation, and crack width ratio (a/w) on the behaviour of crack propagation, peak load, and post-peak response.

The specimens used in this research were prepared using the vacuum bagging technique, with a chosen number of fiber glass cloth layers and fiber orientation. The experimental results provided information regarding the peak load, post-peak

response, fracture energy and stress intensity factor of the notched composite materials specimen under repeated loading/unloading cyclicity. The load versus crack opening displacement as well as crack length, fracture toughness and fracture energy versus number of loading cycles are produced for different specimens. Based on the experimental results, concepts of fracture mechanics are applied to evaluate stiffness degradation, fracture toughness and fracture energy evolution associated with crack growth.

In addition, a linear elastic fracture mechanics approach combined with continuum damage representation is used to predict the response of specimens (peak load and crack opening displacement). This effort has also generated a new crack band model for computational purposes.

A new formula is derived to compute delamination and interlaminar buckling loads using the finite element method. By matching the analytical near crack tip displacement field with the finite element approximation, the crack-axial stress magnitude is established, and therefore an accurate assessment of the buckling load responsible for delamination of composites is accurately evaluated.

A comprehensive derivation of the fracture inelastic zone size and shape in anisotropic solids is presented. An adaptation of Hill's failure criterion is used to derive the shape of the inelastic zone. The findings explain the "banded" shape of the damage zone observed during crack growth.

Acknowledgments

I would like to express my sincere gratitude to my advisor, Professor M. L. Ayari for his guidance toward choosing my topic of research, generous support and never ending patience during my years of graduate studies at the University of Manitoba. Beyond matters of engineering, his wisdom and kindness have had a positive influence on my life. I was extremely fortunate to have had him as my advisor. I also extend my thanks to my committee members, Professor J. Glanville, Professor A. Shah, Professor K. Tandon, and the external examiner Professor K. Soudki for their valuable suggestions and comments.

I certainly extend my gratitude to Professor N. Sepehri for his kindness and early valuable advice in directing me to work in this area. Additionally, I am grateful to have had the opportunity to interact closely with Professor N. Popplewell throughout the courses he taught in the department. His advices are greatly appreciated. My thanks also extend to my friends and colleges, Doug Roberge and Paul Labossiere for their help in my experimental setup at the Thermo-Mechanics Laboratory.

The financial support of Al-Fateh University in Tripoli, the Libyan Secretariat of Education, and the Canadian Bureau for International Education (CBIE) is greatly appreciated.

Appreciation is also given to the National Science and Engineering Research Council of Canada (NSERC), and the faculty of graduate studies at the University of Manitoba, for their assistance.

I am truly indebted to my family, specially my father Al-Haj Ramadan Abdussalam and my wonderful mother Mabrouka Faraj, my brothers Ali, Assadeg, Muftah, Ahmed and Aimen and my sisters Fatima and Assma, without whose constant support, infinite love, encouragement, and continuous prayers and care throughout my life this work not have been possible.

Finally, by no means the least, I specify appreciate the understanding and patience offered to me by my wife Zainab Inbaia, and the incentive provided for further studies and harder effort by my children. I also extend my appreciation to my five Angels ISRA, ENAS, SAFA, MARWA, and AMIRA for allowing so much time to be deprived from them while daddy has to work.

Contents

List of Tables

List of Figures

Nomenclature

K_I, K_{II}, K_{III}	Mode I, Mode II and Mode III Stress Intensity factors
K_{Ic}^1, K_{IIc}^2	Critical Stress Intensity Factor for Crack along Direction 1 and 2, Respectively
K_{Ic}^β	Fracture Toughness of a Crack Oriented at an Angle β with Respect to Direction 1
r, θ	Polar Coordinates
x, y	Cartesian Coordinates
$[K]$	Stress Intensity Factor Matrix
$[K]_c$	Fracture Toughness Matrix
$[R]$	Stress Function Matrix
$[R]_c$	Stress Function Matrix when Critical Stress Intensity Reaches Fracture Toughness

G_I	Mode I Strain Energy Release Rate
G_{II}	Mode II Strain Energy Release Rate
G_{III}	Mode III Strain Energy Release Rate
G_T	Total Strain Energy Release Rate
G_C	Critical Value of Strain Energy Release Rate
AF	The Axial Stress Factor
a	Half Real Crack Length
u, v, w	Displacement Components in x, y, and z Directions
$\triangle U$	Displacement Increment
$\triangle W$	Work Done Increment
A	Crack Extension Area
l	Length of Mesovolum Element
S	Damage Strenth Material Parameter
S_D	Damage Sectional Area
ϵ_e	Uniaxial Elastic Strain

D	Damage Variable
E	Young's Modulus
σ_{xx}	Normal Stresses Near the Crack Tip in x Direction in Cartesian Coordinate
σ_{yy}	Normal Stresses Near the Crack Tip in y Direction in Cartesian Coordinate
τ_{xy}, τ_{xz}	Shear Stresses Near the Crack Tip in Cartesian Coordinate
σ_{rr}	Normal Stresses Near the Crack Tip in Radial Direction in Polar Coordinate
$\sigma_{\theta\theta}$	Normal Stresses Near the Crack Tip in Radial Direction in Polar Coordinate
$\tau_{r\theta}$	Shear Stresses Near the Crack Tip in Polar Coordinate
ν	Poisson's Ratio
δ	Process Zone Length
COD	Crack Opening Displacement
IZL	Inelastic Zone Length

Other symbols and abbreviations used are defined in the text.

Chapter 1

INTRODUCTION

1.1 Overview

The rapidly expanding applications of composite materials in the recent past has provided much optimism for the future of engineering design and technology. For the last few decades, composite materials have become more and more prevalent in engineering applications. The desire for lightweight and stronger materials spurred the development of high strength and low ductility materials such as fiber-reinforced matrix composites. Components made of fiber reinforced composites have been used in the fields of mechanical, aeronautical and aerospace engineering (the high technology of composites have evolved in the aerospace industry only in the last twenty years). The properties of a composite are usually different from that of the original materials. Often this translates into high strength-to-weight ratios which is an attractive property, especially in the field of aeronautics. Filament-wound pressure vessels using glass fibers were the first critical application for modern composites.

Fiber-reinforced composite materials consist of fibers of high strength and modulus embedded in, or bonded to a matrix material with distinct interfaces (boundaries)

between them. Both the fibers and the matrix retain their physical and chemical identities, yet produce a combination of properties that cannot be achieved with any of the constituents acting alone.

There are several types of fibers used such as carbon, aramid, and glass. Glass fibers are the most commonly used because they can be produced at a relatively low cost. The matrix is the binding material of a composite. Its main function is to support the fibers and also to play an important role in transmitting the applied load to the fibers.

In general, fibers are the principal load carrying members, while the surrounding matrix keeps them in the desired location and orientation, acting as a load transfer medium between fibers. and protecting them from environmental damage. Many fiber reinforced composite materials offer a combination of strength and modulus that are either comparable to or better than many of the traditional metallic materials. Traditional structural materials, such as steel and aluminum alloys are considered isotropic since they exhibit nearly equal properties irrespective of the direction of measurement. In general, the properties of fiber-reinforced composites depend strongly on the direction of measurements. For example, the tensile strength and modulus of a unidirectionally oriented fiber reinforced laminate reaches a maximum when these properties are measured in the longitudinal direction of the fibers. At any other angle of measurement, these properties are lower. The minimum value is observed at 90^0 to the longitudinal direction.

Like metals, composites are notch sensitive and lose much of their structural integrity when damaged. The damage may be in the form of delamination, which reduces the strength and stiffness and thus limits the life of a structure. The delamination between each layer is a common failure mode in laminated composites. Other modes of damage occur through matrix cracking. Because the mechanical response

of composites is brittle in nature, it is important to study the applicability of fracture mechanics concepts to assess failure of these materials.

1.2 Thesis Objectives

The overall objective of this thesis is to study the failure mechanisms in composite materials. To this end, concepts of fracture mechanics and continuum damage mechanics are adapted and when necessary extended to interpret crack behaviour and matrix failure.

The specific objectives of the thesis are:

1) to experimentally determine the behavior of crack growth;

2) to investigate the effect of several geometric parameters. such as thickness (number of layers) and fiber orientation on relevant fracture parameters;

3) to develop analytical models to represent progressive damage and crack propagation in composite materials.

1.3 Scope of Work

A comprehensive experimental and analytical investigation is conducted to study and determine the behavior of crack growth in composite materials. The focus of this thesis is mainly on mode I failure processes. The post-peak regime of uniaxially loaded notched specimens is characterized and the relevant fracture parameters such as fracture toughness K_{IC} and fracture energy G_f are measured. Ultimately, it is intended to study the applicability of Linear Elastic Fracture Mechanics (LEFM) and

other models proposed for different engineering materials to assess structural integrity of parts made of composite materials.

This work also intends to study the effect of various geometrical parameters such as thickness and fiber orientation on crack behavior. An analytical model is developed to represent the progress of damage in the matrix and crack propagation in composite materials. A hybrid fracture mechanics/continuum damage model based on test results, is proposed for simulating the progress of failure in composites.

1.4 Thesis Organization

- Chapter 2 gives information on engineering applications of composite materials. This information contains details on the basic constituent, manufacturing, and application of composite materials.

- Chapter 3 presents an extensive literature survey which covers related topics to this research. Delamination of composite material and matrix cracking are the two main topics covered in this literature. Methods of reducing delamination are also presented. Damage, fracture, and failure of composite materials are discussed in detail in this chapter.

- In Chapter 4, modeling techniques based on strength, linear elastic fracture mechanics and continuum damage mechanics are covered.

- Chapter 5 presents a derivation of a formula which gives the axial load at the tip of a crack formed by a delamination mode of failure. This load can be compared to a buckling limit load for delamination safety assessment studies.

- In Chapter 6, the characteristics of crack tip inelastic zone in anisotropic media, are presented. This work extends classical developments proposed for metals to

composites, assuming anisotropic behaviour.

- In chapter 7, the experimental investigation is explained in details. Specimen preparation and test results along with calculations of fracture toughness and fracture energy are presented.
- In chapter 8, constitutive modeling of composite, modeling of damage and fracture in composite specimens along with the determination of critical load and crack opening displacement are presented.
- In chapter 9, Finite Element description of crack growth in composites is summarized.
- Finally in chapter 10, conclusions and recommendations for future work concerning crack growth description are presented.
- Appendix A, contains experimental results, presented in figures that show the post peak response of the different tested specimens.
- Appendix B, contains tables that give some typical properties of metallic and composite materials.
- Appendix C, contains various photos of specimen preparation using vacuum bagging technique, experimental apparatus used in testing, and some typical specimens after testing.

Chapter 2

FIBER REINFORCED COMPOSITES

2.1 General

The term "composite" refers to an assembly of different materials, which when used together, enables them to reflect properties not obtainable by either constituent material [72]. The term "advanced composites" refers to the group of materials usually used in the aerospace industry. Composite materials were developed because no single, homogeneous structural material could be found that had all of the desired attributes for a given application in the aerospace industry.

Fiber-reinforced composites can be classified into broad categories according to the matrix used: polymer, metal, ceramic, and carbon matrix composites (see Table 2.1). Polymer matrix composite include thermoset or thermoplastic resins reinforced with glass, carbon (graphite), aramid (kevlar), or boron fibers. They are used primarily in relatively low temperature application. Metal matrix composite consist of metal or alloys reinforced with boron, carbon (graphite), or ceramic fibers. Their

maximum use temperature is limited by the softening or melting temperature of the metal matrix. Ceramic matrix composites consist of ceramic matrices reinforced with ceramic fibers. They are best suited for very high temperature applications. For example carbon/carbon composite consist of carbon or graphite matrix reinforced with graphite yarn or fabric. They have unique properties of relatively high strength at high temperatures coupled with low thermal expansion and low density.

Basically, the key to producing composite structures is the resin matrix. Its primary purpose is to transfer the load from one fiber to the next, and from the bundle or groups of reinforcements into adjacent structures which may be embedded in the composite or adhesively bonded to it at a later stage. The resin material thus distributes the load within the structure so that each reinforcing fiber carries a proportional share of the total load. Because it is mechanically important, this fiber/resin interface has been the subject of a great deal of work in the composite industry over the last twenty years, particularly for the case of E-glass fibers.

2.2 Material Constituents

The major constituents in a fiber-reinforced composite material are the reinforcing fibers and the matrix. As mentioned earlier, the fiber reinforcement can be glass, Kevlar, carbon, boron fibers, or any of a number of other fibers, all of which are very small in diameter and very strong, imparting a high degree of strength to the resin matrix. This added strength is so large that the performance of a composite as a structure is really another order of magnitude when compared to the strength of the resins by themselves. Other constituents that may also be found are the coupling agents, coatings and fillers. Coupling agents are applied to the fibers to improve their wetting with the matrix as well as to promote across the fiber-matrix interface. Both in turn promote a better load transfer between the fibers and the matrix. Fillers

are used with some polymeric matrices primarily to reduce cost and improve their dimensional stability.

High stiffness and strength usually require a high proportion of fibers in the composite. This can be achieved by aligning a large number of fibers into a thin sheet (alumina or ply). The thickness of the lamina is usually in the range of 0.1 to 1.0 mm. If continuous fibers are used in making a lamina, they may be arranged in unidirectional or in a bidirectional orientation as shown in Figures (2.1 a and b). A lamina can be constructed using discontinuous (short) fibers in a matrix. The fibers can be arranged in a unidirectional orientation or in a random orientation see Figures (2.1 c and d). Discontinuous fiber reinforced composites have lower strength and modulus than continuous fiber composite. However, with random orientation of fibers, it is possible to obtain nearly equal mechanical and physical properties in all direction in the plane of lamina.

The thickness required to support a given load or maintain a given deflection in a fiber-reinforced composite structure is obtained by staking and welding together a number of sheets (laminates), each having the fibers oriented either in one direction or in different direction, to form a laminate (see Figure 2.2).

2.2.1 Fibers

Fibers are the principal constituents in fiber reinforced composites. The strength and stiffness of a composite is provided by the fibers which are selected to carry the majority of the load applied to the composite element and they occupy a large portion of the volume fraction in a laminate. A number of commercially available fibers and their properties are listed in Tables (B 1 and B 2) in Appendix B.

One of the most commonly used fibers among the new composite materials is the carbon fiber. This fiber is manufactured from rayon or pan fibers, it can also be made

Table 2.1: Types of Composite Materials [23]

matrix Type	Fiber	Matrix
Polymer	E-glass S-glass Carbon (Graphite) Aramid (Kevlar) Boron	Epoxy Polyimide Polyester Thermoplastics (PEEK, Polysulfone, etc.)
Metal	Boron Borsic Carbon (Graphite) Silicon carbide Alumina	Aluminum Magnesium Titanium Copper
Ceramic	Silicon carbide Alumina Silicon nitride	Silicon carbide Alumina Glass-ceramic Silicon nitride
Carbon	Carbon	Carbon

from pitch fibers which are produced directly from oil or coal. Carbon and graphite materials are quite new. The first commercial fibers were produced in the early 1970's. Among the advantages of carbon fibers are their exceptionally high tensile strength to weight ratio as well as tensile modulus to weight ratios, high fatigue strength and very low coefficient of linear thermal expansion, where they can maintain their strength up to 2000^oC, thus providing the dimensional stability required in space applications. Due to the high cost of these fibers, they are mostly used in the aerospace industry, where weight saving is more critical than cost.

Glass fibers commonly used are the E-glass and S-glass. In addition to these glass types, there are others that are not usually included in advanced composites because they are used in different fields. For example, the C-glass, is used for chemical resistance in the manufacture of tanks, ducts, blower hoods, fan housings, and other structures, where resistance to corrosion is required. In addition to the different formulations used to make up the glass, the fibers themselves can be quite different. For instance, a simple glass fiber, as the primary ingredient, can be one of any twenty-four different yarns. All of these are made from about seven different sized filaments ranging in diameter from 0.0013 inches (Glass fibers) to 0.00051 inches (K-fibers) as shown in Tables (B 1 and B 2) in Appendix B.

Another new fiber gaining wide acceptance is Kevlar. This man-made material manufactured by Dupont has many of the attributes of the Carbon fiber because of its high strength and high modulus. It also has a unique property to a degree which neither Carbon nor glass fibers have, that is adequate fracture toughness. There are two types of Kevlar: Kevlar 29 and Kevlar 49. The Kevlar that usually finds its way into structures is Kevlar 49. It is of equal strength but has a higher modulus than Kevlar 29. Unlike Carbon fibers, Kevlar does not conduct electricity. It also has a low compressive strength and modulus compared to the high tensile properties. Kevlar acts more like a glass fiber to transmit electric radiation such as radomed and

antenna windows. The diameter of Kevlar fibers and the way they are handled are similar to both carbon and glass fibers, but the form in which the material is available differs.

A large variety of fibers are available as reinforcement for composites. The fiber provides virtually all of the load carrying characteristics of the composite. The desirable characteristics of most reinforcing fibers are high strength, high stiffness, and relatively low density. Each type has its own advantages and disadvantages, as listed in Table (2.2).

Fiber properties are studied by different researchers such as Jones [55], Feldman [34] and Holloway [45]. A number of commercially available fibers and their tensile properties are listed in Table (B 2). Generally, the average tensile strength and modulus of fiber strands are lower than those measured on a single filament. Tensile stress-strain diagrams for all reinforcing fibers in use are linear, up to the point of failure as shown in Figure (2.3). They also exhibit very low strain to failure and brittle failure mode.

2.2.2 Matrix

The matrix is essentially the binder material of the composite. The purpose of the composite matrix is to hold the fibers together in the structure unit by virtue of its cohesive and adhesive characteristics, to transfer and distribute the applied load to and between fibers, to protect them from environments and external damage, and in many cases contributes some needed property such as ductility, toughness, or electrical insulation [38].

The matrix resin also provides many other essential functions such as: keeping the reinforcing fibers in the proper orientation and position so that they can carry the intended loads, distribute the loads more or less evenly among the fibers, provide

Table 2.2: Advantages and Disadvantages of Reinforced Fibers [23]

Fiber	Advantages	Disadvantages
E-glass, S-glass	High strength Low cost	Low strength Short fatigue life High temperature sensitivity
Aramid (Kevlar)	High tensile strength Low density	Low compressive strength High moisture absorption
Boron	High stiffness High compressive strength	High cost
Carbon(AS4, T300, C600)	High strength High stiffness	Moderately high cost
Graphite (GY-70, pitch)	Very high stiffness	Low strength High cost
Ceramic (silicon carbide, alumina)	High stiffness High temperature	Low strength High cost

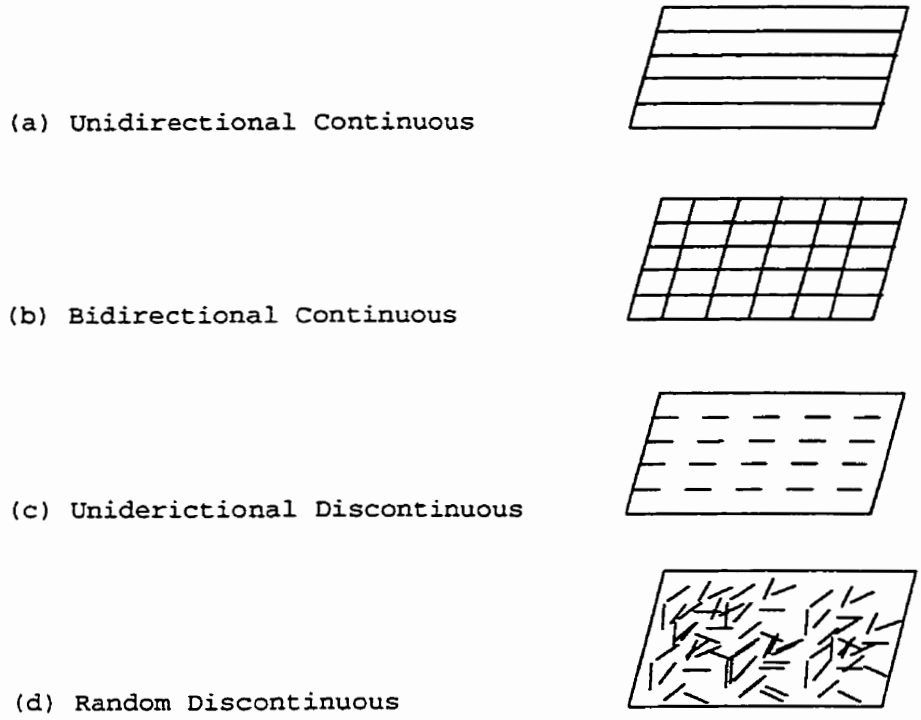

Figure 2.1: Unidirectional Lamina [70].

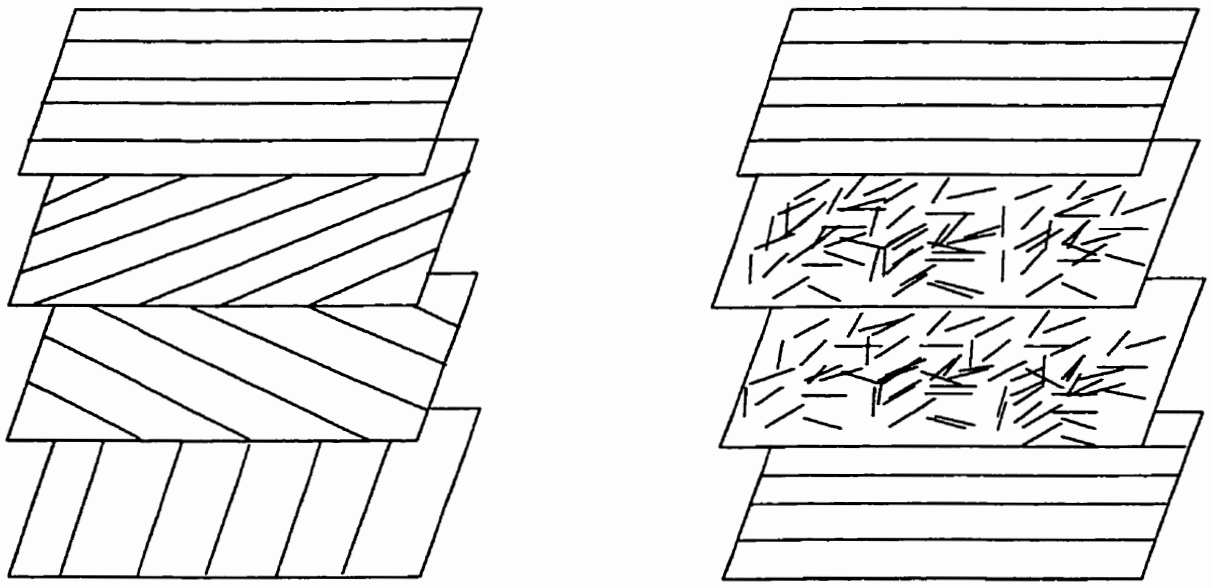

Figure 2.2: Typical Laminates [70].

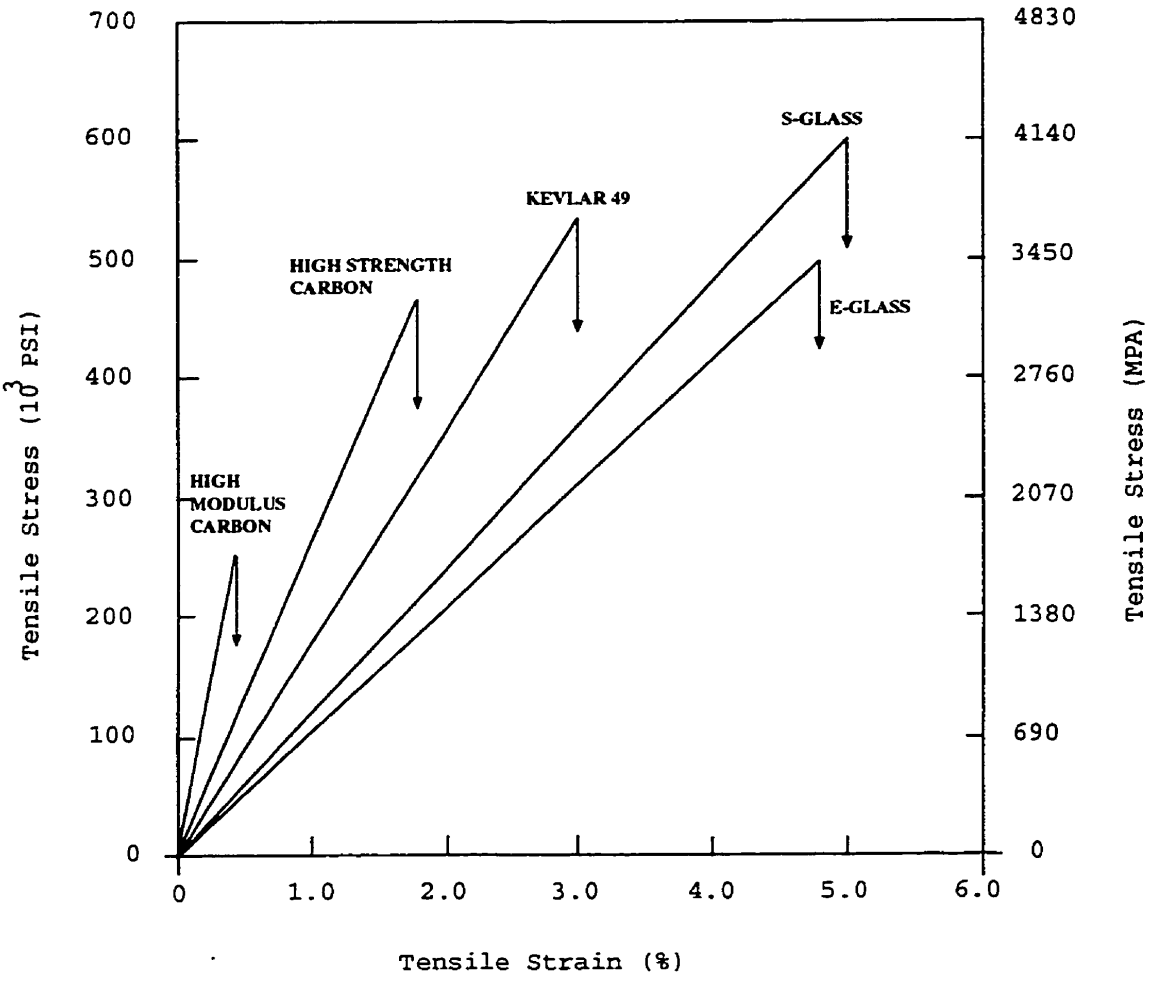

Figure 2.3: Tensile Stress-Strain Diagram for Various Reinforcing Fibers [70].

resistance to crack propagation and damage, and provide all of the inter-laminar shear strength of the composite. A strong interface strength between the fiber and the matrix is obviously desirable, so that the matrix is capable of developing a mechanical or chemical bond with the fiber. However selection of a matrix has a major influence on the inter-laminar shear as in-plane shear properties of the composite material. The former is an important design consideration for structures under bending loads, whereas the latter is important for design under torsional loads.

There are mainly four types of matrices in composites: polymeric, metallic, ceramic, and carbon. (see Table 2.1). The most commonly used matrices are polymeric, which can be thermosets (epoxies, polyimide, polyester), in which these molecular chain become cross linked after heating, or thermoplastics polymers, in which the molecular chain are not connected [23]. The most important advantages of thermoset polymers are their thermal stability and chemical resistance. They also exhibit less creep and stress relaxation than thermoplastics polymers. The disadvantages are their limited storage life (before the final shapes are moulded) at room temperature, long fabrication time in the mould and low strains to failure, as shown in Figure (2.4), which also contribute to their low impact strength.

Generally the matrix has poor mechanical characteristics. Experimental studies on polymers reveal that matrix behaviour is dependent on time of rate and frequency of the load application and the ambient temperature [42]. In fact the stress-strain curves for typical polymers and other resin materials will be influenced by all these conditions. At high loading rates or short duration of loading, the polymer matrix behaves in a rigid, brittle manner. At low loading rates or long durations of loading, the same material behaves in a ductile manner and shows high toughness values. Temperature has a degrading effect on the mechanical properties of the matrix as shown in Figure (2.5).

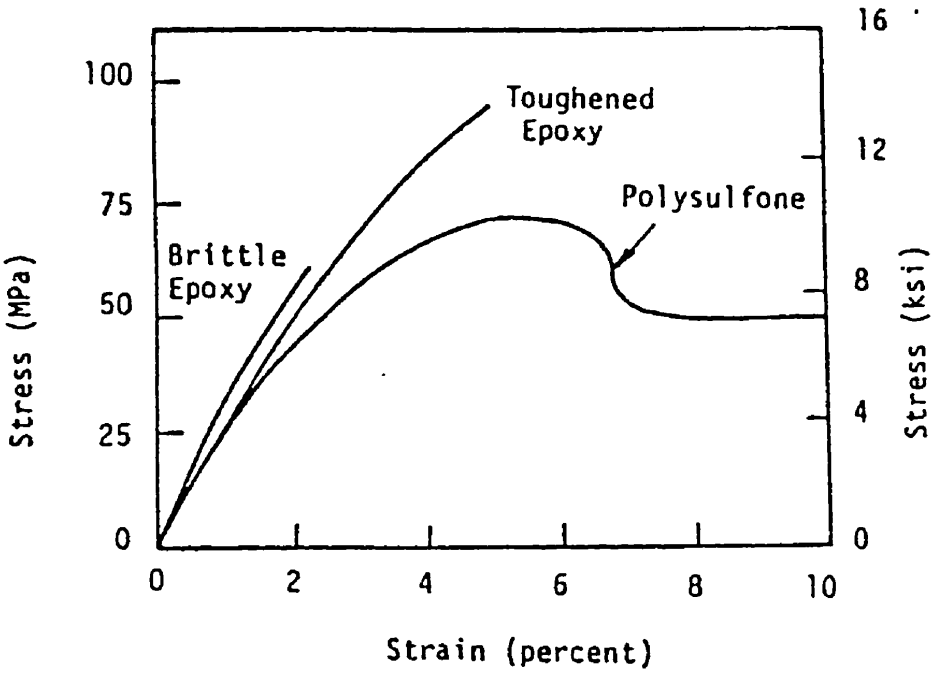

Figure 2.4: Tensile Stress-Strain of a Thermosetting Polymer (Epoxy) and a Thermoplastics Polymer (poly sulfone) [70].

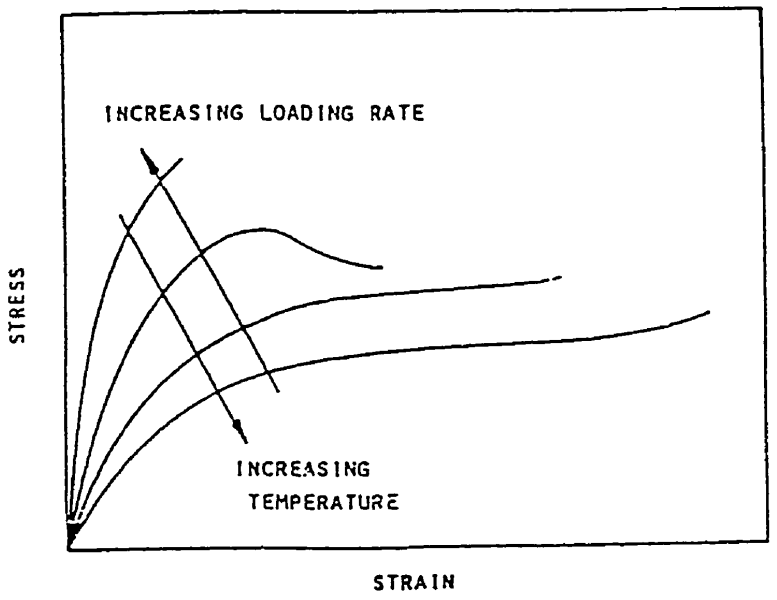

Figure 2.5: Effect of Temperature and Loading rate on the Stress-Strain Behaviour of Polymeric Solids [70].

2.3 Processing and Manufacturing of Composites

Various processes have been developed for manufacturing composite materials and composite structures. Composite materials are fabricated using wet lay up, filament winding, compression molding, injection molding, pultrusion, prepreg, resin transfer molding, sheet molding compounds, bag molding process, and auto clave molding. The early manufacturing method for fiber-reinforced composites used a hand lay-up technique. Although hand lay-up is a reliable process, it is by nature very slow and labor intensive. In recent years, particularly due to the interest generated in all types of industry, there is more emphasis on the development of manufacturing methods that can support high production rates. This section describes the different processes used to fabricate composites.

2.3.1 Filament Winding

Filament winding is one of the classic techniques for fabricating fiber reinforced polymers [38]. This method is widely used to produce structures such as helicopter blades, spherical pressure vessel, oxygen tanks, power transmission shafts, jet engine fan blades and tubing. The filament winding process (see Figure 2.6) consists first of pulling a large number of fiber roving from a series of creels into a liquid resin bath containing liquid resin and other ingredients, such as pigment and UV absorbers. Fiber tension and orientation are often controlled by electrically-programmed equipment, but simple forms winding are performed manually. The rovings are gathered before entering the resin bath, then they pass through a textile thread board or stainless steel comb. After removing the excess resin from the roving using wiping device, the fibers are wound on the mandrel. Fiber orientation is controlled by the transverse speed of the fiber winding head and the rotational speed of the mandrel. After winding the number of layers to generate the desired thickness, the filament-wound

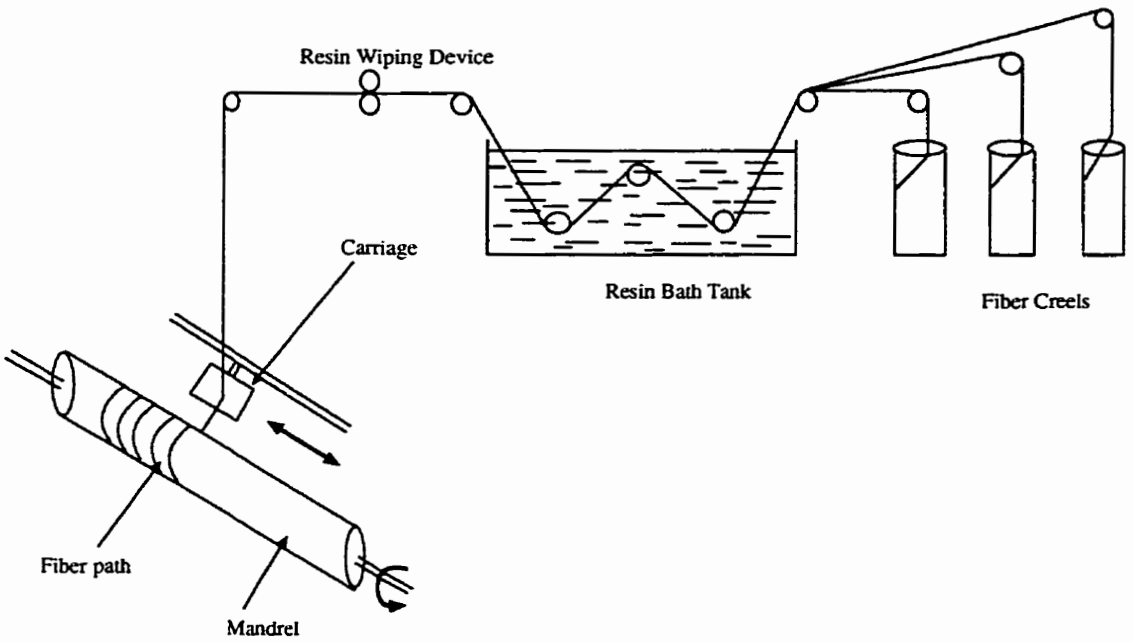

Figure 2.6: Schematic of Filament Winding Process [70].

part is generally cured on the mandrel. The uncured composite undergoes a high-temperature for few hours to harden the matrix. After complete curing, the mandrel is removed. Finally, finish machining or surface finishing may be needed for these parts in order to achieve the desired dimensions.

The advantages of this process are: fiber orientation can be controlled, easy alignment of fibers to carry torsional or circumferential loads effectively, highly automated processing, repeatable processing and fibers can be packed together very tightly to produce high fiber volume fraction. Some disadvantage of the filament process may be encountered: delaminations, fiber wrinkles, and voids which may appear because of poor fiber wet-out and presence of air bubbles in the resin bath.

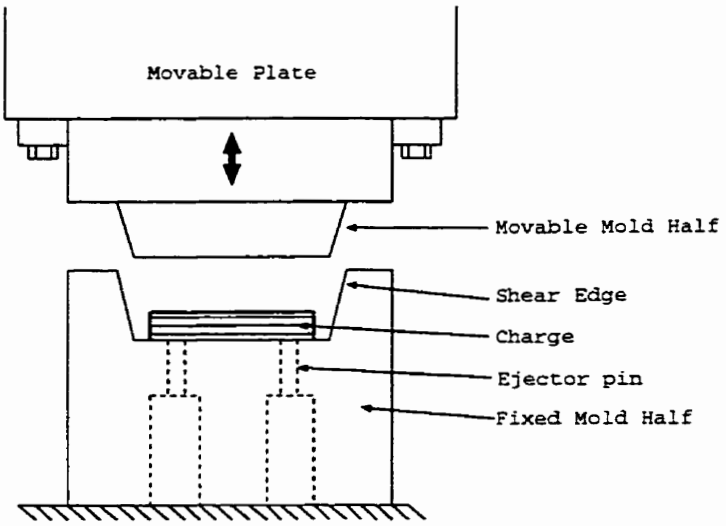

Figure 2.7: Schematic of a Compression Molding Process [70].

2.3.2 Compression Molding

Compression molding is often referred to as matched metal die molding (see Figure 2.7). To start the compression molding operation, first the material containing the fiber and resin are placed in a metal cavity. Then, the composite is compressed under pressure and heated by a top metal punch (or cavity) to compact, flow, and cure the material to a rigid shape having the form of the metal cavity. Finally, the mold is opened and the part is removed, often with the aid of ejector pins.

The principal advantage of this molding process is its ability to produce large parts with many different cross sections and complex geometries in a short period of time. Non-uniform thickness, ribs, flanges and holes can be incorporated during the compression molding process. Additionally, metal inserts can be placed in the mold as part of the operation to yield an integrally molded part. Finally, high strength parts can be obtained by using continuous fiber reinforcement at high volume fractions.

The main defect in this process is that, as in any molding operation involving long flow paths, it is extremely difficult to control the preferential orientation of the

fibers. With compression molding, the presence of high shear zones can create fiber orientations that deviate from the ideal random orientation. As a result the molded part will have its strength and modulus of elasticity higher in the direction of the fiber orientation rather than in the transverse direction.

2.3.3 Prepregs

A major breakthrough in composite manufacturing technology occurred with the development of "prepreg sheets", which are sheets consisting of fibers precoated with polymer resin. In this process, fibers may be in the form of continuous rovings, mat, or woven fabric. Epoxy is the primary matrix material in prepreg sheets. The width of the prepreg sheet may vary from less than 25 mm to over 457 mm. The thickness of the ply cured from prepreg sheets is normally in the range of 0.13 to 0.25 mm. Most prepreg sheets are made by the hot-melt process (see Figure 2.8).

The fabrication of a laminated structure with prepreg sheets evolves simply by "laying-up" the sheets at the required orientation on a mold, stacking layers of tape in the required stacking sequence, and then curing the assembly under elevated temperature and pressure. Towards the end, the prepreg sheets are backed up with a release film or waxed paper. The backup material is separated from the prepreg sheet just before it is placed in the mold. The normal storage life before molding is 6 to 8 days at $23^{o}C$ [70].

2.3.4 Sheet Molding Compounds

Sheet molding compounds (SMC) are thin sheets of fibers precompounded with a thermoset resin and used primarily in compression molding processes. It is an important innovation in composite manufacturing which is used extensively in the au-

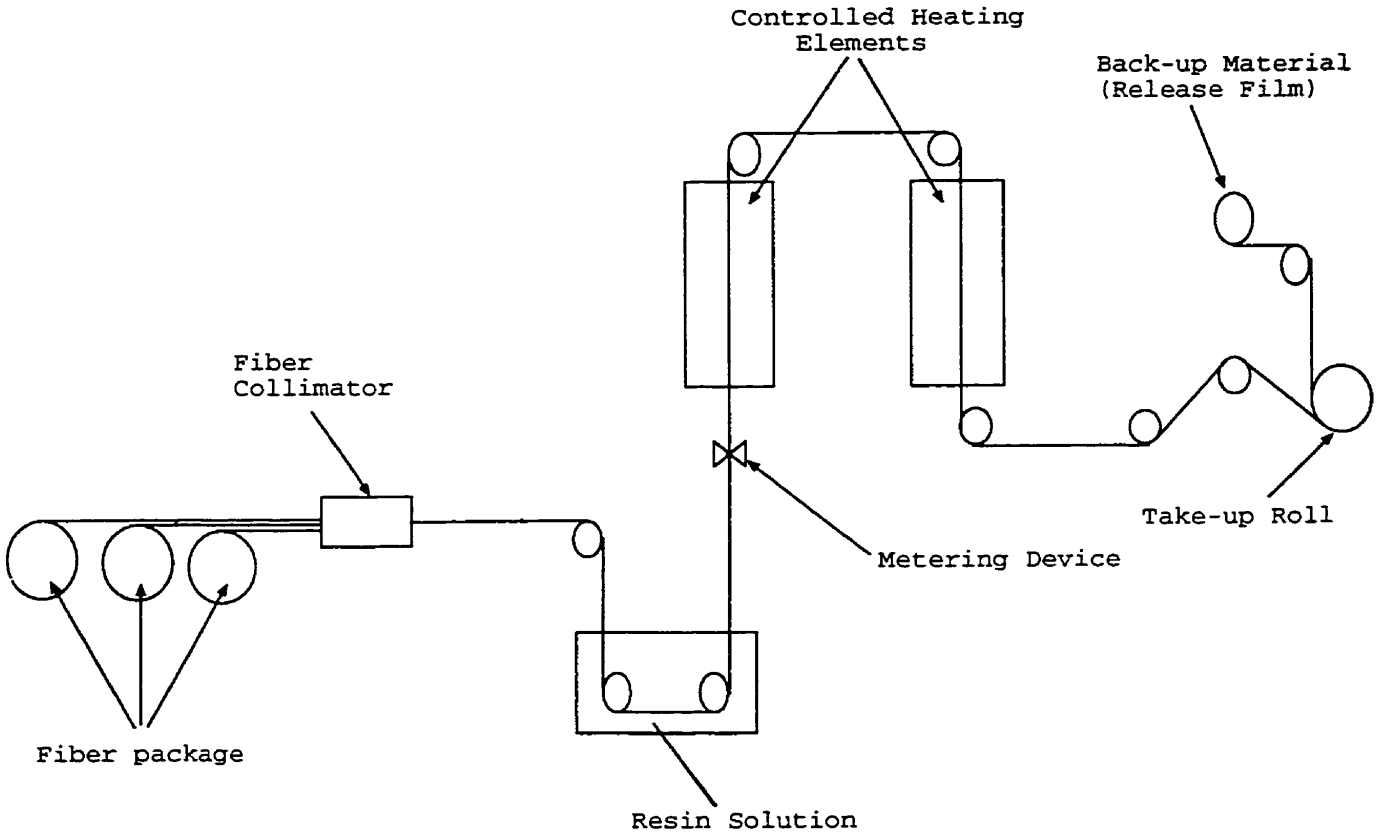

Figure 2.8: Schematic of Prepreg Manufacturing.

tomotive industry. The SMC consists of a relatively thick, chopped fiber-reinforced resin sheet. SMC is made of thermosetting resin, reinforcing fibers, thickeners, and other fillers deposited on a carrier film to form a sheet of material. The cured sheet is compression-molded under heat and pressure into the final part.

There are various types of SMC sheets which are commonly used such as:

i) SMC-R which contains randomly oriented discontinuous fibers. Nominal fiber content (by weight percent) is usually indicated by two-digit numbers after the letter R. for example, the fiber content in SMR-R30 is 30% by weight.

ii) SMC-CR which contains a layer of unidirectional continuous fibers on top of a layer of randomly oriented fibers. Nominal fiber contents are usually indicated by two-digit numbers after the letters C and R. For example, nominal fiber contents in SMC-C40 R30 are 40% by weight of unidirectional continuous fiber and 30% by weight of random discontinuous fibers.

iii) XMC which contains continuous fibers arranged in an X-pattern, where the angle between interlaced fibers is between 5 to 7 degrees. Additionally, it may also contain randomly oriented discontinuous fibers interspersed with the continuous fibers.

SMC-R and SMC-CR sheets are manufactured on a sheet moulding compound machine as shown schematically in Figure (2.9). The resin paste is prepared by mechanically blending various components as; inhibitor to prevent premature curing of the resin, release agent acts as an internal lubricant, fillers to reduce shrinkage, thickener to increase viscosity of the compound. The resin paste is placed on two moving polyethylene carrier films. Continuous roving are fed into the chopper arbor which is commonly set to provide 25 mm long discontinuous fibers. Chopped fibers are deposited randomly on the bottom resin paste. For SMC-CR sheets, parallel

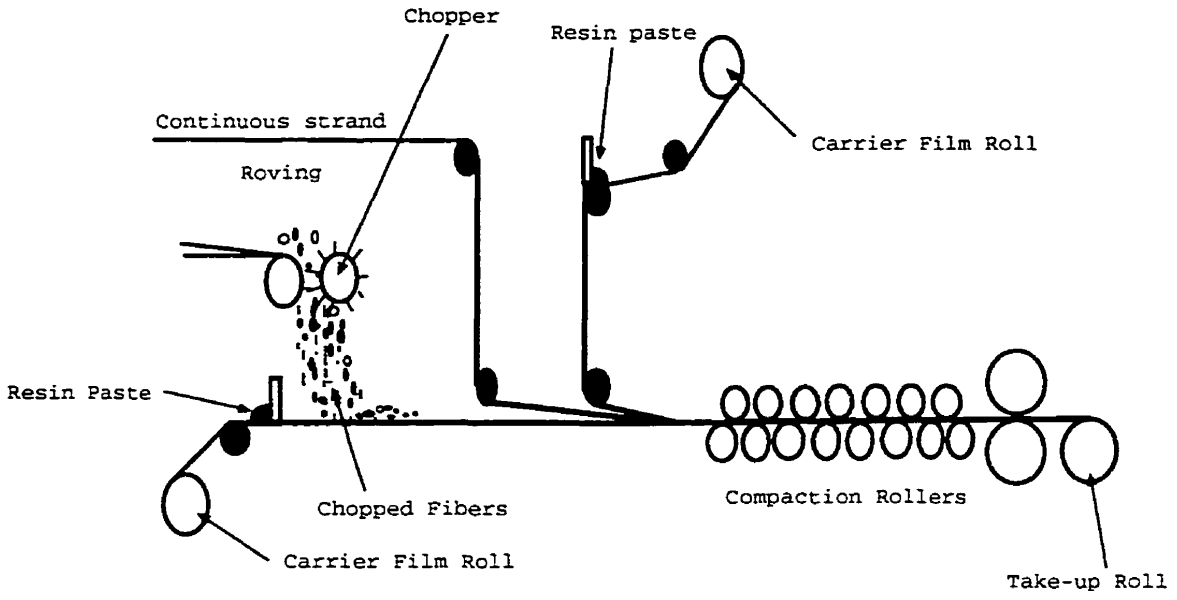

Figure 2.9: Schematic of Sheet Moulding Compound Operation.

lines of continues strand roving are fed on the top of the chopped fiber layer. After covering the fibers with top resin paste, the carrier films are pulled through a number of compacting rolls to form a sheet that is wound around a take up roll. XMC sheets are manufactured by filament winding. Chopped fibers are deposited on the continuous fiber layer during the time of winding. After the derived thickness is obtained the built up material is cut. At the end of manufacturing SMC sheets are allowed to thicken at 30^oC for 1-7 days. Then the sheets can be either compression molded or stored at 0^oC for future use.

2.3.5 Bag Molding Process

The bag molding is one of the oldest and most versatile processes used for manufacturing composites parts. It is commonly used in the aerospace industry where high production rate is not an important consideration. This process is designed to hold wet-out laminate in a specific shape until the resin system has cured. They may vary

widely in shape, size and method of construction.

The starting material for the bag molding is a prepreg that contains fibers in a particularly cured epoxy resin. The schematic of a bag molding process is shown in Figure (2.10). The mold surface is covered with a Teflon-coated glass fabric, to prevent sticking in the mold, on which the prepreg plies are laid up in the desired fiber orientation angle as well as the desired sequence. The layer by layer operation can be performed either manually or by controlled automatic-tape machines. After laying up the prepreg, a slight pressure is applied to adhere the prepreg to the proceeding ply in the lay-up. A porous release cloth and bleeder papers are placed on the top of the prepreg stack to absorb excess resin. The complete lay-up is covered with another sheet of Teflon-coated glass fabric. The entire assembly is placed inside a preheated autoclave where a combination of external pressure and vacuum is applied to density separate plies into a solid laminate.

The vacuum bagging technique is used to prepare specimens for the experimental program of this research. This technique is explained in details in chapter 7 of this thesis.

2.3.6 Pultrusion

Pultrusion is the process of pulling a continuous fiber/resin mixture through a heated die to form a structural element (Figure 2.11). Among the common pultruded products are various types of beams and channel sections, hollow tubes, flat sheets and wide flanged beams. Continuous strand rovings and mats are pulled from one end of the line to the resin bath which contains the liquid resin, curing agents, stabilizers and fire retardant. The fiber resin stream is first pulled through a series of performers that distribute the fiber bundles evenly, squeeze out the excess resin and bring the material into the final configuration. The cured member leaves the die as a finished

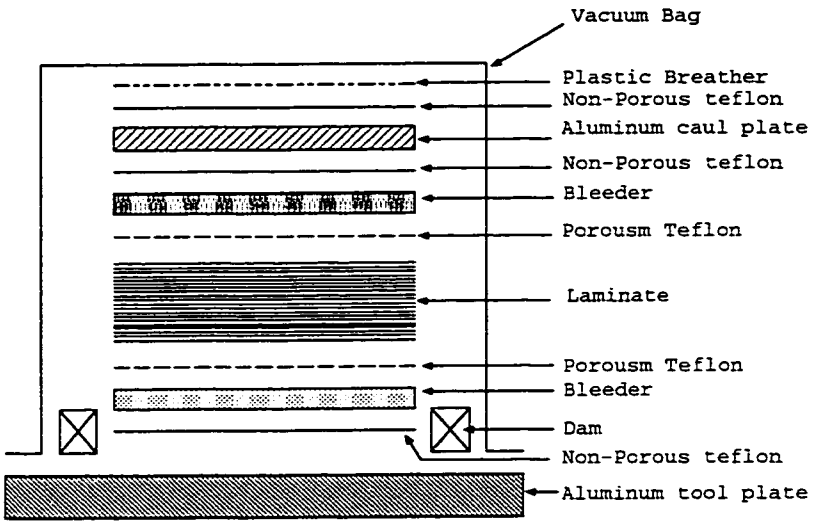

Figure 2.10: Schematic of a Bag Molding Process.

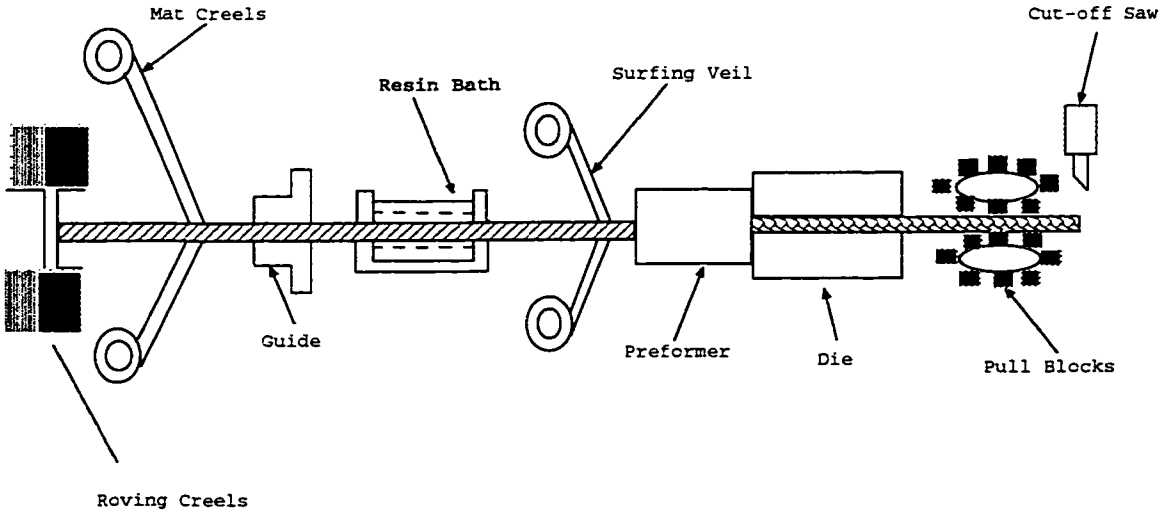

Figure 2.11: Schematic of Pultrusion Process.

part requiring only cutting to desired length at the end of the line.

The advantages of this process are such as a relatively low-cost production method, continuous processing, fibers in various layers can be oriented as desired, pultruded parts have high strength and stiffness in the direction of fiber alignment, and finished cured products need only to be cut to required lengths. Some disadvantages have been mentioned in many references such as constant cross-section parts are required, secondary operation are required for bolt holes, fitting and attachments and material combination such as mat fabric and industrial fibers are difficult to pultrude [70].

2.3.7 Resin Transfer Molding

In resin transfer molding (RTM), several layers of dry continuous strand mat, woven, roving or both are placed in a closed metal mold and the liquid resin is injected under pressure (see Figure 2.12). The resin and hardener are premixed before injection into the mold. As the resin spreads throughout the mold, it displaces the entrapped air through the air vents and impregnates the fibers. After the parts have cured, they are pulled out of the mold. The starting material in the RTM process can perform that already has the shape of the desired product. This perform is fabricated by spraying chopped fiber rovings on to a preshaped screen.

The advantages of the RTM process are: very low tooling cost and simple cleaning requirements, fast molding cycles, excellent system for limited production and it is faster than compression molding. Because of these advantages, the RTM process has been successfully used for molding cabinet walls, water tanks and boat hulls.

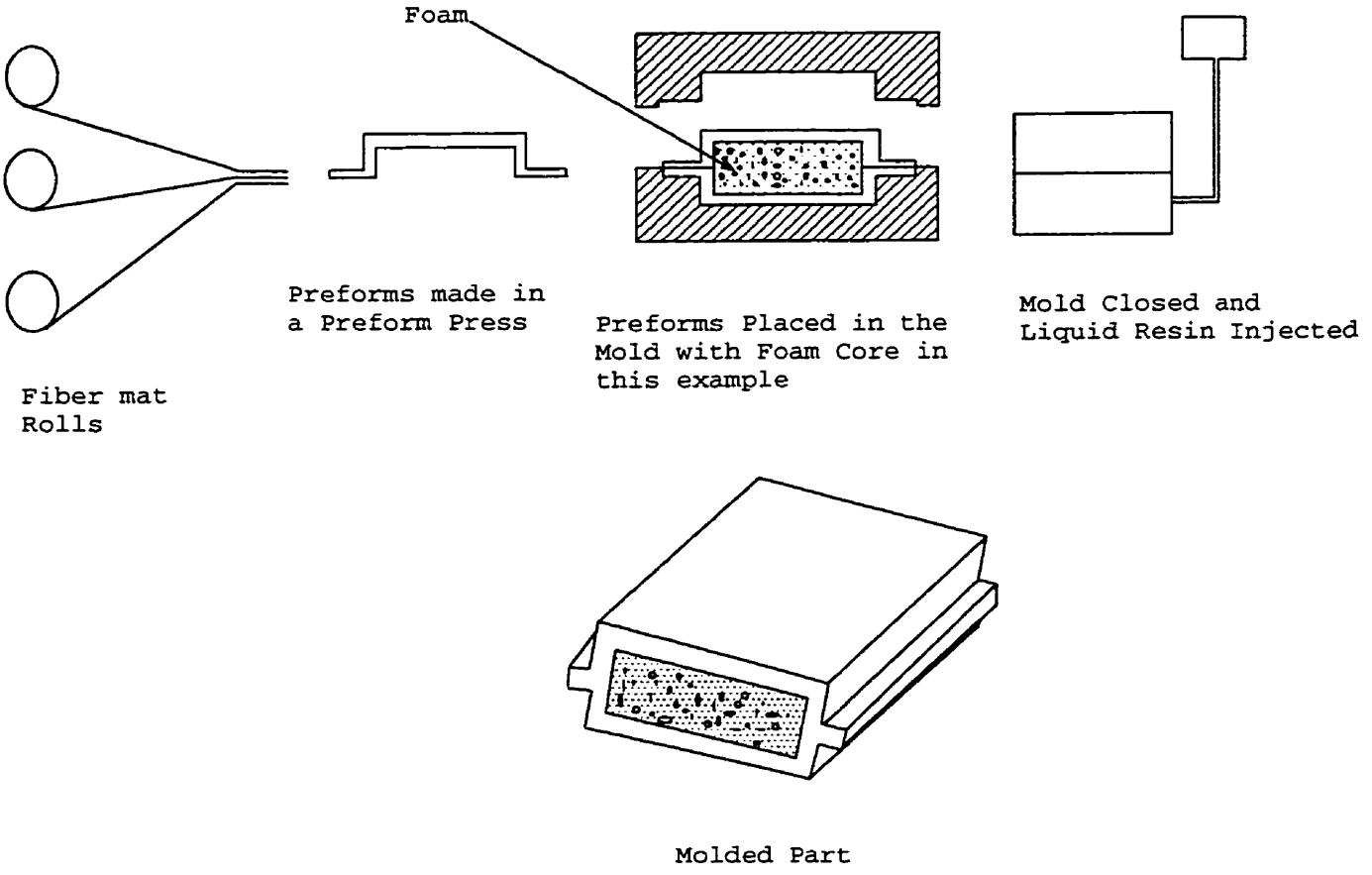

Figure 2.12: Schematic of the RTM Process.

2.4 Applications

Commercial and industrial applications of fiber reinforced composites are so varied that it is almost impossible to list them all. A potential for weight saving with composites exists in many engineering fields and putting them to actual use would require careful design practices and appropriate process developments based on the understanding of their unique mechanical and physical characteristics.

Practical weight savings may range from 15 to 30 percent depending on the application. Technical advantages of selective reinforcement are such as reduced metallic stress levels due to the addition of high stiffness materials, increased fatigue life, and reduction of dynamic vibrations or flutter problems by increasing local stiffness.

In the following sections, an overview of various applications of composite materials will be discussed briefly.

2.4.1 Space Applications

Composites have become the basic material for major aerospace vehicles. Weight reduction is the primary reason for using fiber reinforced composites in many space vehicles due to the expensive rates imposed on launch. By using carbon fiber reinforced composites, it has been found that there is a weight savings of about 40 percent over an all-titanium space frames.

The other major factor in the selection of composite materials for many space applications is their stability over a wide temperature range. Composites reinforced with Carbon and Kevlar fibers have high specific strength and modulus and low coefficient of thermal expansion, making them particularly attractive for space vehicles. Many carbon fiber reinforced epoxy laminates can be "designed" to produce a coefficient of thermal expansion (CTE) close to zero. In addition, they have much lower

specific gravity as well as higher strength and higher stiffness to weight ratios.

Such a unique combination of mechanical properties and CTE has led to a number of applications for carbon fiber reinforced epoxies in artificial satellites. One such application is found in the support structure for mirrors and lenses in the Hubble space telescope (Figure 2.13). Since the temperature in space may vary between -100^0C and 100^0C, it is critical that the support structure be dimensionally stable, or else, large changes in the relative position may cause tremendous distortion in the acquired data.

In general, there are many space components which have been fabricated using composites such as the support struts, truss structures, camera mounts, plate forms, pressure vessels, tanks and shells. Perhaps, the most efficient use of composites from both cost and performance view point is in the design and fabrication of shells for various space applications. Satellites orbiting space today contain over 4000 composite parts. The space shuttle itself (Figures 2.14 and 2.15) uses advanced composites in several areas, resulting in 1633 Kg weight reduction over the initial all-material design [93].

Moreover, composites have become an essential material for fabricating two major antenna components for commercial advanced telecommunications operating in space. These two major components are the antenna dish support ribs and the electronic package and radome support struts. Another notable composite application on space shuttles is the pay-load bay doors, which is the largest composite structure ever built. The right and left hand doors are each 18.3m long (Figure 2.14). Another application is the Canadian remote manipulator system, which is a mechanical arm used to deploy and retrieve payloads from the shuttle cargo bay. The arm is a composite tubular boom that is 411 Kg in weight, 15m in length, and 381 mm in diameter [93].

Figure 2.13: Overall View of the Hubble Space Telescope.

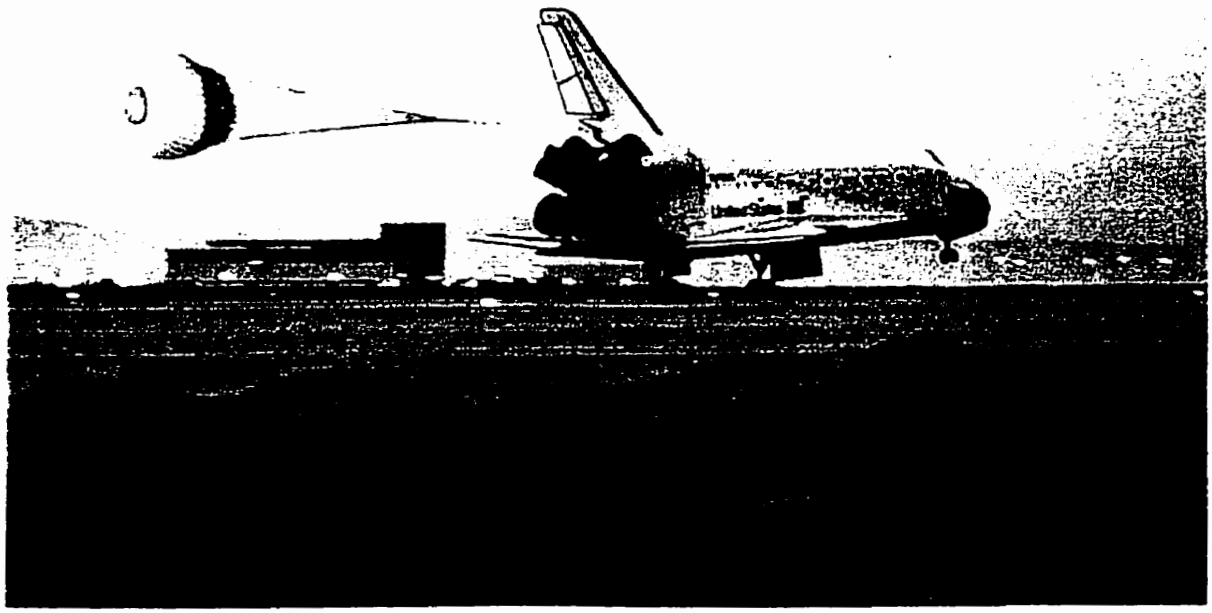

Figure 2.14: Space Shuttle on Landing.

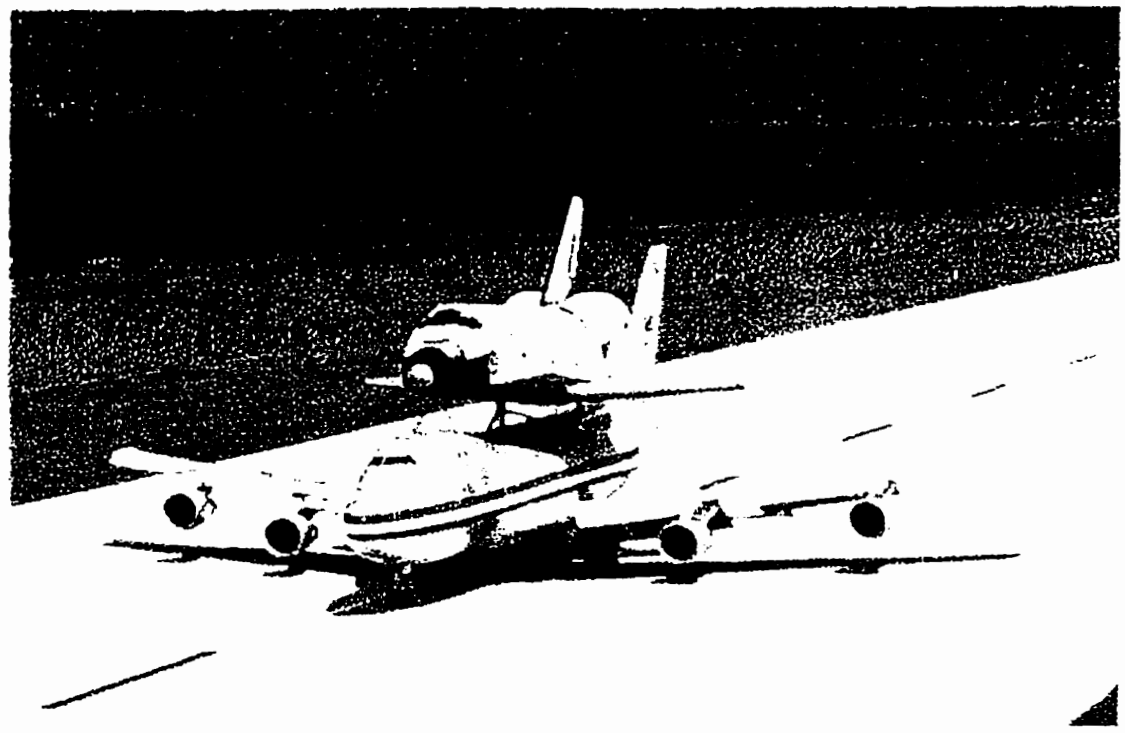

Figure 2.15: Space Shuttle Carried by Boeing 747.

2.4.2 Aircraft and Military Applications

The major structural application for fiber-reinforced composites are in the field of military and commercial aircrafts for which weight reduction is critical for higher speeds and increased payloads. Because composites are strong, durable, and damage tolerant, they have become an increasingly attractive alternative to metal for many aircraft components. The aircraft industry has found that proper use of these advanced fiber reinforced composite materials offers the potential for reducing the weight of aircraft structures by as much as 50 percent [16]. Based on that, carbon fibers, or carbon fibers combined with Kevlar 49 fibers, have become the primary material in many wing, fuselage, and empennage components. As an example, the current commercial production aircrafts such as the Boeing 757, 767, and the airbus A310 are using reinforced composites in different components such as forward wings, main landing gear doors, ailerons, flaps, rudders, elevators, and many other components. In addition, composites are also widely used in the interiors of commercial aircraft. The interior parts such as overhead luggage compartments, side-walls, ceilings, floors, cargo liners, and bulk heads are made in general of fiber reinforced epoxy or phenolic resin honeycomb sandwich constructions. The phenolic resin system is used because of its excellent fire resistant properties [16].

In military aircraft industries, fiber reinforced composites have been utilized for more than 45 years. The bulk of this use has been glass fiber reinforced plastics, which have provided both improved structural efficiency and lower cost. Recently, carbon fiber reinforced composites are being used widely in military aircraft industry, as an example see Figure (2.16). These composites make up approximately 10 percent of the structural weight and more than 50 percent of the surface area. They are used in the wing skins, the horizontal and vertical tail boxes, the wing and tail control surfaces, the speed break, the leading edge extension, and various doors. The

unlimited advantages of fiber composites have made these material very attractive in this field.

In addition to weight saving advantage, on the basis of fatigue life to weight ratio, filamentary composites show substantial improvements over titanium which is the best metallic material to resist fatigue. This improvement can be as much as 100 percent over titanium [16]. Good notch insensitivity with attendant low crack propagation also greatly improves the fatigue properties of filament composite materials. Absolute corrosion resistance is a characteristic uncommon to all metal structures. The high resistance to impact of filamentary composite materials helps localize damage and maintain it around the area of damage. Projectile impacts are localized to an area only slightly greater than that of the projectile itself, whereas in metal structures when cracks are initiated they may tear the skin of materials over a large area. The stress concentration around the crack in metal are extremely high and tend to assist propagation, whereas in filamentary composite materials the stress concentrations remain low and only slow crack propagation may occur in the area of damage.

For helicopters, applications include the use of composites in skin surface, where sixty percent of the outer skin surface is constructed of Kevlar reinforced composites, doors, fairings, and access panels. Fiber-reinforced epoxies are also used in rotor blades for many military and commercial helicopters. Besides the weight, which is in the range of 25 percent, the first advantage of using composite materials in blade applications is the manufacturing flexibility of these materials. The composite blades can be molded into complex airfoil shapes with little or no additional manufacturing costs.

In the case of missiles, composites have demonstrated the wide range of characteristics necessary to satisfy the operational requirement of missiles. High stiffness and strength and minimum weight are the major reasons for the use of graphite compos-

ites for critical structural members of missiles systems [16]. The properties mentioned and weight reduction purposes, which in turn increases the missile range as well as its payload capacity, have made the composites widely used in this important field.

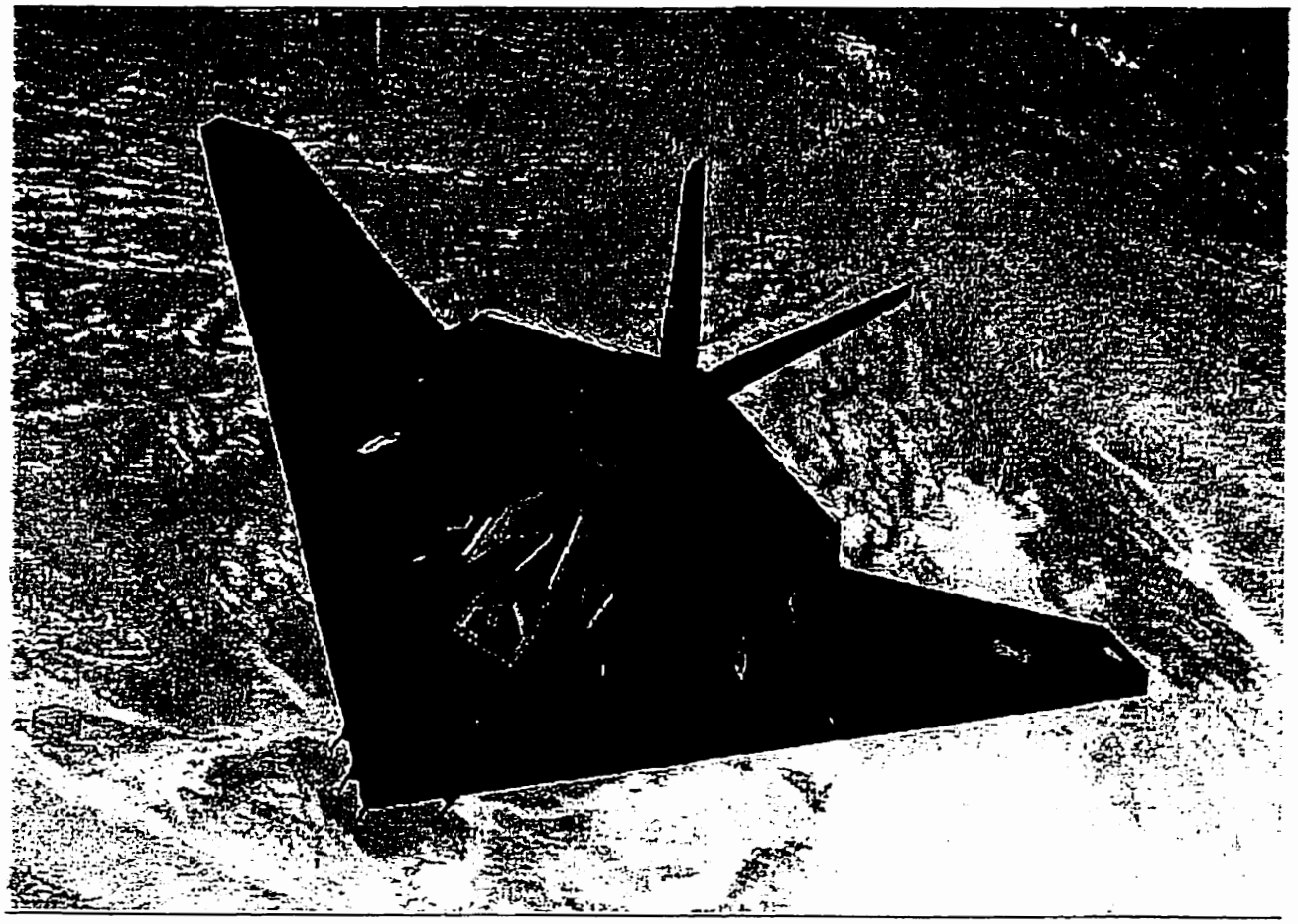

Figure 2.16: F117 Aircraft in Flight.

2.4.3 Marine Applications

Glass fiber-reinforced polyester laminates have found use in marine applications ever since their introduction as a commercial material in the 1940's. In recent years,

Kevlar 49 fibers are replacing glass fibers in some of these applications. Among the application areas are boat hulls, decks, bulkheads, frames, and some other parts. The principal advantage here is also weight reduction, which translates into higher cruising speed, acceleration and fuel efficiency. Other advantages are increased stiffness, increased damage resistance, durability and ease of handling. The combination of light weight, increased stiffness and excellent impact resistance have resulted in the rapid entry of Kevlar 49 composites into the canoe and kayak industry. Canoe and kayak hulls reinforced with Kevlar 49 are as much as 35 percent lighter by weight than fiber glass composites or aluminum hulls [112]. Recently, Kevlar 49 composites are used to fabricate about 80 percent of canoes and kayaks that engage in many sea sports.

Other applications of Kevlar 49 are manufacturing of the hulls of both large and small racing sailboats where the light weight increases speed, provides optimum weight distribution, and facilitates portability. It is also used in the manufacturing of hulls and decks of small fishing boats. In large yachts, using composites in building drive shafts have increased hull life because of the reduced vibration. A civil built prototype submarine for offshore work has been constructed with an unpressurized aramid-epoxy outer hull in place of glass fiber to allow greater payload and increased operational range and endurance. The new material offers a better combination of low weight, improved stiffness, and impact toughness [112].

2.4.4 Automotive Applications

The manufacturing and design of fiber-reinforced composite materials for the automotive industry are significantly different from those of aircraft applications. One obvious difference is in the volume of production, which may be hundreds of pieces per hour of automotive components compared with a few hundred pieces per year for

the aircraft industry. Composites of Kevlar 49 are now being used for a number of automotive parts where stiffness, strength, damage resistance, fatigue resistance and vibration damping properties are important, as well as weight savings. Many racing cars use graphite and Kevlar composites to save weight, eliminate environmental problems and give strength and ductility. Using composites in chassis of a racing cars achieves a 35 percent weight reduction over aluminum and is 50 percent stiffer [16].

In trucks, glass fiber composites are used in the cabins and containers manufacturing. Truck cabs and containers made of glass-fiber composites have reduced the weight by 33 percent and eliminated corrosion at the rear doors of the trucks. Compression molded SMC method is used for fabricating these doors which replace the steel ones. These doors are produced in lower tooling costs and reduced weight, while providing corrosion resistance and meeting the desired performance requirements. Composites are also used in manufacturing engine parts such as push rods, rocker arms, pistons and cylinder heads. Using such advanced composites in engines not only reduces engine weight but also allows engine to turn at higher speed and produces more power.

In spite of all these advantages, the issue of the high cost of composite materials particularly carbon fibers and Kevlar 49 fiber-reinforced materials, have remained critical compared to the traditional material of construction for automobiles which has been low cost mild steel. The development of efficient, low cost production methods for the mass production of composite automotive components will accelerate and expand the use of composites for these applications.

2.4.5 Other Commercial and Civil Engineering Applications

Other areas where composites are making progress include electronics, tanks and pressure vessels, buildings and bridges, sports equipments, music equipments and

medical equipments. In electronics the composites are widely used in manufacturing many components such as microphones, ribs to protect printed-circuit boards, and different types of antennas and satellites and space electrical systems.

In chemical applications the composites are used in pressure vessels and tank industries. Such applications include supply tanks for home water systems, swimming-pool filters, and water- softener tanks.

In sports, composites of Kevlar 49 offer weight savings in construction of sports equipment of various types with no sacrifice in stiffness and strength. Kevlar 49 has excellent vibration damping and damage resistance. The favorable composite properties have led to the adoption of Kevlar 49 composites for reinforcing tennis rackets, fishing rods, snow skis, and golf club shafts.

In civil engineering construction, composite materials have been used widely in buildings . bridges, and other structures. Recently, the C-bar new forcing rods for concrete has been designed to reinforce concrete operating in corrosive environments (e.g. roadway structures exposed to de-icing, salt and structures built in or close to sea water) as well as applications where low electric conductivity or electromagnetic neutrality is required. This type of C-bar is manufactured using a continuous pultrusion compression molding process. Other applications in civil engineering structures is in the use of carbon fiber (sheets and rods) composites to repair, protect, and strengthen concrete structures.

The use of these composites materials for bridge construction is one important applications that is being explored in order to lessen the pervasive corrosion problems of steel and reinforced concrete members. Prestressing tendons made of fiber reinforced composite materials are one of the most promising applications of this new material for bridges. Also, the repair and rehabilitation of existing structures represents a potential large scale use.

Chapter 3

LITERATURE SURVEY

3.1 Background

Composites are materials blending the desirable properties or behavior of two or more constituent materials to achieve improved stiffness, strength, and toughness at reduced weight. Composites subjected to repeated applications of stress can fatigue in a variety of mechanisms. In composites with uniformly strong reinforcing fibers, failure may occur by fatigue in the matrix, producing excessive delamination and loss of bending stiffness [12]. Repeated stress cycling can then produce delamination by matrix fatigue along the element-matrix interface between some of the isolated element fractures. Once enough of these isolated fractures have been joined by delamination to produce an effective critical transverse crack, the composite will fracture in a brittle manner. This chapter introduces the causes of delamination, growth and effect of delamination, prediction of delamination, and methods of reducing delamination in composite materials.

3.2 Linear Elastic Fracture Mechanics

Modern Linear Elastic Fracture Mechanics (LEFM) is based on the premise that the strength of the singular elastic stress field induced by a sharp crack may be completely characterized by the stress intensity factor (S.I.F.) [41]. Calculation of the stress intensity factor is the central element of fracture mechanics. Accurate determination of the SIF is particularly important in fracture testing, where its value at the onset of unstable crack growth is regarded as a material property: the fracture toughness K_{IC}.

Most of the early work on fracture of composite materials involved investigations of the applicability of linear elastic fracture mechanics, which had been originally developed for the analysis of through-thickness cracks in homogeneous, isotropic metals. The origin of fracture mechanics can be traced back to the seminal work of Griffith [40], who explained the discrepancy between the measured and predicted strength of glass by considering the stability of a small crack. The stability criterion was developed by an energy balance. The application of the Griffith-type analysis to composites presents some difficulties, but, fortunately, many of these problems have been solved over the years since Griffith's early work when researchers around the world focused their attention on fracture of metals in the fifties, and subsequently on fracture of concrete and rocks in the seventies and eighties. Irwin [50] and Orowan [79] modified the Griffith's analysis to include energy absorption due to plastic deformation at the crack tip.

The applicability of linear elastic fracture mechanics to unidirectional composites, in which the crack direction is "predetermined" to be parallel to the fibers was established in early studies by Wu [122, 120]. Wu developed an interaction relationship for combined Mode I and Mode II fracture using primarily center-notched tension specimens. Fracture of cross-ply composites has been studied using center or edge-notched

tension specimens and notched bend specimens [82, 7]. Slepetz and Carlson [101] have carried out experimental work on compact tension specimens of unidirectional and cross-ply S-glass/epoxy and graphite/epoxy. They concluded that, in unidirectional specimens, fracture toughness is dependent on the crack length in early stages of crack growth due to fiber bridging. At certain crack lengths the toughness remains constant with additional crack growth. On the other hand, they found that cross-ply graphite specimens do not exhibit a dependence of toughness on crack length.

In general, linear elastic fracture mechanics is invalid for circular holes and blunt notches in composites should be self evident, since LEFM theory assumes sharp cracks [3]. If, however, a sharp slit is introduced in a composite panel, as shown in Figures (3.1 and 3.2), were central sharp crack is introduced under uniaxial and biaxial stresses, the validity of fracture mechanics is less obvious.

In resent years, the solution to several problems encountered with composites have been provided by the use of several analytical techniques. The two leading techniques, are referred to as the "stress intensity factor" approach and the "strain energy release rate" approach. These two methods will be presented in the following sections.

3.2.1 Stress Intensity Factors

By considering the stress distribution around the crack tip and referring to plane stress condition in the vicinity of a uniaxially loaded crack, as show in Figure (3.3), Westgaard [113] used the complex stress function approach to show that the stress state for the isotropic case at a point P, defined by the polar coordinates (r, θ), can be expressed as:

$$\left.\begin{aligned} \sigma_x &= \frac{K_I}{\sqrt{2\pi r}} F_1(\theta) \\ \sigma_y &= \frac{K_I}{\sqrt{2\pi r}} F_2(\theta) \\ \tau_{xy} &= \frac{K_I}{\sqrt{2\pi r}} F_3(\theta) \end{aligned}\right\} \tag{3.1}$$

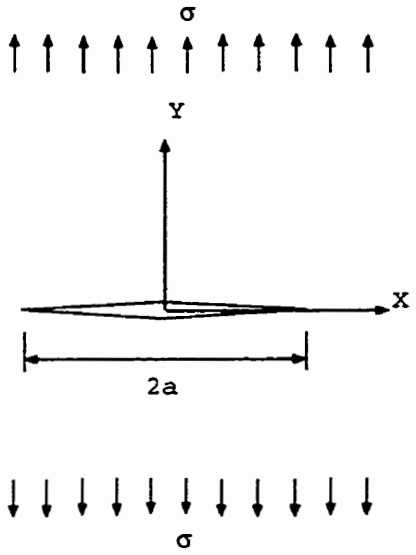

Figure 3.1: Mode I Crack under Uniaxial Stress State.

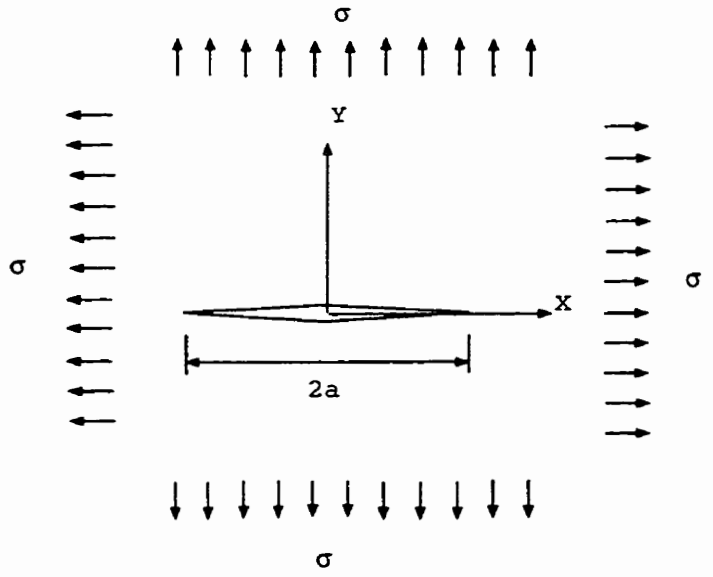

Figure 3.2: Mode I Crack under Biaxial Stress State.

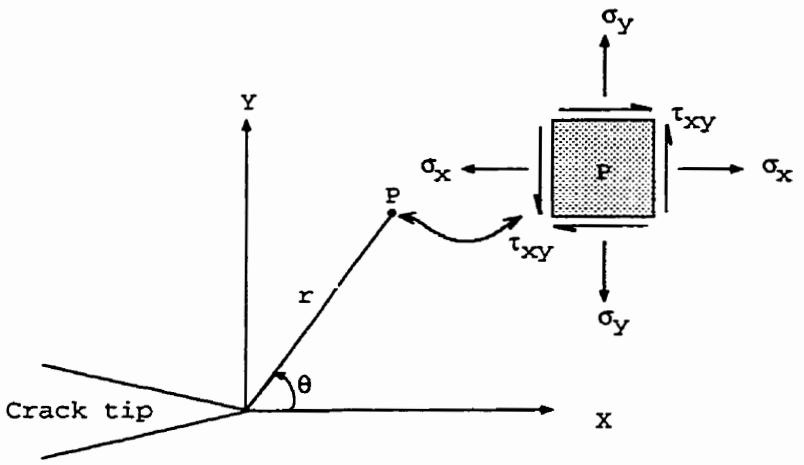

Figure 3.3: Stress at the Tip of a Crack under Plane Stress.

Where K_I is the stress intensity factor for the crack opening mode, and it is defined as:

$$K_I = \sigma\sqrt{2\pi a} \tag{3.2}$$

and $F_i(\theta)$ are trigonometric function of the angle θ. Irwin [51] also recognized that the term $\sigma\sqrt{2\pi a}$ controls the magnitude of the stress at a point (r, θ) near the crack tip. The critical value of the stress intensity factor, K_{IC}, corresponding to the critical stress σ_c, at which the crack propagates, is the fracture toughness:

$$K_{Ic} = \sigma_c\sqrt{2\pi a} \tag{3.3}$$

The fracture toughness K_{IC} is a material property which can be determined experimentally. Thus, if the fracture toughness of a material is known, then the fracture mechanics analysis can be used to find the critical crack size, a_c, or to find the critical stress, σ_c.

Several experimental investigations, e.g. Wu [120], Konish [61] and Parhizgar[80], have shown that the concepts of a critical stress intensity factor can describe the fracture behaviour of through-thickness cracked unidirectional composites and laminates.

In another report, the simple crack growth assumed in the Griffth-type analysis does not occur in composites with random fiber orientation. As an alternative to crack growth, the concept of a damage zone ahead of the crack tip in short fiber composites has been proposed by Gaggar and Broutman [35]. No systematic measurement or quantification of the damage process was addressed in the work of Gaggar and Broutman. Chapter 9 of this thesis proposes an indirect method to properly evaluate the loss of stiffness during crack growth. As it will be shown, the rate of change (degradation) in the elastic modulus may be approximated to be constant.

3.2.2 Strain Energy Release Rate Approach

The strain energy release rate has an easily understood physical interpretation which is equally valid for either isotropic or anisotropic materials, and is also related to the stress intensity factor. The strain energy release rate approach has proved to be a powerful tool in both experimental and computational studies of crack growth.

Following the explanation given by Gibson [38], consider a through-thickness cracked linear elastic plate under a uniaxial load, as shown in Figure (3.4a). An increase in the load, P, from the unloaded condition causes a linearly proportional change in the displacement, u, at the point of application of the load as shown in the load displacement plot in Figure (3.4b). If the load increases and reaches P_I and the corresponding displacement reaches u_I, the crack extends a small increment Δa. The crack extension causes the load to drop by an amount ΔP and the displacement to increase by an amount Δu. The strain energy G_I is defined by Corten [21] as:

$$\begin{aligned} G_I &= \lim_{\Delta A \to 0} \frac{\Delta W - \Delta U}{\Delta A} \\ &= \frac{dW}{dA} - \frac{dU}{dA} \end{aligned} \tag{3.4}$$

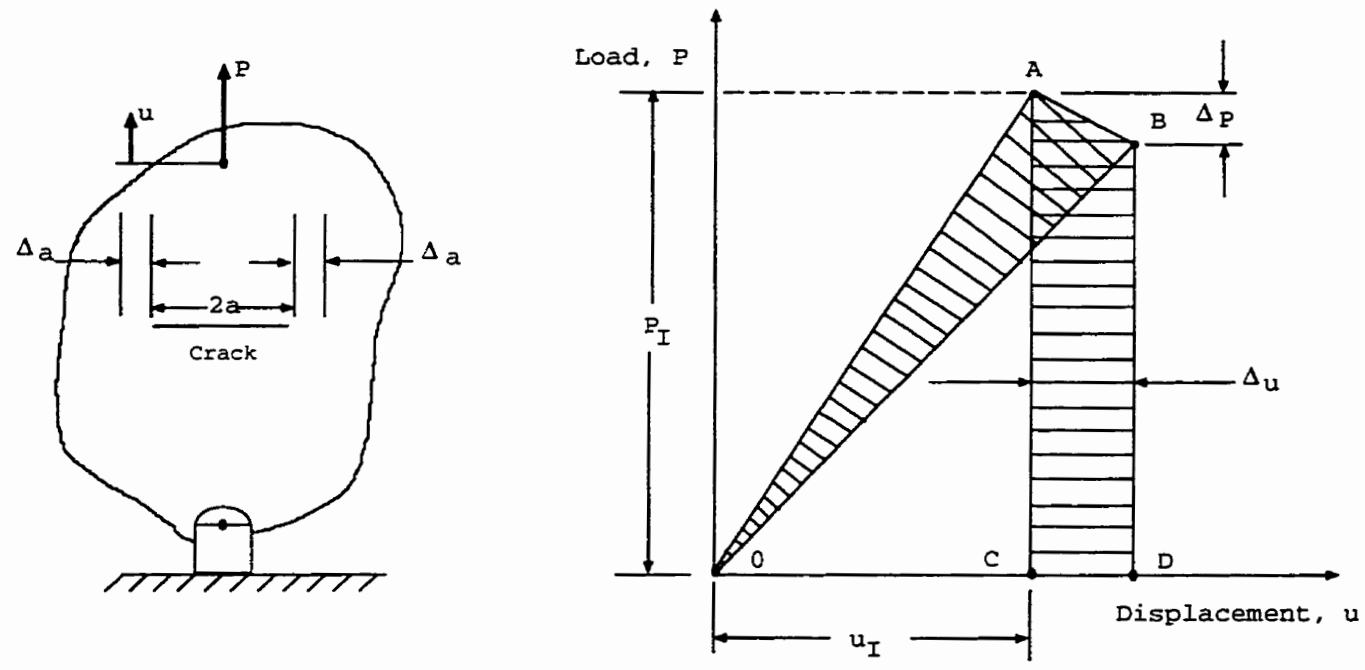

Figure 3.4: Loaded Plate and Corresponding Load-displacement Curve Used for Strain Energy Release Rate Analysis [38].

If the system compliances, S, is given by:

$$S = \frac{u}{P} \tag{3.5}$$

the potential energy U of the plate is

$$U = \frac{1}{2}Pu = \frac{1}{2}SP^2 \tag{3.6}$$

so that

$$\frac{dU}{dA} = SP\frac{\partial P}{\partial A} + \frac{1}{2}P^2\frac{\partial S}{\partial A} \tag{3.7}$$

The incremental work done W during the crack extension is approximately

$$\Delta W = P(\Delta u) \tag{3.8}$$

and

$$\frac{dW}{dA} = PS\frac{\partial P}{\partial A} + P^2\frac{\partial S}{\partial A} \tag{3.9}$$

Finally the strain energy release rate can be written as

$$G_I = \frac{P^2}{2}\frac{\partial S}{\partial A} \tag{3.10}$$

for a plate of constant thickness, t, and $\partial A = t\partial a$, the strain release energy is written as

$$G_I = \frac{P^2}{2t}\frac{\partial S}{\partial a} \tag{3.11}$$

and the critical strain energy release rate is given by

$$G_{IC} = \frac{P_c^2}{2t}\left(\frac{\partial S}{\partial a}\right)_C \tag{3.12}$$

The strain energy release rate is related to the stress intensity factor:

$$K_I^2 = G_I E \tag{3.13}$$

It is also shown by Cruse [22] that for a through-thickness mode I crack in an orthotropic laminate having N angle-ply components, the critical strain energy release rate is given by

$$G_{IC} = \frac{\sum_{i=1}^{N} G_{Ici} t_i}{t}. \tag{3.14}$$

where

G_{IC} is the critical strain energy release rate for the laminate

G_{Ici} is the strain energy release rate for the i^{th} angle-ply component

t is the total laminate thickness

t_i is the thickness of the i^{th} angle-ply component

The strain energy release rate is useful in the characterization of the crack growth rate under cyclic loading. This relationship between fatigue crack growth rate and strain energy release rate is demonstrated mathematically by Erdogan and Paris [81].

3.3 Damage Mechanics

The fundamental reason for studying damage mechanics is to understand why and how materials break. Together with physics, material science and chemistry, this knowledge allows us to improve the mechanical properties of materials and design new multi materials such as composite materials. The practical reason for studying damage mechanics is to predict when materials, as they are currently made, break when subjected to mechanical and thermal loading. (This involves the analysis of real components of material structures under real loading situations).

3.3.1 Definition of Damage

The damage of materials is the progressive physical process by which they break. The mechanics of damage is the study, through mechanical variables, of the mechanisms involved in this deterioration when the materials are subjected to loading [64]. At the microscale level, this is the accumulation of micro-stress in the neighborhood of defects or interfaces and the breaking of bond, which both damage the material. At the mesoscale level of the representative volume element, this is the growth and the coalescence of microcracks or microvoids which together initiate crack. At the macroscale level it is the growth of the crack in question. The first two stages may be studied by means of damage variables of the mechanics of continuous media defined at the mesoscale level. The third stage is usually studied using fracture mechanics with variables defined at the macroscale level.

Based on one-dimensional surface damage, damage may be defined also as the "effective" surface density of intersection of microcracks and cavities in most damaged section. To illustrate this concept, let us consider a three-dimensional mesovolume element containing a single circular crack loaded in mode I by force F perpendicular to the plane of the crack (see Figure 3.5). The overall damage defined by the continuum damage theory is the damage in the plane of the crack i.e:

$$D = \frac{\delta S_D}{\delta S} \tag{3.15}$$

or

$$D = \frac{\pi a^2}{l^2} k \tag{3.16}$$

Where k is the correction factor due to the stress concentration in the vicinity of the crack tip line to define the effective damage area. From which k can be calculated as a function of a/l as:

$$k = \frac{16\,(1-\nu^2)}{3\pi}\frac{a}{l} \simeq 1.55\frac{a}{l} \tag{3.17}$$

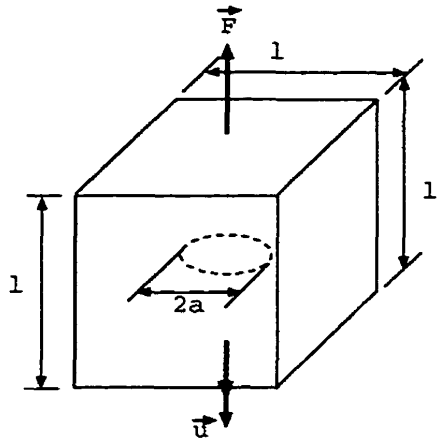

Figure 3.5: Single Cracked Meso Volume Element [64].

This indicates that for a given a/l, the value of the damage is always smaller than the crack density.

3.3.2 Manifestations of Damage

Damage manifest itself in different forms, depending on the material structure, loading, and environmental effects, as thermal loads. Classification of different forms of damage may be as follows:

1) Brittle damage: The damage is called brittle when a crack is initiated at the mesoscale without a large amount of plastic strain.

2) Ductile damage: The damage is called ductile when it occurs simultaneously with plastic deformations larger than a certain threshold.

3) Creep damage: When a material is loaded at elevated temperature, for instance a temperature above 1/3 of the melting temperature, the plastic strain involves viscosity; i.e. the material may be deformed at constant stress.

4) Low Cycle Fatigue Damage: When a material is subjected to a cyclic loading at high values for stress or strain, damage develops together with cyclic plastic strain after a period of incubation proceeding the phases of nucleation and propagation of microcracks. The degree of damage localization is higher than for ductile or creep damage.

5) High Cycle Fatigue Damage: When the material is loaded with lower values of stress, the plastic strain at the mesolevel remains small and is often negligible.

3.3.3 Measurement of Damage

3.3.3.1 Variation of the Elasticity Modulus

This is a non direct measurement based on the influence of damage elasticity though the state coupling i.e:

$$\varepsilon_e = \frac{\sigma}{E(1-D)} \tag{3.18}$$

If we set $\tilde{E} = E(1-D)$ as the effective elasticity modulus of the damaged material, the volume of the damage may be derived from measurements of $\tilde{E}$; provided that Young's modulus E is known then damage is given by,

$$D = 1 - \frac{\tilde{E}}{E} \tag{3.19}$$

This method requires accurate strain measurements. Strain gauges are commonly used and $\tilde{E}$ is most accurately measured during unloading. Chapter 9 proposes a systematic procedure to evaluate the damage D.

3.3.3.2 Ultrasonic Waves Propagation

Another technique for evaluating damage based on the variation of the elasticity modulus consists of measuring the speed of ultrasonic waves. For frequencies higher

than 200 kHz, the longitudinal wave speed (v_L) and transverse wave speed (v_T) in a linear isotropic elastic cylindrical medium are defined [64] as:

$$v_L^2 = \frac{E}{\rho} \frac{1-\nu}{(1+\nu)(1-2\nu)} \tag{3.20}$$

and

$$v_T^2 = \frac{E}{\rho} \frac{1}{2(1+\nu)} \tag{3.21}$$

Where E is Young's modulus, ρ the density and ν poisson's ratio. A measure of the longitudinal wave speed of a damaged material gives:

$$\tilde{v}_L^2 = \frac{\tilde{E}}{\tilde{\rho}} \frac{1-\nu}{(1+\nu)(1-2\nu)} \tag{3.22}$$

Where $\tilde{E}$ and $\tilde{\rho}$ are the damaged elastic modulus and density. Poisson's ratio does not vary with damage if elasticity is isotropic, and damage is scalar. The damage can be calculated as:

$$D = 1 - \frac{\tilde{E}}{E} = 1 - \frac{\tilde{\rho}}{\rho} \frac{\tilde{v}_L^2}{v_L^2} \tag{3.23}$$

If the damage consists mainly of microcracks or if small caviation is considered, then $\left(\frac{\tilde{\rho}}{\rho}\right) \simeq 1$ and:

$$D \simeq 1 - \frac{\tilde{v}_L^2}{v_L^2} \tag{3.24}$$

3.3.3.3 Other Methods

Several other methods, which are based upon the influence of damage on some physical or mechanical measurable properties, can be used. These methods are based on variation of the microhardness, density, electrical resistance (potential drop method), and variation of the cyclic plasticity response.

Most of these methods were used successfully to measure damage. As far as the survey is concerned, agreement between the results obtained by different methods was

shown to be sufficient for some practical accuracy involved. However, a conclusion, depending on the kind of damage involved, choose of the proper method of damage measurement remains very important to come up with acceptable results.

3.4 Damage Mechanics in Composite Materials

Damage mechanics in composite materials is quite different from that of homogeneous and isotropic materials and, thus, the basic concepts and assumptions that have been applied to simpler materials are not valid.

A unique property of composite materials is their evolutionary failure characteristic. The inhomogeneity of the microstructure provides numerous paths in which loads can be redistributed around the damage region. Thus, the ability to predict the strength of high performance composite materials under complex loading conditions is required for design with such materials. Because composite materials are frequently used in structures subjected to dynamic loads, it is also important to fully understand their response to cyclic loads.

Because of the inhomogeneity of the microstructure of composites, the integrity and response of the composite are affected more by the effective accumulated subcritical damage than by any single damage event. For laminated composites, this subcritical damage takes the form of matrix cracks, delaminations, debonding, and fiber fractures. Because the transfer of load away from the damaged area influences the damage evaluation in adjacent areas, the stresses at the ply level play an important role in the evaluation of damage and the ultimate failure of the structure. Thus, this unique failure process that makes composites an attractive material has also limited their efficient use in structures.

In recent years, many researchers have devoted considerable effort to the investi-

gation of damage in composite materials. Although they were able to detect, identify, and monitor damage details during the process of failure, the individual details that combine to form the damage state which controls the fracture of composite materials, is not understood.

In 1991, Lo, Allen and Harris [69] presented the evolution of matrix cracking in crossply laminates subjected to fatigue loading condition. They found that the stress distribution behaviour is dependent on the load amplitude. They also reported the existence of other types of damage, such as delamination, will alter the redistribution of stress among the plies and thus the evolution of the damage state. Adams et al. [1] studied damage in reinforced plastics and reported that damage in specimens fabricated from reinforced plastics could be detected by a reduction in stiffness and an increase in damping. Also, Cawley and Adams [14] successfully tested the frequency measurement principle on composite structures made in the presence of damage.

Manivasagam et al.[71] studied the characterization of damage progression in composites using the fundamental frequency degradation of layered composite materials with damage progression. They report in their work that the frequency measurement were performed during progressive cracking and progressive debonding and delamination. They concluded that, using vibration measurement techniques, the presence of damage and its size are detected simply from changes in the natural frequencies without the need of any further analysis.

3.5 Delamination in Composite Materials

A commonly observed failure mode in laminated composite materials is the delamination between the composite layers. Delamination may develop during manufacture due to incomplete curing or may result from the interlaminar stresses created by

impact. Failure of fiber composites consists of initiation, subcritical damage development and ultimate failure. Edge delamination is one of the important component of subcritical damage [54].

In laminated composite materials. matrix cracking and local delamination from matrix cracks are also important damage mechanisms that contribute to stiffness loss and eventual failure [90]. Furthermore, delamination may grow under cyclic loading. This growth redistributes the stresses in the plies of the laminate, and may influence residual stiffness, strength and fatigue life [78].

3.5.1 Causes of Delamination

Delamination may result from interlaminar stresses created by impact, eccentricities in structural load paths or from discontinuities in the structure. Besides mechanical loads. the moisture and temperature may also cause interlaminar stresses in a laminate.

3.5.1.1 Free Edge Stresses

The occurrence of interlaminar stresses near free edges of laminated composites is an important phenomenon. and is attributed to the mismatch in Poisson's ratio (ν) and coefficient of neutral influence ($\eta_{xy,x}$) between layers [37]. If there is no mismatch of ν or $\eta_{xy,x}$ between layers, interlaminar stresses do not exist even if there is a mismatch in elastic and shear moduli [43].

3.5.1.2 Delamination Caused by Impact

When a laminate is hit by a projectile or is subjected to an impact, the hit generates highly localized deformation gradients which cause large transverse shear and normal

stresses that can cause the damage to propagate and eventually failure of the laminate. This amount and type of damage in the laminate depends upon the size, type and geometry of the laminate, impact energy and the loading at the time of impact.

3.5.1.3 Delamination Caused by Matrix Cracking

Another cause of delamination development in a laminate is the matrix cracking in off-axis plies. These off-axis ply cracks create interlaminar stresses. These interlaminar stresses frequently cause local delamination which grow along ply interface near matrix cracks.

3.5.2 Effect of Delamination

The tensile static and cyclic loading behaviour of quasi-isotropic graphite/epoxy laminates reported by Reinfsinder, Stinchcomb and Coworker [84], indicate that the damage developed in the form of matrix cracks and delamination does not appear to influence the residual strength. Subsequently, Garg [37] and other researchers showed that delamination plays a critical role in affecting the compressive behavior of a laminate. Grag states that it may cause localized buckling and high interlaminar shear and normal stresses at the edges of the buckled region. This effect is depicted in Figure (3.6). Such a phenomenon is designated as instability-related delamination growth. Whitcomb [114] studied such delamination growth in compressively loaded members and concluded that, for a laminate with one surface delaminated partially (Figure 3.6), the critical load P_c decreases with the increase in delamination length a. Yin, Semites and Coworkers [94, 126, 127] also studied the delamination growth due to compressive loads in various laminates under different edge conditions. Similar effect on the buckling behavior of composites with delamination have been shown by Majumdar and Suryanarayan [73]. Rholdes, Williams and Coworkers [116] studied

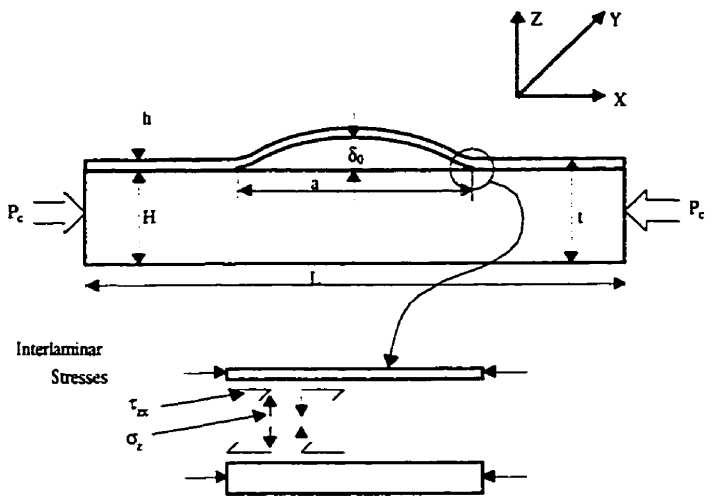

Figure 3.6: Delaminated Laminate under Compression.

the compression behavior of impact damaged composite panels. These studies have indicated that the residual strength significantly deteriorates with increase in impact velocity (or impact damage). Also, fatigue loading of delamination panel may accelerate damage growth, particularly under compressive cyclic loading. This tends to reduce the residual strength and stiffness. Such behavior was studied by several researchers [36, 114, 95] where the delamination was either caused by impact or by implanted flaws.

3.5.3 Growth of Delamination

Delamination growth depends upon the stress state at the crack tip which is governed by the mixed mode stress intensity factors involving K_I,K_{II} & K_{III} or the strain energy release rates G_I,G_{II} and G_{III}. It is not necessary that all three modes exist and one or two modes may dominate fracture propagation. For example, the analysis by Wang [109] for edge delamination at the interface of angle ($\pm\theta$) laminates show that K_{II} is considerably lower than K_I and K_{III} and edge delamination is dominated

by K_{III} i.e. the tearing mode. The growth of edge delamination is a stable fracture process in laminates subjected to tensile loading [78], i.e. applied load has to be increased to force the delamination to grow. Such growth has been characterized by O'Brien [78] using the concept of crack growth resistance (R-curve). He considered that G_C is a material property and is independent of ply orientation. This is contrary to the observations of Johannesson and Bliksted [54] for delamination of angle ply laminates. Their studies have shown that G_C is strongly dependent on the ratio $\frac{K_{III}}{K_I}$ for angle ply laminate.

The mixed mode delamination growth is not observed to follow a single propagation law. Various laws have been used by different investigators to fit their test data. The simplest mixed mode delamination propagation law is defined as "the delamination growth which occurs when the total strain energy release rate $G_T = G_I + G_{II}$ reaches a critical value G_C". i.e.

$$G_T = G_I + G_{II} = G_C \tag{3.25}$$

Equation (3.25) may describe the mixed mode delamination growth only for the materials when $G_{IC} = G_{IIC}$. Rybicki et al. [89] and O'Brien [78] have used Equation (3.25) to describe their mixed mode delamination growth.

For most of the graphite/epoxy composites, Equation (3.25) may not adequately describe the delamination growth. A more appropriate interaction relation to describe the delamination growth is given in [68] as:

$$\left(\frac{G_I}{G_{IC}}\right)^m + \left(\frac{G_{II}}{G_{IIC}}\right)^n = 1, \tag{3.26}$$

Where the exponents m and n have different values for the different cases.

Hahn [21] has proposed another mixed mode crack propagation law as:

$$(1-g)\left(\frac{G_I}{G_{IC}}\right)^{\frac{1}{2}} + g\left(\frac{G_I}{G_{IC}}\right) + \left(\frac{G_{II}}{G_{IIC}}\right) = 1 \tag{3.27}$$

where $g = \frac{G_{IC}}{G_{IIC}}$

For composites with epoxy matrices $g \approx 0.1 - 0.2$. For negligible g, Equation (3.27) is similar to Equation (3.26), with $m = 1/2$ and $n = 1$.

Russell and Street [88] also studied various crack propagation laws and demonstrated that mixed mode delamination growth may be better represented by Wu's tensor polynomial criterion [121]. Russel and Street modified Wu's original criterion from the plane stress to plane strain condition which are more appropriate for delamination problems. The plane strain model was found to fit the experimental data for mixed mode delamination fairly well.

Various test methods have been considered for measuring the growth of delamination. Wilkins et al. [115] tested double cantilever beam (DCB) specimens and cracked lap shear (CLS) specimens under displacement controlled conditions where P vs δ curves are obtained for various crack lengths, a. The DCB specimen. , consist of two cantilever beams joined at the end of the crack tip as shown in Figure (3.7A). The compliance of system is expressed as:

$$C = \frac{8a^3}{WEh^3} \tag{3.28}$$

where E is longitudinal modulus and h is the thickness of each beam, and the energy release rate is

$$G = \frac{3P^2C}{2Wa} \tag{3.29}$$

To characterize mode II delamination, several specimens such as cracked lap shear (CLS) specimen [115] (see Figure 3.7B) were considered, in which the P vs δ curves may be obtained for various crack length and the value of G_C may be obtained using

$$G_C = \frac{P_C^2}{2W^2}\left[\frac{1}{(Eh)_2} - \frac{1}{(Eh)_1}\right] \tag{3.30}$$

where subscripts (1) and (2) refer to the sections indicated in Figure (3.7B).

Russel and Street [88] used the end notched flexure (ENF) specimen, which is the same as the DCB but it is located in a three point flexure and results in almost pure in-plane shear delamination growth by mode II. An expression for mode II delamination of G_{IIC} using the beam theory is given as:

$$G_{IIC} = \frac{9P_C^2 a^2 C}{2W(2L^3 + 3a^3)} \tag{3.31}$$

where Pc is the critical load for delamination, W, L and a are defined in Figure (3.7C) and C is the compliance defined by

$$C = \frac{(2L^3 + 3a^3)}{8EhW} \tag{3.32}$$

where E is the flexural modulus and $2h$ is the thickness of the specimen.

3.5.4 Prediction of Delamination Behavior

3.5.4.1 Prediction of Interlaminar Stresses

Prediction of delamination behavior in composites has been an important subject for many years. Most of previous work has focused on determination of the stresses in the boundary layer near the free edges whether curved or straight. The analytical approach to such problems have been to determine stress intensity factors at the tip of the crack and at the interface of two or more isotropic layers or transversely isotropic half planes which was derived by Erdogan and Gupta [31] and England [28].

Because of its complexities, the analytical solution to edge delamination has been rather limited. Therefore more emphasis has been placed on the use of either finite difference as Altus, Rotern and Shmeli [2], or finite element methods as Kim and Hong [58] and Spilker and Chou [102].

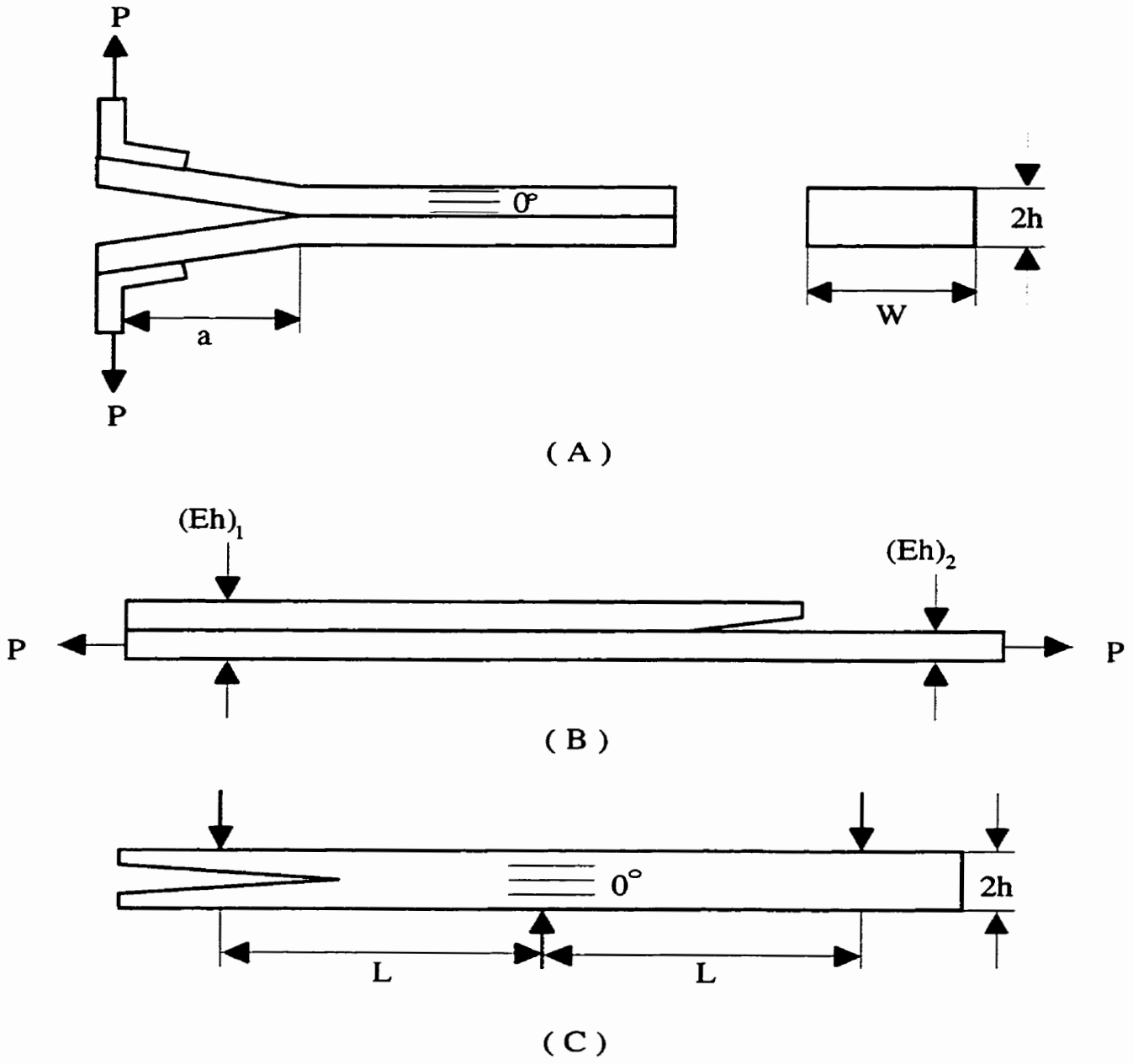

Figure 3.7: A) Double Cantilever Beam (DCB) Specimen. B) Cracked Lap Shear (CLS) Specimen. C) End Notched Flexure (ENF) Specimen.

3.5.4.2 Onset of Delamination

There are two approaches to predict delamination: one based on fracture mechanics and the other based on strength. Rybicki, Schmueser and Fox [89], modeled the edge delamination utilizing finite element method. They found that the strain energy release rate remained nearly constant during the propagation of delamination. This indicates that the critical strain energy release rate (G_C) may be a useful criterion for delamination growth. This observation that G remaining constant with delamination propagation has been noted by other researchers as Altus, Rotern and Shmueli [2] and Whitcomb [114]. However, Garg [36] stated that, the fracture mechanics approach in predicting the delamination onset appears to be more accurate than the strength approach. Thus, delamination has been predicted using the strain energy release rate approach and other failure criteria. O'Brien [78] suggested the strain energy release rate approach for prediction initiation and growth of delamination.

Kim and Sonic [60] studied the onset of delamination by using the average stress criterion. The average stress criterion assumes that the initiation of delamination occurs when the average value of interlaminar stress over the critical length reaches prescribed interlaminar strength. Brewer and Lagace [10] introduced the quadratic delamination criterion to predict initiation of delamination based on free edge stress distributions. They reported good agreement between the results calculated by the quadratic delamination criterion and experimental ones.

Sung Yi [125] extended the quadratic delamination criterion to take into account time-dependent creep rupture strengths by some modified expression for time dependent average stresses. For more details one can refer to ref. [125].

3.5.5 Matrix Cracking

Wang and Chang [108], found in their studies that fiber-reinforced laminated composites are vulnerable to transverse concentrated loading as low-velocity impact can cause significant internal damage in the form of matrix cracks and delamination. Experimental observations done by Wu and Springer [123], Gosse and Mori [39] have shown that these matrix cracking and delamination resulting from impact or quasi-impact appear concurrently. This strongly indicates the existence of strong interaction between matrix cracking and delamination during impact.

Recent studies of two-dimensional impact by Choi and Chang [17, 18] showed that matrix cracking is the initial impact damage mode. Two types of matrix cracks such as shear crack embedded inside the material and bending crack which appears in the outermost layers of the laminate were found to initiate delamination. Additionally, delamination induced by impact or quasi-impact always propagate more extensively in the direction of the fibers than in the transverse direction of the fibers of the bottom layers next to the delamination interface.

Liu, Kutlu and Chang [68] studied the damage mechanism and mechanics of laminated composites subjected to transverse concentrated loading. In their investigation, an analytical model was proposed for analyzing the response of the composite beam beyond initial damage resulting from transverse concentrated loading. The Liu, Kultlu and Chang [68] model considers matrix cracking in addition to delamination and interaction between matrix cracking and delamination. Basically, the model consists of three parts: a stress analysis, a contact analysis and a failure analysis. Because matrix cracking and delamination growth in laminated composite beams subjected to transverse concentrated loading were the major concern of this study, fiber breading was not considered. An appropriate failure criterion was adopted for predicting the initiation of matrix cracking and delamination. A fracture analysis based on linear

elastic fracture mechanics theory was utilized for modeling the growth of the initial damage. They described the matrix failure criterion as

$$\left(\frac{\sigma_{yz}}{S_i}\right)^2 + \left(\frac{\sigma_{yy}}{Y_t}\right)^2 = e_M \tag{3.33}$$

Where S_i is the inter-laminar shear strength within the laminate under consideration, and Y_t is the insitu ply transverse tensile strength. The occurrence of matrix cracking is predicted when the value of e_M is equal to or greater than unity. They expressed the delamination failure criterion in their study as

$$\left(\frac{\sigma_{ZZ}}{Y_t}\right)^2 + \left(\frac{\sigma_{YZ}^2 + \sigma_{XZ}^2}{S_i^2}\right) = e_d^2 \tag{3.34}$$

Where σ_{YZ} and σ_{XZ} are the interlaminar shear stresses, and σ_{ZZ} and σ_{YY} are the out-of-plane normal stress and in-plane transverse normal stress respectively within the element under consideration. The occurrence of delamination at the interface is predicted when the value e_d is equal to or greater than unity.

Whenever the combined state of stresses satisfies either one of the criteria, initial failure was predicted. The corresponding failure criterion indicates the initial mode of failure. Once the initial failure was predicted, fracture analysis was then applied to simulate the growth of local damage when the applied load continued to increase. They also suggested in their study that in order to simulate crack propagation, a small initial crack was introduced immediately after the occurrence of the initial failure, depending upon the type of the failure mode. For matrix cracking, they suggested a vertical crack to be immediately generated in the failed ply at the location where matrix cracking was predicted. Finally, at the end of their study they concluded that the delamination growth induced by interplay bending cracks is stable and progressive, but the one induced by interplay shear-cracks is very unstable and catastrophic. For more details on this subject, the reader is refered to ref. [68].

3.5.6 Methods of Reducing Delamination

3.5.6.1 Improved Resins

The delamination growth in a composite depends on its interlaminar fracture toughness which in turn depends on the toughness of the matrix material. Williams and Rhodes [116], Choi and Coworkers [18] demonstrated that tough resins can significantly reduce damage caused by impact and substantially improve the residual strength following impact.

3.5.6.2 Through Thickness Reinforcement

Using polyester and Kevlar yarns at various stitch spacing and pitch for stitching through the thickness graphite/epoxy laminates, Dexter and Funk [24] demonstrated a considerable improvement in damage tolerance. However, the stitching reduces the compressive and tensile strength of laminate compared to unstitched laminate for undamaged specimens by about $20 - 25\%$.

3.5.6.3 Interleafing

Interleafing of the laminate, i.e. sandwiching thin films of high toughness and shear strain thermoplastic between graphite/epoxy layers has been demonstrated by Evans et al [33] to be an effective way to improve the damage tolerance of composites.

3.5.6.4 Design Consideration

It has already been stated that the cause of delamination is the interlaminar stresses which are dependent on the lay-up sequence. Kim [59] suggested that the reinforcement of free edges is an effective way to prevent and/or delay initiation of delamination. His study has indicated that the reinforcement of edges of various delamination

prone laminates by fiber glass cloth significantly delays or prevents the initiation of edge delamination.

3.6 Fracture of Composite Materials

The fracture and fatigue behaviour of composite materials is obviously one of the more challenging and certainly one of the most important technological areas to be investigated and understood. Application of the principles of linear elastic fracture mechanics to these materials is limited not only by the anisotropic and inhomogeneous nature of composites but also by the fact that the individual components may be capable of plastic deformation.

Fracture, whether brittle or ductile, whether in nearly homogeneous materials or in composites, is governed more or less sensitively by macroscopic discontinuities and imperfections such as cracks, holes and inclusions. It can not be understood without a full description of such micro structural features. The fracture behaviour of composite materials has recently become a major concern, as engineering composites have begun to appear in critical structural applications. Fracture of fiber-reinforced composite, however, is often controlled by numerous microcracks distributed throughout the material, rather than a single macroscopic crack. There are situations where fracture mechanics is appropriate for composites, but it is important to recognize the limitations of theories that were intended for homogeneous materials.

3.7 Stress Field Around an Interface Crack Between Dissimilar Materials

The accurate evaluation of the strength of an interface crack between dissimilar materials such as composites becomes very important because fracture often occurs at the interface. Therefore, the singular stress and displacement fields for an interface crack is of concern to many scientists and researchers. One of the early investigations in this field was by Williams [117] in 1959, who used an eigen function approach to determine the singular character of the extensional stress near the tip of the crack at the interface between two materials. He found that the stresses have an oscillatory character.

From 1963 to 1965 Erdogan [29, 30] used complex variable formulation in examining the case of two half-planes bonded to each other along a finite number of straight line segments and evaluated the stress distributions near the end of the crack. In his study, he found that stresses due to violent oscillations occur near the ends of the cracks. This problem was also studied by England [27] in 1965 and he concluded that the solution to the problem of a single line crack opened by equal and opposite normal pressures between two bonded dissimilar half-planes, is physically inadmissible since it predicts that the upper and lower surfaces of the crack should later wrinkle and overlap near the ends of the crack. Rice and Sih [96, 85] in 1965, applied the complex variable technique of Muskhelishvili [75] combined with eigenfunction expansion to explicitly obtain the expression of stress components in the vicinity of a crack tip. They also conclude that the significant stresses are inversely proportional to the square root of the radial distance from the crack front and have an oscillatory character.

Theocaris and Gdouto [105, 106] derived the stress functions to solve the problems

under various boundary conditions. However, in case of the interface crack between dissimilar materials, Ishikawa and Kohno [52] found that the stress functions which was derived by Theocaris and Gdoutos [105, 106] are restricted to the case where the shear-modulus and Poisson ratios of the dissimilar materials satisfy certain conditions. The stress functions which were derived by Theocaris and Gdoutos [105, 106] were improved in 1993 by Ishikawa and Kohno [52] so that they can be used for the materials with arbitrary moduli and ratios. By using these improved stress functions, the energy release rate for the extension of the crack, as well as the singular stress and displacement fields around the tip of the crack is obtained. They also show that the solutions obtained were identical to those obtained by Rice and Sih as well as those by Sun and Jih [104].

Alternately, total strain energy release rate, G_i was used as a fracture parameter for interfacial crack propagation. It was found by Mulville and Mast [74] that the total strain energy release rate remained relatively constant as the crack propagated along the bond. Moreover, the total energy release rate approach eliminated problems associated with oscillating singularities. Sun and Jih [104] in 1987 used crack-closure method to calculate the strain energy release rates associated with mode I and mode II. It was shown analytically that mode I and mode II strain energy release rates for the interfacial crack in bi-material plates are not well defined due to the presence of oscillatory terms. However, it was found numerically that G_I and G_{II} depend on the choice of the assumed crack extension.

Kelly, Hills and Nowell [57] in 1994 used the method of distributed dislocations to formulate the plane problem of crack between a circular elastic inclusion and an elastically dissimilar matrix. Results are given for the crack-tip stress intensity factors for several sizes of cracks, and it is shown that as the crack angle becomes large, the open mode intensity falls, and eventually the crack tips close. Dhaliwal and Saxena [25] in 1992 considered the problem of determining the stress intensity factor when

two bonded dissimilar non-homogeneous layers contain an interface Griffith crack, and when the faces of the crack are subjected to antiplanar shear stress. Numerical results are presented for the stress intensity factor using Fourier transformation and Erdogan's approach. The numerical results showed that the stress intensity factor K decreases rapidly as the thickness of the two layers decrease. For the case of the two layers of equal thickness, and the interface crack subjected to an antiplane constant shear stress, they concluded that the stress intensity factor decreases rapidly as thickness increases. Following this, in 1993, Xu and Reifsnider [124] studied fiber cracks or microcracking formed in the process of manufacturing due to mismatch of fiber and matrix thermal expansion coefficients propagation in composites due to transverse tensile fracture mechanics (LEFM). They investigated the effect of fiber volume fraction, fiber anisotropy, and fiber-matrix mechanical property mismatch on the fiber crack propagation and concluded that the fiber mechanical anisotropy seems to have little effect on the fiber cracking for transverse loads.

3.8 Numerical Modeling

Numerical methods of stress analysis are powerful tools which can produce solutions for complex problem such as the ones of composite materials [8]. The finite element modeling for the prediction of crack propagation in composite materials have found widespread use in the fracture mechanics field. There are two basic approaches to model a crack using the finite element method: the smeared crack model and the discrete crack model. Historically, the first crack models were discrete [76], however, the smeared crack model is introduced by Rashid [83] which has been adopted by most of finite element codes and the discrete model was discarded primarily for convenience.

3.8.1 Smeared Crack Modeling

In this approach, the cracked material is assumed to remain as a continuum; the cracks are "smeared out" in a continuous fashion. Rather than representing a single discrete crack. This approach has the effect of representing an infinite number of parallel fissures across the cracked material element. These parallel fissures are assumed to form in the planes (or surface for axisymmetric problems) perpendicular to the maximum principal stress (or strain) direction. After the first cracking has occurred, it is assumed that the cracked material becomes orthotropic or transversely isotropic, with one of the material principal axes being oriented along the direction of cracking.

The model smears the crack over one or more finite elements by defining an orthotropic stress-strain relation for those elements. This would assign a zero Young's modulus to the element in the direction normal to the crack, and a fraction of the original shear modulus is retained [5]. Thus as the crack propagates, the [D] matrix of the cracked elements varies while the topology (or element connectivity) is not affected.

3.8.2 Discrete Crack Modeling

In the discrete crack model, a crack is represented by an inter-element gap and during crack growth the mesh topology continuously changes and its elastic properties are kept constant. further-more in the discrete approach, the mesh is modified, automatically, to represent the cracking process [47]. In the case of arbitrary cracking, local remeshing is introduced to existing elements and performed for each crack at each increment of cracking. Singular elements are introduced at a true crack tip to model the singular stress field in accordance with linear elastic fracture mechanics (LEFM).

In the early 80's there has been a renewed interest in the discrete model. Since

then, discussions about the merits of discrete versus smeared crack models kept on being addressed. As a result of that, much has been written about the phenomenological and computational aspects of each model [6], [62]. As far as the two models are concerned, some of the recent smeared crack models are beginning to look like discrete ones. In fact, there is a need for both models, but discrete crack models should be used when a precise crack profile is sought.

Chapter 4

FAILURE MODELING OF COMPOSITE MATERIALS

4.1 Introduction

This chapter addresses the mathematical modeling of composites failure. Three classes of models are proposed in the literature: strength-based models, fracture based models and continuum based models. Two major contributions are proposed herein. The first contribution establishes a systematic numerical procedure to determine interlaminar buckling in finite element analysis using a correlation technique. The second contribution addresses hybrid fracture mechanics-continuum damage mechanics model to simulate crack growth in composites using the finite element method.

4.2 Failure of Fiber Composites - Strength Approach

Because of the complexity of the failure process, it may be desirable to regard the strength of a unidirectional fiber composite subjected to a single principal stress component as a quantity to be measured experimentally, rather than deduced from constitutive properties. At the level of unidirectional composites, it is important to examine the effect upon failure of the individual constituents to develop an understanding of the nature of the possible failure mechanisms.

The strength of the fiber composite clearly depends on the orientation of the applied load with respect to the direction in which the fibers are oriented as well as whether the applied load is tensile or compressive.

4.2.1 Axial Tensile Strength

The simplest model for the tensile failure of a unidirectional fiber composite subjected to a tensile load in the fiber direction is based on elasticity solution of uniform axial strain throughout the composite. Generally, the fibers have a lower strain to failure than the matrix, and composite fracture occurs at the strain of the fibers alone.

When the bond strength between the fibers is high enough to prevent interface failure, local stress concentrations may cause fiber failure to propagate through the matrix, to and through adjacent fibers. Alternatively, the stress concentration in adjacent fibers may cause one or more of such fibers to break before failure of the intermediate matrix. If such a crack or such fiber break continue to propagate, the strength of the composite may be no greater than that of the weakest fiber. As the applied load continue to increase, new fiber failure at other locations in the material will appear and internal damage will results.

4.2.2 Axial Compressive Strength

Both strength and stability failures must be considered for compressive loads parallel to the fibers of unidirectional composite. Microbuckling is the load failure mechanism for axial compression. The energy method has been used for evaluation of the buckling stress for these modes. This procedure considers the composite as stressed to buckling load. The strain energy in this compressed but straight pattern (extension mode) is then compared to an assumed buckling deformation pattern (shear mode) under the same load. The condition of instability is given by equating the strain energy change to the work done by the external loads during buckling.

4.2.3 Matrix Mode Strength

When failure in composite materials occurs without fracture of fibers, This is known as matrix mode of failure. This kind of failure mode can happen when the material subjected to transverse tension or compression and axial shear loading conditions. Micro-mechanical analyses of these failure modes are complex because the critical stress states in the matrix, are highly non-uniform, and are very dependent upon local geometry. As a result, it appears that the most fruitful approaches will be those that consider average states of stress.

4.2.4 Strength-based Finite Element Modeling

As mentioned in the literature review, the smeared crack is best fit to model failure on the bases of the "strength approach".

At the constitutive level, a finite element may be considered to be linear elastic isotropic or anisotropic to simulate an initial undamaged state. A multilayered element may be used to simulate individual plies. While tensile failure is simulated by

introducing a discontinuity in the displacement field across the direction of maximum principal stress, within the element, when the maximum principal stress reaches a limiting value, compressive failure is introduced by removing the local capacity of the element to transmit compressive forces, while the former task is an easy one to implement, the latter presents serious difficulties due to incompatibility problems across inter-element boundaries.

4.3 Failure of Fiber Composites-Fracture Mechanics Approach

In this section a brief summary is provided of the basic concepts and definitions employed in the theory of linear elastic fracture mechanics.

4.3.1 Introduction

The application of fracture mechanics concepts to crack growth has made substantial progress over the last three decades. The process which causes cracking of a components subjected to loading can generally be broken into two distinct phases-initiation and propagation. The prediction and measurement of crack propagation is of significant importance for the design of loaded components and the measurement assessment of service life. Linear elastic fracture mechanics is based on the concepts of stress intensity factors. Using complex functions, Westergaard was the first to determine the stress and displacement field near the tip of a sharp crack [113].

Subsequently Irwin [51] introduced the concepts of stress intensity factor defined as

$$\begin{Bmatrix} K_I \\ K_{II} \\ K_{III} \end{Bmatrix} = \lim_{r \to 0, \theta \to 0} \sqrt{2\pi r} \begin{Bmatrix} \sigma_{22} \\ \sigma_{12} \\ \sigma 23 \end{Bmatrix} \tag{4.1}$$

where σ_{ij} are the near crack tip stresses, and K_I, K_{II}, K_{III} are associated with three independent kinematic movements of the upper and lower crack surfaces with respect to each other, as shown in Figure (4.1) the displacement modes are:

- *Opening Mode I*: in which the two crack surfaces are pulled apart in the y direction, but where the deformations are symmetric about the x-y and x-z planes.
- *Shearing Mode II*: in which the two crack surfaces slide over each other in the x-direction, but where the deformations are symmetric about the x-y plane and skew symmetric about the x-z plane.
- *Tearing Mode III*: in which the crack surfaces slide over each other in the z-direction, but where the deformations are skew symmetric about the x-y and x-z planes.

4.3.2 Near Crack Tip Stress and Displacements in Isotropic Cracked Solids

Using Irwin's concept of the stress intensity factors which characterizes the strength of the singularity at a crack tip, the near crack tip (i.e. $r << a$) stresses and displacements can be expressed as [5]:

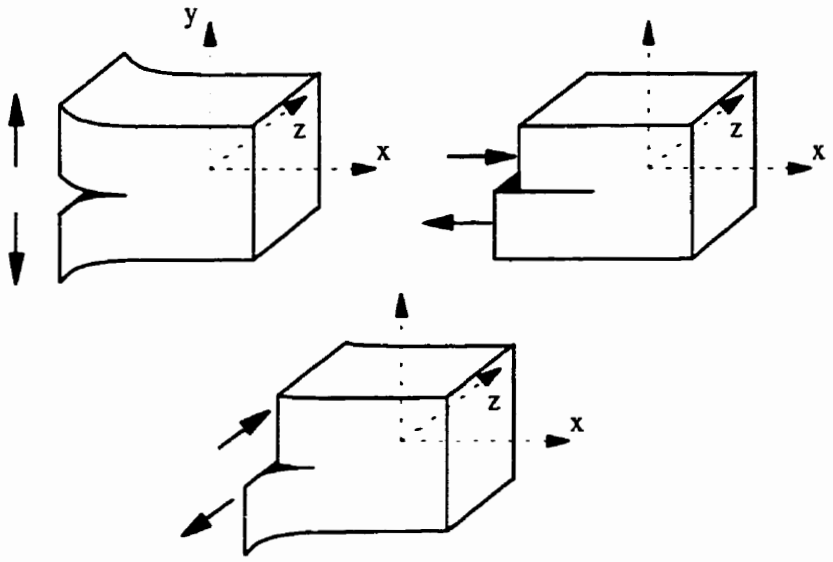

Figure 4.1: Independent Modes of Crack Displacement.

- Mode I loading:

$$\sigma_x = \frac{K_I}{(2\pi r)^{\frac{1}{2}}} \cos\frac{\theta}{2}\left[1 - \sin\frac{\theta}{2}\sin\frac{3\theta}{2}\right] \tag{4.2}$$

$$\sigma_y = \frac{K_I}{(2\pi r)^{\frac{1}{2}}} \cos\frac{\theta}{2}\left[1 + \sin\frac{\theta}{2}\sin\frac{3\theta}{2}\right] \tag{4.3}$$

$$\tau_{xy} = \frac{K_I}{(2\pi r)^{\frac{1}{2}}} \left[\sin\frac{\theta}{2}\cos\frac{\theta}{2}\cos\frac{3\theta}{2}\right] \tag{4.4}$$

$$\sigma_z = \nu\left(\sigma_x + \sigma_y\right) \tag{4.5}$$

$$\tau_{xy} = \tau_{yz} = 0 \tag{4.6}$$

$$u = \frac{K_I}{G}\left[\frac{r}{2\pi}\right]^{\frac{1}{2}} \cos\frac{\theta}{2}\left[1 - 2\nu + \sin^2\frac{\theta}{2}\right] \tag{4.7}$$

$$v = \frac{K_I}{G}\left[\frac{r}{2\pi}\right]^{\frac{1}{2}} \sin\frac{\theta}{2}\left[2 - 2\nu - \sin^2\frac{\theta}{2}\right] \tag{4.8}$$

$$w = 0 \tag{4.9}$$

- Mode II loading:

$$\sigma_x = \frac{K_{II}}{(2\pi r)^{\frac{1}{2}}} \sin\frac{\theta}{2}\left[2 + \cos\frac{\theta}{2}\cos\frac{3\theta}{2}\right] \tag{4.10}$$

$$\sigma_y = \frac{K_{II}}{(2\pi r)^{\frac{1}{2}}} \sin\frac{\theta}{2}\left[\cos\frac{\theta}{2}\cos\frac{3\theta}{2}\right] \tag{4.11}$$

$$\tau_{xy} = \frac{K_{II}}{(2\pi r)^{\frac{1}{2}}} \cos\frac{\theta}{2}\left[1 - \sin\frac{\theta}{2}\sin\frac{3\theta}{2}\right] \tag{4.12}$$

$$\sigma_Z = \nu\left(\sigma_x + \sigma_y\right) \tag{4.13}$$

$$\tau_{xz} = \tau_{yz} = 0 \tag{4.14}$$

$$u = \frac{K_{II}}{G}\left[\frac{r}{2\pi}\right]^{\frac{1}{2}} \cos\frac{\theta}{2}\left[2 - 2\nu + \cos^2\frac{\theta}{2}\right] \tag{4.15}$$

$$v = \frac{K_{II}}{G}\left[\frac{r}{2\pi}\right]^{\frac{1}{2}} \cos\frac{\theta}{2}\left[1 - 2\nu + \sin^2\frac{\theta}{2}\right] \tag{4.16}$$

$$w = 0 \tag{4.17}$$

- Mode III loading:

$$\tau_{xz} = \frac{K_{III}}{(2\pi r)^{\frac{1}{2}}} \sin\frac{\theta}{2} \tag{4.18}$$

$$\tau_{yz} = \frac{K_{III}}{(2\pi r)^{\frac{1}{2}}} \cos\frac{\theta}{2} \tag{4.19}$$

$$\sigma_x = \sigma_y = \sigma_z = \tau_{xy} = 0 \tag{4.20}$$

$$w = \frac{K_{III}}{G}\left[\frac{2r}{\pi}\right]^{\frac{1}{2}} \sin\frac{\theta}{2} \tag{4.21}$$

$$u = v = 0 \tag{4.22}$$

For some applications, it is more convenient to rewrite the above near crack tip stresses in polar coordinates, in which case their expression is given by:

- Mode I loading:

$$\sigma_r = \frac{K_I}{\sqrt{2\pi r}} \cos\frac{\theta}{2}\left[1 + \sin^2\frac{\theta}{2}\right] \tag{4.23}$$

$$\sigma_\theta = \frac{K_I}{\sqrt{2\pi r}} \cos\frac{\theta}{2}\left[1 - \sin^2\frac{\theta}{2}\right] \tag{4.24}$$

$$\tau_{r\theta} = \frac{K_I}{\sqrt{2\pi r}}\left[\sin\frac{\theta}{2}\cos^2\frac{\theta}{2}\right] \tag{4.25}$$

- Mode II loading:

$$\sigma_r = \frac{K_{II}}{\sqrt{2\pi r}}\left[-\frac{5}{4}\sin\frac{\theta}{2} + \frac{3}{4}\sin\frac{3\theta}{2}\right] \tag{4.26}$$

$$\sigma_\theta = \frac{K_{II}}{\sqrt{2\pi r}}\left[-\frac{3}{4}\sin\frac{\theta}{2} - \frac{3}{4}\sin\frac{3\theta}{2}\right] \tag{4.27}$$

$$\tau_{r\theta} = \frac{K_{II}}{\sqrt{2\pi r}}\left[\frac{1}{4}\cos\frac{\theta}{2} + \frac{3}{4}\cos\frac{3\theta}{2}\right] \tag{4.28}$$

4.3.3 Mixed Mode Crack Propagation Models

Once the stress intensity factors (K_I, K_{II}, K_{III}) have been numerically (or analytically) computed and the material fracture toughness K_{IC} experimentally determined, a fracture initiation criterion encompassing these variables is sought. This criterion will:

1) Determine the angle of incipient propagation, θ_0, with respect to the crack axis.

2) Determine if the stress intensity factors are in such a critical combination as to render the crack locally unstable and force it to propagate. For mode I problems, fracture initiation occurs if:

$$K_I \geq K_{IC} \tag{4.29}$$

The determination of a fracture propagation criterion for an existing crack in mode I and II would require a relationship between K_I, K_{II} and K_{IC}. This relationship would have the form:

$$F(K_I, K_{II}, K_{IC}) = 0 \tag{4.30}$$

and would be analogous to the one between the two principal stresses and a yield stress

$$F_{yld}(\sigma_1, \sigma_2, \sigma_3) = 0 \tag{4.31}$$

Such an equation may be the familiar Von-Mises criterion. In the absence of a widely accepted criterion for mixed mode crack growth, three of the most widely used criterion are discussed below.

4.3.3.1 Maximum Circumferential Tensile Stress

Erdogan and Sih [32] presented the first mixed-mode fracture initiation theory, the Maximum Circumferential Stress Theory. It is based on the knowledge of the stress state near the tip of a crack, and expressed in polar coordinates. The Maximum Circumferential Stress Theory states that the crack extension starts:

1) At its tip in a radial direction;

2) In the plane perpendicular to the direction of largest tension;

3) When $\sigma_{\theta\,\max}$ reaches a critical material constant.

It can be easily shown that σ_θ reaches its maximum value when $\tau_{r\theta} = 0$. Adding the two contributions to σ_θ given by Equations (4.25 and 4.28) we obtain:

$$\tau_{r\theta} = 0 \Longrightarrow \frac{\cos\theta_0}{2}\left[K_I \sin\theta_0 + K_{II}\left(3\cos\theta_0 - 1\right)\right] = 0 \tag{4.32}$$

this equation has the following two solutions: $\theta_0 = \pm\pi$ trivial and

$$K_I \sin\theta_0 + K_{II}\left(3\cos\theta_0 - 1\right) = 0 \tag{4.33}$$

The angle of crack propagation can be explicitly solved for:

$$\tan\theta_0 = \frac{1}{4}\frac{K_I}{K_{II}} \pm \frac{1}{4}\sqrt{\left(\frac{K_I}{K_{II}}\right)^2 + 8} \tag{4.34}$$

Finally equating the maximum circumferential tensile stress to a material dependent critical value, we obtain:

$$\sigma_{r\theta}\sqrt{2\pi r} = K_{IC} = \cos\frac{\theta_0}{2}\left[K_I\cos^2\frac{\theta_0}{2} - \frac{3}{2}K_{II}\sin\theta_0\right] \tag{4.35}$$

This last equation can be normalized and rewritten as :

$$\frac{K_I}{K_{IC}}\cos^3\frac{\theta_0}{2} - \frac{3}{2}\frac{K_{II}}{K_{IC}}\cos\frac{\theta_0}{2}\sin\theta_0 = 1 \tag{4.36}$$

Equations (4.36 and 3.34) give the onset and direction of crack growth in mixed mode problems.

4.3.3.2 Maximum Energy Release Rate

Another theory, based on the application of the Griffith-Irwin potential energy release rate criterion, states that the crack will grow in the direction along which the potential energy release per unit crack extenuation will be maximum and the crack will grow when this energy (release rate) reaches a critical value.

A solution to this complex mathematical problem was proposed by Hussain et al.[46]. They propose the following expression for the plane strain energy release rate associated with an infinitesimal extension of the crack tip at an angle :

$$\begin{aligned} G(\theta) &= \frac{4}{E}\left(\frac{1}{3+\cos^2\theta}\right)^2\left(\frac{1-\frac{\theta}{\pi}}{1+\frac{\theta}{\pi}}\right)^{\frac{\theta}{\pi}} \\ &\times \left[\left(1+3\cos^2\theta\right)K_I^2 8\sin\theta\cos\theta K_I K_{II} + \left(9-5\cos^2\theta\right)K_{II}^2\right] \end{aligned} \tag{4.37}$$

The fracture locus predicted by the $G_{\theta\max}$ theory is :

$$
\begin{aligned}
G_{\theta max} &= 4\left(\frac{1}{3+\cos^2\theta}\right)^2\left(\frac{1-\frac{\theta_0}{\pi}}{1+\frac{\theta_0}{\pi}}\right)^{\frac{\theta_0}{\pi}} \\
&\times \left[\left(1+3\cos^2\theta_0\right)\left(\frac{K_I}{K_{IC}}\right)^2 + 8\sin\theta_0\cos\theta_0\frac{K_IK_{II}}{K_{IC}^2} + \left(9-5\cos^2\theta_0\right)\left(\frac{K_{II}}{K_{IC}}\right)^2\right] \\
&= 1
\end{aligned} \tag{4.38}
$$

4.3.3.3 Minimum Strain Energy Density Criteria

The Minimum Strain Energy Density Theory, formulated by Sih, has been receiving a lot of attention [97]. It states that fracture initiates from the crack tip in direction, θ, along which the strain energy density at a critical distance is minimum, and when this minimum reaches a critical value, cracking occurs.

$$\frac{\partial U}{\partial V} = \frac{1}{r_0\pi}\left(a_{11}K_I^2 + 2a_{12}K_IK_{II} + a_{22}K_{II}^2\right) = \frac{s}{r_0} \tag{4.39}$$

where

$$a_{11} = \frac{1}{16G}\left[\left(1+\cos\theta\right)\left(k-\cos\theta\right)\right] \tag{4.40}$$

$$a_{12} = \frac{\sin\theta}{16G}\left[2\cos\theta-(k-1)\right] \tag{4.41}$$

$$a_{22} = \frac{1}{16G}\left[(k+1)\left(1-\cos\theta\right)+\left(1+\cos\theta\right)\left(3\cos\theta-1\right)\right] \tag{4.42}$$

$k = 3-4\nu$ for plane stress and $k = \frac{3-4\nu}{1+\nu}$ for plane strain, and G is the shear modulus. The fracture locus predicted by this theory is given by:

$$\frac{8G}{(k-1)}\left[a_{11}\left(\frac{K_I}{K_{IC}}\right)^2 + 2a_{12}\left(\frac{K_IK_{II}}{K_{IC}^2}\right) + a_{22}\left(\frac{K_{II}}{K_{IC}}\right)^2\right] = 1 \tag{4.43}$$

4.3.4 Implementation

Algorithmically, the angle of crack propagation θ_0 is first obtained, and the criteria assessed for the local fracture stability. If the pair of the stress intensity factor (SIF) is inside the fracture loci given above, then that crack cannot propagate without sufficient increase in stress intensity factors. If outside the loci, the crack is locally unstable and will continue to propagate:

1) With an increase in the SIF (and the energy release rate G), thus resulting in a global instability and failure of the structure (crack reaching a free surface).

2) Or with a decrease in the SIF (and the energy release rate G), due to stress redistribution and the SIF pair goes back within the locus.

Also, it should be indicated that a crack tends to propagate in a direction which minimizes the $\frac{K_{II}}{K_I}$ ratio, i.e. a crack under mixed-mode loading will tend to re-orient itself so that is minimized. Thus during its trajectory a crack will most often be in that portion of the normalized $\frac{K_I}{K_{IC}} - \frac{K_{II}}{K_{IC}}$ space where the three theories are in close agreements.

4.4 Nonlinear Fracture Mechanics

Both linear and nonlinear fracture mechanics theories are used to describe crack initiation, crack propagation of different components and structures under various loading conditions. The relationship between load and deformation of a structural component subjected to a increasing load can often be nonlinear during the process of slow stable crack growth regardless of weather the material behaves in a linear or nonlinear fashion [98]. This nonlinearity can, in general, be attributed to a crack

growth at the microscopic scale and material deforming beyond the yield point which corresponds to damage done at the microscopic scale level. The nonlinearity ahead of a crack is modeled usually by extending the true crack to account for the nonlinear zone ahead of it and apply a closing pressure which is derived from the postpeak response of uniaxially loaded member. This approach is commonly referred to as the fictitious crack model. The commonly used fracture mechanics parameters are: stress intensity factor K [56], strain energy release rate G [98], the J integral [86, 87], crack tip opening displacement $CTOD$ [77].

4.5 Continuum Damage Mechanics

The fundamental notion of continuum damage mechanics is to represent the damage state of material in terms of appropriate interval state variables, such as the damage parameters and the internal stress. Mechanical equations can then be established to describe the evolution of the internal variables and the mechanical behaviour of the damage materials. The coupling effect between damage processes and the stress-strain behaviour of materials can thus be described. Continuum damage mechanics (CDM) is also classified as a local approach of fracture since only local field variables are considered necessary in order to determine the onset of cracking, failure,..etc. It does not have the limitation due to different modes of failure (e.g. I,II,III) [19, 20], or due to the scale of yielding and finite deformation such as the one required by the fracture mechanics parameters approach [103].

4.6 Relationship Between Fracture Mechanics and Continuum Damage Mechanics

Different theories and models have been put forward to explain mechanics of fracture, damage, fatigue and creep deformation. From the point of view of macro-mechanics, there are generally two schools of taught in fracture and creep fracture problems. the fracture mechanics approach [92] and the continuum damage approach [63].

Both fracture mechanics and continuum damage mechanics are tools to deal with problems of material failure. The two approaches are complementary to each other [64]. In fracture mechanics problems, material failure is usually caused by the initiation and propagation of one major crack in the specimen. It is usually assumed that only the material at the crack tip experience damage or degradation, while the material in other parts of the specimen is not influenced.

In Continuum Damage Mechanics, the final failure is caused by progressive degradation of the material. The damage is distributed unevenly throughout the material and therefore influences its properties at every point depending upon the degree of damage. The final failure of the material is caused by the evolution and accumulation of the damage, i.e continuum damage mechanics is used to describe material deterioration before and after a macro-cracks is formed [65]. As an example, when the accumulated damage at a particular point reaches a critical value, the material at the point is regarded as having lost its load-carrying capacity and damage is "complete". Figure (4.2) shows the relationship between fracture mechanics and continuum damage mechanics as complementary science [15].

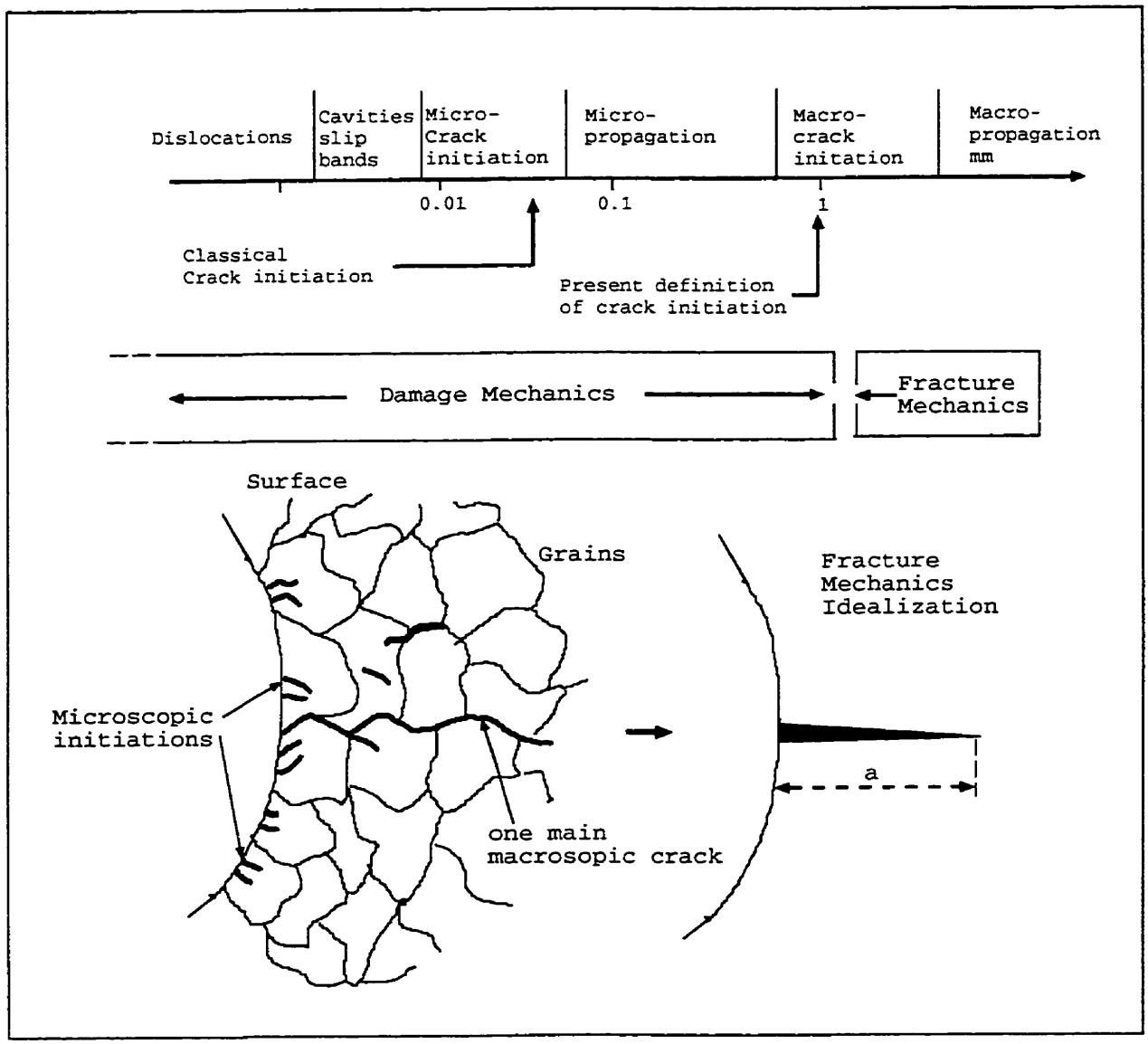

Figure 4.2: Fracture Mechanics and Continuum Mechanics as Complementary Sciences.

Chapter 5

FINITE ELEMENT COMPUTATION OF INTERLAMINAR BUCKLING LOAD

5.1 Introduction

Interlaminar fractures caused by compressive stresses did not get enough attention in computational mechanics, since cracking is caused mainly by tensile and shearing loads. Further developments are required to extract the parameters giving the effective axial stress ahead of the crack tip with an arbitrary orientation and subjected to a general loading configuration.

As an extension to the correlation technique, used for determination of stress intensity factors, the near crack tip displacement field expression is correlated with

the corresponding finite element one to define the parameter representing the effective axial stress ahead of the crack tip. For an initial flaw between two laminates, finite element computation of the axial stress along the crack direction is impossible due to the limitation of the approximation. This chapter presents a derivation of the proper formula for determining the effective axial stress ahead of a crack tip in two-dimensional finite element analysis using singular elements.

5.2 Background

Computational fracture mechanics addresses two important engineering problems: failure investigation and safety assessment of solids and structures. In problems of the first kind, we attempt to trace the response of the structure either in real time or in a pseudo-time and recover the collapse mechanism by nucleating and propagating cracks in a discretized continuum. In problems of the second kind, we start from the assumption that cracks and defects exist due to material imperfection or human error in construction and/or conception. Safety is then assessed by deciding whether cracks are stable or need to be propagated further. A critical crack length can be established with a parallel safety factor. In both exercises, fracture nucleation and propagation have to be correctly modeled within a continuum, and relevant fracture parameters have to be accurately defined. To this end, singular elements for crack tip modeling in computational fracture mechanics has become widely used because they do not require any alteration of a standard finite element code and only pre and post-processing additional work has to be performed. To be more specific, the pre-processing consists of documenting the topology of the cracks (nodes along the crack(s) faces), and the post-processing consists of evaluating expressions for the stress intensity factors. The correct determination of stress intensity factors is done by matching. The square root singular terms in the analytical near crack tip displacement field and the finite

element approximation of the displacement field was first introduced by Tracey [107] and Shih et al. [13] in the two dimensional case and later generalized by Ingraffea and Manu [48] for the three dimensional case.

Fortunately, the formula for stress intensity factor (SIF) does not depend on the type of shape functions used in the finite element implementation of the singular element. As a matter of fact, the collapsed eight-node serendipity element and any degenerate six-node element would have the same expressions for SIF extraction. Similar conclusion is reached for three dimensional quadratic singular elements (derivation can be found in [4]). From an engineering point of view, we need not to worry about the type of approximation being used in the finite element package, and only the correct formula for SIF extraction are needed.

Erroneous results can be found when conventional linear elastic fracture mechanics is used to predict the direction of crack extension and the onset of crack propagation in dominantly compressive fields. The $1/\sqrt{r}$ singular terms of the solution used to extract the stress intensity factors does not account for compression/tension along the axis of the crack. Meanwhile, the higher order term r^0 in the analytical solution of the stress field (which corresponds to the $1/r$ term in the displacement field expressions), could contain the necessary information on the intensity of the axial stress field that is known to drive cracks in compressive fields [26]. In this chapter, a generalization of the correlation technique for stress intensity factor extraction, to account for the axial compressive or tensile field, is presented. The effect of non-uniformity of the remote axial stress on the behavior of the crack is examined and more importantly, new fracture criteria for compressive fracture is addressed. For crack problems, the method of eigenfunction expansion, among others, give a systematic way for deriving the complete (i.e. including higher order terms) expressions interms of the close form solution of the stress and displacement fields about a crack tip. Following Williams [118], and the notation of Sih and Liebowitz [99], the stresses and displacements can

be expressed as follows:

$$\sigma_\theta = \frac{r^{-\frac{1}{2}}}{2}\left[a_1\left(\frac{3}{2}\cos\frac{\theta}{2}+\frac{1}{2}\cos\frac{3\theta}{2}\right)+a_2\left(\frac{3}{2}\sin\frac{\theta}{2}+\frac{3}{2}\sin\frac{3\theta}{2}\right)\right] + 4a'_1\sin^2\theta + ... \quad (5.1)$$

$$\sigma_r = \frac{r^{-\frac{1}{2}}}{2}\left[a_1\left(\frac{5}{2}\cos\frac{\theta}{2}-\frac{1}{2}\cos\frac{3\theta}{2}\right)+a_2\left(\frac{5}{2}\sin\frac{\theta}{2}-\frac{3}{2}\sin\frac{3\theta}{2}\right)\right] + 4a'_1\cos^2\theta + ... \quad (5.2)$$

and the displacement field is given by:

$$u_r = \frac{r^{\frac{1}{2}}}{2\mu}\left[a_1\left((\kappa-\frac{1}{2})\cos\frac{\theta}{2}-\frac{1}{2}\cos\frac{3\theta}{2}\right)+a_2\left((\kappa-\frac{1}{2})\sin\frac{\theta}{2}-\frac{3}{2}\sin\frac{3\theta}{2}\right)\right] + \frac{r}{2\mu}(\kappa-1+2\cos 2\theta)a'_1 + ... \quad (5.3)$$

$$u_\theta = \frac{r^{\frac{1}{2}}}{2\mu}\left[a_1\left((-\kappa-\frac{1}{2})\sin\frac{\theta}{2}+\frac{1}{2}\sin\frac{3\theta}{2}\right)+a_2\left((\kappa+\frac{1}{2})\cos\frac{\theta}{2}-\frac{3}{2}\cos\frac{3\theta}{2}\right)\right] + \frac{r}{2\mu}(a'_2(\kappa+1)-2a'_1\sin 2\theta) + ... \quad (5.4)$$

where r, θ are the polar coordinates, a_1, a_2 are the stress intensity factors, $AF = 4a'_1$ is the axial stress factor which is equal to the remote applied axial stress in the case of uniformly, axially losded, cracked plate. κ is a constant which depends on poisson's ratio and the nature of the problem (i.e. plane stress or plane strain) and μ is the coefficient of friction.

In the numerical counterpart (FEM), if we consider the 2D singular element generated from a collapsed eight-noded isoparametric element, as well as the one generated from a degenerate six-noded element, it can be shown that the approximation of the displacement field along the face (A,B,C) in Figure (5.1) is given by:

$$u' = u'_A + (-3u'_A + 4u'_B - u'_C)\sqrt{\frac{r}{L}} + (2u'_A + 2u'_C - 4u'_B)\frac{r}{L} \quad (5.5)$$

where u' can be either u or v,and L is the singular element length.
By equating the r term in Equation (5.3), taken at $\theta = \pi$ to the r term in the approximated finite element displacement in Equation (5.5), we get :

$$a'_1 = -\frac{2\mu}{L(\kappa+1)}(2u_A + 2u_C - 4u_B) \tag{5.6}$$

taking into account both faces of the crack, we obtain

$$a'_1 = -\frac{2\mu}{L(\kappa+1)}(2u_A + u_C + u_E - 2(u_B + u_D)) \tag{5.7}$$

5.3 Numerical Extraction of the Axial Stress Factor

In order to check the accuracy and validate the expression of the axial stress factor, three test cases with known analytical solutions are analyzed. The first case consists of a cracked plate loaded uniformly in the crack-axis direction. The second test problem consists of a large plate which simulate the classical half plane subjected to a point load at its free surface. The plate has a crack in different positions. The third problem studies the effect of load concentration on the axial stress at the tip of a crack.

5.3.1 Case I: Uniformly Loaded Cracked Plate

In order to check the formula giving the axial stress factor, a plate loaded axially by a uniform unit pressure, as shown in Figure (5.2), is analyzed. As expected, the analytical solution is recovered and the axial stress factor is found to be equal to unity. Hence the formula is capable of recovering a uniform pressure with a 100% accuracy.

5.3.2 Case II: Half Plane Problem

A large plate which simulates a half plane is subjected to a line load along its thickness. The plate has a crack with position varies as shown in figure (5.3). The analytical solution for this problem (see e.g. [53]) is given by:

$$\sigma_r = \frac{r^{-\frac{1}{2}}}{2}\left[a_1\left(\frac{5}{2}\cos\frac{\theta}{2} - \frac{1}{2}\cos\frac{3\theta}{2}\right) + a_2\left(\frac{5}{2}\sin\frac{\theta}{2} - \frac{3}{2}\sin\frac{3\theta}{2}\right)\right] + 4a'_1\cos^2\theta + ... \tag{5.8}$$

The numerical solution, evaluated using expression (5.7) is compared with the closed form solution as illustrated in Figure (5.5). It can be stated that the expression of the axial stress factor provides an accurate way of determining the stress level along the crack.

5.3.3 Case III: Effect of Load Concentration Ahead of a Crack Tip

The total load from the previous analysis (Case I) is applied over 80 %, 60 %, 40 % , and 0 % (concentrated load case) of the total area of the same plate as shown in Figure (5.4). In each case, we extract both mode I stress intensity factor K_I and the axial stress factor AF. From the results, summarized in Figure (5.6), it is found, that while a crack aligned with a uniform stress field would not alter the stress distribution, when the applied axial stress field is no longer uniform, the crack starts feeling a higher axial stress intensity and ultimately under a concentrated load a crack suffers twice as as much as if the loading were uniformly applied. Also the crack buckles up to give a non-zero mode I SIF when the remote load tends to become closer to concentrated force. The axial stress factor as well as K_I are increasing functions of the crack length. This is an important finding from a fracture mechanics point of view, as the

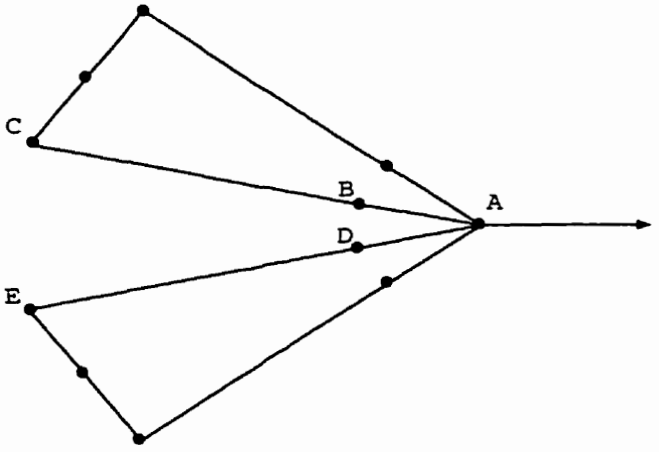

Figure 5.1: 2D Crack Tip Model.

stability of the crack can be related to one single material parameter, similar to the one adopted in mode I fracture (i.e. $K_I \leq K_{IC}$).

5.4 Conclusion

A finite measure of the axial stress intensity ahead of the tip of the crack (Axial Stress Factor) is made possible. This factor may play a role in the compressive cracking mechanism found in dams and mining environments. The finite element extraction of the axial stress factor is successfully derived and implemented using regular singular elements.

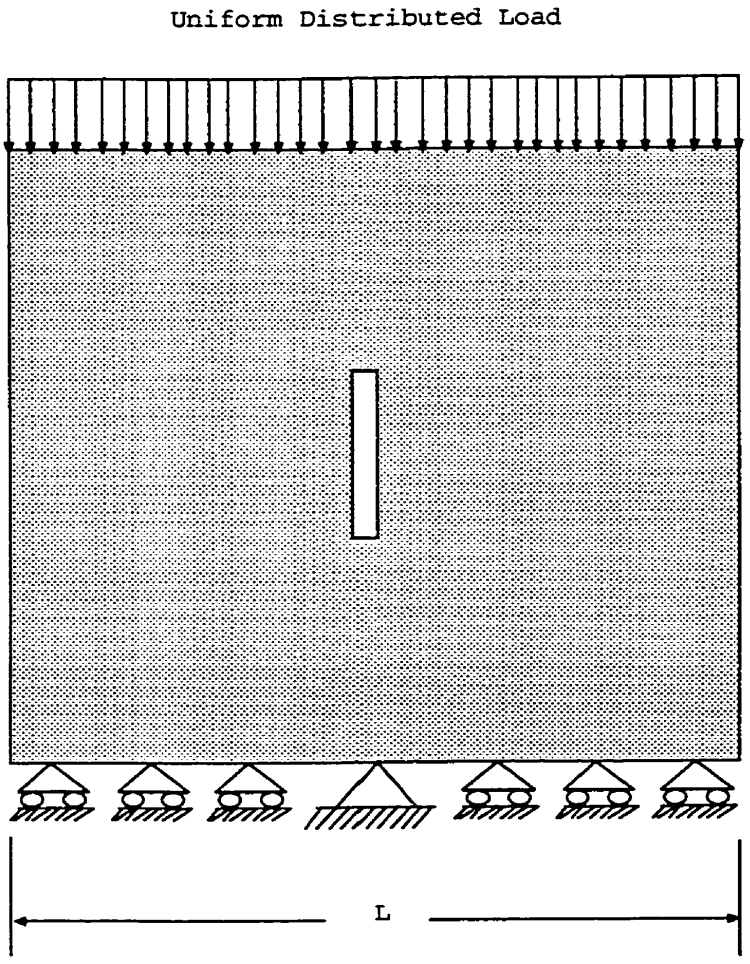

Figure 5.2: Case I: Uniformaly Distributed Load.

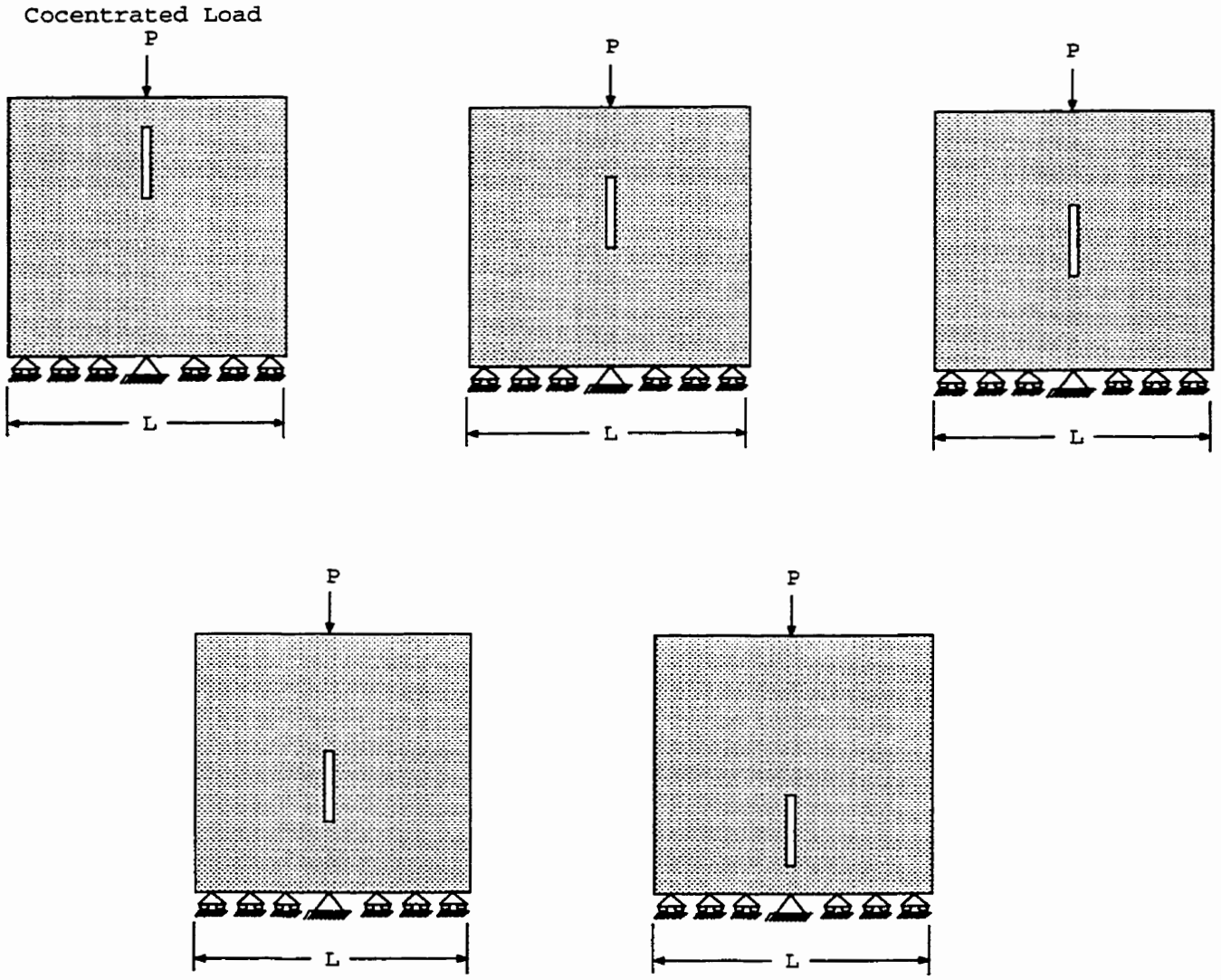

Figure 5.3: Case II: Axial Concentrated Load at the Mid of the Plate.

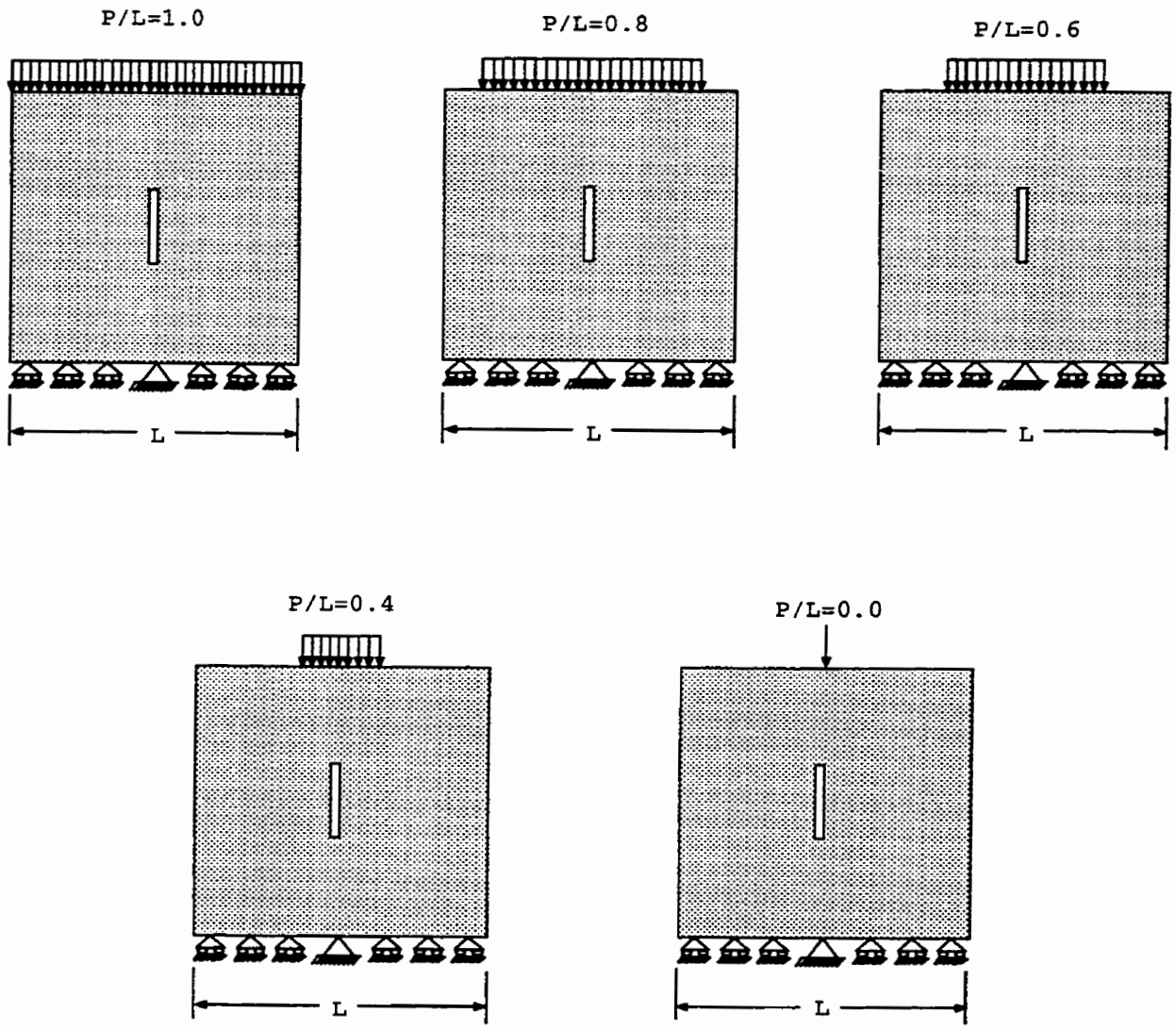

Figure 5.4: Effect of the Uniformity of the Remote Stress on AF.

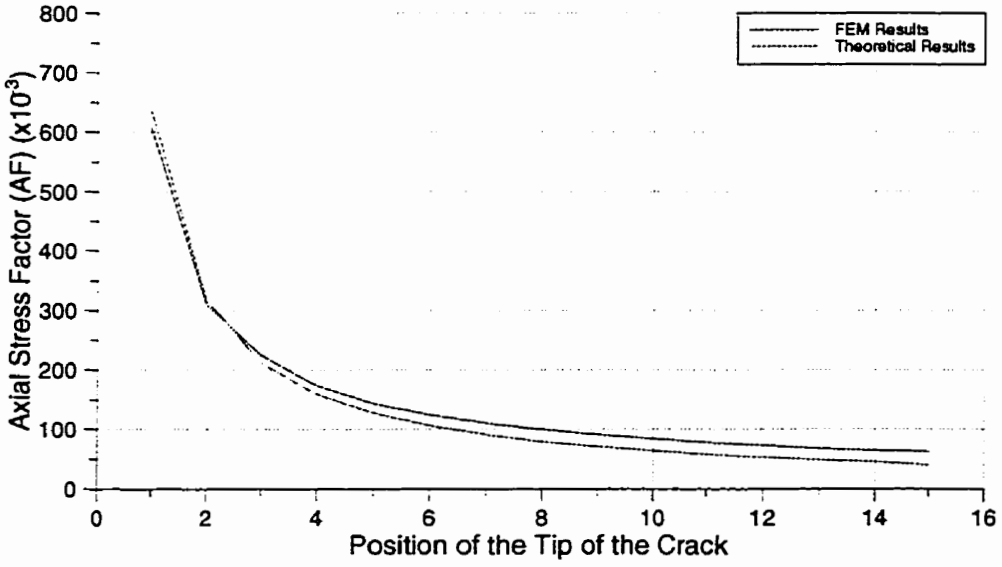

Figure 5.5: Effect of the Position of the Crack Tip on AF.

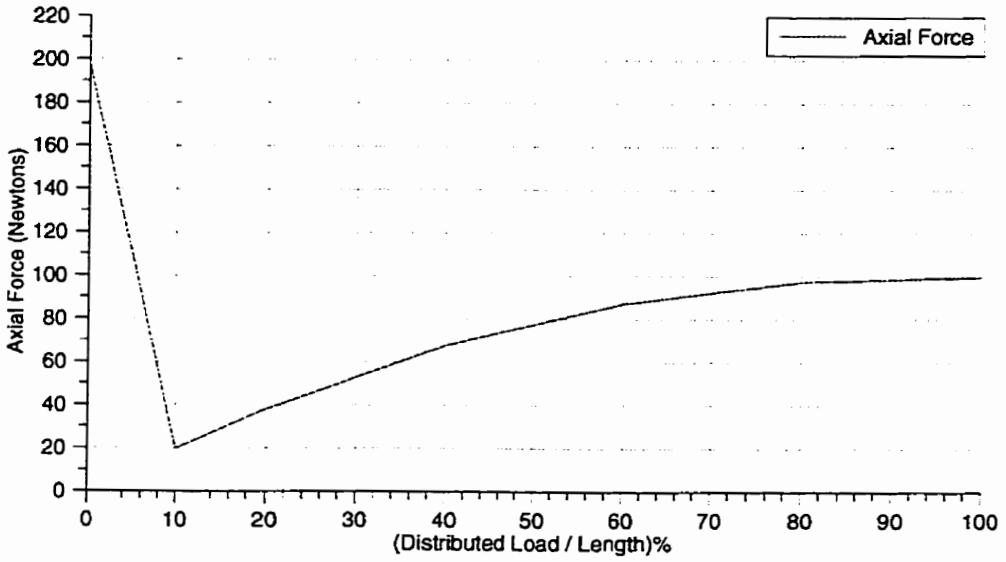

Figure 5.6: Effect of the Uniform Distributed Load on AF.

Chapter 6

CRACK TIP INELASTIC ZONE IN ANISOTROPIC MEDIA

6.1 Introduction

Composites of oriented fiber glass, composite of whisker reinforced metal, wood, rock and roller compacted concrete are most often orthotropic and anisotropic from point to point [66]. With the wide recognition of the need for the accounting for the anisotropic nature of many natural and man-made materials, crack propagation in anisotropic material must be governed by appropriate mixed mode models. Although considerable attention has been given in recent years to this problem in ideally brittle isotropic materials [32], [97], and despite the fact that the stress field solution for anisotropic bodies was developed more than twenty years ago [100], little research was focused on the mixed-mode crack propagation and crack tip inelastic zone of the latter. Development on this problem was made by Saouma, et al. [91], Ayari [5], and Ingraffea [49]. They extended the maximum circumferential tensile stress theory to anisotropic solids. However, they did not account on how important the size of the

inelastic zone and what shape it has under anisotropic conditions?

In this chapter, a comprehensive derivation of the fracture inelastic zone size and shape in anisotropic solids, is presented. Some energy models of anisotropic materials are discussed using uniaxial and biaxial stress assumptions. Under uniaxial stress assumptions, Hill's yield criterion [44] is adapted to seek the shape of the inelastic zone. It is found that material parameters play an important role in the inelastic zone shape and size, under mode I, mode II and mixed mode I-II loadings. Under the biaxial stress state, the inelastic zone size is found to be larger than the theoretical one calculated under uniaxial assumption. Finally, a comparison is made between these models and conclusions are drawn.

6.2 Stress and Displacement Field in Anisotropic Bodies

In examining the stability of cracks, and referring to Figure (6.1), it is customary to determine the stress in the neighborhood of the crack tip so that the relationship between the elastic stresses and the input energy rate in crack extension may be established. Sih, Paris and Irwin (1965) have shown that the basic concept of isotropic fracture mechanics can be extended to the anisotropic case. In 1968, Sih and Liebowitz [66] obtained the following stress distribution and displacements in the neighborhood of a crack tip: For the plane symmetric case,

$$\left.\begin{aligned} \sigma_x &= \frac{K_I}{\sqrt{2\pi r}} F_{Ix}(s_1, s_2, \theta) \\ \sigma_y &= \frac{K_I}{\sqrt{2\pi r}} F_{Iy}(s_1, s_2, \theta) \\ \tau_{xy} &= \frac{K_I}{\sqrt{2\pi r}} F_{Ixy}(s_1, s_2, \theta) \end{aligned}\right\}, \tag{6.1}$$

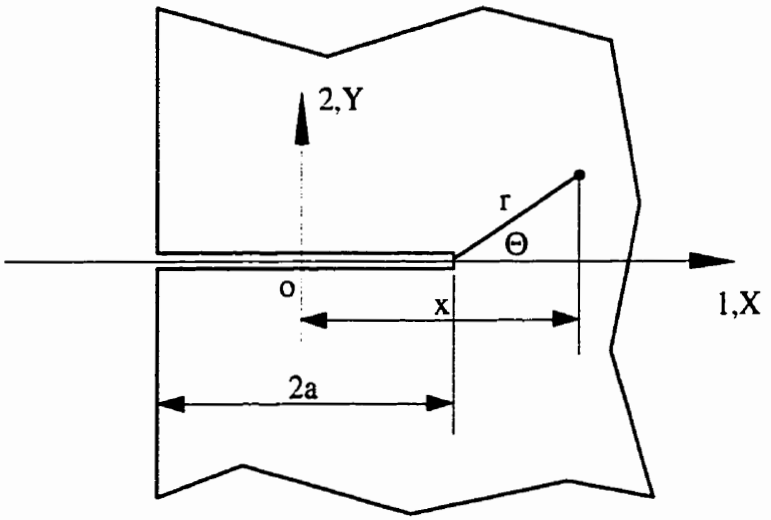

Figure 6.1: A Crack in a Homogeneous Anisotropic Elastic Solid.

where

$$\left.\begin{aligned} F_{Ix}(s_1,s_2,\theta) &= \mathrm{Re}\left[\frac{s_1 s_2}{s_1-s_2}\left(\frac{s_2}{(\cos\theta+s_2\sin\theta)^{\frac{1}{2}}}-\frac{s_1}{(\cos\theta+s_1\sin\theta)^{\frac{1}{2}}}\right)\right] \\ F_{Iy}(s_1,s_2,\theta) &= \mathrm{Re}\left[\frac{1}{s_1-s_2}\left(\frac{s_1}{(\cos\theta+s_2\sin\theta)^{\frac{1}{2}}}-\frac{s_2}{(\cos\theta+s_1\sin\theta)^{\frac{1}{2}}}\right)\right] \\ F_{Ixy}(s_1,s_2,\theta) &= \mathrm{Re}\left[\frac{s_1 s_2}{s_1-s_2}\left(\frac{1}{(\cos\theta+s_1\sin\theta)^{\frac{1}{2}}}-\frac{1}{(\cos\theta+s_2\sin\theta)^{\frac{1}{2}}}\right)\right] \end{aligned}\right\} \tag{6.2}$$

and

$$\left.\begin{aligned} u_x &= K_I\sqrt{2\pi r}\,\mathrm{Re}\left(\frac{1}{s_1-s_2}\left[s_1 p_2(\cos\theta+s_2\sin\theta)^{\frac{1}{2}}-s_2 p_1(\cos\theta+s_1\sin\theta)^{\frac{1}{2}}\right]\right) \\ u_y &= K_I\sqrt{2\pi r}\,\mathrm{Re}\left(\frac{1}{s_1-s_2}\left[s_1 q_2(\cos\theta+s_2\sin\theta)^{\frac{1}{2}}-s_2 q_1(\cos\theta+s_1\sin\theta)^{\frac{1}{2}}\right]\right) \end{aligned}\right\} \tag{6.3}$$

For the plane skew-symmetric case,

$$\left.\begin{aligned} \sigma_x &= \frac{K_{II}}{\sqrt{2\pi r}}F_{IIx}(s_1,s_2,\theta) \\ \sigma_y &= \frac{K_{II}}{\sqrt{2\pi r}}F_{IIy}(s_1,s_2,\theta) \\ \tau_{xy} &= \frac{K_{II}}{\sqrt{2\pi r}}F_{IIxy}(s_1,s_2,\theta) \end{aligned}\right\} \tag{6.4}$$

where

$$\left.\begin{aligned} F_{IIx}(s_1,s_2,\theta) &= \mathrm{Re}\left[\frac{1}{s_1-s_2}\left(\frac{s_2^2}{(\cos\theta+s_2\sin\theta)^{\frac{1}{2}}}-\frac{s_1^2}{(\cos\theta+s_1\sin\theta)^{\frac{1}{2}}}\right)\right] \\ F_{IIy}(s_1,s_2,\theta) &= \mathrm{Re}\left[\frac{1}{s_1-s_2}\left(\frac{1}{(\cos\theta+s_2\sin\theta)^{\frac{1}{2}}}-\frac{1}{(\cos\theta+s_1\sin\theta)^{\frac{1}{2}}}\right)\right] \\ F_{IIxy}(s_1,s_2,\theta) &= \mathrm{Re}\left[\frac{1}{s_1-s_2}\left(\frac{s_1}{(\cos\theta+s_1\sin\theta)^{\frac{1}{2}}}-\frac{s_2}{(\cos\theta+s_2\sin\theta)^{\frac{1}{2}}}\right)\right] \end{aligned}\right\} \tag{6.5}$$

and the displacement are given by

$$\left.\begin{aligned} u_x &= K_{II}\sqrt{2\pi r}\mathrm{Re}\left(\tfrac{1}{s_1-s_2}\left[p_2\left(\cos\theta+s_2\sin\theta\right)^{\frac{1}{2}}-p_1\left(\cos\theta+s_1\sin\theta\right)^{\frac{1}{2}}\right]\right) \\ u_y &= K_{II}\sqrt{2\pi r}\mathrm{Re}\left(\tfrac{1}{s_1-s_2}\left[q_2\left(\cos\theta+s_2\sin\theta\right)^{\frac{1}{2}}-q_1\left(\cos\theta+s_1\sin\theta\right)^{\frac{1}{2}}\right]\right) \end{aligned}\right\} \tag{6.6}$$

The first observation to be made is that stress singularity at the crack tip is of the order of $1/\sqrt{r}$. Moreover, the stress distribution near a crack tip depends on the configuration and loading of the anisotropic body as well as the material properties. Equations (6.1-6.6) represent the most general state of stress and displacement around the crack tip bodies with anisotropy. In these equations, s_1, and s_2 are the roots of the characteristic equation:

$$a_{11}s^4-2a_{16}s^3+\left(2a_{12}+a_{66}\right)s^2-2a_{26}s+a_{22}=0 \tag{6.7}$$

For the case of rectilinear transverse anisotropy, the number of elastic constants a_{ij} is reduced to six [67]. The constants p_j and q_j (j=1,2) are given by:

$$\left.\begin{aligned} p_j &= a_{11}s_j^2+a_{12}-a_{16}s_j \\ q_j &= a_{12}s_j+\tfrac{a_{22}}{s_j}-a_{26} \end{aligned}\right\} \tag{6.8}$$

Also, the stress field near a crack tip under mixed mode loads can be summarized as:

$$\left.\begin{aligned} \sigma_x &= \tfrac{K_I}{\sqrt{2\pi r}}F_{Ix}+\tfrac{K_{II}}{\sqrt{2\pi r}}F_{IIx} \\ \sigma_y &= \tfrac{K_I}{\sqrt{2\pi r}}F_{Iy}+\tfrac{K_{II}}{\sqrt{2\pi r}}F_{IIy} \\ \tau_{xy} &= \tfrac{K_I}{\sqrt{2\pi r}}F_{Ixy}+\tfrac{K_{II}}{\sqrt{2\pi r}}F_{IIxy} \end{aligned}\right\} \tag{6.9}$$

For the purpose of reducing the lengthy algebra, the above equations are formulated in matrix form. Hooke's Law is written as:

$$[\varepsilon]=[A]\,[\sigma]\,, \tag{6.10}$$

where

$$[\varepsilon]=\left\{\begin{array}{ccc}\varepsilon_x & \varepsilon_y & \gamma_{xy}\end{array}\right\}^T \tag{6.11}$$

and

$$[\sigma] = \left\{ \begin{array}{ccc} \sigma_x & \sigma_y & 2\tau_{xy} \end{array} \right\}^T \tag{6.12}$$

The compliance matrix [A] for anisotropic solids with principal directions of symmetry can be expressed as:

$$[A] = \left[\begin{array}{ccc} a_{11} & a_{12} & \frac{1}{2}a_{16} \\ a_{12} & a_{22} & \frac{1}{2}a_{26} \\ a_{16} & a_{26} & \frac{1}{2}a_{66} \end{array} \right] \tag{6.13}$$

The stress field near a crack tip under mixed mode loading, given by system of Equations (6.9) can be summarized as:

$$[\sigma] = \frac{1}{\sqrt{2\pi r}} [R][K] \tag{6.14}$$

where

$$[K] = \left\{ \begin{array}{cc} K_I & K_{II} \end{array} \right\}^T \tag{6.15}$$

and.

$$[R] = \left[\begin{array}{cc} F_{Ix} & F_{IIx} \\ F_{Iy} & F_{IIy} \\ 2F_{Ixy} & 2F_{IIxy} \end{array} \right] \tag{6.16}$$

6.3 Fracture Toughness Characterization of Anisotropic Solids

The fracture toughness is no longer uniquely defined as in the case of isotropic materials. However, for homogeneous transversely isotropic solids with elastic constants modulus E_1, E_2, G_{12} and ν_{12}, two values are needed to characterize the brittle behavior of the crack K_{Ic}^1 and K_{Ic}^2, where directions "1" and "2" are oriented along the principal planes of elastic symmetry, (see Figure 6.2).

It should be noted that if the applied load and material propagation are aligned symmetrically with reference to the crack, pure mode I displacement occurs in isotropic materials, while a "parasitic" crack sliding displacement occurs in anisotropic materials.

A symmetric loading for anisotropic materials can induce mode II deformation. This can be deduced from Equation (6.1) when a non-zero τ_{xy} resulting in a pure mode I loading at θ=0. In particular, if the material is orthotropic and the crack is aligned with one of the principal planes of elastic symmetry, then it can be shown that the roots $s_i = \alpha_i + i\beta_i$ of Equation (6.7) fall in to one of three categories:

$$\begin{aligned} &\alpha_1 = \alpha_2 = 0, && \beta_1 \neq \beta_2; \\ &\alpha_1 = \alpha_2 = 0, && \beta_1 = \beta_2; \\ &\alpha_1 = -\alpha_2 && \beta_1 = \beta_2. \end{aligned} \tag{6.17}$$

Finally, the toughness K_{Ic}^{β}could be assumed to follow the polar variation of the stress state as introduced by Saouma et al. [91], where K_{Ic}^{β} is a function of K_{Ic}^{1} and K_{Ic}^{2}, hence

$$K_{Ic}^{\beta} = K_{Ic}^{1}\cos^2\beta + K_{Ic}^{2}\sin^2\beta \tag{6.18}$$

It can be further assumed (for the purpose of parametric numerical studies) that the ratio of the fracture toughness in both directions is equal to the ratio of the elastic moduli:

$$K_{Ic}^{2} = K_{Ic}^{1}\frac{E_1}{E_2} \tag{6.19}$$

6.4 Uniaxial Crack Tip Inelastic Zone Size

Following metal plasticity we distinguish two methods, a first order approximation of the inelastic zone size in which the normal stress is set equal to the strength σ_y, and

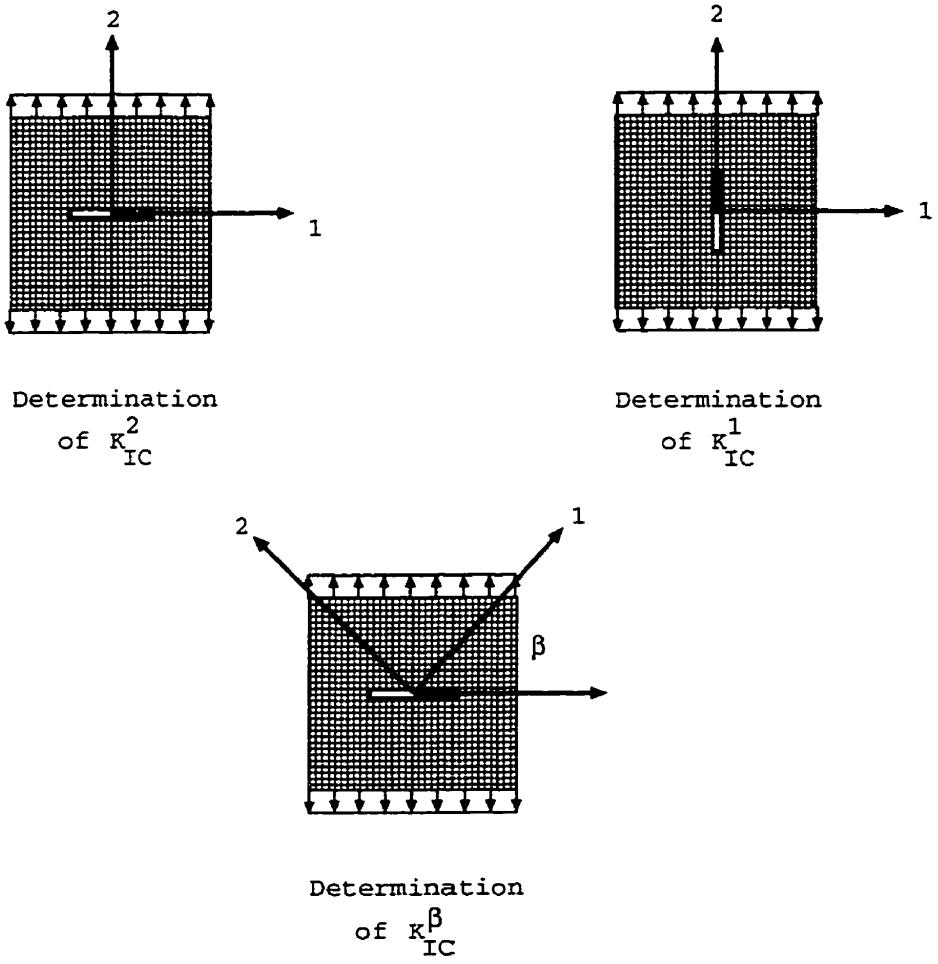

Figure 6.2: Fracture Toughness for Homogeneous Anisotropic Solids.

a second order approximation in which the size of the inelastic zone is determined based on energy balance arguments.

6.4.1 First Order Approximation

In this model, the state of stress is considered as uniaxial and only the σ_y component ahead of the crack is taken into account. Following Irwin's classical approximation of the inelastic zone, r_p^*, which can be determined by simply equating the singular expression of the normal stress σ_y to the uniaxial tensile strength σ_s of the anisotropic solids. From Equation (6.1), and under pure mode I (θ= 0) we obtain:

$$\sigma_y = \frac{K_I}{\sqrt{2\pi r_p^*}} = \sigma_s \tag{6.20}$$

Eliminating K_I by using the far-field stress ($\sigma = \frac{K_I}{\sqrt{\pi a}}$), we have the nondimensional inelastic zone length:

$$\frac{r_p^*}{a} = \frac{1}{2}\frac{\sigma^2}{\sigma_s^2} \tag{6.21}$$

6.4.2 Second Order Approximation

In the second order approximation, we account for the post-peak stress distribution. In the original *Irwin's* model [5, 11] a perfectly plastic model was assumed for the post peak stress distribution. This assumption is reasonable for metals. For this study we will be considering a continuum damage-based model in which the degradation process is represented by means of two separate models:

First, a linear model in which the stress σ_y ahead of the crack tip is assumed to have a linear distribution and second, a nonlinear model in which σ_y is assumed to be a function of the crack opening displacement.

6.4.2.1 Linear Function of Position (σ_y=f(r))

In this model, the determination of the inelastic zone length (IZL) is accomplished by assuming the existence of a fictitious crack which extends to a length $a+\delta$, as shown in Figure (6.3). The fictitious crack is assumed to obey LEFM and therefore would have a fictitious singular field. To relate the fictitious crack to the actual crack, a transfer of energy taking place between a ligament under the singular stress distribution ahead of the effective crack, A, to the inelastic zone ahead of the physical crack, we set the area A to be equal to the area B. Area A is given by:

$$A = \int_0^{r_p^*} \sigma\sqrt{\frac{a+\delta}{2r}}dr - r_p^*\sigma_s + \frac{1}{2}xr_p^* \tag{6.22}$$

or

$$A = \sigma\sqrt{2\,(a+\delta)}r_p^* - r_p^*\sigma_s + \frac{1}{2}\sigma_s\frac{\left(r_p^*\right)^2}{\delta + r_p^*}, \tag{6.23}$$

and area B is given by:

$$B = \frac{1}{2}\sigma_s\frac{\delta^2}{\delta + r_p^*} \tag{6.24}$$

The requirement $B = A$ yields:

$$\frac{1}{2}\sigma_s\frac{\delta^2}{\delta + r_p^*} = \sqrt{\sigma 2\,(a+\delta)}r_p^* - r_p^*\sigma_s + \frac{1}{2}\sigma_s\frac{\left(r_p^*\right)^2}{\delta + r_p^*} \tag{6.25}$$

From this equation, two non-dimensional parameters arise, the loading parameter $\beta = \frac{\sigma}{\sigma_s}$, and a non-dimensional geometric parameter $\lambda = \frac{\delta}{a}$. The inelastic zone length from the second order approximation is given by:

$$\frac{IZL}{a} = \frac{\beta^2\,(4-\beta)}{2\,(1-\beta)} \tag{6.26}$$

6.4.2.2 Elastic-Plastic Stress Distribution

For, comparison, one can assume an elastic-plastic stress profile for the damaged zone ahead of the tip. In such a case, following a similar procedure as in section (6.4.2.1),

we obtain:

$$\frac{1}{2}\sigma_s\delta = \int_0^{r_p^*} \sigma\sqrt{\frac{a+\delta}{2r}}dr - r_p^*\sigma_s \tag{6.27}$$

which leads to

$$\frac{IZL}{a} = \frac{\beta^2(3-\beta^2)}{2(1-\beta^2)} \tag{6.28}$$

6.4.2.3 Perfectly-Plastic Stress Degradation

Under the assumption of perfect plasticity, the following result is found:

$$\sigma_s\delta = \int_0^{r_p^*} \sigma\sqrt{\frac{a+\delta}{2r}}dr - r_p^*\sigma_s \tag{6.29}$$

The expression of $IZL = \delta + r_p^*$ is given by

$$\frac{IZL}{a} = \frac{\beta^2(4-\beta^2)}{2(2-\beta^2)} \tag{6.30}$$

Figure (6.4) shows the variation of $\frac{IZL}{a}$ versus β in the range $0.0 \leq \frac{IZL}{a} \leq 0.3+\frac{1}{2}\beta^2$. From Figure (6.4), it is evident that the real inelastic zone length is located between curve *oa* and curve *oc*.

6.5 Shape of the Inelastic Zone under Biaxial Stress Assumption

In this section we consider the biaxial state of stress around the crack tip. We substitute the near crack tip stress field into the expression of an adequate yield function and determine the radius of the inelastic zone. This approach is very similar to the uniaxial *Irwin's* first order approximation with the only difference, that a surface is being sought as inelastic zone ahead of the crack tip. Assuming that the material contains three mutually orthotropic planes of symmetry at every point, and

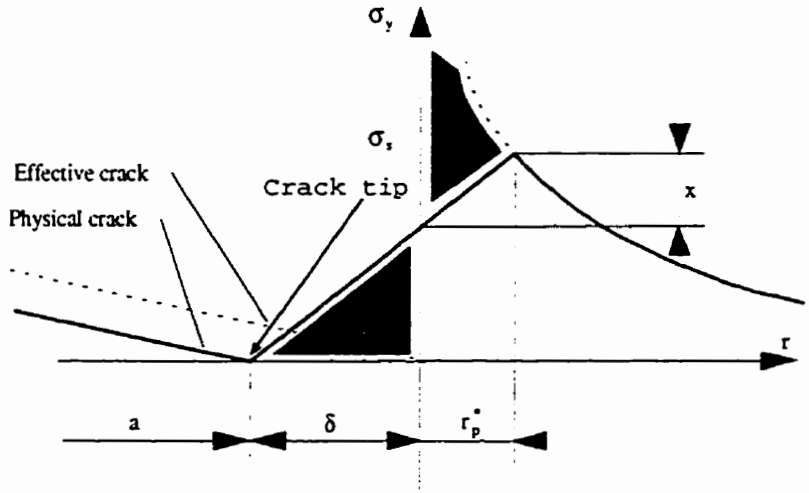

Figure 6.3: Second Approximation Fracture Model ($\sigma_y = f(r)$)[5]

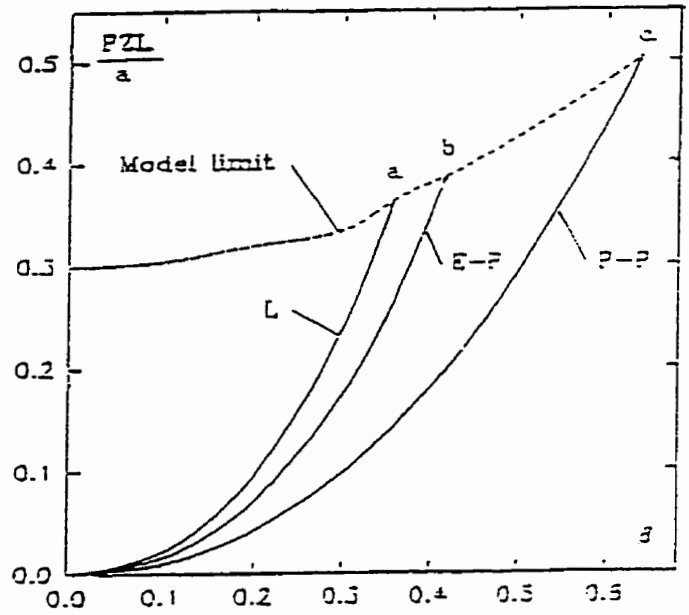

Figure 6.4: Normalized Inelastic Process Zone Size.

referring to the coordinate axes x, y to be the symmetry axes, it follows that the sign of a given shear stress should not contain first powers and therefore,

$$F(\sigma_y - \sigma_z)^2 + G(\sigma_z - \sigma_x)^2 + H(\sigma_x - \sigma_y)^2 + 2L\tau_{yz}^2 + 2M\tau_{zx}^2 + 2N\tau_{xy}^2 = 1 \quad (6.31)$$

where F, G, L, M and N are material constants. Equation (6.31) was utilized by Hill [44] and was applied to a number of technological problems. The yield function can be expressed in terms of the principal stresses. First, we note that, in general, when the reference axes are principal ones, the shear stress components vanish and may be written in the form:

$$F(\sigma_2 - \sigma_3)^2 + G(\sigma_3 - \sigma_1)^2 + H(\sigma_1 - \sigma_2)^2 = 1 \quad (6.32)$$

If X, Y and Z are the tensile strengths in the principal directions, Equation (6.31) reduces to

$$F(0 - 0)^2 + G(0 - \sigma_1)^2 + H(\sigma_1 - 0)^2 = 1 \quad (6.33)$$

or

$$G + H = \tfrac{1}{X^2} \quad (6.34)$$

Similarly,

$$H + F = \tfrac{1}{Y^2} \quad (6.35)$$

and

$$F + G = \tfrac{1}{Z^2} \quad (6.36)$$

On the other hand, recall that for plane problems, the principal stresses are given by:

$$\left.\begin{matrix}\sigma_{\max} \\ \sigma_{\min}\end{matrix}\right\} = \frac{1}{2}(\sigma_x + \sigma_y) \pm \frac{1}{2}\sqrt{(\sigma_x - \sigma_y)^2 + 4\tau_{xy}^2} \quad (6.37)$$

Substituting the equations for near crack tip stress field in-to the above expressions, we finally obtain,

$$\left.\begin{matrix}\sigma_{\max}\\ \sigma_{\min}\end{matrix}\right\} = \frac{K_I}{2\sqrt{2\pi r}}\left[(F_{Ix}+mF_{IIx}+F_{Iy}+mF_{IIy})\right.$$
$$\left. \pm \sqrt{(F_{Ix}+mF_{IIx}-F_{Iy}-F_{IIy})^2+4\,(F_{Ixy}+mF_{IIxy})^2}\right] \quad (6.38)$$

Having obtained the near crack tip principal stresses, we consider now the plane stress and plane strain cases separately.

6.5.1 Plane Stress State

In this case, the normal and shear stresses in the z direction vanish (i.e. $\sigma_z = \tau_{zx} = \tau_{yz} = 0$). The yield function is written then as follows

$$\sigma_1^2 + \sigma_2^2 - \frac{2R}{R+1}\sigma_1\sigma_2 = Y^2 \quad (6.39)$$

where, $R = 2\left(\frac{Z}{Y}\right)^2 - 1$. Substituting the principal stresses given by Equation (6.37) into Equation (6.38), we obtain the following expression, which gives the boundary of the plastic zone as a function of θ,

$$r = r(\theta) = \frac{K_I^2}{8\pi Y}\left[(\Lambda_1+\Lambda_2)^2 + (\Lambda_1-\Lambda_2)^2 - \frac{2R}{1+R}\left(\Lambda_1^2-\Lambda_2^2\right)\right] \quad (6.40)$$

in which,

$$\Lambda_1 = F_{Ix} + mF_{IIx} + F_{Iy} + mF_{IIy}. \quad (6.41)$$

$$\Lambda_2 = \sqrt{(F_{Ix}+mF_{IIx}-F_{Iy}-mF_{IIy})^2 + (F_{Ixy}+mF_{IIxy})^2} \quad (6.42)$$

and m is the loading ratio.

6.5.2 Plane Strain State

In this case, the strain in the z direction is zero (i.e. $\varepsilon_z = 0$). The principal stresses are given by

$$\left.\begin{aligned} \sigma_1 &= \frac{K_I}{2\sqrt{2\pi r}}(\Lambda_1 + \Lambda_2) \\ \sigma_2 &= \frac{\nu K_I}{\sqrt{2\pi r}}\Lambda_1 \\ \sigma_3 &= \frac{K_I}{2\sqrt{2\pi r}}(\Lambda_1 - \Lambda_2) \end{aligned}\right\} \tag{6.43}$$

Similarly, we have

$$r = r(\theta) = \frac{K_I^2}{4\pi Y^2}(\{(\Gamma_1 + \Gamma_2)(1-k) + \Gamma_3 k\}) \tag{6.44}$$

where,

$$\left.\begin{aligned} \Gamma_1 &= \Lambda_2 - (1-2\nu)\Lambda_1 \\ \Gamma_2 &= 4\Lambda_2^2 \\ \Gamma_3 &= \Lambda_2 + (1-2\nu)\Lambda_1 \end{aligned}\right\} \tag{6.45}$$

In the above $K = HY^2$. Figure (6.5) and Figure (6.6) show the shapes of the inelastic zone for different values of the loading ratio m under the plane stress and plane strain conditions.

6.6 The Crack Tip Opening Displacement:

When the inelastic zone is large in comparison with the crack size, we have to consider non-linear fracture mechanics concepts as opposed to linear elastic fracture mechanics. By applying a correction factor, the displacement of crack surface is given by

$$COD = \frac{4\sigma}{E}\sqrt{\left(a + r_p^*\right) - x^2} \tag{6.46}$$

where, $a + r_p^*$ is the effective crack length. The crack tip opening displacement at the tip of the physical crack is found for $x = a$. Since $r_p^* \ll a$, the COD is determined as:

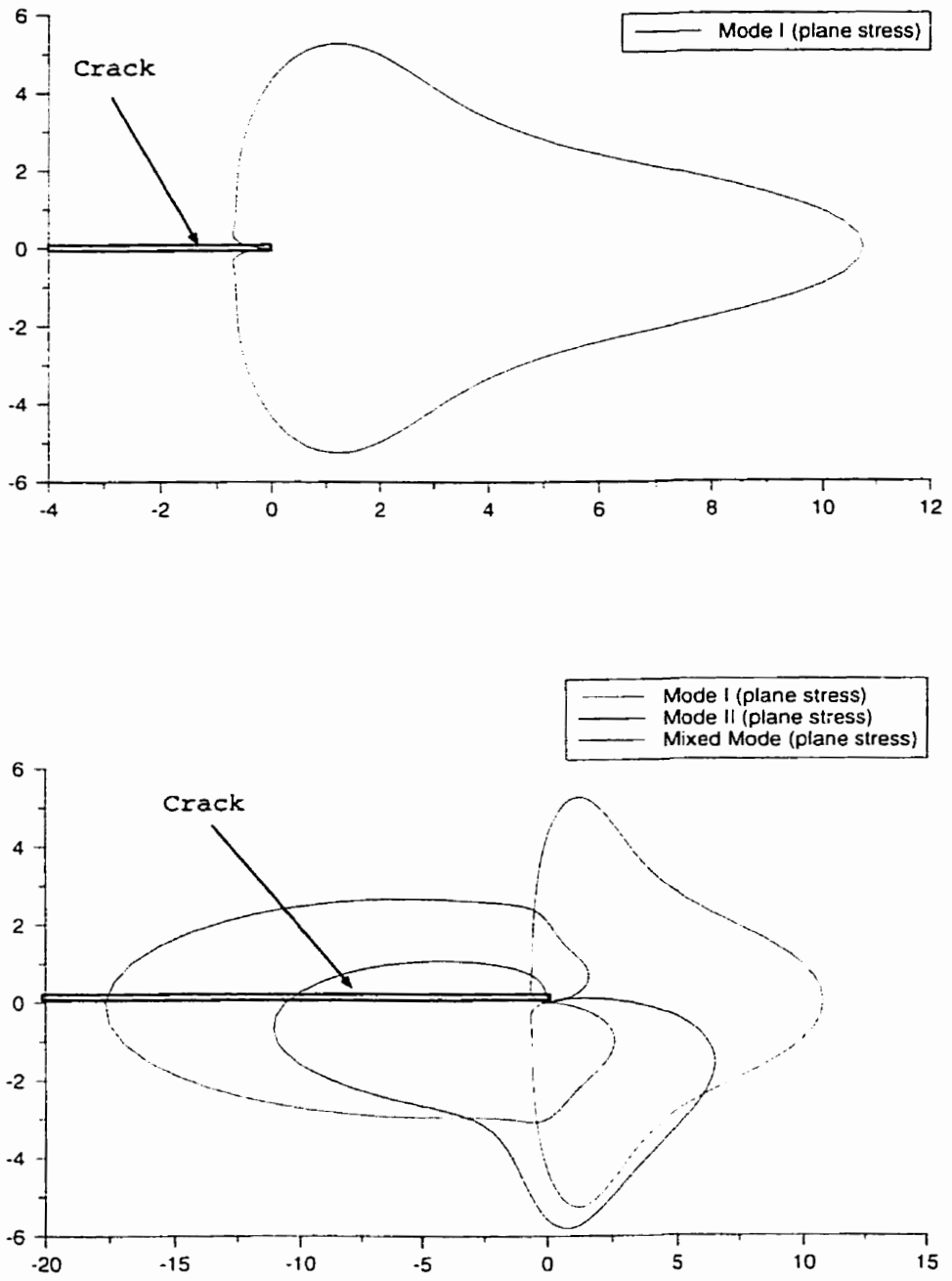

Figure 6.5: Inelastic Zone Shapes for Plane Stress State

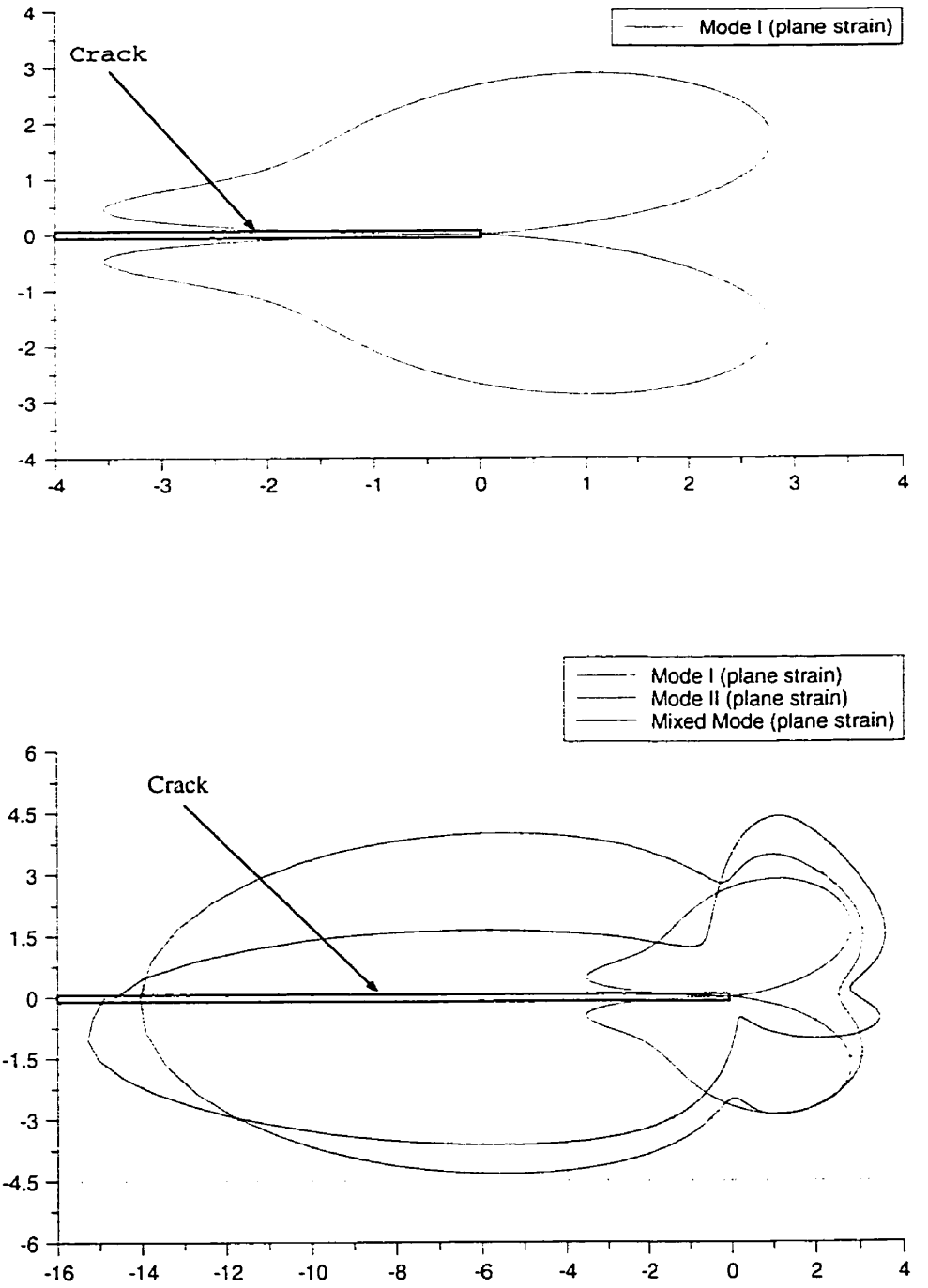

Figure 6.6: Inelastic Zone Shapes for Plane Strain State

$$COD = \frac{4\sigma}{E}\sqrt{2ar_p^2} \tag{6.47}$$

or

$$COD = \frac{4}{\pi}\frac{K_I^2}{E\sigma_s} \tag{6.48}$$

6.7 Discussion and Conclusion:

Under uniaxial stress assumption, three models have been presented. The inelastic zone sizes for anisotropic media would be within the range of curve L, abc and $P-P$.

For the biaxial stress state, *Hill's* yield criterion was adapted to seek the shape of the inelastic zone. We assumed a variation of the loading parameters m between 0 and 10. where $m = 0$ corresponds to pure mode I. $m = 10$ corresponds to near pure modeII loading (numerically this assumption was very close to pure modeII), and $m = 1$ to mixed mode. The parametric study yield the results for the shapes of inelastic zone shown in Figures (6.5 and 6.6), for plane stress and plane strain states. From these results the following conclusions are made:

(1) When $E_1 > E_2$, the inelastic zone for mode I is much larger than the one for the isotropic case. The inelastic zone size for mode II is smaller than the one of mode I.

(2) When $E_1 < E_2$, both inelastic zone shapes and size are very similar to the isotropic case. The only difference is that mode I has a got very narrow zone in comparison with the isotropic one.

(3) The actual shape of the inelastic zone found here is quit large, This may be because the yielding zone goes past the limitation of $\frac{r}{a} \ll 1$.

Chapter 7

EXPERIMENTAL PROGRAM

7.1 Introduction

A total of 75 tests were performed at the thermomechanics laboratory of the University of Manitoba to study the behavior of crack propagation and the effect of inelastic zone size. The composite under testing consists of fiberglass cloth with a West System epoxy matrix. The investigation examined the effect of thickness (i.e. number of layers) of the cloth and the fiber orientation. The composite material used in this investigation is manufactured as flat panels using the vacuum bagging technique.

A Instron loading frame 8562 was used for all the tests carried out in this research (see Figure (7.1)). The Instron dynamic testing system is an all-digital system designed specifically for testing the strength and measuring the physical properties of materials. The system consists of several major components: a load frame for the test forces to push or pull against, a force producing device (the electric actuator), a load measuring device (the load cell), a source of servo electric power (the electric power pack), and a means to control the system (the electronic control). The load frame is a very ruggedly constructed structure which provides a solid against which

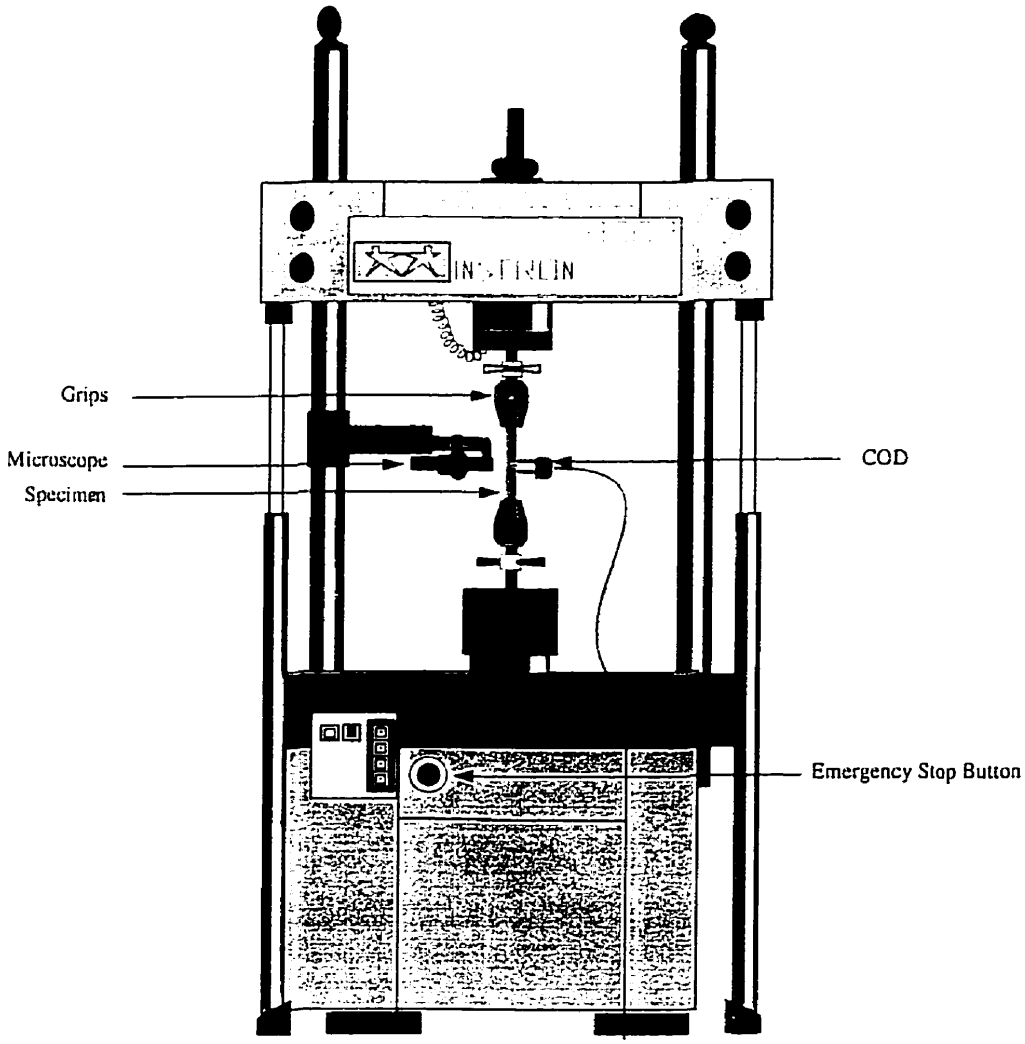

Figure 7.1: The Instron Test Machine and the COD device.

the test forces can react, and also serves as a support for the actuator and the load cell. It consists of a support base, a fixed table, and a movable cross-head riding on cylindrical vertical columns. The actuator is the driving mechanism of the system. It is essentially an electric motor driven rod with helical screw threads cut into its exterior surface. A load cell is a load measurement and control device that converts a mechanical force into an electrical signal that can be measured by the control system. Thus the load cell is a key element in the servo action of the system. The amplifier used in the experiment is a Measurements Group Strain Gage Conditioning Amplifier model 2310. This piece of equipment is used to provide an excitation for the strain gauges and amplifies the signal from the strain gauges. It can provide a excitation from 0.5 to 15Vdc and is equipped with a fully adjustable gain, frequency filter and automatic bridge balance. a 5V excitation with an amplification of 3500 was used to obtain the desired range and accuracy of measurement. The output signal range is from 0 to 10 V which is fed into the computer for storage.

7.2 Crack Opening Displacement (COD) Gauge

The C.O.D. gauge is used to measure the displacement of two knife edges placed in the vicinity of the crack opening (see Figure 7.2). Since a similar device was not readily available. The gauge used in the tests was constructed in the Lab. (see figure 7.3). It consists of two cold rolled stainless steel cantilever beams to which four strain gauges are bonded. Two of which are in compression and two are in tension. The strain gauges are connected to form a full bridge. The strain gauges are excited using an amplifier and calibration of the device is checked periodically. The range of motion of the device is 6.5 mm to 9.5 mm and the initial deflection for the knife edges for the experimentation is maintained at 7.5 mm. The device was verified to produce linear response over the operating range within 0.5 percent and is easily able to measure

displacements of the order of 0.0005 mm .

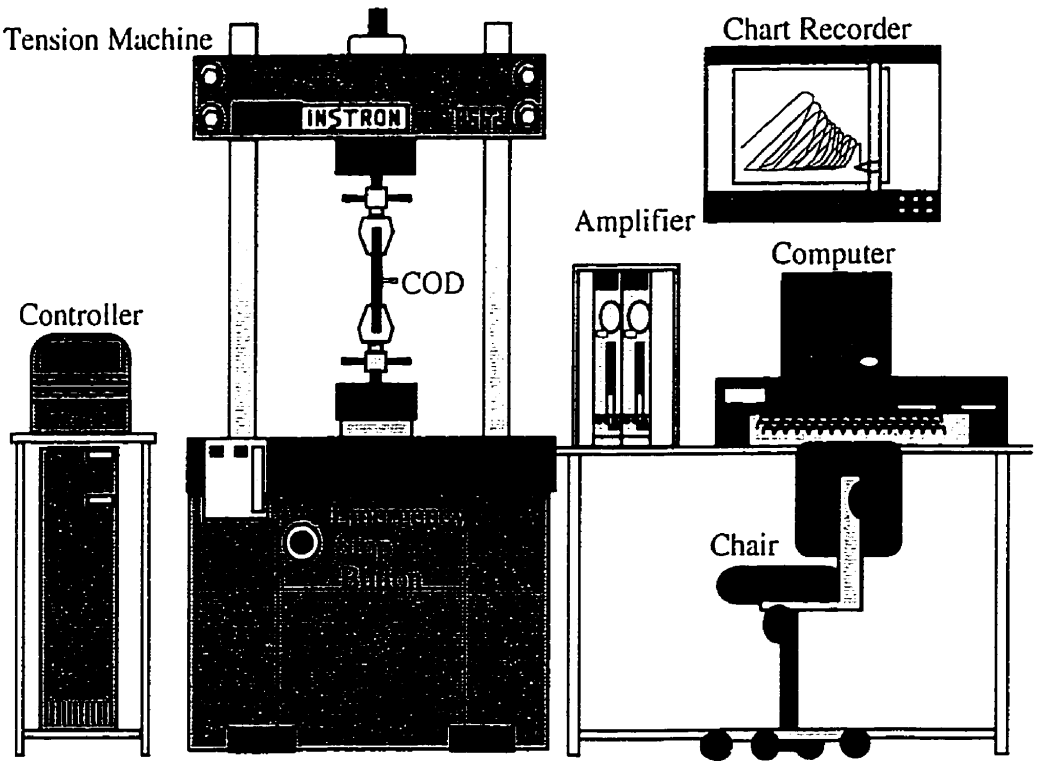

Figure 7.2: Experimental Setup.

7.3 Specimen Preparation and Vacuum Bagging Technique

As discussed in section 2.3.5 in Chapter II, vacuum bagging (or vacuum bag laminating) is a clamping method that uses atmospheric pressure to hold the adhesive

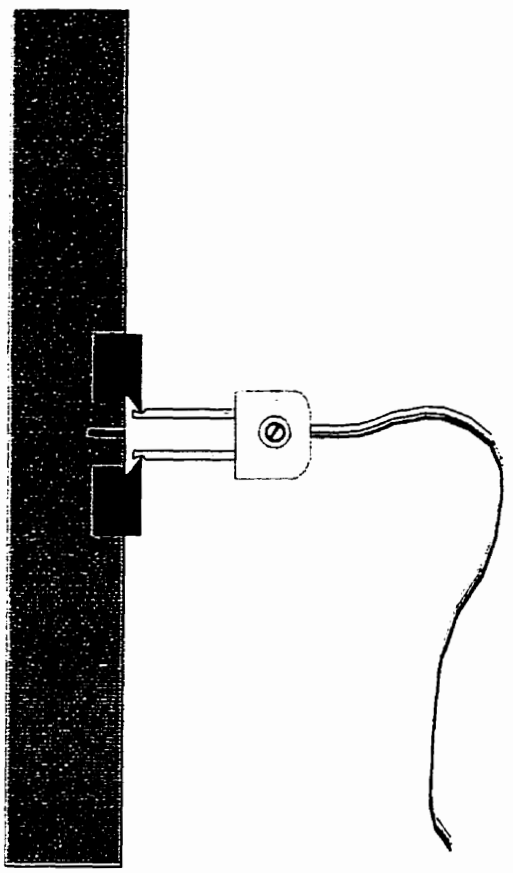

Figure 7.3: Specimen with COD Gage and Movable Knife-Edges.

coated components of a laminate in place until the adhesive cures. The laminates are sealed within an airtight envelope. The envelope may be an air-tight mold on one side and an air-tight bag on the other. When the bag is sealed to the mold, pressure on the inside and outside of the mold is equal to atmospheric pressure, approximately 736.6 mm (29 inches) of Mercury (Hg), or 14.7 psi (101.35 KPa). A vacuum pump is then used to evacuate air from the inside of the envelope. The pressure differential between the inside and outside of the envelope determines the amount of clamping force on the laminate (see Figure 7.4).

Vacuum bagging offers many advantages over conventional clamping or stapling techniques. Vacuum bagging delivers firm, evenly distributed pressure over the entire surface regardless of the type or quantity of material being laminated. It also allows for greater control over excess of adhesive in the laminate, resulting in higher fiber-to-resin ratios. This translates into high strength-to-weight ratios and cost advantages to the builder. Another advantage lies in the simplicity and variety of the molds that can be used. Since atmospheric pressure provides equal and even clamping pressure to the back of the mold, the mold only has to be strong enough to hold the laminates in their desired shape until the epoxy has cured. Therefore, molds can be relatively light weight and easy to build. The components of the vacuum bagging system are shown in Figure (7.4), which include specialized equipment and commonly available materials which are vacuum pumps, vacuum bagging material, release fabric, breather material, vacuum bag, mastic sealant, and plumbing system. The heart of a vacuum system is the vacuum pump. Vacuum pumps are mechanically similar to air compressors, but work in reverse so that air is drawn from the closed system and exhausted to the atmosphere. A variety of other materials are needed to complete the vacuum system and assist the laminating process. The release fabric is a treated material to prevent bonding to epoxy, and can be perforated to separate the breather and the laminate. Excess epoxy can pass through the perforated release fabric which can be pealed from

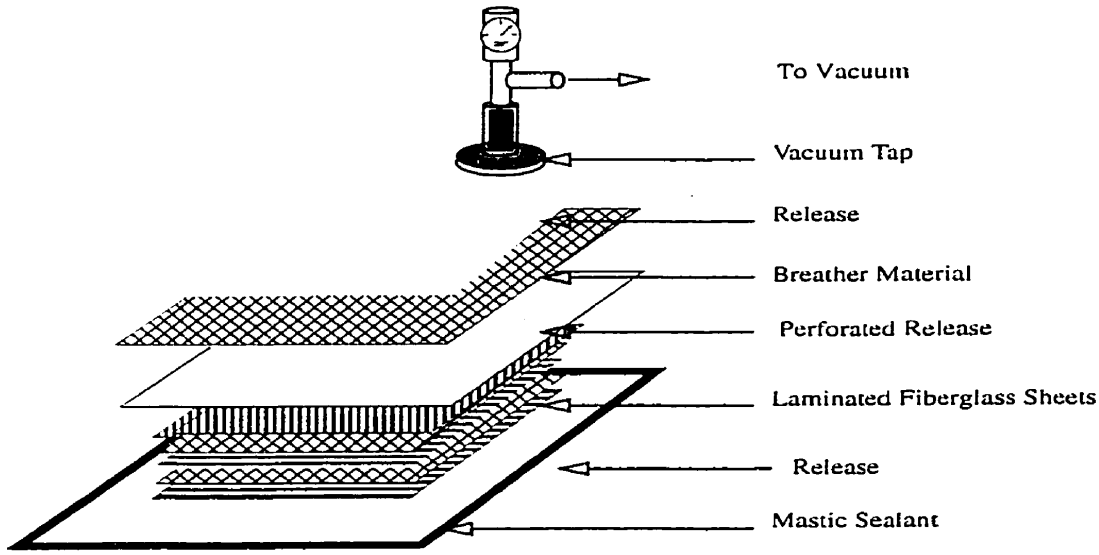

Figure 7.4: Fiberglass Panel Lay-up using The Vacuum Bagging Technique.

the laminate after the adhesive cures.

A variety of release materials are produced specifically for vacuum bagging operations. They are known as release fabric, peel ply, or release film. Many are designed for use at elevated temperatures or to control the amount of resin passing through them. A breather (or Bleeder) cloth allows air from all parts of the envelope to be drawn to a manifold by providing a slight air space between the bag and the laminate. The vacuum bag, in most cases, forms half of the airtight envelope around the laminate. For higher pressure and temperature applications, specially manufactured vacuum bag material should be used.

Generally, the better the airtight seal and bag material, the smaller the required pump. Poor seals or materials which allow air leakage, require larger pump capacity in order to maintain satisfactory vacuum pressure. Mastic is used to provide a continuous airtight seal between the bag and the mold around the perimeter of the mold. The mastic may also be used to seal the point where the manifold enters the bag and to repair leaks in the bag or plumbing. The plumbing system provides an air-tight passage from the vacuum envelope to the vacuum pump, allowing the pump to remove air and reduce the air pressure in the envelope. A basic system consists of flexible hose or rigid pipe, a trap and a port that connects the pipe to the envelope.

7.4 Epoxy Matrix

Bisphenol-epoxide A type (West System 105) resin is a clean, light-amber, low-viscosity, epoxy resin that can be cured in a wide temperature range to yield a high strength, rigid solid which has excellent cohesive properties and is an outstanding bonding adhesive and moisture vapor barrier. Two types of hardeners are formulated for use with 105 resin depending on the final application. Polyamine (West System

205) hardener is used for general bonding, barrier coating and fabric applications. It is formulated to cure at lower temperature and to produce a rapid cure that develops its physical properties quickly at room temperature. The preparation of the resin mix is performed as follows:

Dispense the proper portions of the resin and hardener into a mixing pot. Stir the two ingredients together thoroughly with a wooden mixing stick (1 to 2 minutes is recommended). Heat is generated by the chemical reaction that cures the epoxy. The time required for the epoxy-hardener mixture to transit from a liquid to a solid state is known as the cure time. This time is divided in three phases: open time, or wet lay-up time (liquid state), initial cure (gel state) and final cure (solid state).

7.5 Specimen Preparation

The test specimens are prepared in the following process. First, panels of fiberglass are manufactured using the vacuum bagging technique, with the chosen number of fiberglass cloth layers and fiber orientation, see Figure (7.4). These panels are allowed to cure for a minimum of 24 hours at room temperature. Next, the specimen size and orientation is recorded on the surface of each panel. The specimen has a length of 250 mm and a width of 25 mm as shown in Figure (7.5). The total gauge length between grips is 140 mm. The specimens are cut using a bandsaw. Since the cutting procedure may cause local delamination, the specimens are cut 0.7 mm larger than required. Each specimen is then hand sanded to the final shape with successively finer grits of sandpaper. Dimensions are verified with digital Vernier calipers. Each specimen must be within 0.03 mm in order to maintain decent accuracy within the experiment. For specimens requiring an initial crack, the location of the crack is marked on the specimen. The crack is then cut with a thin bandsaw blade at low speed in order to ensure minimal damage of the cut surface. The length of the crack is then verified to

be 6.25 mm (see Figure 7.5).

7.6 Test Procedure

The test equipment is connected as shown in Figure (7.6) where the arrows indicate the transfer of information between test equipment. The specimen is placed between the grips and locked into place. The COD gauge is fixed to the specimen between the knife edges which are either glued or screwed to the specimen on either side of the crack opening. Using the control keys of the Instron Tension Machine, the slack is removed prior to loading of the specimen. The Instron self-calibration routine is initiated using the controller. Using a computer program, written exclusively for this experiment and based on displacement control, loading and unloading of the specimen proceeded. The loading and unloading rates are chosen to be as slow as possible, between 0.06-0.1 mm/min in the case of loading and 0.09-0.1 mm/min in the case of unloading. This ensures that the operator is able to reverse the load when the crack begins to propagate, without breaking the specimen. Because of this slow loading and unloading rates each test takes from 7 to 9 hours to complete. The load value, the total elongation and the C.O.D. measurement for a number of loading and unloading cycles are recorded by the computer. These results can then be plotted. Typical results are shown in Figures 7.11, 7.12, 7.13 and 7.14 in the next section. The rest of the results are depicted in Appendix (A).

7.7 Test Results

The experimental work consisted of testing several uncracked specimens with different thicknesses (number of layers) to determine the initial elastic modulus and

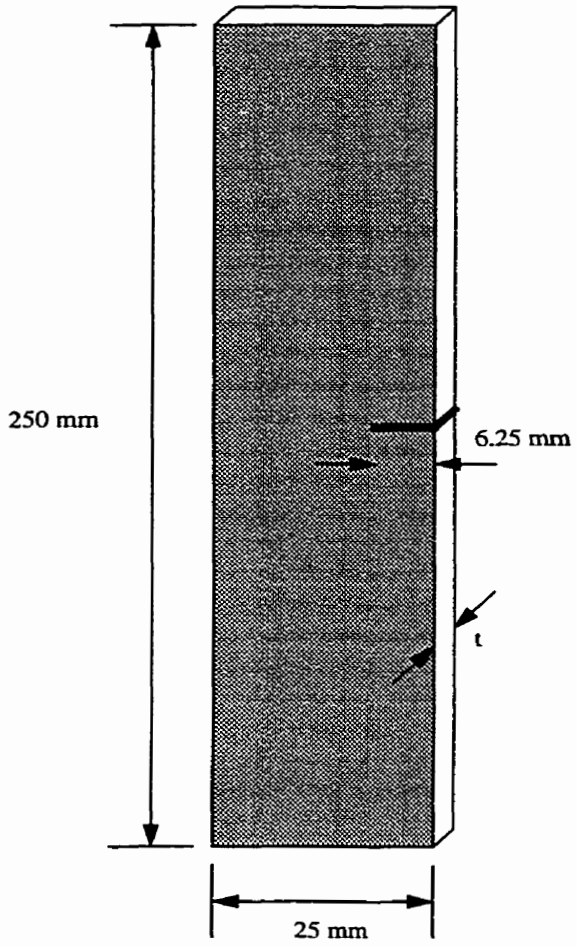

Figure 7.5: Tension Test Specimen Dimension.

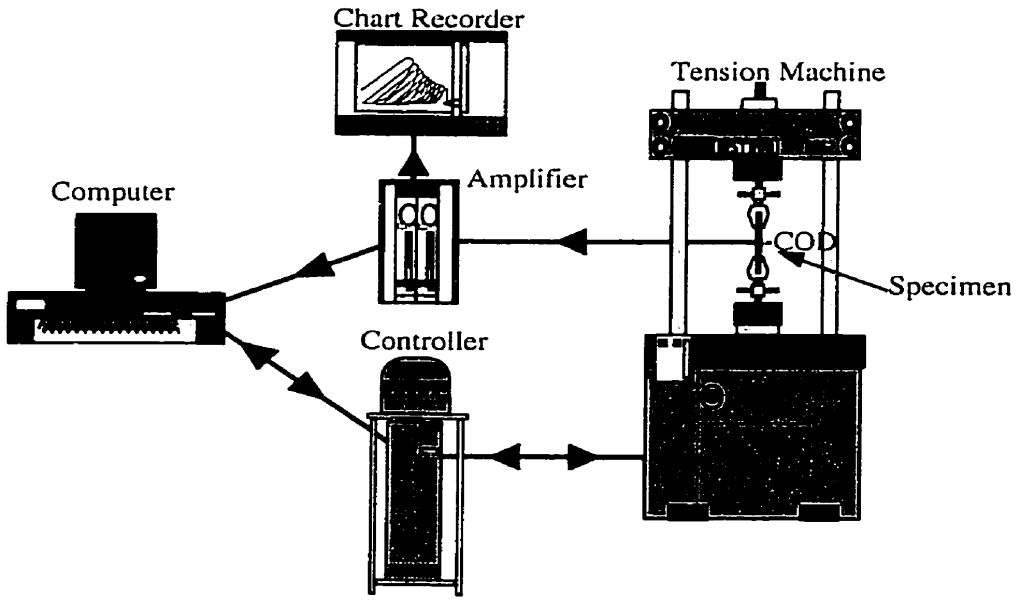

Figure 7.6: Connection Lay-out.

the elastic strength. The initial elastic modulus is found to be equal to 14.37 GPa. When the load transfer between the matrix and fibers takes place for the first time, the response remains linear, but with a secondary modulus of $9.87GPa$ (see Figure 7.7), corresponding to a drop of about 30 %. The tensile strength is evaluated to be 312 MPa at the peak. During the test, the vertical load and crack opening displacements were monitored and recorded using a standard data acquisition system.

The load versus displacement measured at a gauge length of 140 mm and the crack opening displacement are presented in Tables (7.1, 7.2, 7.3, and 7.4), which gives the number and type of specimen used in this investigation. The results were repeatable within an accuracy of 3 % in the evaluation of the peak load and compliances. The post response of the COD reading indicates that the specimen loses energy as the number of loading cycles increases. This decrease is caused by a localized energy dissipation in the vicinity of the crack. Unloading/reloading cycles, which were used to monitor the change in the specimen compliance or flexibility, were performed. The experiment was performed number of cycles in which the crack propagates or sometimes until the specimen splits in two halves. The loading process was COD controlled and, since the COD is a monotonically increasing function of time during the fracture process, it is possible to capture the post-peak response for all the tested specimens. This means it was possible to detect the catastrophical softening branch of the load-COD curve. In this way, a phenomenon unstable in nature was made stable in practice. While the load decreased beyond the peak load, the crack opens and grows in a stable manner.

From the results presented in this Chapter and in Appendix A, it can be seen that the COD first gradually increased, following a linear curve. A non-linear prepeak response is observed which is associated with slow crack growth and thus the formation of a fracture plastic zone turning the notch into a crack. At around the peak load, the COD decreases, thus effectively reducing the load. The load is then

Table 7.1: Test Group # 1

Number of layers	Fiber Orientation	Thickness (mm)	Peak Load (N)	Number of Cycles
12	0/90/0	2.05	3398	50
16	0/90/0	2.50	4310	50
16	0/45/90	3.00	5372	50
20	0/90/0	3.25	6904	50

Table 7.2: Typical Results for 12 Layers Specimen of (0/90/0) Fiber Orientation

Cycle Number	Applied Load (N)	Total Elongation (mm)	COD Reading (mm)	Crack Length (mm)
1	3398	1.18	0.19	6.25
5	3303	1.24	0.22	6.90
10	3271	1.29	0.28	7.15
15	3043	1.28	0.32	8.20
20	2620	1.23	0.35	9.03
25	2303	1.20	0.39	10.0
30	1869	1.17	0.43	11.40
35	1855	1.19	0.48	12.85
40	1631	1.21	0.55	13.93
45	1225	1.21	0.62	15.60
50	1026	1.21	0.66	17.05

Table 7.3: Test Group # 2

Number of layers	Fiber Orientation	Thickness (mm)	Peak Load (N)	Number of Cycles
12	0/90/0	2.05	3308	50
16	0/90/0	2.50	4678	50
16	0/45/90	3.00	5481	50
20	0/90/0	3.25	6908	50

Table 7.4: Typical Results for 16 Layers Specimen of (0/90/0) Fiber Orientation

Cycle Number	Applied Load (N)	Total Elongation (mm)	COD Reading (mm)	Crack Length (mm)
1	4678	1.55	0.25	6.25
5	4161	1.58	0.28	7.85
10	3490	1.50	0.33	9.80
15	2988	1.43	0.38	11.25
20	2326	1.36	0.39	11.95
25	1661	1.30	0.45	13.65
30	1266	1.30	0.52	15.15
35	1145	1.32	0.58	16.45
40	835	1.34	0.65	19.85

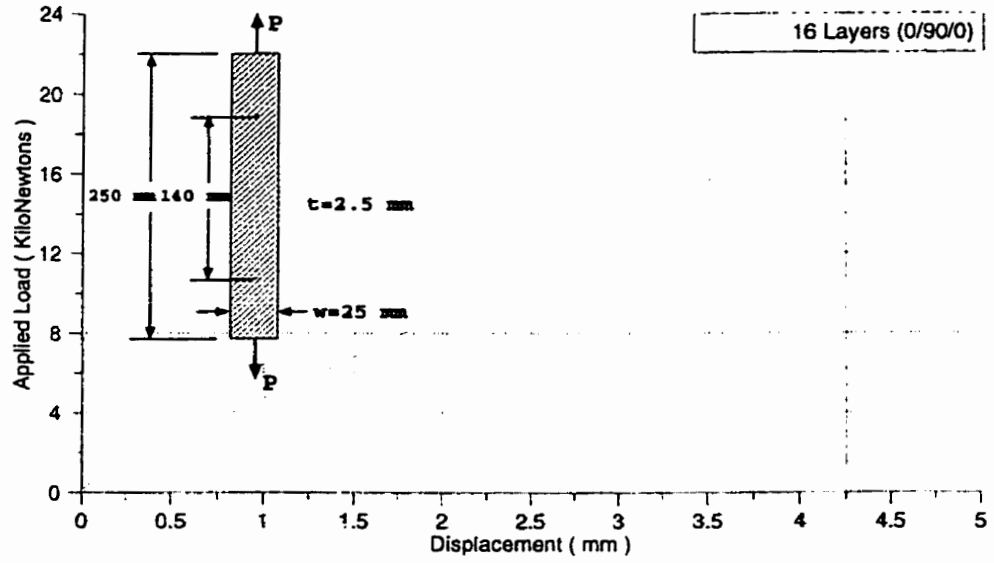

(a)

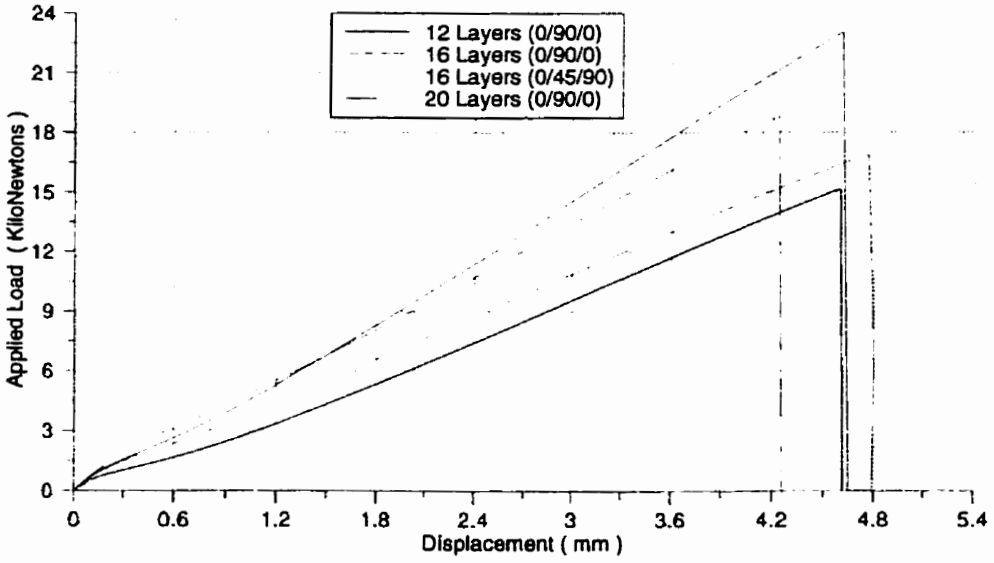

(b)

Figure 7.7: Typical Uniaxial Tensile Test a) for 16 Layers Specimen b) for Different Specimens.

reapplied and the response would be extended in to the post-peak regime. Following the peak load, is the softening or the crack propagation stage where the non-linearity occurs. This non-linearity is caused by the formation of micro cracks ahead of the notch as the matrix begins to fail. This is characterized by an increase in displacement and corresponding decrease in load (see Figures from 7.9 to 7.16)

According to the results obtained, the peak load increases with the thickness. For example the peak load for twelve layers cracked specimen is 3.4kN, while for sixteen and twenty layers specimens peaks of 4.1kN and 6.9kN were obtained respectively (table 7.1). The strength of the specimen may also be effected by the fiber orientation. The test results showed that the peak load that can be carried by (0/45/90) fiber orientation is larger than those carried by a specimen with the same number of layers but with fiber orientation (0/90/0). The notch width ratio also affects the load-displacement and load-COD response. Different notch-width ratio specimens has been tested ($a/w = 0.2, 0.25, 0.35, 0.45$). Both load-elongation and load-COD responses were captured. Typical results of load-COD are shown in Figure (7.8). It is shown that by decreasing the relative notch depth ratios, the curve becomes steeper with increase in the brittleness, and the load capacity and stiffness increases.

Attempts were made to conduct load-COD behavior for specimens with inclined crack experimentally as shown in Figures (7.17,7.18,7.19 and 7.20). Failure mode in the notched specimens under this mixed mode loading were more complex than the open loading mode [110, 111].

Generally, in an inclined notch , the crack grew initially along a direction away from the original crack plane, then changed its direction, and became normal to the tensile loading. Again, in the mixed-mode fracture very little stable crack growth was observed, and fracture occurred in an unstable manner. A typical fractured specimen with inclined crack is shown in Appendix (C).

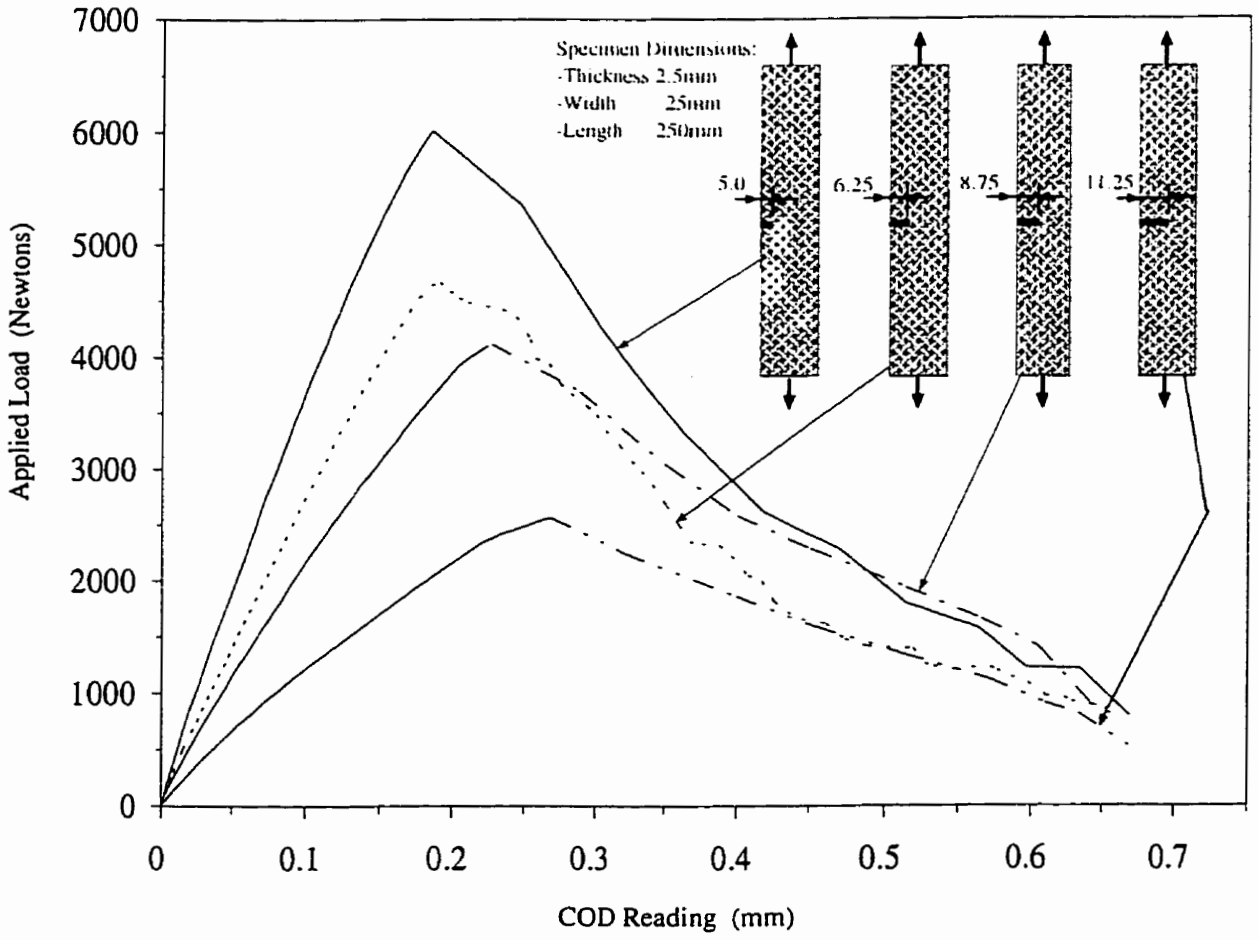

Figure 7.8: Experimental Load-COD Response of Sixteen-layers Specimen of (0/90/0) Fiber Orientation ($a/w = 0.2, 0.25, 0.35, 0.45$) .

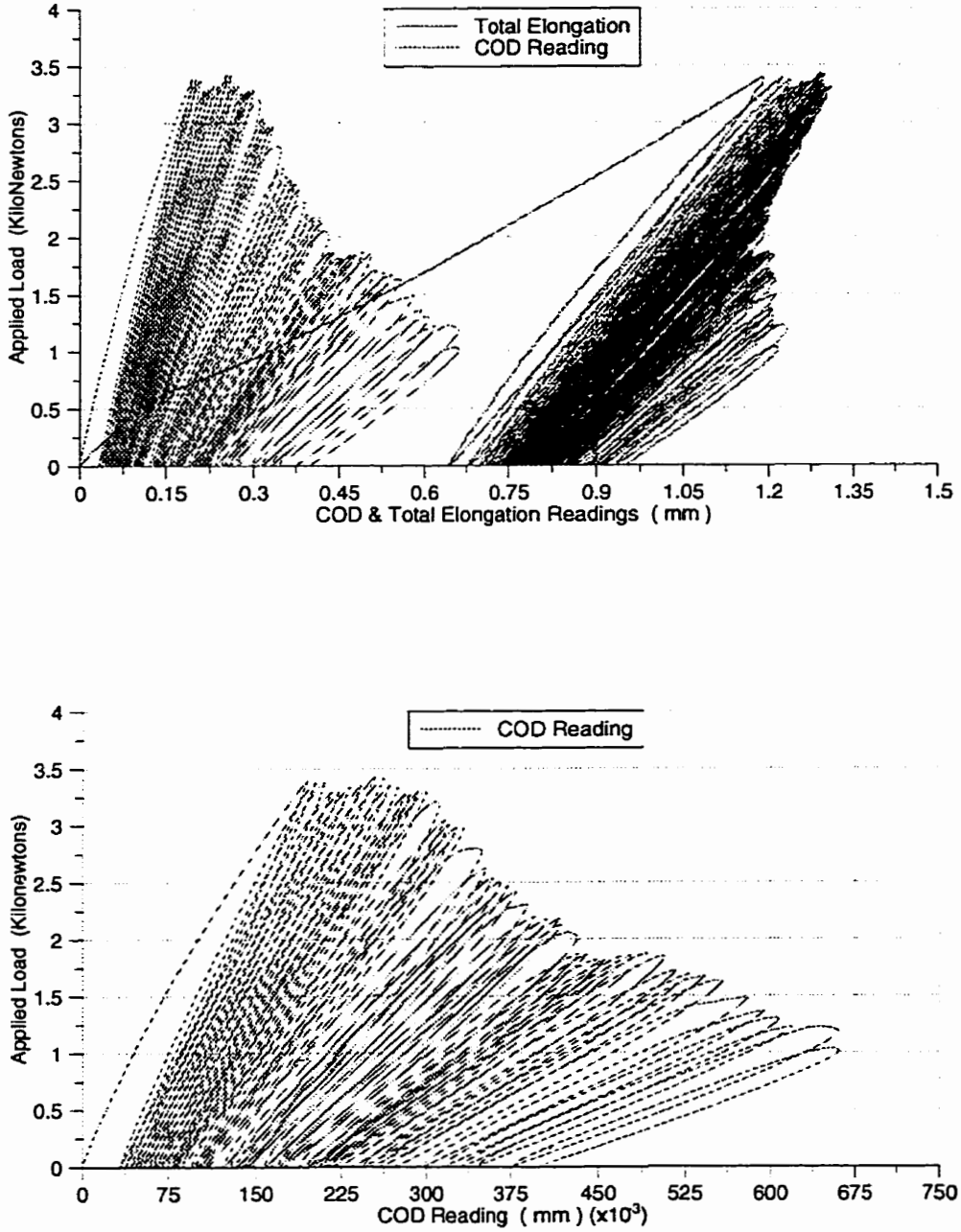

Figure 7.9: Response of 12 Layers Specimen of (0/90/0) Fiber Orientation.

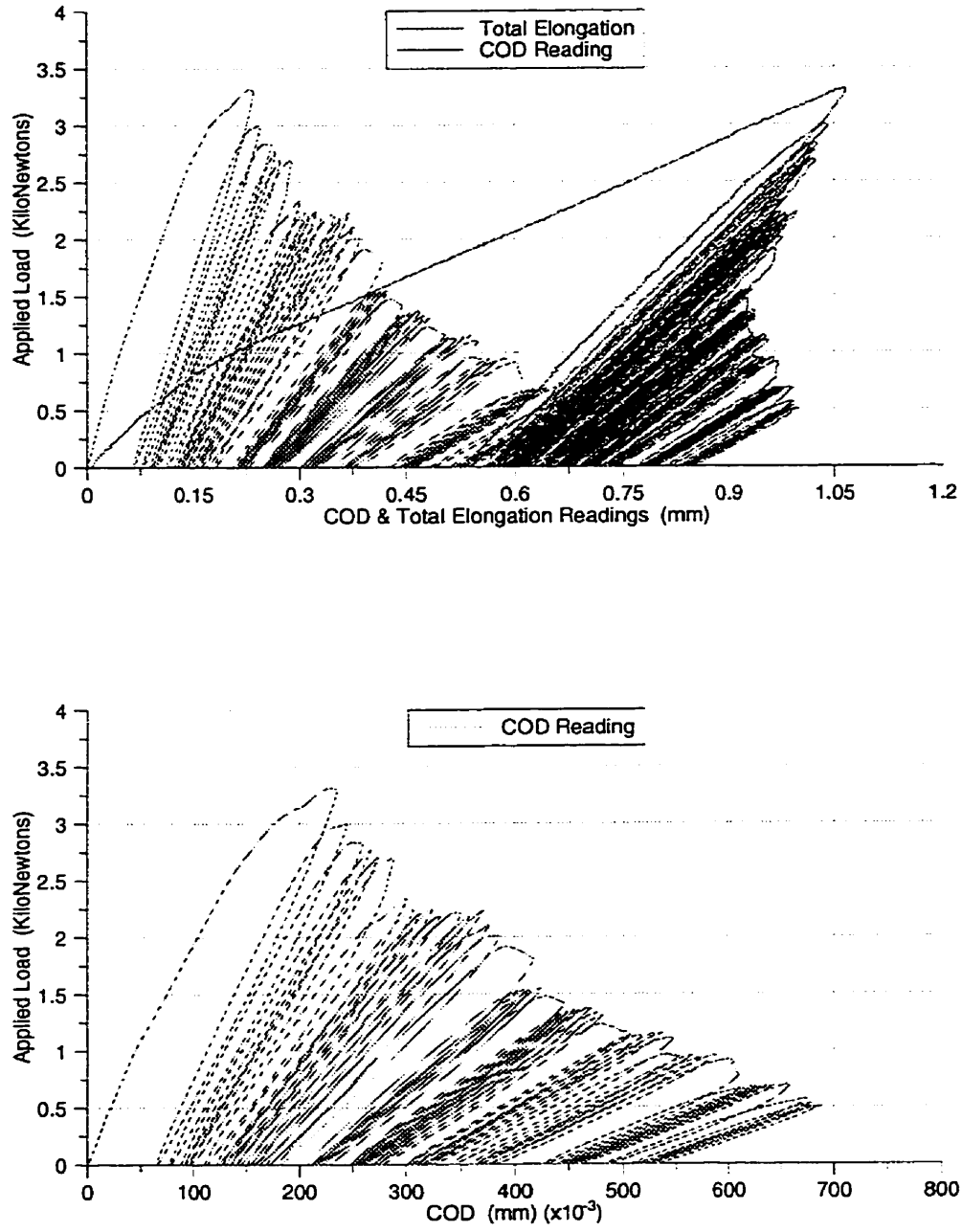

Figure 7.10: Response of 12 Layers Specimen of (0/90/0) Fiber Orientation.

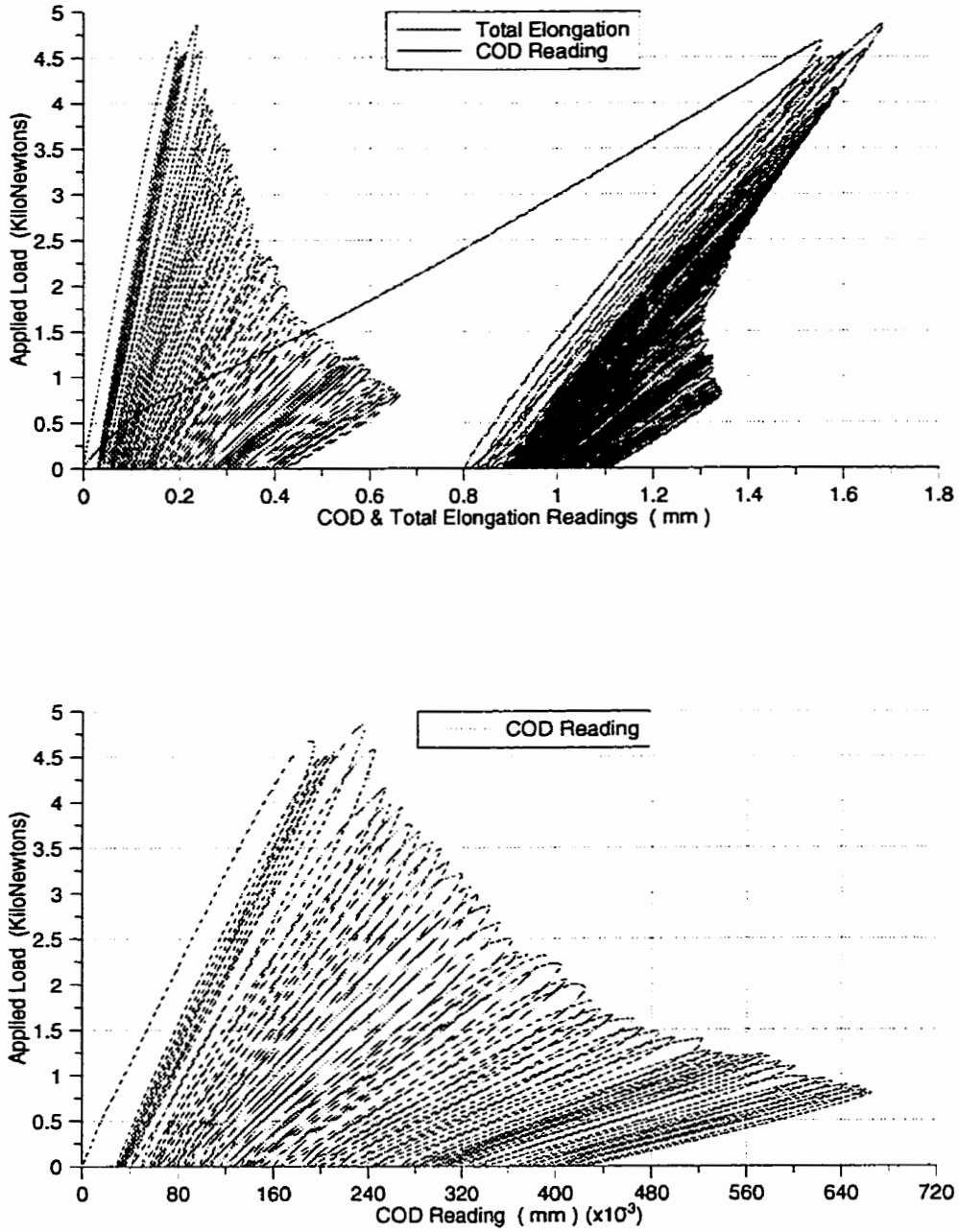

Figure 7.11: Response of 16 Layers Specimen of (0/90/0) Fiber Orientation.

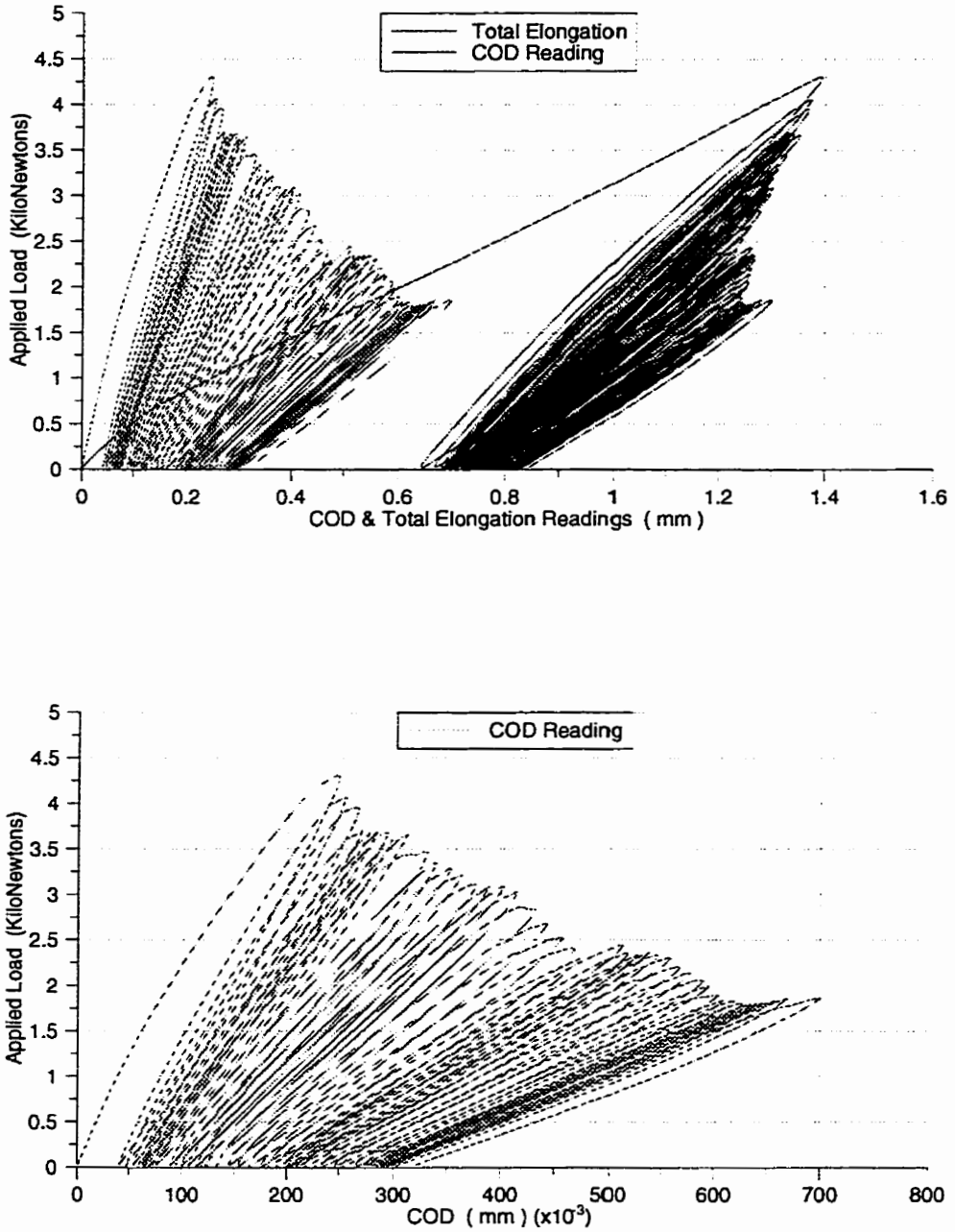

Figure 7.12: Response of 16 Layers Specimen of (0/90/0) Fiber Orientation.

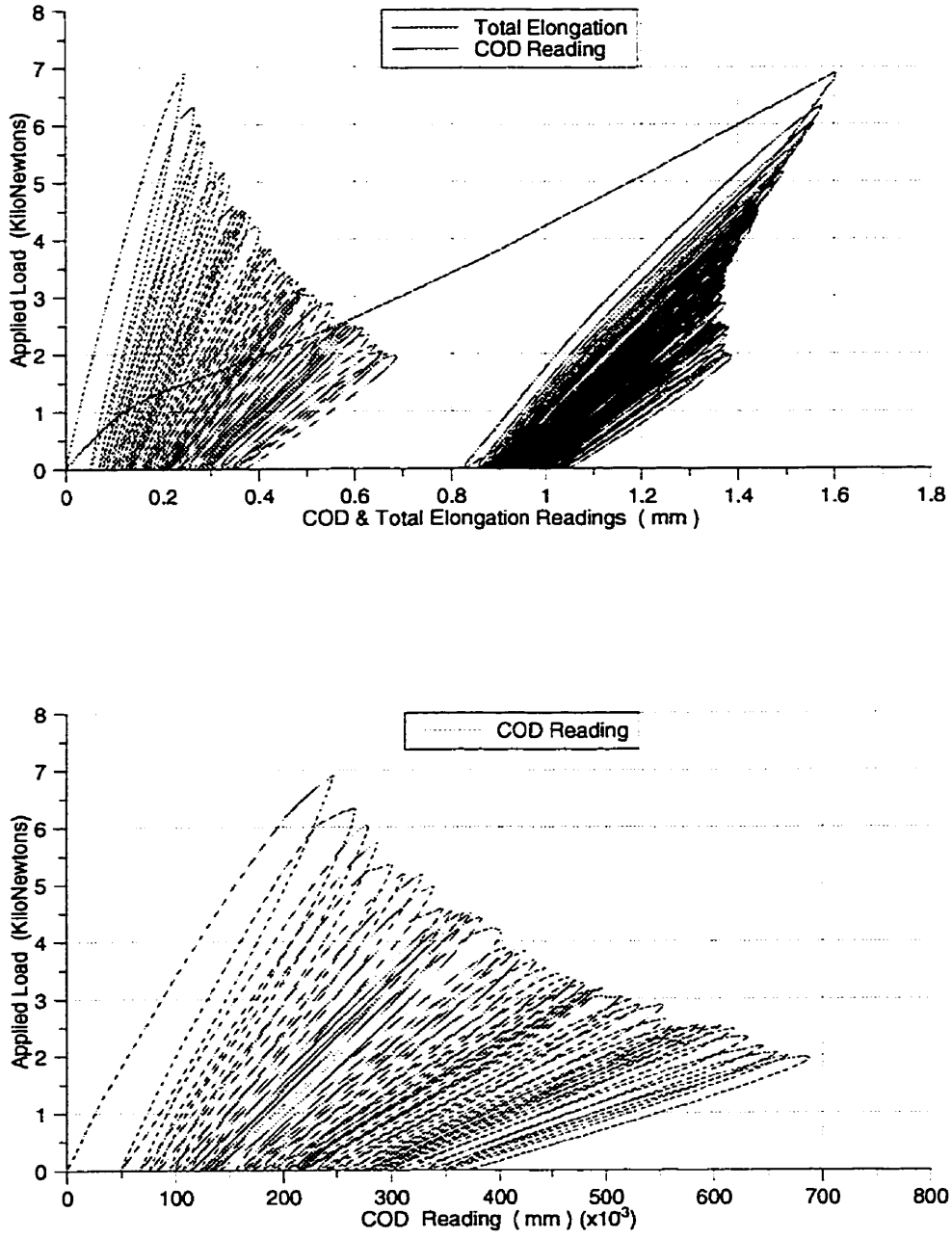

Figure 7.13: Response of 20 Layers Specimen of (0/90/0) Fiber Orientation.

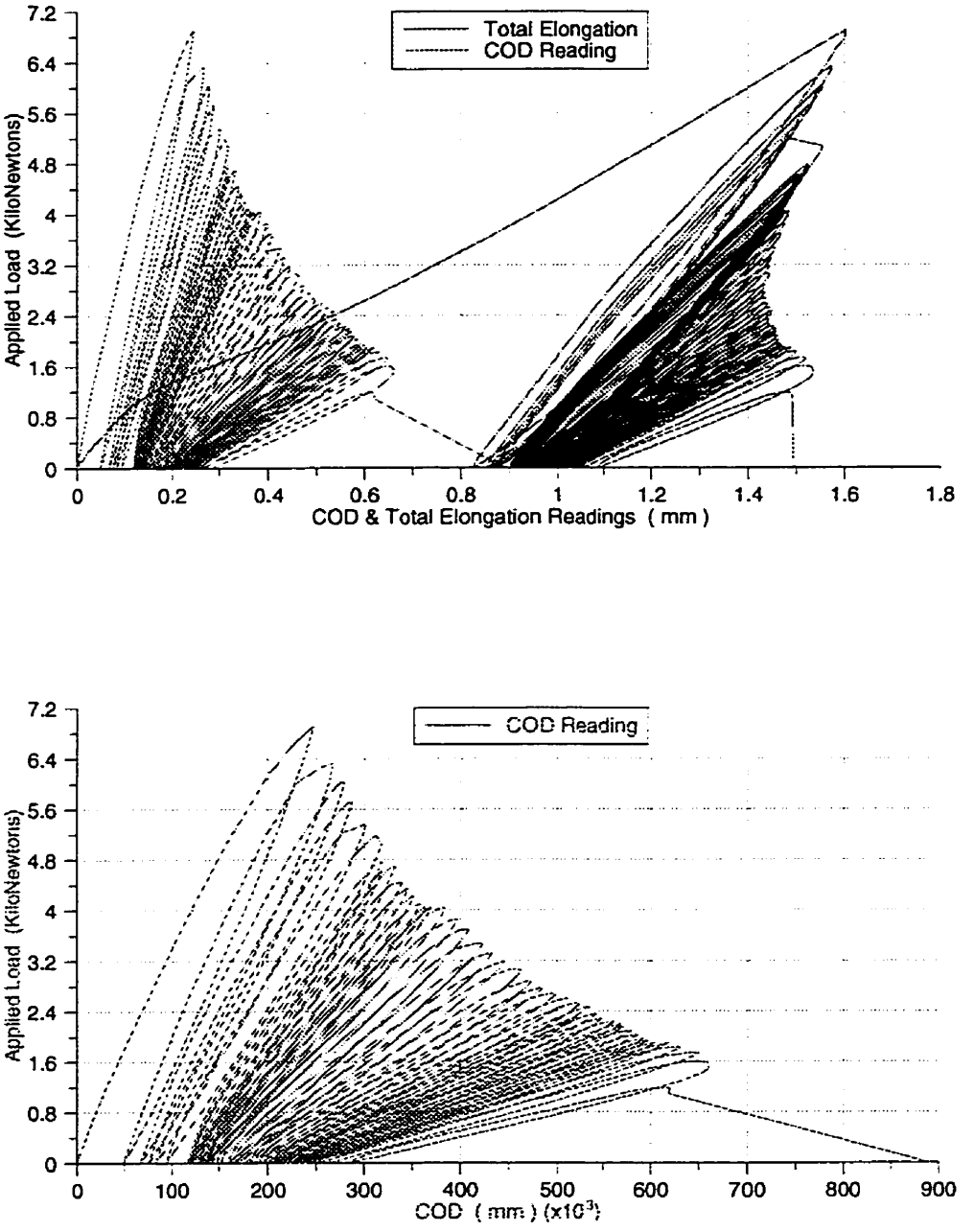

Figure 7.14: Response of 20 Layers Specimen of (0/90/0) Fiber Orientation.

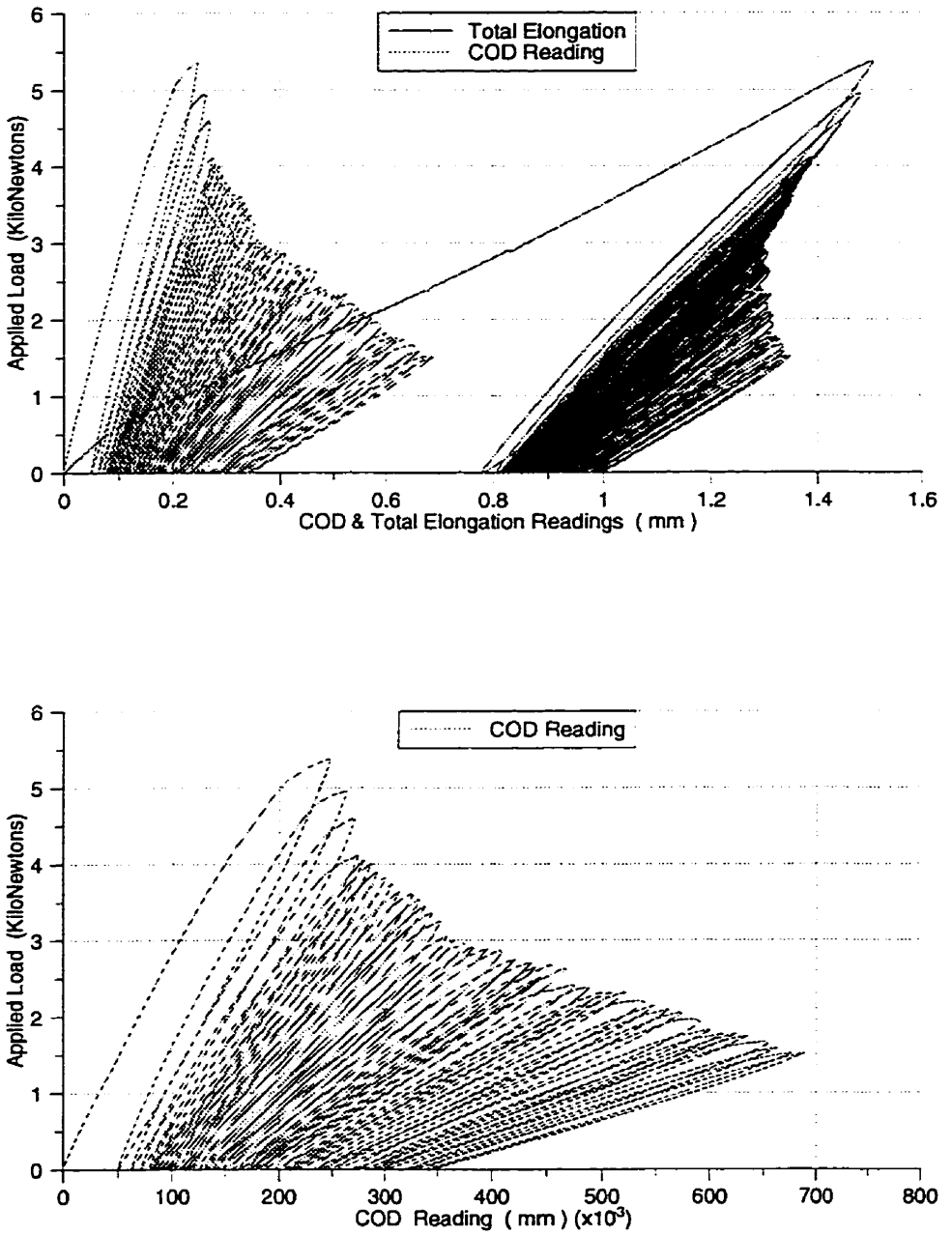

Figure 7.15: Response of 16 Layers Specimen of (0/45/90) Fiber Orientation.

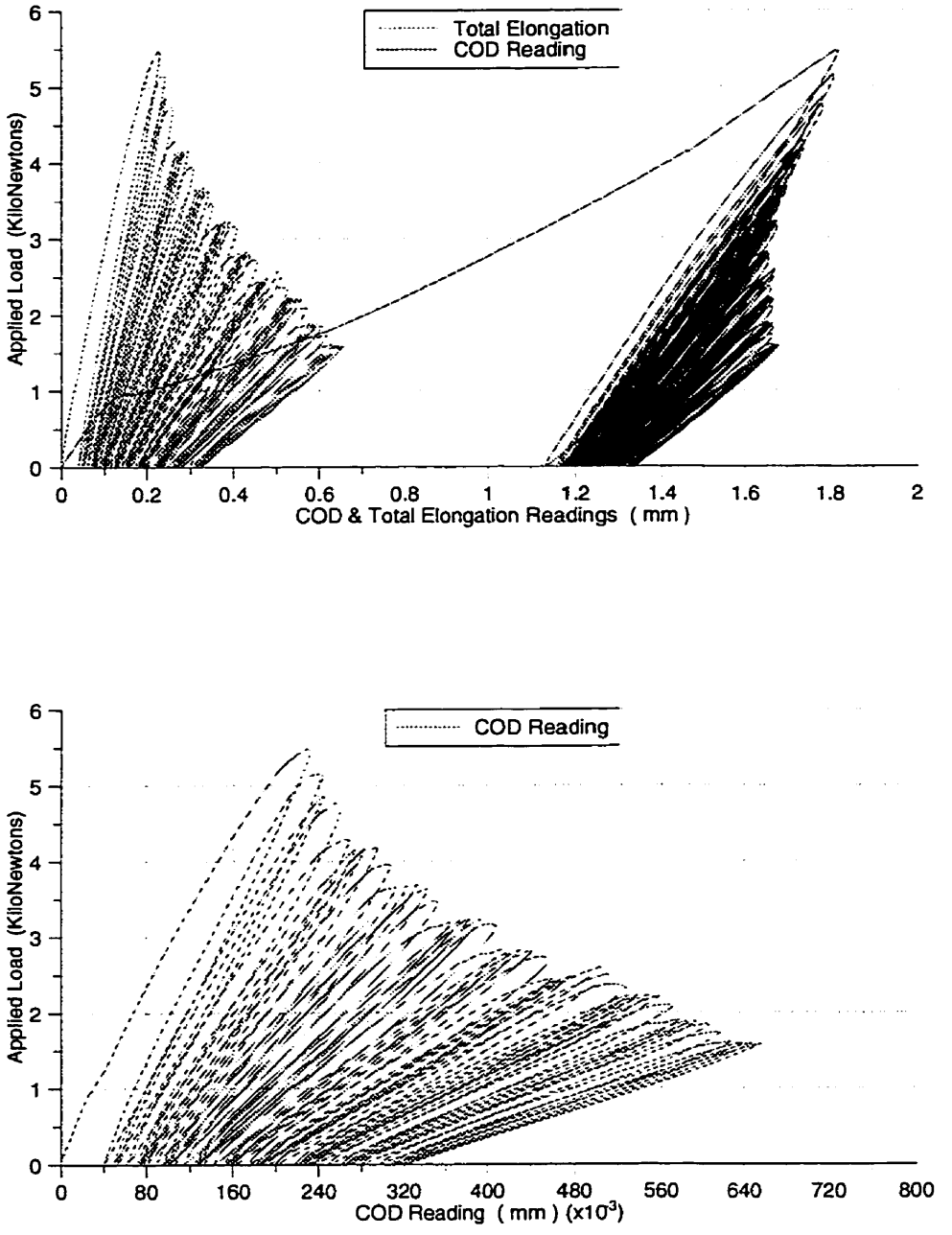

Figure 7.16: Response of 16 Layers Specimen of (0/45/90) Fiber Orientation.

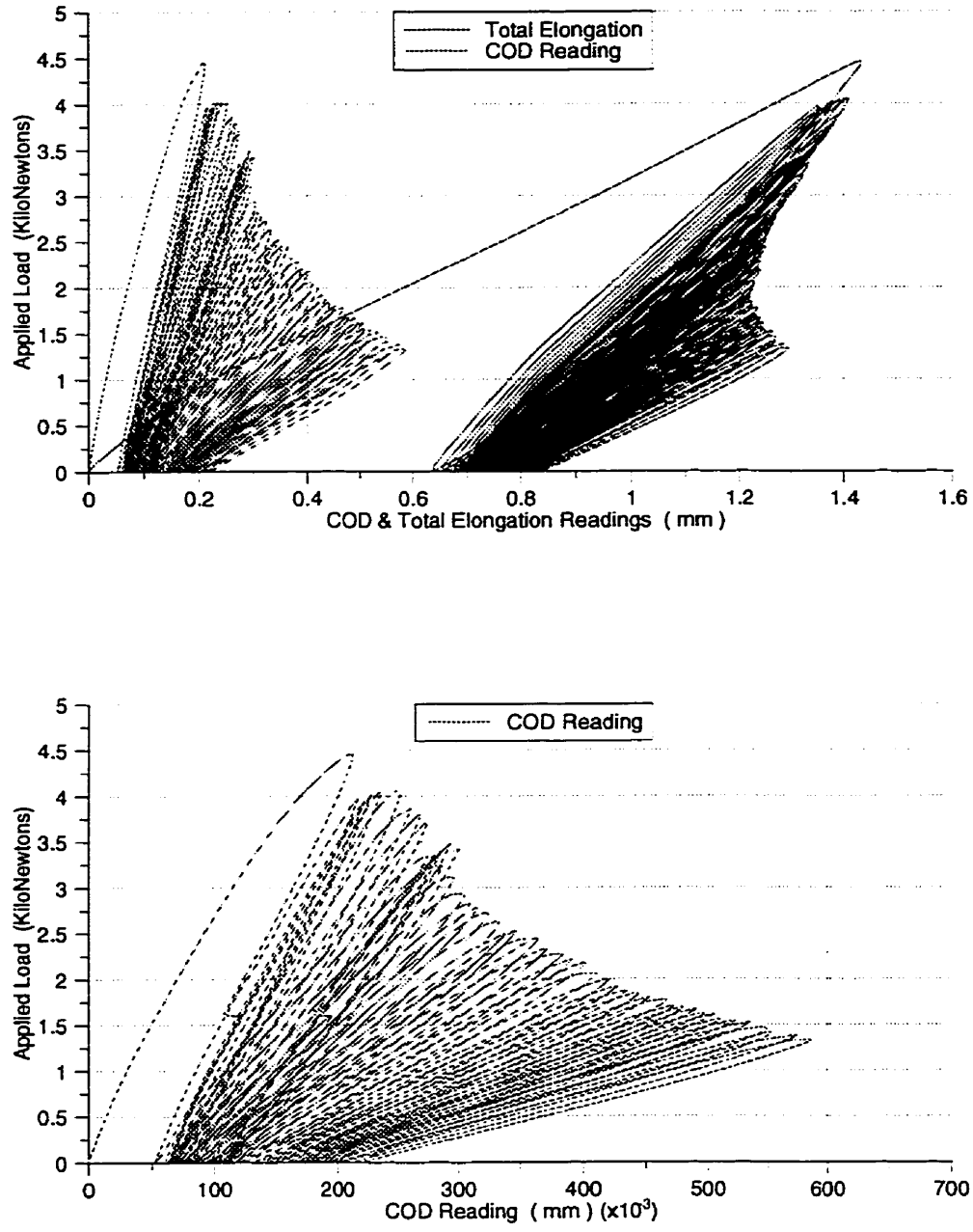

Figure 7.17: Response of 12 Layers Specimen with Inclined Crack and (0/90/0) Fiber Orientation.

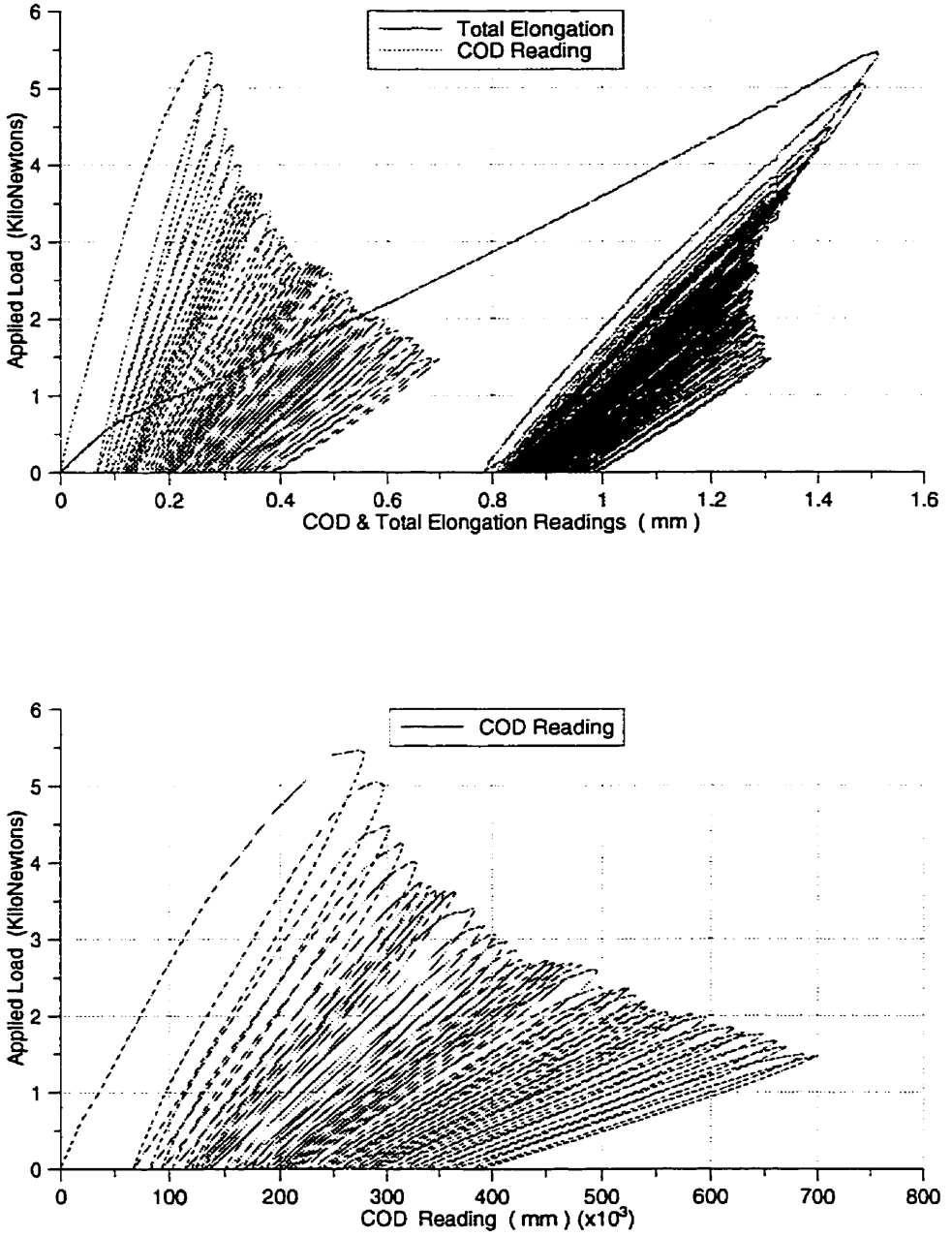

Figure 7.18: Response of 16 Layers Specimen with Inclined Crack and (0/90/0) Fiber Orientation.

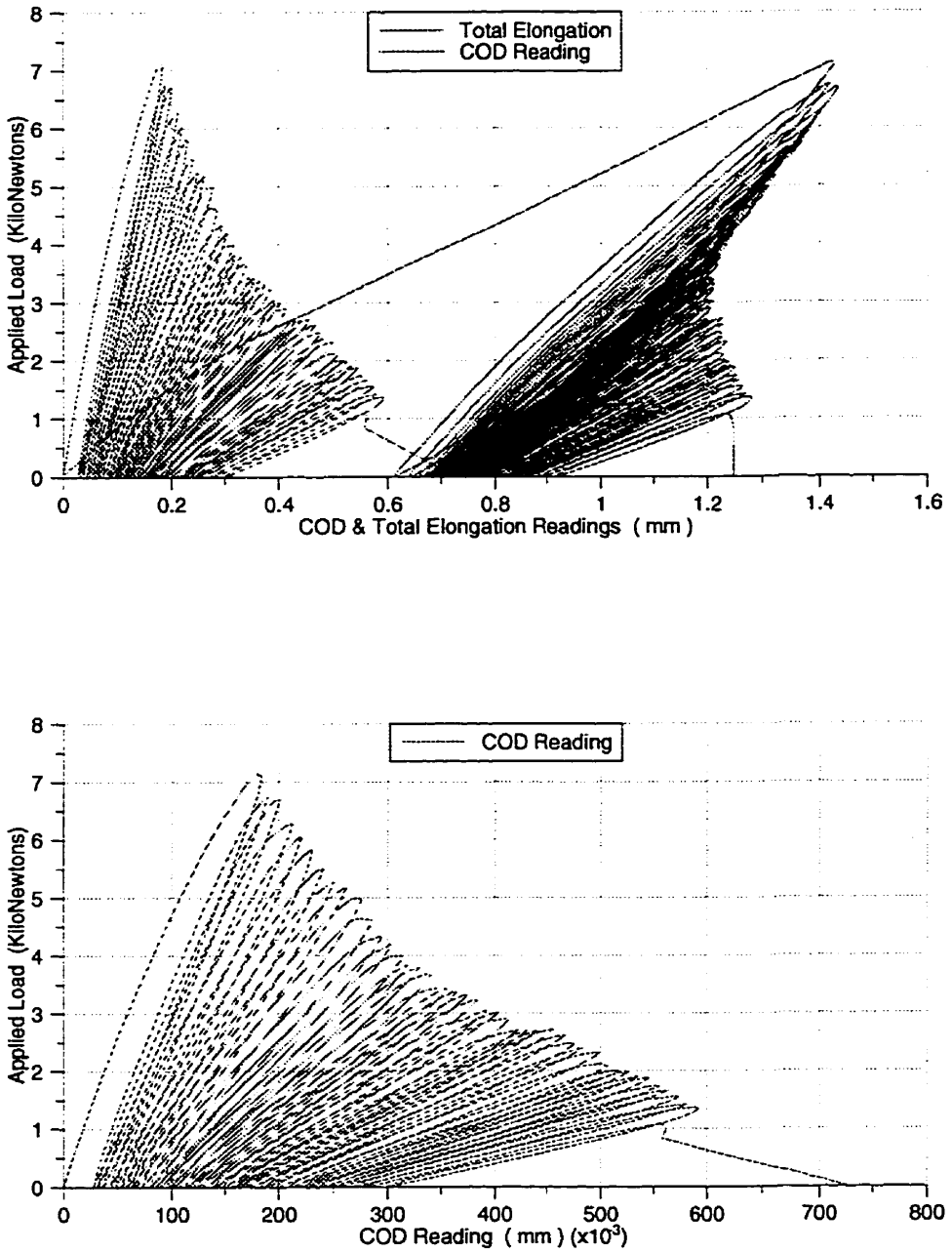

Figure 7.19: Response of 20 Layers Specimen with Inclined Crack and (0/90/0) Fiber Orientation.

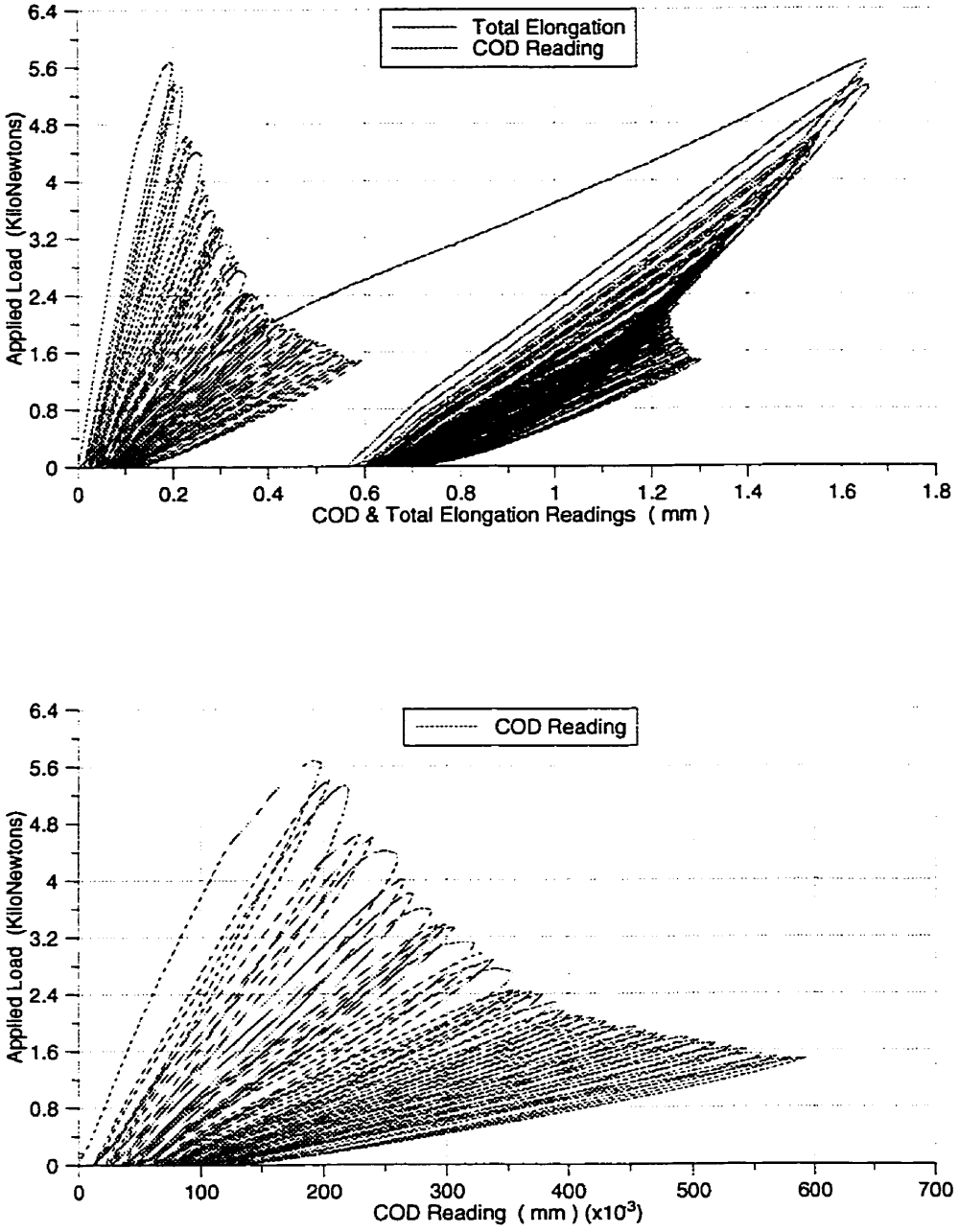

Figure 7.20: Response of 16 Layers Specimen with Inclined Crack and (0/45/90) Fiber Orientation.

Chapter 8

STIFFNESS DEGRADATION AND ENERGY DISSIPATION

8.1 Introduction

In this chapter, the effect of various geometric parameters such as specimen thickness and fiber orientation on the material degradation is addressed. As was shown in chapter 7, the load versus crack opening displacement presents a well defined post-peak regime which can be described by a simple bilinear model. Based on the experimental results, concepts of fracture mechanics are applied to evaluate stiffness degradation in composite materials and are discussed in this chapter.

8.2 Test Results

From the results shown in Figures (8.1a, 8.1b and 8.2a), it appears that the Load-COD response is first measures linearly, followed by a non-linear pre-peak response. This nonlinear regime is associated with the formation of a fracture tip inelastic zone

and a small slow crack growth. At the peak load, and soon after the crack start to grow, the COD decreases, thus effectively reducing the load. The load is then re-applied and the response extends into the post-peak regime. Following the peak load is the softening or the crack propagation stage where strong nonlinearity occurs. This nonlinearity is caused by the formation of micro cracks ahead of the notch as the matrix begins to fail. This is characterized by an increase in displacement and a corresponding decrease in load as shown in Figures (8.1a and 8.1b).

The peak load increases with thickness as shown. For example from Figures (8.1a, 8.1b and 8.2a), the peak load for a twelve layer cracked specimen is 3.4 kN, while for similar sixteen and twenty layer specimens peaks of 4.1 kN and 6.9 kN are obtained respectively. It is worth noting that the strength of the specimen can also be affected by the fiber orientation. Test results presented in Figure (8.2a) show that the peak load carried by a (0/45/90) fiber orientation is larger than the one carried by a specimen with the same number of layers but with a fiber orientation of (0/90/0).

Clearly, we have a manifestation of stiffness degradation and loss of carrying capacity. From the plot of load versus crack opening displacement, Figures (8.1a, 8.1b and 8.2a), the strength is affected throughout the test. The stiffness decreases as the number of cycles beyond the peak load increases Figures (8.2b). The value of the stiffness is determined for a given cycle. This degradation in stiffness is due to matrix failure at the tip of the crack in the composite and as a result the load is carried predominantly by the fibers.

8.3 Fracture Toughness and Fracture Energy

Under the assumption of linear elastic fracture mechanics (LEFM), fracture toughness can be evaluated using the concepts of effective crack length. The critical load and

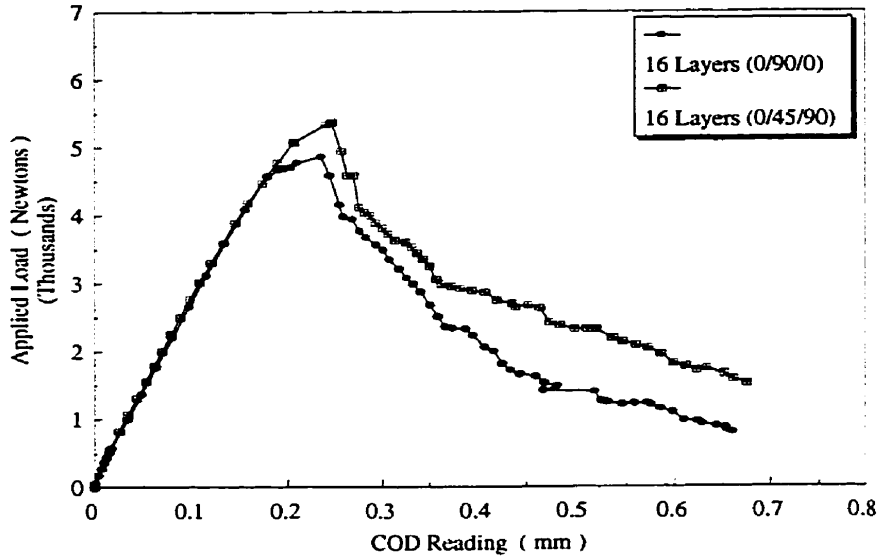

(a)

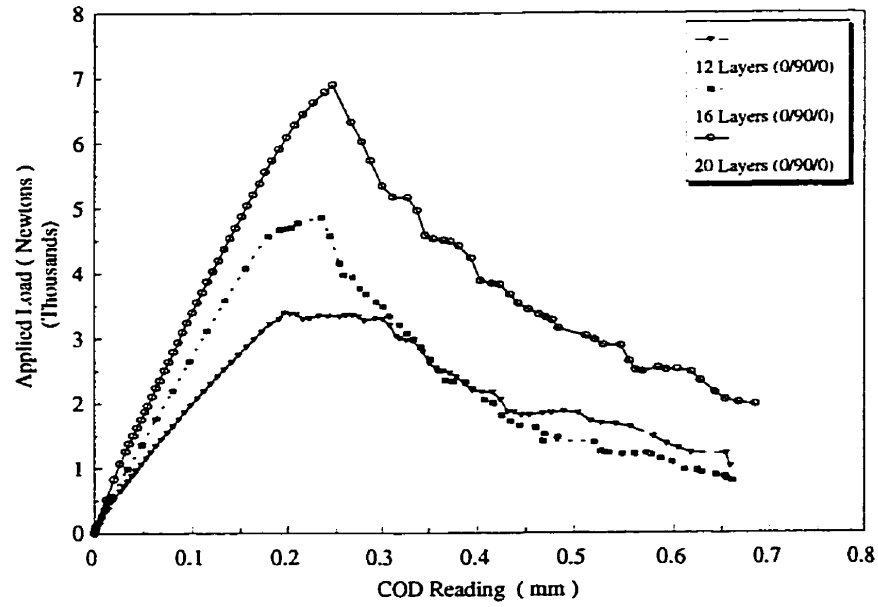

(b)

Figure 8.1: Comparison of the Behaviour of (a) Two Specimens of Different Fiber Orientation, (b) Three Specimens of Different Thickness.

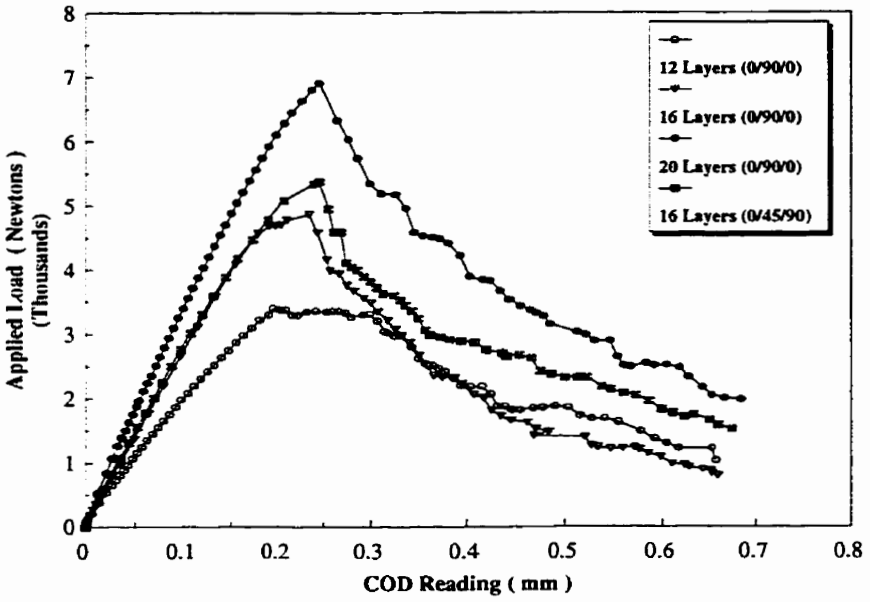

(a)

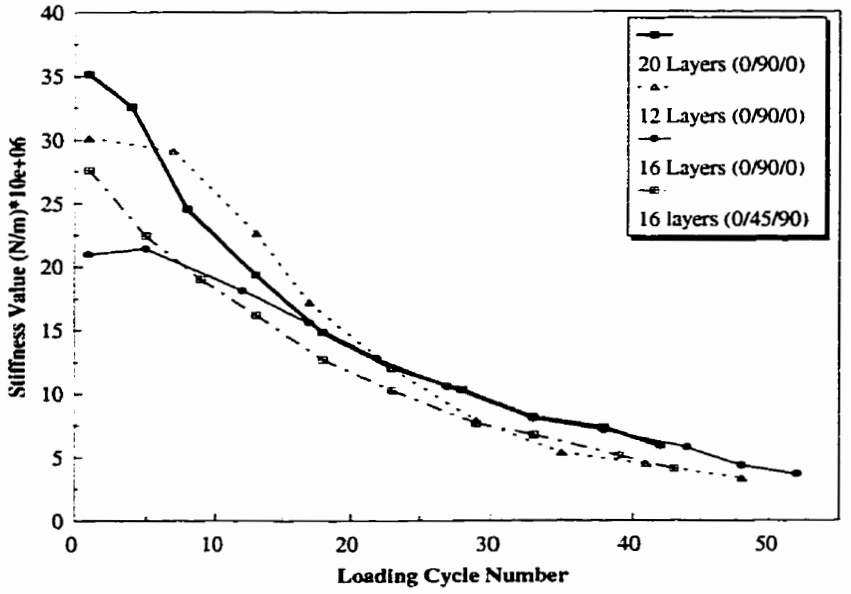

(b)

Figure 8.2: (a) Comparison of the Behaviour of Four Specimens of Different Thickness and Fiber Orientation, (b) Stiffness Degradation under Different Loading Cycles for Different Specimens.

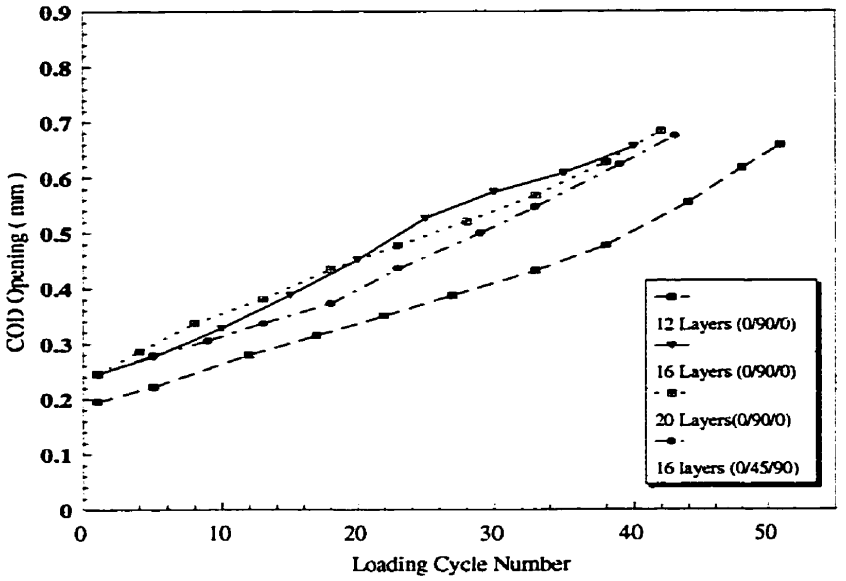

(a)

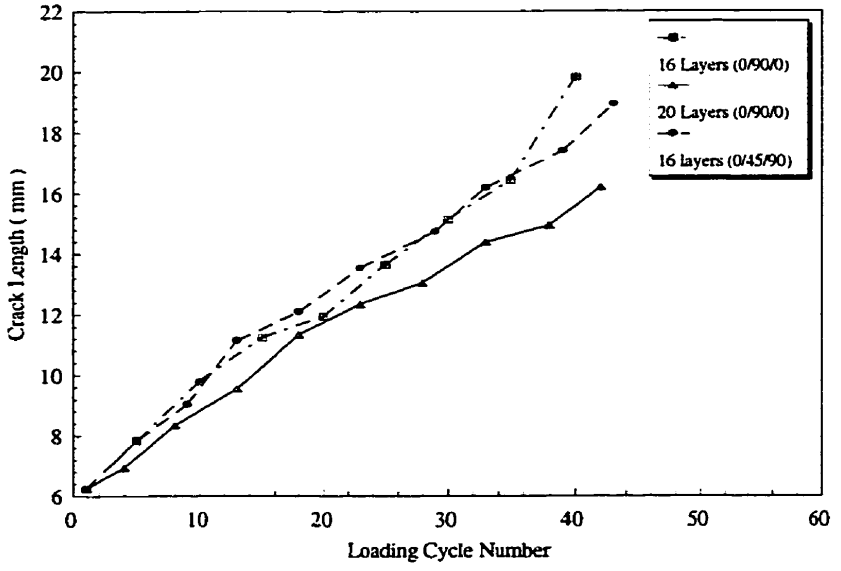

(b)

Figure 8.3: (a) Measured Crack Opening Displacement as a Function of the Number of Loading Cycles, (b) Measured Crack Length as a Function of The Number of Loading Cycles.

the calibration function for a particular specimen depends on the geometry. Specimen geometries used herein have the following calibration function [119]:

$$f\left(\frac{a}{w}\right) = 0.265\left(1-\frac{a}{w}\right)^4 + \frac{0.857+0.265\left(\frac{a}{w}\right)}{\left(1-\frac{a}{w}\right)^{\frac{3}{2}}} \tag{8.1}$$

where a is the crack length and w is the width of the specimen. Specimen geometries used herein have a constant notch to depth ratios equal to 0.25.

The crack advance da is measured using a microscope with an accuracy of 0.001mm which is mounted on to the Instron machine. The effective crack length a_{eff} is defined as the sum of the initial notch length and effective crack advance or extension: $a_{eff} = a_0 + da$, where a_0 is the initial crack length and da is the crack growth during loading. The effective crack length is updated at each cycle and the fracture toughness can be calculated using:

$$K_{IC} = \frac{P_C}{wt}\sqrt{\pi a_{eff}}\left[f\left(\frac{a}{w}\right)\right] \tag{8.2}$$

where

P_C is the corresponding critical load

t is the specimen thickness

a_{eff} is the effective length of the crack

a is the length of the crack or notch

Tables (8.2, 8.4, 8.5 and 8.6) give the values of the fracture toughness K_{IC} obtained for different specimens for different loading cycles. Fracture toughness versus crack length and number of loading cycles are plotted in Figure (8.4a and b). It is clear the fracture toughness is affected by crack length increase as well as the number of loading cycles and applied load.

In general, as can seen from the Figure (8.4a), the K_{IC} values as function of a_{eff} fluctuate between minimum and maximum value. This may be caused by the epoxies

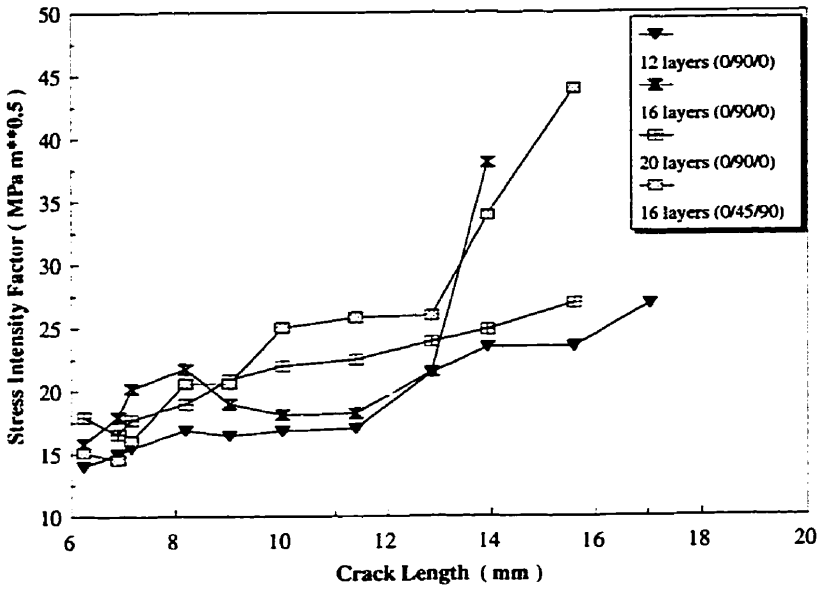

(a)

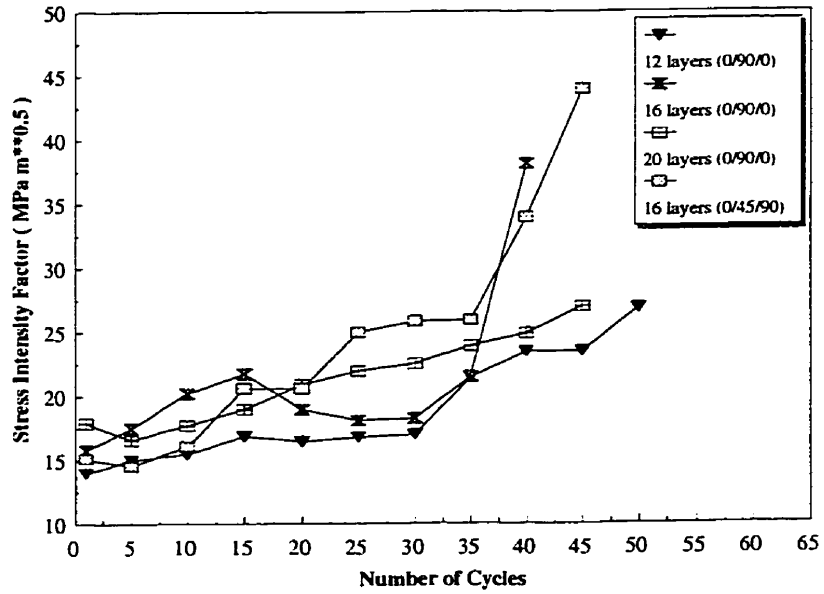

(b)

Figure 8.4: a) Fracture Toughness Versus Crack Length, b) Fracture Toughness Versus Number of Loading Cycles.

hard and weak spots in random manner. It can be seen that the K_{IC} increases in the first stage of the curve, this is because of increasing size of the microcracked zone at the crack tip; which is the stage of formation of the fracture process zone. Then there is sudden decrease of K_{IC} in the second stage. This sudden drop in K_{IC} values may be explained as part of fracture energy is dissipated in crack propagation rather than in the fracture process zone. Finally, the values of K_{IC} starts to increase again at the last stage. This explains the fact that the crack propagates faster and less fracture energy is needed to be dissipated during propagation of the crack.

8.3.1 Determination of Fracture Energy G_f

The fracture energy G_f of a notched specimen is defined as the area under the complete load-deflection curve for a complete fracture of the specimen divided by the ligament area (for details, see ref. [9]), hence, we can write:

$$G_f = \frac{A_T}{(w-a)\,t} \tag{8.3}$$

where A_T is the total area under the load-deflection curve. Using the experimental results, it is also possible to estimate the incremental energy dissipation for each cycle. After the first loading cycle the crack advances to $a = a_0 + \Delta a$, and a new surface area $t\Delta a$ is formed. The work necessary to create this new surface is related to the incremental energy dissipation $G_f^{\Delta a}$ via

$$G_f^{\Delta a} = \frac{A^{\Delta a}}{t.\Delta a} \tag{8.4}$$

where $G_f^{\Delta a}$ is the fracture energy dissipation for a certain loading cycle. $A^{\Delta a}$ is the work necessary to create the new surface (i.e. the area under current loading cycle see Figure 8.5) and $\Delta a.t$ is the ligament area of corresponding to the current loading cycle.

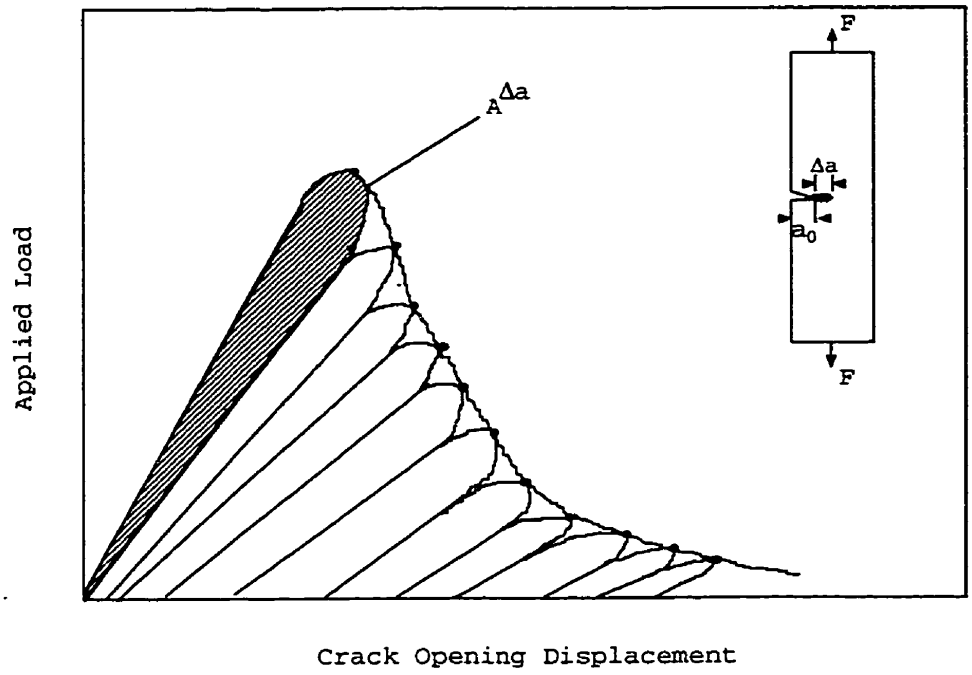

Figure 8.5: Typical Load-COD Response.

The fracture energy is calculated from the measured data and tabulated in Tables (8.1 and 8.3). The results are plotted versus thickness (see Figure 8.6).

The fracture energy calculated from the complete load-deflection curve of each specimen is found to be size dependent (i.e. depends on the ligament length). This response is similar to other engineering materials where the fracture energy G_f depends on the ligament length. Also there are no fracture mechanics parameters which are independent of the size of the specimen.

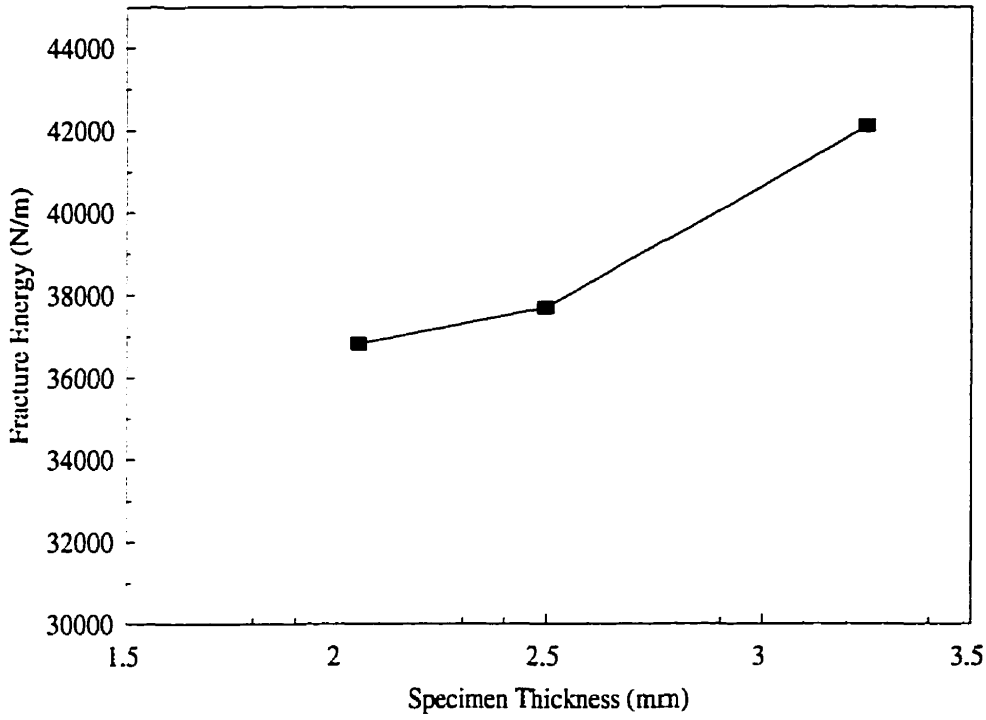

Figure 8.6: Fracture Energy Versus Thickness.

Table 8.1: Calculation of Fracture Energy for Test Group # 1

Number of layers	Fiber Orientation	Thickness (mm)	Peak Load (N)	Fracture Energy (N/m)	Number of Cycles
12	0/90/0	2.05	3398	36820	50
16	0/90/0	2.50	4310	37686	50
16	0/45/90	3.00	5372	34349	50
20	0/90/0	3.25	6904	42113	50

Table 8.2: Typical Results for 12 Layers Specimen of (0/90/0) Fiber Orientation

Cycle Number	Applied Load (N)	Total Elongation (mm)	COD Reading (mm)	Crack Length (mm)	Fracture Toughness ($MPa\sqrt{m}$)
1	3398	1.18	0.19	6.25	13.9
5	3303	1.24	0.22	6.90	15.0
10	3271	1.29	0.28	7.15	15.5
15	3043	1.28	0.32	8.20	16.8
20	2620	1.23	0.35	9.03	16.5
25	2303	1.20	0.39	10.0	16.8
30	1869	1.17	0.43	11.40	16.9
35	1855	1.19	0.48	12.85	20.2
40	1631	1.21	0.55	13.93	23.4
45	1225	1.21	0.62	15.60	23.5
50	1026	1.21	0.66	17.05	26.8

Table 8.3: Calculation of Fracture Energy for Test Group # 2

Number of layers	Fiber Orientation	Thickness (mm)	Peak Load (N)	Fracture Energy (N/m)	Number of Cycles
12	0/90/0	2.05	3308	35903	50
16	0/90/0	2.50	4678	42113	50
16	0/45/90	3.00	5481	35205	50
20	0/90/0	3.25	6908	42310	50

Table 8.4: Typical Results for 16 Layers Specimen of (0/45/90) Fiber Orientation

Cycle Number	Applied Load (N)	Total Elongation (mm)	COD Reading (mm)	Crack Length (mm)	Fracture Toughness ($MPa\sqrt{m}$)
1	5372	1.50	0.24	6.25	15.1
5	4051	1.38	0.28	7.85	14.5
9	3733	1.36	0.31	9.05	16.1
13	3452	1.34	0.34	11.15	20.6
18	2958	1.30	0.37	12.10	20.6
23	2706	1.30	0.43	13.55	24.1
29	2326	1.30	0.51	14.75	25.8
33	2141	1.30	0.54	16.20	31.7
39	1771	1.32	0.62	17.40	34.3
43	1520	1.34	0.67	18.95	43.9

Table 8.5: Typical Results for 16 Layers Specimen of (0/90/0) Fiber Orientation

Cycle Number	Applied Load (N)	Total Elongation (mm)	COD Reading (mm)	Crack Length (mm)	Fracture Toughness ($MPa\sqrt{m}$)
1	4678	1.55	0.25	6.25	15.8
5	4161	1.58	0.28	7.85	17.4
10	3490	1.50	0.33	9.80	20.2
15	2988	1.43	0.38	11.25	21.7
20	2326	1.36	0.39	11.95	18.9
25	1661	1.30	0.45	13.65	18.1
30	1266	1.30	0.52	15.15	18.2
35	1145	1.32	0.58	16.45	21.5
40	835	1.34	0.65	19.85	38.1

Table 8.6: Typical Results for 20 Layers Specimen of (0/90/0) Fiber Orientation

Cycle Number	Applied Load (N)	Total Elongation (mm)	COD Reading (mm)	Crack Length (mm)	Fracture Toughness ($MPa\sqrt{m}$)
1	6904	1.60	0.25	6.25	15.1
4	5736	1.53	0.28	6.95	16.5
8	4965	1.47	0.34	8.35	17.7
13	4422	1.44	0.38	9.55	18.9
18	3678	1.39	0.43	11.35	20.9
23	3280	1.37	0.48	12.35	21.9
28	2984	1.36	0.52	13.05	22.5
32	2489	1.35	0.56	14.40	23.9
38	2335	1.37	0.63	14.95	24.8
42	1972	1.39	0.68	16.20	26.9

8.4 Summary

The effects of thickness and fiber orientation on the fracture of short fiber composite materials are studied. The stiffness degradation, compliances and crack length are measured. Based on the experimental results, the following observations are made:

1) The initial linear response is followed by a secondary response which signals the load transfer between the matrix and the fibers. Prior to the peak load, non linearity occurs due to the formation of micro-cracks in the vicinity of crack tip.

2) The post-peak response is marked with a gradual decrease in stress accompanying an increase in displacement.

3) The strain energy accumulated in the specimen is released at the peak-load and a stable crack propagates with increase in displacement and reduction in the load.

4) The strength of the specimen is clearly affected by the fiber orientation i.e. the load carried by (0/45/90) fiber orientation specimen is larger then the one carried by a specimen with the same number of layers but with fiber orientation (0/90/0). The reason is that as the crack approaches inclined fibers, it changes direction so as to run parallel to them for a considerable distance, sometimes to the end of the fiber, but sometimes eventually turning again to cross the fiber and resume forward progress.

5) The results showed a gradual degradation in the stiffness and a concurrent loss of carrying capacity, i.e. beyond the peak load, the value of stiffness decreases as the number of cycles increases.

6) The post peak regime may be expressed as a bilinear form in terms of the crack opening displacement.

7) The fracture toughness of composite materials decreases with increasing notch-width ratio $\left(\frac{a}{w}\right)$.

8) The fracture toughness is dependent on the specimen thickness.

9) The fracture energy calculated (referred to as G_f) indicates that G_f is affected by the thickness of the specimen and the fiber orientation.

10) Cracks advance linearly as a function of number of loading cycles.

Chapter 9

CONSTITUTIVE MODELING OF COMPOSITES-A FRACTURE MECHANICS APPROACH

9.1 Introduction

Much of the early work on fracture of composites involved investigations of the applicability of linear elastic fracture mechanics. The earliest work in the field of fracture mechanics was done by Griffith in 1920 [40]. The Griffith theory considers that the stress act perpendicular to the axis of the crack and with the crack presumably growing along the crack axis. This type of failure is generally described as Mode I failure, and is the basis for most fracture-based models since that time. Griffith developed the discrepancy between measured and predicted strength of glass by considering the stability of a small crack using an energy balance. This means, with an increase in the tensile load, the crack would propagate when the strain energy release rate associated with crack growth is greater than the surface tension of the new crack. In

1949 and 1950 Irwin [50] and Orowan [79] modified the Griffith analysis to include energy absorption due to plastic deformation at the crack tip. They used several approaches for solving different composite fracture problems. Their approaches, are now referred to as the "stress intensity factor" approach and the "strain energy release rate" approach. Much of the early work in the field of modern fracture mechanics occurred in the nineteen sixties and was devoted to the fracture of metals. In the seventies, research in cementitious materials polarized the bulk of the contributions and numerous models were proposed to explain cracking in concrete. New composite materials emerged in the recent history and better models were required to explain these failure properties.

In a given composite laminate, the fibers have a statistical distribution of strength. As the applied load to a laminate increases, the weaker fibers fail and redistribute their load to the surrounding fibers by a shear transfer mechanism through the matrix. In a notched specimen, when the stress concentration around the crack tip rises, the first fibers to fail in a laminate are those in the immediate vicinity of the notch tip. Consequently, the strain energy released must be absorbed by the surrounding matrix and adjacent fibers. Load may continue to be applied after fiber failure as long as the strain energy released by that fiber can be absorbed by the surrounding matrix and fibers.

The purpose of this chapter is to provide a mathematical interpretation of the underlying failure mechanism behind crack growth in composite materials. By associating the matrix failure partial fiber breakage with a degradation of the elastic modulus ahead of the crack (in a continuum damage sense), the experimental critical load at the onset of crack growth provide us with the progressive degradation of the elastic modulus in the vicinity of the crack tip. The internal parameters, associated with damage is computed. Section 9.3 proposes a new crack model for composite materials.

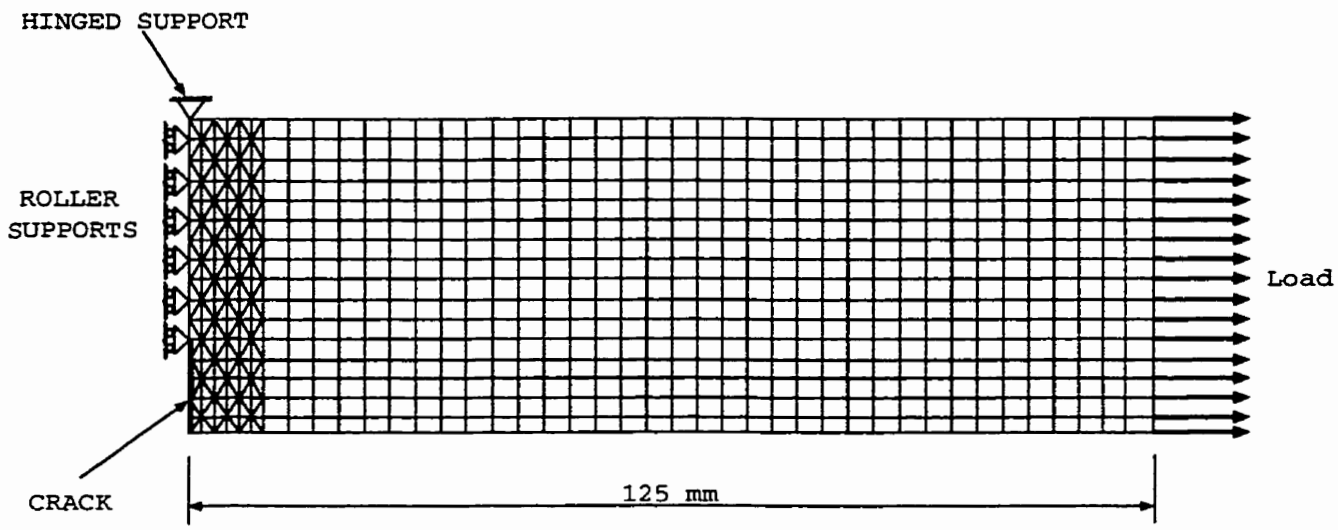

Figure 9.1: Finite Element Mesh for Half of the Specimen.

9.2 Continuum Elastic Degradation

With reference to test results presented in chapter 7, a model will be proposed which duplicates the response of load versus COD by changing the elastic parameters in process zone. Denoting by E_1, E_2 and E_d, the primary, secondary and damaged elastic modulie of the composite. E_1 and E_2 are readily available from the uniaxial tension test shown in Figure (7.7). The damaged modulus, E_d, is the one that would describe the material behaviour at its damaged state. Obviously E_d must have a maximum value equal to E_2 and should decrease with progressive increase of damage in the matrix and fiber breakage. It is intended to determine the evolution of the magnitude of E_d with the progress increase in damage during crack advance. Typical test results for the 12 layers specimen of (0/90/0) fiber orientation are used to calibrate the model. The following steps are followed to determine the evolution of E_d:

(a) First the width of the damage zone (or process zone as referred to in the concrete community) t_d, shown in Figure (9.2 A and B) is measured and found to be equal to 10.4 mm.

(b) From the load-displacement response of Figure (7.7) the primary elastic modulus is obtained (in this case $E_1 = 11.7GPa$) and assigned to the undamaged part of the model i.e. away from the process zone as shown in Figure (9.2 B).

(c) The mesh shown in Figure (9.1) is generated, the elements ahead of the crack tip are first assigned the value of E_1 and when the stress level becomes above σ=19.51MPa the elements are assigned the value of E_2.

(d) The load is increased to the value of the experimental peak of 3399 N (see Figure 7.9), the stress intensity factor is computed and adopted to be $K_I = 13.7MPa\sqrt{m}$ the initial toughness of the material.

(e) At this stage the measured crack advance from the experiment is duplicated in the finite element model by releasing the corresponding support ahead of the notch, thus simulating further crack growth.

(f) In order to reproduce the post peak response of the specimen, the elements of the process zone are assigned a value of E_d=λE_2, where λ decreases by about 5% at each step. Using a unit load, and the value of the fracture toughness, the critical load and the COD are computed indirectly. The values of P_{cr} and corresponding COD are compared with experimental values. This step is repeated (decreasing E_d each time) until a good match with the experimental response is obtained (see Figures 9.3(a and b), 9.4(a and b)).

(g) The crack is advanced and step (f) is repeated. At each crack length, the critical load, and the corresponding values of E_d and damage are recorded.

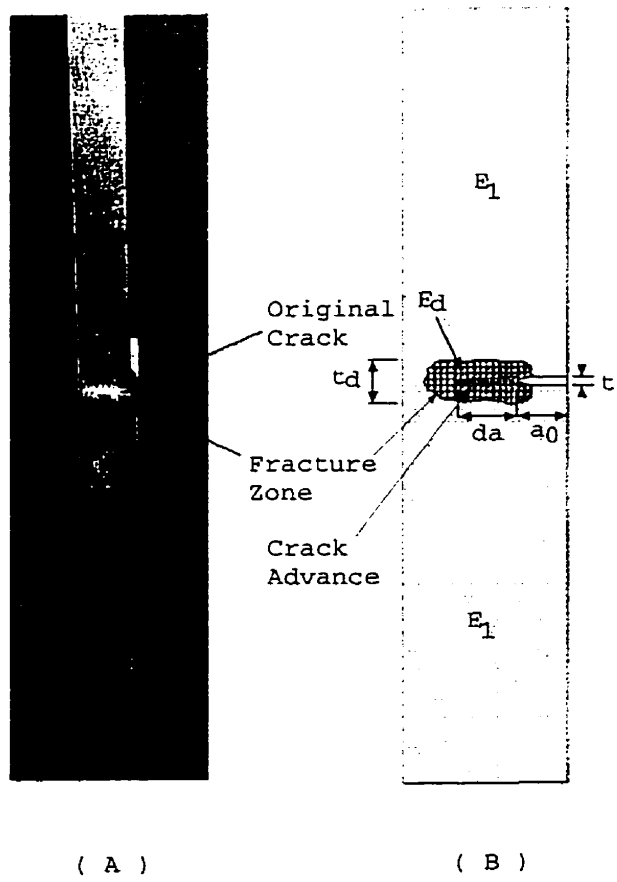

Figure 9.2: Illustration of Process Zone in Front of the Crack tip.

The above procedure was used in all test cases. Typical results are shown for the 12-layers specimens of (0/90/0) fiber orientation. Figures (9.3-9.7) illustrates the matching of the test data with the above analytical procedure. Figures (9.13, 9.12) provide a record of the evolution of E_d as a function of the crack length and COD, respectively.

Table (9.1) and Figure (9.14) show the damage progress as a function of a/a_0. A bilinear fit was found to be adequate in

1) Elastic Modulus as a function of COD ($x = COD$):

$$E(x) = (27.68 * \delta - 33.54)\, x - 5.408 * \delta + 13.36$$

$$Where \left\{ \begin{array}{l} \delta = 0 \ldots\ldots\ldots if \ldots\ldots\ldots 0.0485 \leq x \leq 0.195 \\ \delta = 1 \ldots\ldots\ldots if \ldots\ldots\ldots 0.1950 \leq x \leq 0.605 \end{array} \right\}$$

2) Elastic Modulus as a function of Crack Length ($x = CrackLength$):

$$E(x) = (3.603 * \delta)\, x - 27.02 * \delta + 36.2$$

$$Where \left\{ \begin{array}{l} \delta = 0 \ldots\ldots\ldots if \ldots\ldots\ldots 6.25 \leq x \leq 7.5 \\ \delta = 1 \ldots\ldots\ldots if \ldots\ldots\ldots 7.50 \leq x \leq 15 \end{array} \right\}$$

9.3 Discrete Crack Band New Model

In Chapter 3, three finite element crack models were discussed. These are: "Discrete Crack Model," "Smeared Crack Model," and "Crack Band Model." The experimental investigation on composite specimens showed that crack growth is associated with a simultaneous propagation of a damage zone of constant thickness. In addition, one could establish a procedure to determine the evolution of the internal damage

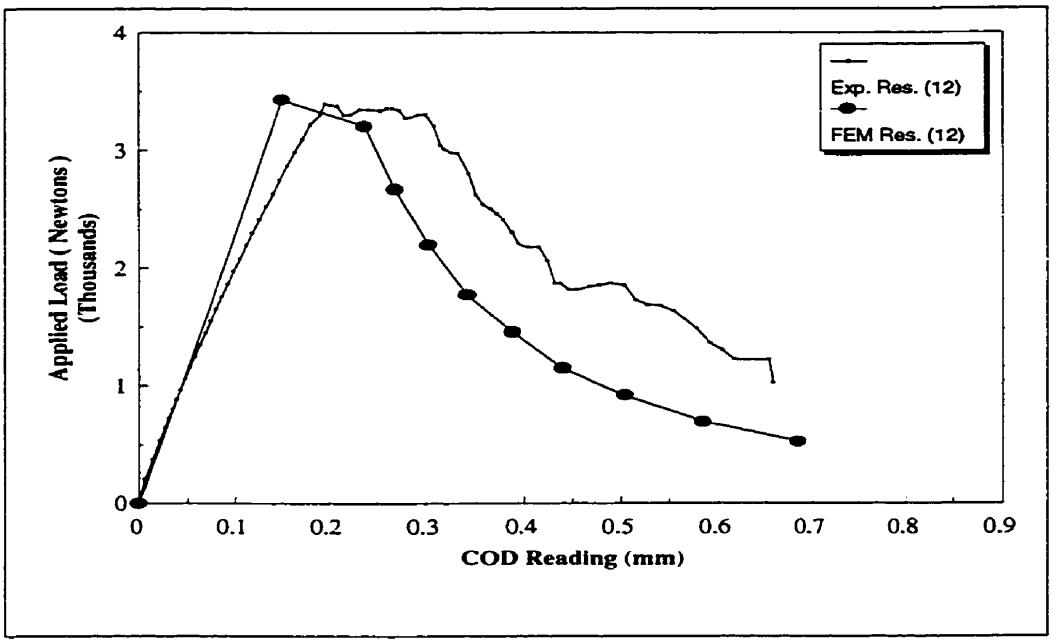

(a)

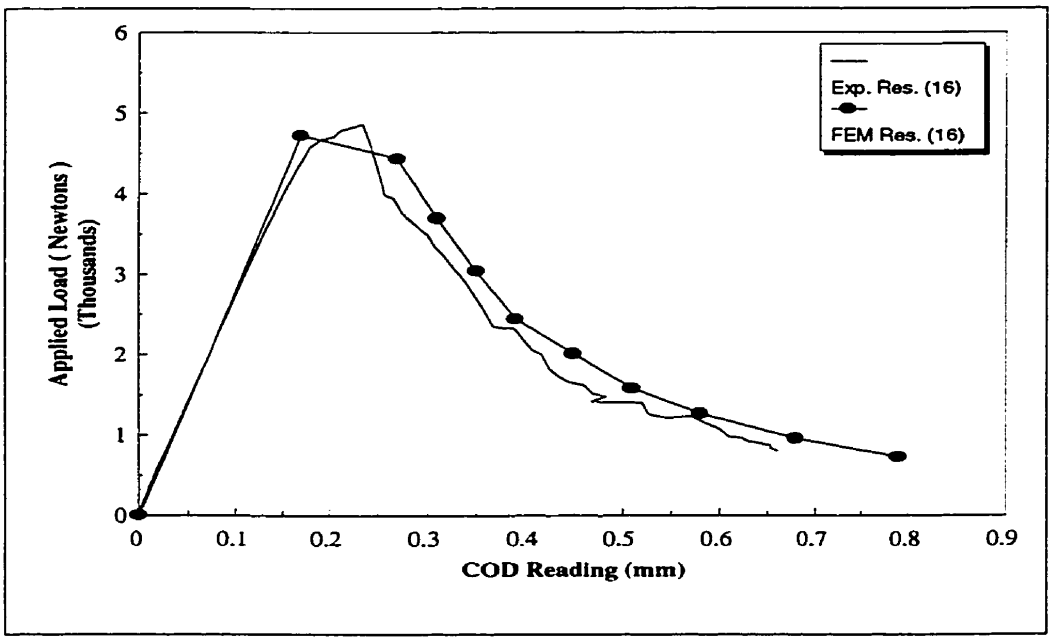

(b)

Figure 9.3: Comparison of Experimental and FEM Results: a) 12 Layers Specimen. b) 16 Layers Specimen of (0/90/0) Fiber Orientation.

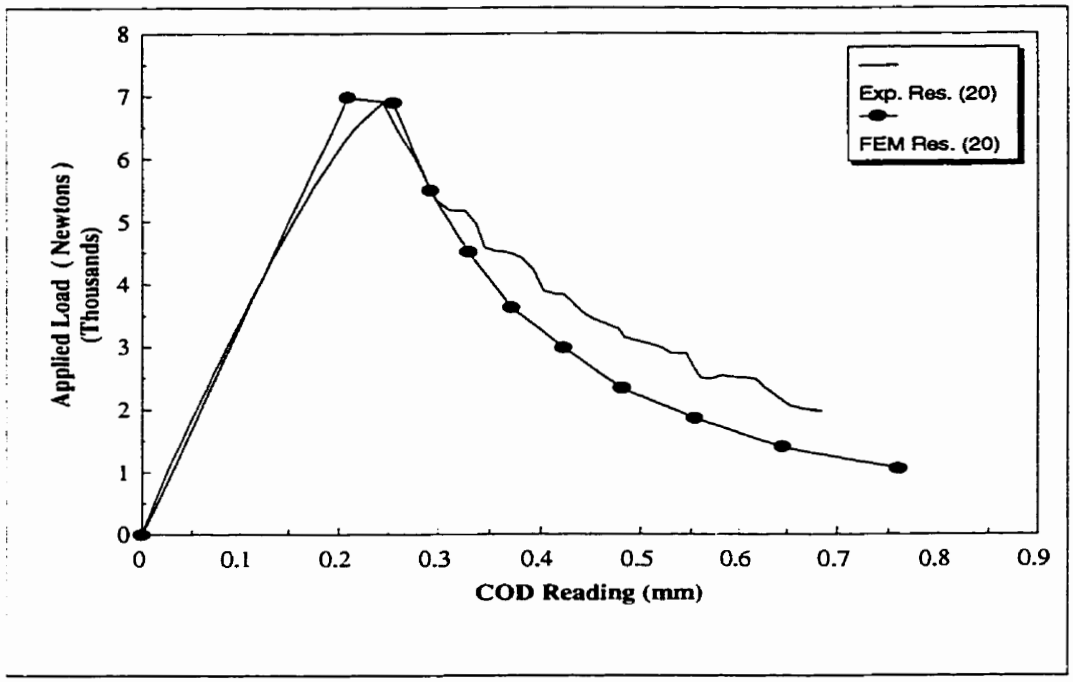

(a)

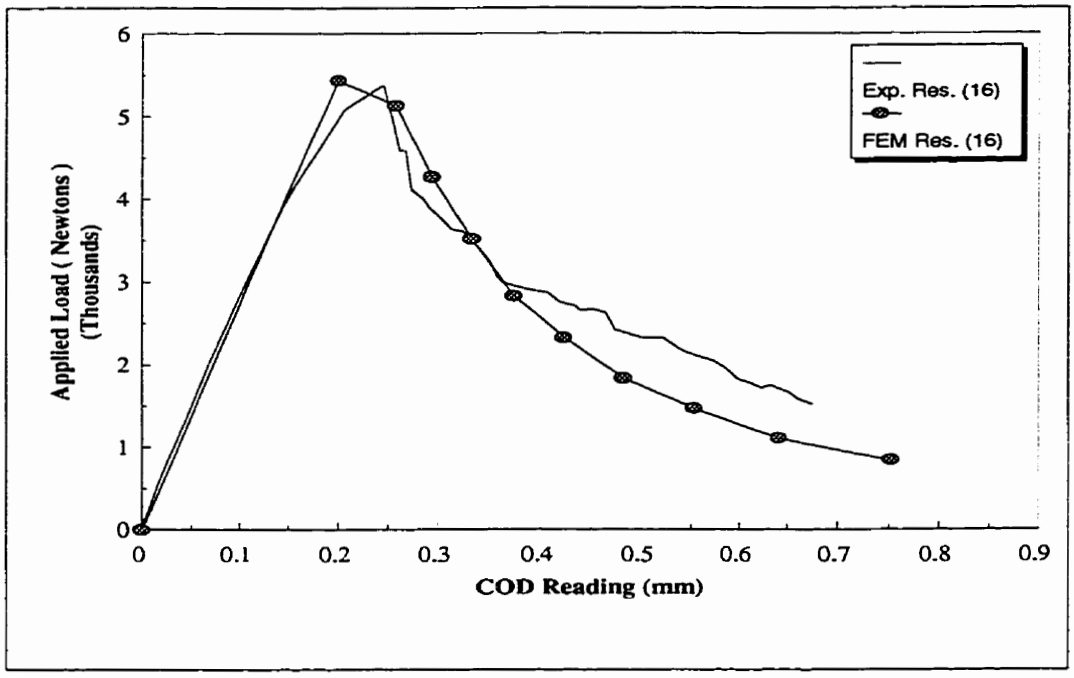

(b)

Figure 9.4: Experimental and FEM Results: a) 20 Layers Specimen of (0/90/0) Fiber Orientation. b) 16 Layers Specimen Of (0/45/90) Fiber Orientation.

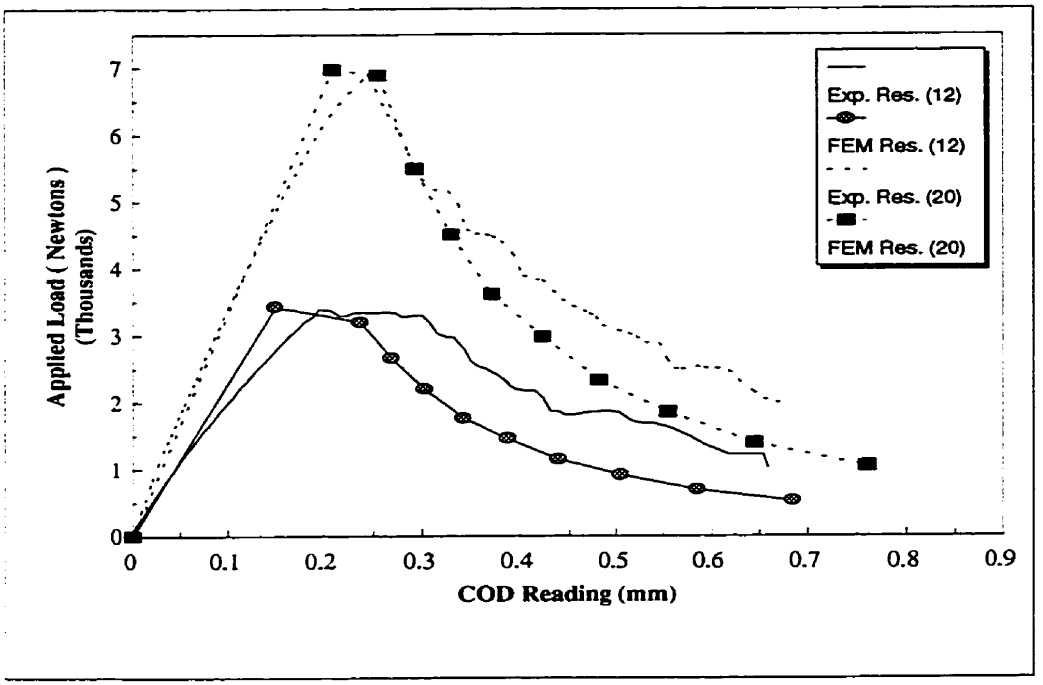

(a)

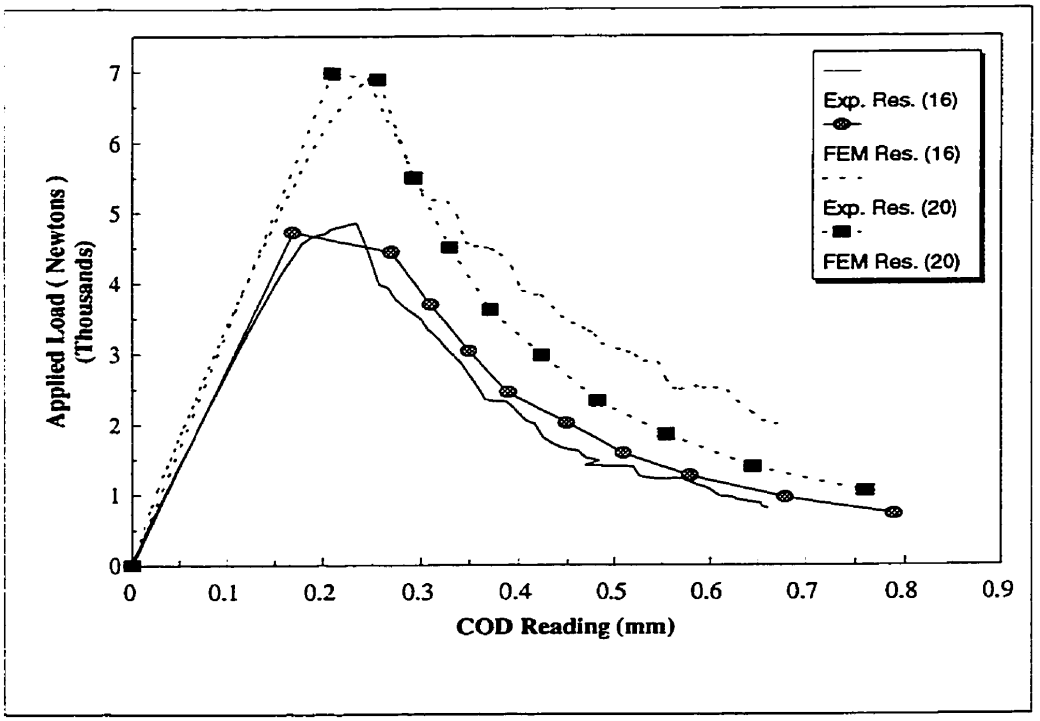

(b)

Figure 9.5: Experimental and FEM Results: a) 12 and 20 Layers Specimens. b) 16 and 20 Layers Specimens of (0/90/0) Fiber Orientation.

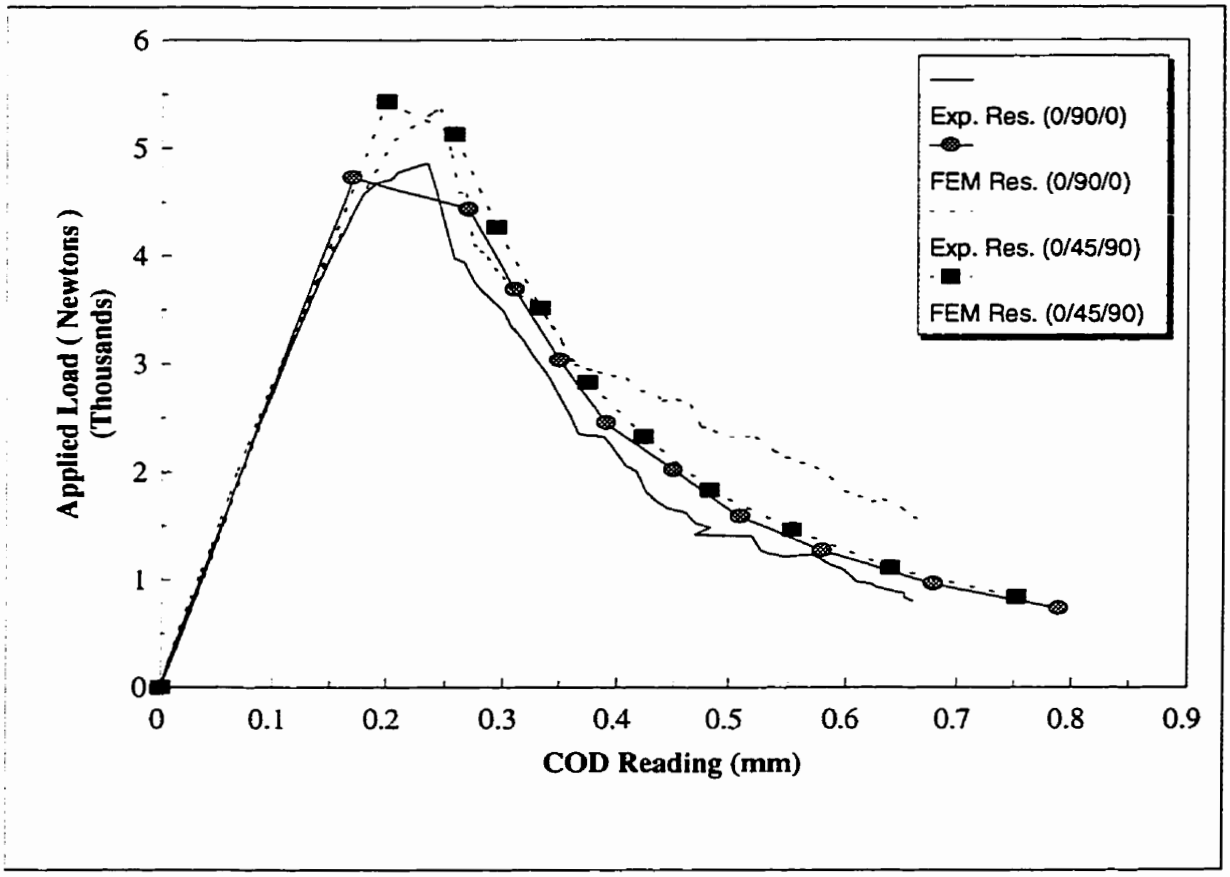

Figure 9.6: Experimental and FEM Results: 16 Layers Specimens of Different Fiber Orientation.

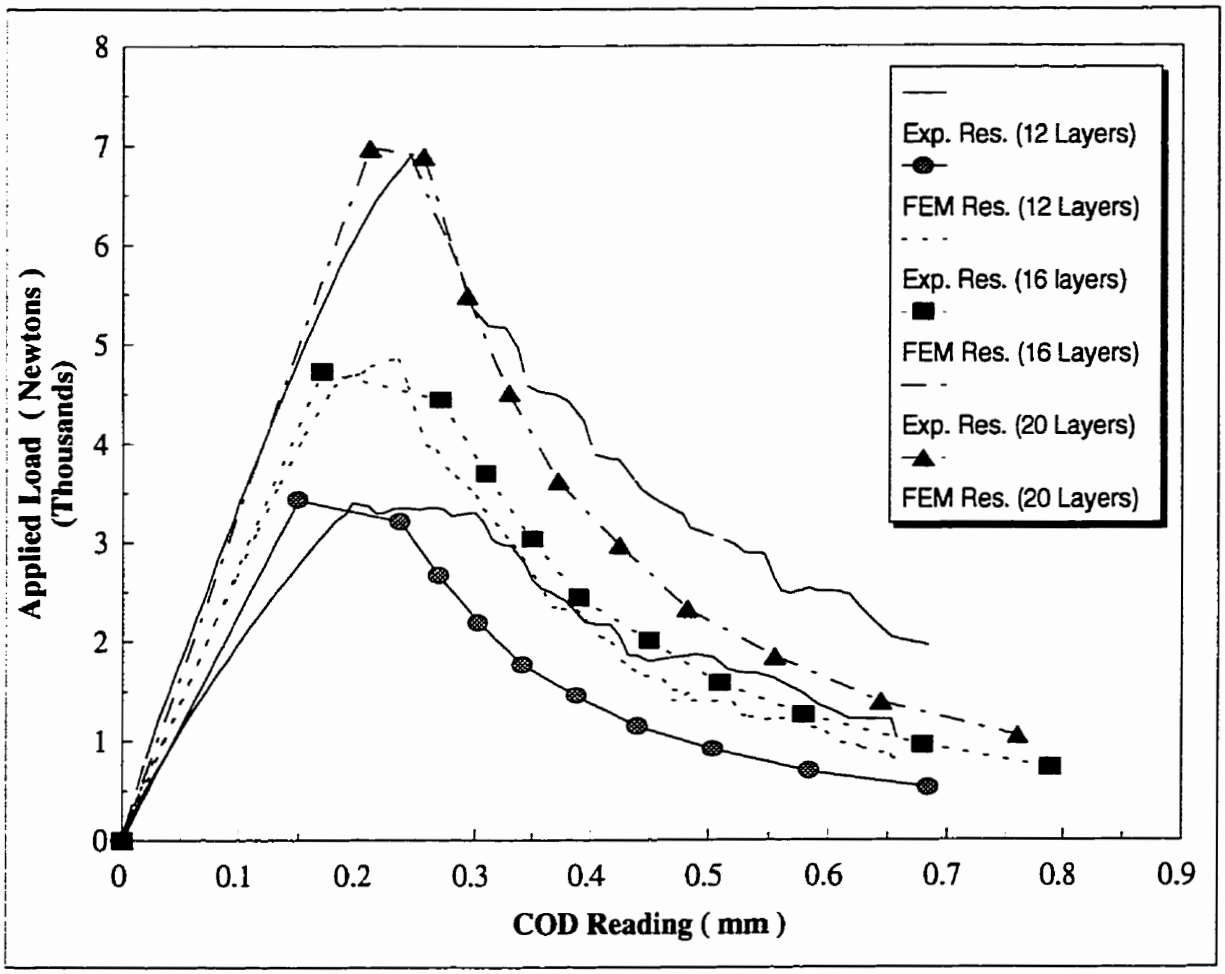

Figure 9.7: Experimental and FEM Results of Three Specimens of the Same Fiber Orientation (0/90/0) but Different Thickness.

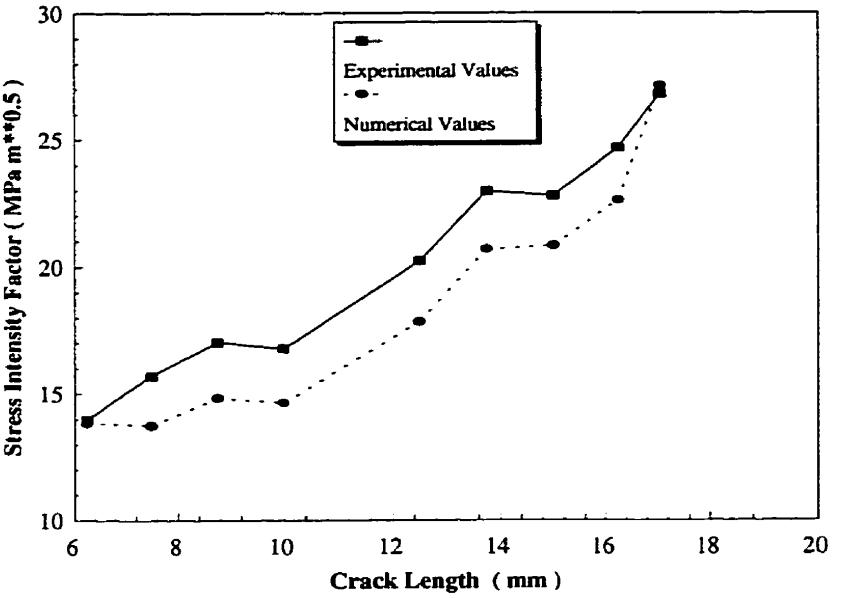

Figure 9.8: Typical Experimental and FEM Results of the Stress Intensity Factor of 12 Layers Specimen of (0/90/0) Fiber Orientation.

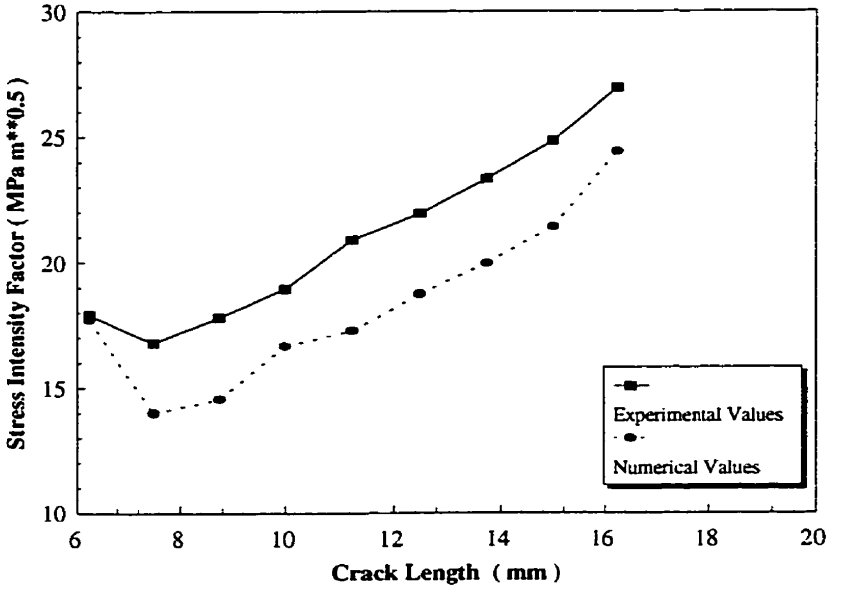

Figure 9.9: Typical Experimental and FEM Results of the Stress Intensity Factor of 20 Layers Specimen of (0/90/0) Fiber Orientation.

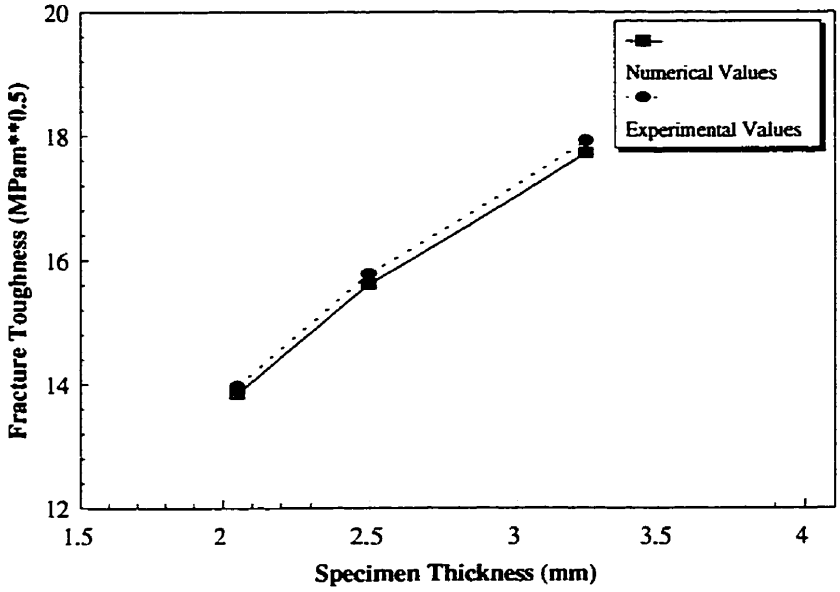

Figure 9.10: Experimental and FEM Values of the Fracture Toughness of Three Specimens of the Same Fiber Orientation (0/90/0) but Different Thickness.

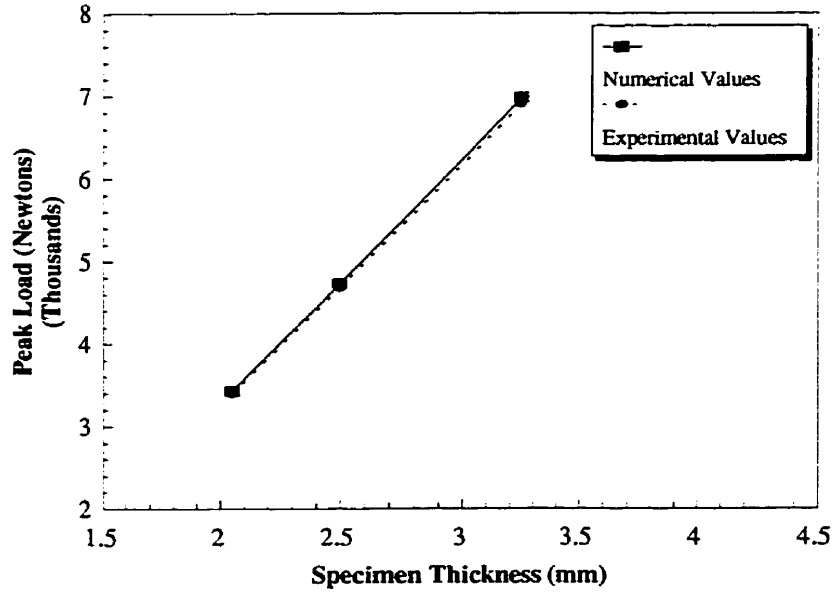

Figure 9.11: Experimental and FEM Values of the Peak Load of Three Specimens of the Same Fiber Orientation (0/90/0) but Different Thickness.

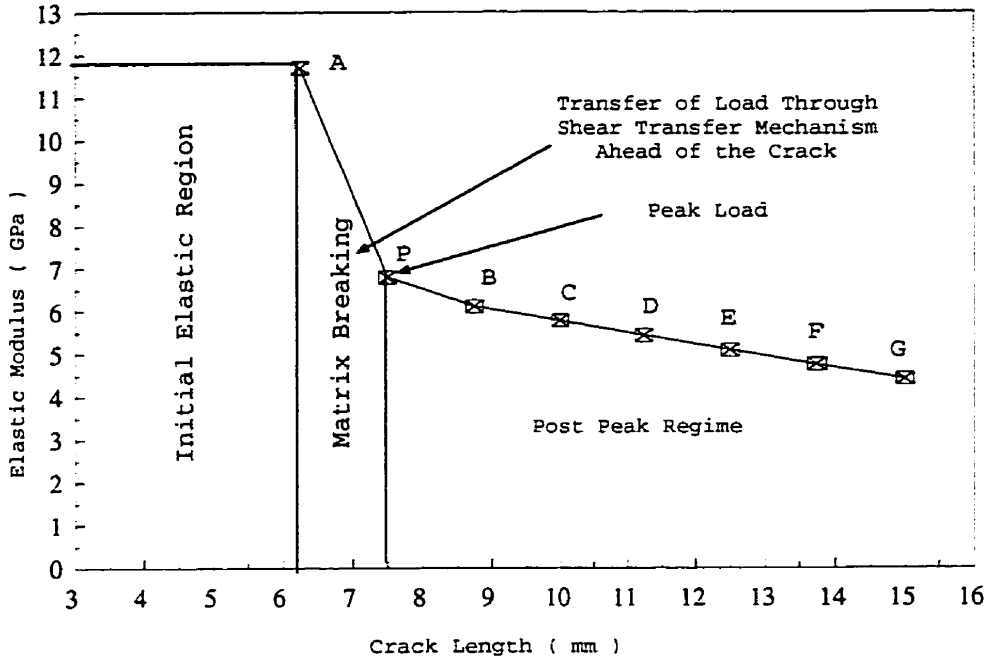

Stiffness Degradation Vs Crack length of
12 Layers Specimen of (0/90/0)

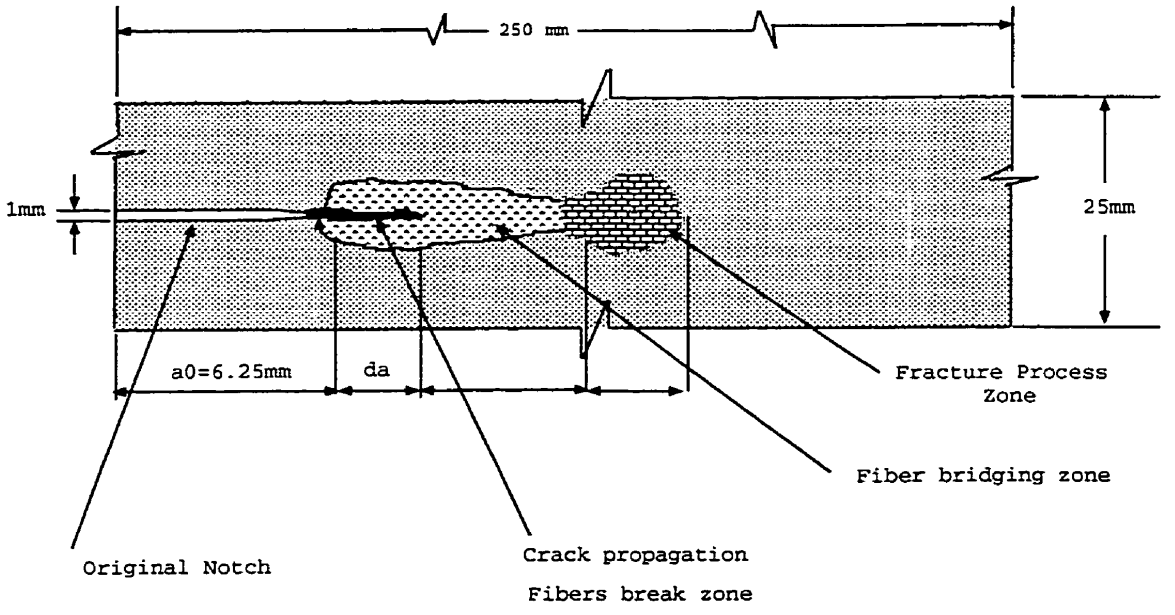

Figure 9.12: FEM Results Showing the Degradation in Stiffness as a Function of Crack Length, and a Diagram Showing the Inelastic Zone in Front of the Crack Tip.

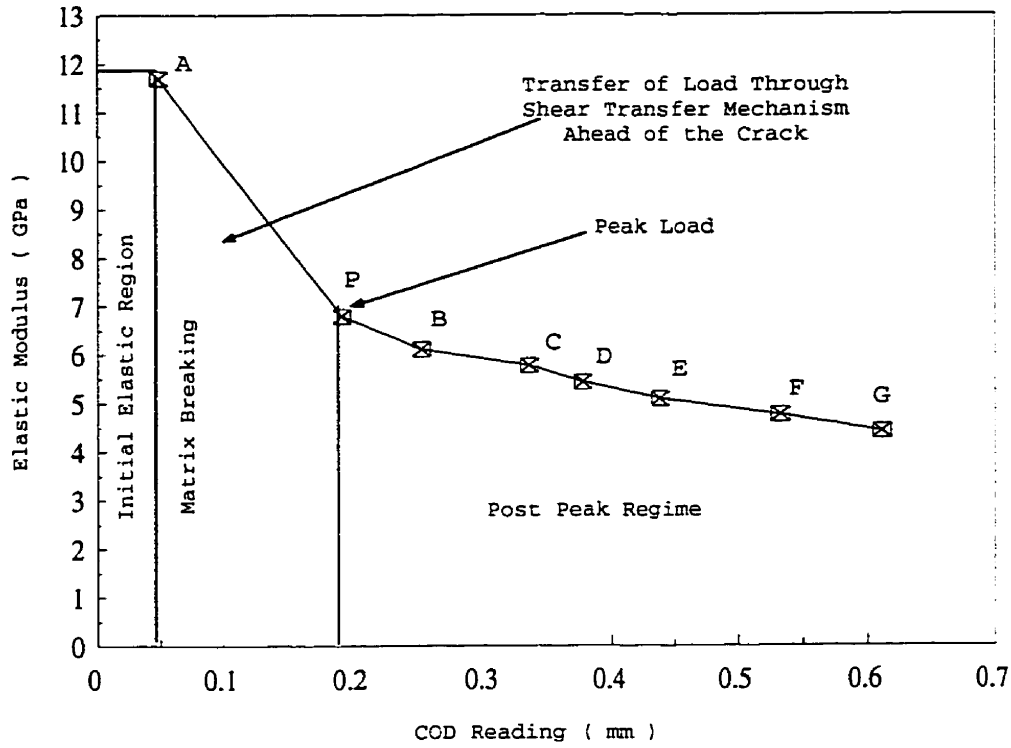

Stiffness Degradation Vs COD of
12 Layers Specimen of (0/90/0)

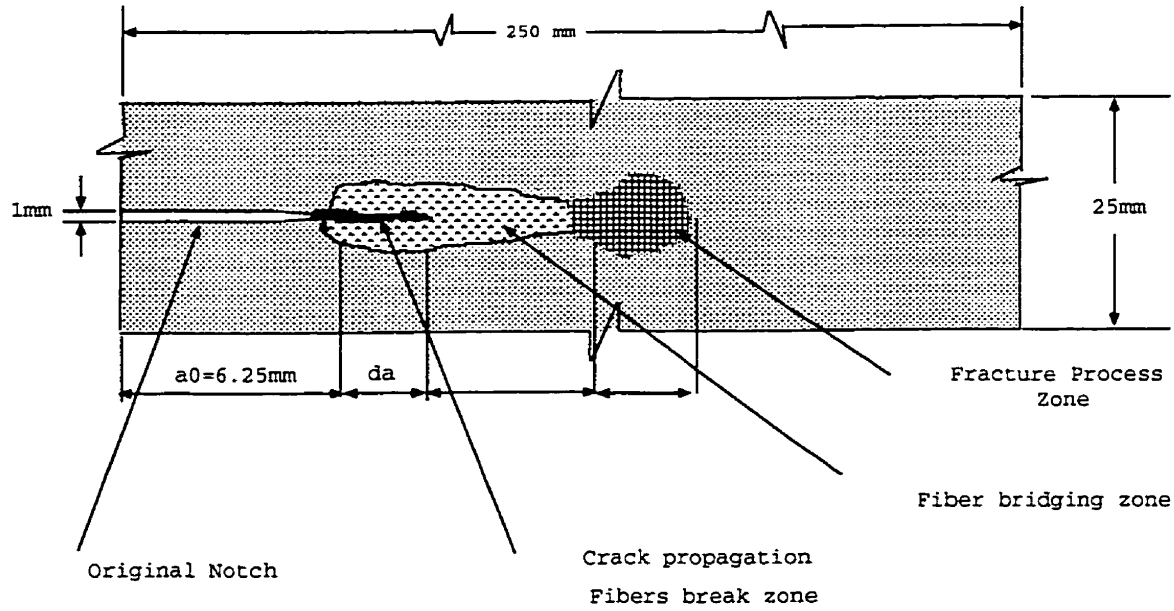

Figure 9.13: FEM Results Showing the Degradation in Stiffness as a Function of COD, and a Diagram Showing the Inelastic Zone in Front of the Crack Tip.

Table 9.1: Typical Results for 12 Layers Specimen of (0/90/0) Fiber Orientation

Applied Load Newtons	Elastic Modulus (GPa)	Crack Length (mm)	COD (mm)	Damage Parameter
3340	6.80	7.50	0.254	0.42
3011	6.12	8.75	0.318	0.48
2464	5.78	10.00	0.372	0.51
1966	5.44	11.25	0.428	0.54
1690	5.10	12.50	0.527	0.56
1304	4.76	13.75	0.604	0.59
1026	4.42	15.00	0.658	0.62

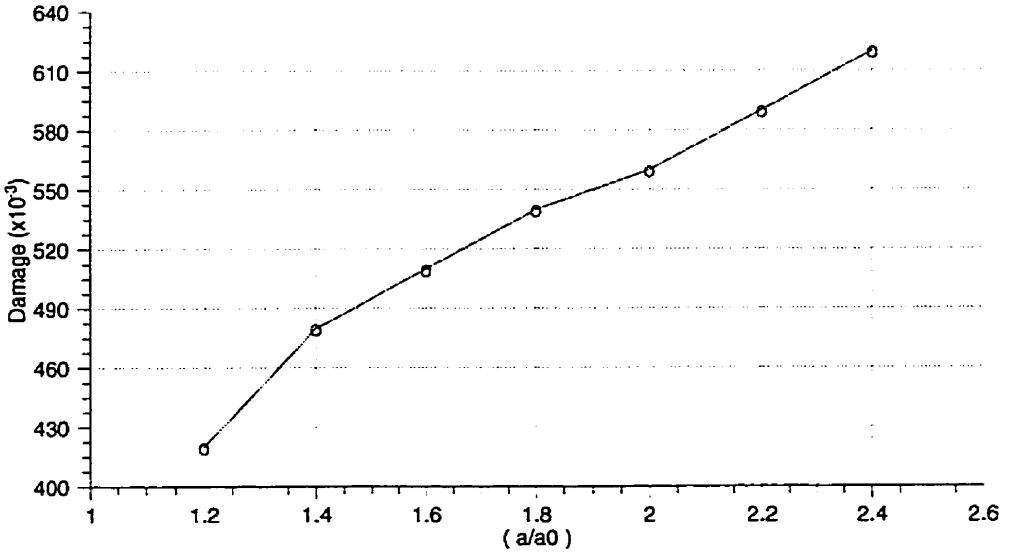

Figure 9.14: Variation of Damage Versus Crack Ratio.

parameter D with crack growth, or equivalently the degradation in elastic modulus E.

In order to duplicate crack growth in composite materials, it is proposed to model crack growth using the discrete crack model and concurrently model the associated surrounding damage evolution with the accumulation of the internal parameter D along and ahead of the crack. As reported in Section (9.2) the width of the damage band in 12 layers fiber glass specimen of (0/90/0) fiber orientation composite is 10.4 mm and the extent of damage is 5.0 mm long ahead of the tip.

9.3.1 Finite Element Implementation

The modeling of crack growth is simulated by continuously updating the mesh topology by, nucleating and growing a discrete crack, and also by propagating a damaged band of thickness 10.3 mm (see Figure 9.2). The elements within the crack band are monitored via the damage parameter D and therefore their elastic modulus will be degraded continuously.

9.3.2 Onset and Direction of Crack Growth

As discussed in Chapter 3, three leading models were proposed in the literature to establish the onset and direction of crack growth in isotropic media. Extensions were also developed to anisotropic continua. However, to the best knowledge of the author, no model which accounts for damage exists today.

Experimental evidence, presented in Appendix (C), show that for an inclined crack the direction of crack growth is always perpendicular to the direction of maximum principal stress at some distance away from the crack tip. Note that This can be

explained by the occurrence of damage ahead of the crack. For the sake of the argument, we consider the limiting case, in which the damage zone ahead of the crack has a nil modulus (i.e. the damage zone is simply a hole) ahead of the crack. Further crack propagation would emanate from the furthest edge of the damage zone away from the tip and in the direction perpendicular to the maximum principal stress. Hence for the case of a specimen with inclined crack, with respect the applied load, the direction of crack propagation occurs in the direction perpendicular to the applied load path. (see Figures C.15, C.17, and C.20) in Appendix (C).

An extension of the minimum strain energy density criterion (see section (4.3.3.3)) may be the best candidate for evaluating the onset of crack growth, due to the fact that its evaluation is performed at a distance "r" from the tip of the crack.

Chapter 10

CONCLUSIONS AND RECOMMENDATION FOR FUTURE RESEARCH

10.1 General

For the past few decades structural composites made of fiber polymers composites have been used in the fields of mechanical, aeronautical and aerospace engineering. Initially, these advanced materials were directed to military applications, principally for aircrafts and space system structures. Currently, a very broad technological and applications base has been established for these materials in different fields of engineering industries.

Putting this new material in actual use requires careful design practices and appropriate developments based on the understanding of their unique mechanical and physical properties. This thesis is intended to contribute to the ongoing effort towards understanding the mechanical and fracture behaviour of composite materials.

10.2 Conclusions

Based on the theoretical, numerical, and experimental investigation, the following conclusions are summarized.

10.2.1 Finite Element Computation of Interlaminar Buckling Load

Generalization of the correlation technique for stress intensity factor extraction, to account for the axial compressive or tensile field, is presented and the following conclusions are made:

1) The proper formula for extracting the effective axial stress ahead of a crack tip is successfully derived as well as the finite element extraction and measure of the axial stress factor ahead of the crack in two dimensional analysis are made possible.

2) It is also found that while a crack aligned with a uniform stress field would not alter the stress distribution, but when the applied load is no longer uniform, the crack starts sensing a higher axial stress intensity and ultimately under a concentrated load a crack suffers twice as much as if the loading were uniformly applied.

3) The axial stress factor as well as K_I are increasing functions of the crack length.

4) The crack buckles up to give a non-zero mode I stress intensity factor when the remote load tends to become closer to concentrated load.

10.2.2 Inelastic Zone Size Case Study in Anisotropic Media

A comprehensive derivation of fracture inelastic zone size and shape in anisotropic solids are presented in this thesis. Energy models were discussed under uniaxial and biaxial stress assumptions. Based on this study the following conclusions are made:

1) Under uniaxial stress assumption, three models were discussed and the inelastic zone size for anisotropic media have been found within the range of the curve $L.abs$ and $P - P$ as shown in Figure (6.4) in chapter 6.

2) Under the biaxial stress state, Hill's yield criterion was adapted to seek the shape of the inelastic zone. This study provided the results for the shapes of inelastic zone shown in Figures (6.5 and 6.6), and the following conclusion are made:

a) When $E_1 > E_2$, the inelastic zone for mode I is much larger than the one of isotropic case.

b) The inelastic zone for mode II is smaller than the one of mode I.

c) When $E_1 < E_2$, both inelastic zone shapes and sizes are very similar to the isotropic case. The only difference is that mode I has a narrow zone in comparison with the isotropic one.

d) For biaxial stress assumption, the real inelastic zone size is larger than the theoretical one.

10.2.3 Experimental Program

The behaviour of cracked fiber reinforced composite material (glass fiber) under mode I loading was investigated. A total of 75 specimens were tested to determine the effect

of various geometric parameters such as: thickness, fiber orientation and the ratio of (a/w) on the behaviour of this material. Based on the experimental investigation the following is concluded:

1) The initial and secondary elastic modulus as well as the tensile strength of the composite specimen were measured.

2) The post-peak response of composite material specimen under tensile cyclic loading is experimentally established.

3) The post-peak response is marked with a gradual decrease in stress accompanying an increase in displacement.

4) The strain energy accumulated in the specimen is released at the peak-load and a stable crack propagates with increase in displacement and reduction in the load.

5) The strength of the specimen is clearly affected by the fiber orientation.

6) There is a gradual degradation in the stiffness and a concurrent loss of the carrying capacity, i.e beyond the peak load, the value of the stiffness decreases as the number of loading cycles increase.

7) The post peak regime may be expressed as a bilinear form in terms of the crack opening displacement.

8) The strength of the specimen is affected by the fiber orientation, i.e the load carried by (0/45/90) fiber orientation specimen is larger than the one carried by a specimen with the same number of layers but with fiber orientation (0/90/0).

9) The fracture toughness of composite materials decreases with increasing notch to width ratio.

10) The fracture toughness is dependent on the specimen thickness.

11) The fracture energy calculated indicates that G_f is affected by the thickness of the specimen and fiber orientation.

12) Cracks advance linearly as a function of number of loading cycles.

10.2.4 Numerical Program

A computer Finite Element Program (SIMEX) is used to calculate the peak load, fracture toughness, COD, and to model the degradation in composite materials. Based on the modeling, the following conclusions are made:

(1) The numerical results obtained using the finite element program (SIMEX) show a good agreement with the experimental results.

(2) Both experimental and numerical results show a gradual degradation in the stiffness and a constant loss of the carrying capacity beyond the post-peak load.

(2) The computed values of E_d produces a secant overall response, i.e. no permanent damage is modeled. The permanent damage (non-recoverable deformation) was not modeled, as it defeats the purpose of this investigation which attempts to produce a simple, yet efficient procedure to model damage in composite.

10.3 Recommendations for Future Research

Experimental and numerical investigations have been carried out to study the fracture parameters, such as stress intensity factor, fracture energy and post peak response

as well as damage of composite materials. The results from this study has demonstrated a very good agreement between the two methods. This agreement provides a potential for further research in the area of combined fracture and damage mechanics in composite materials. The following recommendations with regard to further work in this area are in order.

- Experimental and analytical investigations are recommended to extend the present study to include the effect of other parameters such as: different loading conditions and environmental effect.
- More experimental tests are needed for different types of fiber reinforced composites, such as: carbon FRP and kevlar FRP, under different loading conditions.
- Experimental investigation and numerical verification of the results are recommended for mixed mode crack propagation.
- The finite element extraction of the axial stress factor which is presented in Chapter 5 is recommended to be extended to three-dimensional finite element analysis for extracting the effective axial stress ahead of a crack tip. The stability and prediction of the direction of crack extension are also recommended to be investigated.
- The case study of crack tip inelastic zone in an isotropic media which presented in Chapter 6 needs to be extended to include the effect of material parameters in the inelastic zone shape for both mode I and mode II as well as mixed mode I-II.
- Based on the analytical results of inelastic zone shape presented in Chapter 6, a second order numerical analysis is recommended for predicting the yielding inelastic zone in front of the crack tip.

- Numerical model representing the stiffness degradation of composite materials for mode II and mixed mode crack propagation should be studied.

Bibliography

[1] R. D. Adams, C. J. Pye P. Cawley, and B. J. Stone. "A vibration Testing for Non-destructively Assessing the Integrity of the Structure". *Journal of Mechanical Engineering Science*, 20:93–100, 1978.

[2] E. Altus, A. Rotern, and M. Shmeli. "Free Edge Effect in Angle Ply Laminates-new Three Dimensional Finite Difference Solution". *Journal of Composite Material*. 14:21–30, 1980.

[3] T.L. Anderson. *"Fracture Mechanics , Fundamentals and Applications"*. CRC Press, Inc., 1991.

[4] M. L. Ayari. "Simulation of Mining Excavation". Internal report, Geological Engineering Department, University of Manitoba, 1990.

[5] M.L. Ayari. *"Static and Dynamic Fracture Mechanics of Concrete Gravity Dams"*. PhD thesis, The university of Colorado at Boulder, 1988.

[6] Z. P. Bazant. "Mechanics of Distributed Cracking". *Applied Mechanics Review*, 39(5), May 1986.

[7] P. W. R. Beaumont and B. Harris. "The Energy of Crack Propagation in Carbon Fiber-Reinforced Resin Systems". *Journal of Materials Science*, 7:1265 – 1279, 1972.

[8] M. H. Beleackley and A. R. Luxmoore. "Comparison of Finite Element Solutions with Analytical and Experimental Data for Elastic-Plastic Cracked Problems". *International Journal of Fracture*, 22:15–39, 1983.

[9] W. Brameshuber and H. K. Hilsdorf. "Influence of Ligament Length and Stress State on Fracture Energy of Concrete". *Engineering Fracture Mechanics*, 35 No.1/2/3:95–106, May 1990.

[10] J. C. Brewer and P. A. Lagace. "Quadratic Stress Criterion for Initiation of Delamination". *Journal of Composite Materials*. 22:1141–1155, 1988.

[11] D. Broek. *"Elementary Engineering Fracture Mechanics"*. Noordhoff International Publishers, 1974.

[12] L. J. Broutman and Richard H. Krock, editors. *"Composite Materials (Fracture and Fatigue)"*, volume 5. Academic Press, Inc., 111 Fifth Avenue, New York, New York 10003, 1974.

[13] H. G. De Lorenzi C. F. Shih and M. D. German. " Crack Extension Modeling with Singular Quadratic Isoparametric Elements". *International Journal of Fracture Mechanics.*, 12:647–651, 1976.

[14] P. Cawley and R. D. Adams. "A vibration Technique for Non-distructive Testing of Fiber Composite Structures". *Journal of Composite Materials*, 13:161–175, 1979.

[15] J. L. Chaboche. "Continuum Damage Mechanics, Part 1 and Part 2". *Journal of Applied Mechanics*, 55:59 – 72, 1988.

[16] T. J. Reinhart (Technical Chairman) and M. S. Woods (Technical Editor), editors. *"Engineered Materials Handbook, Composites"*, volume 1. Metal Park, Ohio: ASM International, USA, 1987.

[17] H. T. Choi, H. Y. T. Wu, and F. K. Chang. "A New Approach Toward Understanding Damage Mechanisms and Mechanics of Laminated Composites Due to Low-Velocity Impact, Part II - Analysis". *Journal of Composite Materials*, 25 (12):1012–1038, August 1991.

[18] H.Y. Choi, H. S. Wang, and F. K. Chang. "Effect of Laminate Configuration and Impactor's Mass on the Initial Impact Damage of Graphite/Epoxy Composite plates due to Line-loading Impact". *Journal of Composite Material*, 26 (6):804–827, December 1992.

[19] C. L. Chow and T. J. Lu. "On Evolution Laws of Anisotropic Damage". *Engineering Fracture Mechanics*, 34(3):679 - 701, 1989.

[20] C. L. Chow and K. Y. Sze. "Characterization of Notched Ductile Failure with Continuum Damage Mechanics". *Journal of Engineering Material Technology*, 112:412 - 421, October 1990.

[21] H. T. Corten. "Fracture Mechanics of Composites". In H. Liebowitz, editor, *Fracture - An Advanced Treatise: Volume VII Fracture of Nonmetal and Composite*, pages 675 - 769. Academic Press, New York, 1972.

[22] T. A. Cruse. "Tensile Strength of Notched Composites". *Journal of Composite Materials*, 7:218–229, 1973.

[23] I. M. Daniel and O. Ishai. *"Engineering Mechanics of Composite Materials"*. Oxford University Press, Inc., 200 Madison, New York, New York 10016, first edition, 1994.

[24] H. B. Dexter and J. G. Funk. "Impact Resistance and Interlaminar Fracture Toughness of Through-the-Thickness Reinforced Graphite/Epoxy". In *The Pro-*

ceedings of 27th Structures, Structural Dynamics and Mat. Conference, San Antonio, TX, May 1986.

[25] R. S. Dhaliwal and H. S. Saxena. "Antiplanar Shear Problem for a Crack Between Dissimilar Nonhomogeneous Isotropic Elastic Layers". *Engineering Fracture Mechanics Journal*, 42 No. 4:653–662, 1992.

[26] B. J. Carter E. Z. Lajtai and M. L. Ayari. " Brittle Fracture Criteria for Compression". *Engineering Fracture Mechanics Journal*, 37(1):59–74, 1990.

[27] A. England. "A Crack Between Dissimilar Media". *Journal of Applied Mechanics*, 32:400–402, 1966.

[28] A. H. England. "Viscoelastic Behavior of Heterogeneous Media". *Journal of Applied Mechanics*. 87:631–636. 1985.

[29] F. Erdogan. "The Stress Distribution in a Nonhomogeneous Elastic Plane With Cracks". *Journal of Applied Mechanics*, 85:232–236, 1963.

[30] F. Erdogan. "Stress Distribution in Bonded Dissimilar Materials with Cracks". *Journal of Applied Mechanics*, 87:403–410, 1965.

[31] F. Erdogan and G. D. Gupta. "Layered Composite With an Interface Flow". *International Journal of Solids and Structures*, 7:1089–1107, 1971.

[32] F. Erdogan and G. C. Sih. "On the Crack Extension in Plates under Plane Loading and Transverse Shear". *Journal of Basic Engineering*, 85:519–527, 1963.

[33] R. E. Evans, J. E. Masters, and J. L. Courter. "Toughened Interleafed Composites". In *Conference Proceedings, American Society for Metals*, pages 249–257, Dearborn, Michigan, 2-4 December 1985.

[34] D. Feldman. *"Polymeric Building Materials"*. Elsevier Applied Science Publishers LTD, 1989.

[35] S. K. Gaggar and L. J. Broutman. "The Development of a Damage Zone at the Tip of a Crack in a Glass Fiber Reinforced Polyester Resin". *International Journal of Fracture*, 10:606 – 608, 1974.

[36] A. C. Garg. "Stress Distribution Near Periodic Cracks at the Interface of Two Bonded Dissimilar Orthotropic Half-Planes". *International Journal of Engineering Science*. 19:1101–1114, 1981.

[37] A. C. Garg. "Delamination-A damage Mode in Composite Structures". *Engineering Fracture Mechanics*, 29 No. 5:557–584, 1988.

[38] R. F. Gibson. *"Principles of Composite Material Mechanics"*. McGraw-Hill Inc., 1995.

[39] J. H. Gosse and P. B.Y. Mori. "Impact Damage Characterization of Graphite/Epoxy Laminates". In *Proc. of The Third Technical Conference of American Society for Composite*, pages 334–353, Seattle, WA, 1988.

[40] A. A. Griffith. "The Phenomena of Rupture and Flow in Solids". *Philosophical Transactions of the Royal Society*, 221A:163 – 198, 1920.

[41] Jr. H. J. Konish. "Mode I Stress Intensity Factor for Symmetrically-Cracked Orthotropic Strips". Technical Report ASTM STP 593, American Society for Testing and Materials. 1975.

[42] N. K. Hassan. *"Multi-Bolted Connections for Fiber Reinforced Plastics Structural Members"*. PhD thesis, Ain Shams University, 1994.

[43] C. T. Herakovich. "On The Relationship Between Engineering Properties and Delamination of Composite Materials". *Journal of Composite Materials*, 15:336–348, July 1981.

[44] R. Hill. *"The Mathematical Theory of Plasticity"*. Oxford University Press, Amen House, London E.C.4, first edition, 1950.

[45] L. Holloway. "Polymer, Fiber and Composite Material Properties and Manufacturing Techniques". In L. Holloway, editor, *Polymers and Polymer Composites in Construction*, pages 5–31. Thomas Telford Ltd., London, 1990.

[46] M. A. Hussain, S. L. Pu, and J. H. Underwood. "Strain Energy Release Rate for a Crack Under Combined Mode I and Mode II," Fracture Analysis. *ASTM, STP 560*, pages 2–28, 1974.

[47] A. R. Ingraffea and W. H. Gerstle. "Non-Linear Fracture Models for Discrete Crack Propagation". In S. P. Shah, editor, *Application of Fracture Mechanics to Cementitious Composites*, E: Applied Sciences - No. 94, pages 247–285. Martinus Nijhoff Publishers, 1984. proceedings of the NATO Advanced Research Workshop on Application of Fracture Mechanics to Cementitious Composites, Northwestern University, Evanston, Illinois,USA.

[48] A. R. Ingraffea and C. Manu. "Stress-Intensity Factor computations in Three Dimensions with Quarter-Point Elements". *International Journal of Numerical Methods in Engineering*, 15(10):1427–1445, 1980.

[49] A. R. Ingraffea and C. Manu. "Stress-Intensity Factor Computations in Three Dimensions with Quarter-Point Elements". *International Journal of Numerical Methods in Engineering*, 15 No. 10:1427 – 1445, 1980.

[50] G. R. Irwin. "Fracture of Metals". *American Society of Metals*, pages 147 – 166, 1949. Cleveland, OH.

[51] G. R. Irwin. "Analysis of Stress and Strain Near the End of a Crack Traversing a Plate". *Journal of Applied Mechanics*, 24:61 – 364, 1967.

[52] H. Ishikawa and Y. Kohno. "On The Stress Functions for Stress Field Around an Interface Crack Between Dissimilar Materials". *International Journal Of Engineering Science*, 31, No. 4:583–591, 1993.

[53] J. C. Jaeger and N. G. W. Cook. *"Fundamentals of Rock Mechanics"*. Methuen & Co. Ltd., 11 New Fetter Lane, London E.C.4., 1969.

[54] T. Johannesson and M. Blikstad. "A Fractographic Study of the Delamination Process". Technical report, Report From linkoping Institute of Tech., linkoping, Sweden, 1984.

[55] R. M. Jones. *"Mechanics of Composite Materials"*. Scripta Book Co., 1975.

[56] E. H. Jordan and G. J. Meyers. "Fracture Mechanics Applied to Nonisothermal Fatigue Crack Growth". *Engineering Fracture Mechanics*, 23:345 – 358, 1986.

[57] P. Kelly, D. A. Hills, and D. Nowell. "Curved Interface Cracks Between Elastically Dissimilar Media, With Application to the Analysis of Circular Inclusions". *International Journal of Mechanics Science*, 36, No. 3:173–181, 1994.

[58] K. S. Kim and C. S. Hong. "Delamination Growth in Angle-Ply Laminated Composites". *Journal of Composite Material*, 20:423–438, 1986.

[59] R. Y. Kim. "A Technique for Preventation of Delamination". *AFWAL-TR-82-4007*, pages 218–230, 1982.

[60] R. Y. Kim and S. R. Soni. "Experimental and Analytical Studies on the Onset of Delamination in Laminated Composites". *Journal of Composite Materials*, 18:70–80, January 1984.

[61] H. J. Konish, J. L. Swedlow, and T. A. Cruse. "Experimental Investigation of Fracture in an Advanced Composite". *Journal of Composite Materials*, 6:114 – 124, 1972.

[62] L. Leibengood, D. Darwin, and R. H. Dodds. "Parameters Affecting Finite Element Analysis of Concrete Structures". *Journal of Structural Engineering, ASCE*. 112(2), February 1986.

[63] J. Lemaitre. "Local Approach of Fracture". *Engineering Fracture Mechanics*, 25 No. 5/6:523 – 537, 1986.

[64] J. Lemaitre. *"A Course on Damage Mechanics"*. Springer-Verlag, Berline Heidelberg, Germany, 1992.

[65] J. Lemaitre and J. Dufailly. "Damage Measurements". *Engineering Fracture Mechanics*, 28 No. 5/6:643 – 661, 1987.

[66] H. Liebowitz. *"Fracture, An Advanced Treatise"*, volume II. Academic Press, New York & London, 1968.

[67] S. G. Likhnitskii. *"Theory of Elasticity of an Anisotropic Body"*. Mir Publisher, Moscow, (English Translation), 1981.

[68] S. Liu, Z. Kutlu, and F. Chang. "Matrix Cracking and Delamination in Laminated Composite Beams Subjected to a Transverse Concentrated Line Load". *Journal of Composite Materials*, 27 No. 5:436–465, 1993.

[69] D. C. Lo, D. H. Allen, and C. E. Harris. "A Continuum Model for Damage Evolution in Laminated Composites". In *ASTM Special Technical Publication*

Proceedings of the 23rd National Symposinum on Fracture Mechanics., number 1189 in ASTM STP, pages 680–695, Texas, USA., June 18-20 1991. American Society of Testing And Materials.

[70] P. K. Mallick. *"Fiber Reinforced Composites Materials, Manufacturing, and Design"*. Marcel Dekker, Inc., New York, New York 10016, second revised and expanded edition, 1993.

[71] S. Manivasagam and K. Chandrasekaran. "Characterization of Damage Progression in Layered Composites". *Journal of Sound and Vibration*, 152(1):177–179, 1992.

[72] A. C. Marshall. *"Composite Basics"*. Marshall Consulting, California, USA, 1985.

[73] P. M. Mujumdar and S. Suryanarayan. "Buckling of Beams with Delaminations". In *Proc. of International Conference on Composite Material Structures*, pages 273–283, Madras, India, 6-9 January 1988.

[74] D. R. Mulville and P. W. Mast. "Strain Energy Release Rate for Interfacial Cracks Between Dissimilar Media". *Engineering Fracture Mechanics Journal*, 18:55–56, 1976.

[75] N. I. Muskhelishvili. *"Some Basic Problems of Mathematical Theory of Elasticity"*. P. Noordoff limited, Groningen, The Netherlands. 4th edition, 1963. Translated from Russian by J. R. M. Radok.

[76] D. Ngo and A. C. Scodelis. "Finite Element Analysis of Reinforced Concrete Beams". *Journal of the American Concrete Institute*, 64(3), March 1967.

[77] R. D. Nicholson and C. L. Formby. "The Validity of Various Fracture Mechanics Methods at Creep Temperatures". *International Journal of Fracture*, 11 No. 4:595 - 604, 1975.

[78] T. K. O'Brien. "Characterization of Delamination onset Growth in a Composite Laminates". In K. L. Reifsnider, editor, *Damage in Composite Materials*, number 775 in ASTM STP, pages 140–167, Virginia Polytechnic Institute and State University., 1982.

[79] E. Orowan. "Fatigue and Fracture of Metal". MIT Press, 1950. Cambridge, MA.

[80] S. Parhizgar, L. W. Zachary, and C. T. Sun. "Application of the Principles of Linear Fracture Mechanics to the Composite Materials". *International Journal of Fracture*, 20:3 - 15. 1982.

[81] P. C. Paris and F. Erdogan. "A Critical Analysis of Crack Propagation Laws". *Transaction of ASME, Journal of Basic Engineering*, 85:528 - 534, 1963.

[82] D. C. Phillips. "Fracture Mechanics of Carbon Fiber Laminates". *Journal of Composite Materials*, 8, April 1974.

[83] Y. R. Rashid. "Analysis of Prestressed Concrete Pressure Vessels". *Nuclear Engineering and Design*, 7(4), April 1968.

[84] K.L. Reifsnider, E.G. Henneke, W.W. Stinchcomb, and J.L. Duke. . In *Proc. Int. Union of Theor. Appl. Mech*, pages 339–390, blacksburg, Virginia, 1982. Pergamon Press, New York.

[85] J. Rice and G. Sih. "The Problems of Cracks in Dissimilar Media". *Journal of Applied Mechanics*, 32:418 - 423, June 1965.

[86] J. R. Rice. "A Path Independent Integral and the Approximate Analysis of Strain Concentration by Notches and Cracks". *Journal of Applied Mechanics*, pages 379 - 386, June 1968.

[87] J. R. Rice. "Inelastic Constitutive Relations for Solids: an Internal-Variable Theory and its Application to Metal Plasticity". *Journal of Physics and Solids*, 19:433 - 455, 1971.

[88] A. J. Russell and K. N. Street. "Moisture and Temperature Effects on the Mixed-Mode Delamination Fracture of Unidirectional Graphite/Epoxy". *ASTM STP*, 876:349–370, 1985.

[89] E. F. Rybicki, D. W. Schmueser, and J. Fox. "An Energy Release Rate Approach for Stable Crack Growth in the Free-edge Delamination Problem". *Journal of Composite Materials*, 11:470–487, October 1977.

[90] S. A. Salpekar and T. K. O'Brien. "Analysis of Matrix Cracking and Local Delamination in $(0/\theta/-\theta)_s$ Graphite Epoxy Laminates Under Tensile Load". *Journal of Composites Technology and Research*, 15 No. 2:95 - 100, 1993.

[91] V. E. Saouma, M. L. Ayari, and D. A. Leavell. "Mixed Mode Crack Propagation in Homogeneous Anisotropic Solids". *Engineering Fracture Mechanics*, 27 No. 2:171–189, 1987.

[92] A. Saxena. "Creep Crack Growth in High Temperature Ductile Materials". *Engineering Fracture Mechanics*, 40 No. 4/5:721 - 736, 1991.

[93] M. M. Schwartz. *"Composite Materials Handbook"*. McGraw-Hill, Inc., USA, 1984.

[94] G. J. Semites, S. Salaam, and W. L. Yin. "Effect of Delamination of Axially Loaded Homogeneous Laminated Plates". *IAA Journal*, 23:1437–1444, 1985.

[95] M. J. Shuart and J. G. Williams. "Comparison behavior of +45 - Dominated Laminate with a Circular Hole or Impact Damage". *AIAA*, 25:115–122, 1986.

[96] G. Sih and J. Rice. "The Bending of Plates of Dissimilar Materials With Cracks". *Journal of Applied Mechanics*, 86:477–482, 1964.

[97] G. C. Sih. "Strain Energy Factors Applied To Mixed Mode Crack Problems". *International Journal of Fracture Mechanics*, 10:305, 1974.

[98] G. C. Sih and B. V. Kiefer. "Nonlinear Response of Solids due to Crack Growth and Plastic Deformation". In N. Perrone and S. N. Atluri, editors, *Nonlinear and Dynamic Fracture Mechanics*, volume 35, pages 135 - 156. The American Society of Mechanical Engineering, 1979.

[99] G. C. Sih and H. Liebowitz. "Mathematical Theories of Brittle Fracture". In H. Liebowitz, editor. *Fracture an Advanced Treatise*, volume 2. Academic Press, New York, 1968.

[100] G. C. Sih, P. C. Paris, and G. R. Irwin. "on Cracks in Rectilinearly Anisotropic Bodies". *International Journal of Fracture Mechanics*, 1:189 - 203, 1965.

[101] J. M. Slepetz and L. Carlson. "Fracture of Composite Compact Tension Specimens". Technical Report ASTM STP 593, American Society for Testing and Materials, 1975.

[102] R. L. Spilker and S. C. Chou. "Edge Effects in Symmetric Composite Laminates: Importance of Satisfying the Traction-Free-Edge Condition". *Journal of Composite Material*, 14:2–20, 1980.

[103] B. Sun. *"Characterization of Creep Deformation and Damage of Metallic Materials at High Temperature"*. PhD thesis, University of Manitoba, June 1994.

[104] C. T. Sun and C. J. Jih. "On Strain Energy Release Rates for Interfacial Cracks in Bi-Material Media". *Engineering Fracture Mechanics Journal*, 28, No. 1:13–20, 1987.

[105] P. Theocaris and E. Gdoutos. "Stress Singularities at Equal Angle Biwedges and Two-Material Composite Half Planes With Rough Interfaces". *Journal of Applied Mechanics*, 43:64, 1976.

[106] P. Theocaris and E. Gdoutos. "Experimental Solution of Flexed Plates by the Method of Caustics". *Journal of Applied Mechanics*, 13:107–111, 1977.

[107] D. M. Tracey. "Discussion of 'On the Use of Isoparametric Finite Elements in Linear Fracture Mechanics". *International Journal of Numerical Methods in Engineering*, 11:401–402, 1977.

[108] H. S. Wang and F. K. Chang. "Curvature Effect on Impact Damage in Laminated Composites Subjected to Low-Velocity Impact". In *The Proceedings of English International Conference on Composite Materials*, pages 28–K–I–28–K–II, Honolulu, HI, 1991.

[109] S. S. Wang. "Fracture Mechanics for Delamination Problems in Composite Materials". *Journal of Composite Materials*, 17:210–223, 1983.

[110] S. S. Wang, E. S. M. Chim, T. P. Yu, and D. P. Gotez. "Fracture of Random Short-Fiber SMC Composite". *Journal of Composite Materials*, 17:299–315, July 1983.

[111] S. S. Wang, E. S. M. Chim, and N. M. Zahlan. "Fatigue Crack Propagation in Random Short-Fiber SMC Composite". *Journal of Composite Materials*, 17:250–266, May 1983.

[112] A.A. Watts, editor. *"Commercial Opportunities for Advanced Composites"*. Number 704 in ASTM STP. American Society for Testing and Materials, Philadelphia, Pa. 19103, 1980. ASTM Special Technical Publication.

[113] H. M. Westergaard. "Bearing Pressures and Cracks". *Journal of Applied Mechanics*, 61:A49 – A53, 1939. Transaction of the ASME, Series E.

[114] J. D. Whitcomb. "Analysis of Instability-Related Delamination Growth of a Through-Width Delamination". *ASA-TM-86301*, 1984.

[115] D. J. Wilkins, J. R. Eisenmann, R. A. Camin, W. S. Margolis, and R. A. Benson. "Characterizing Delamination Growth in Graphite-Epoxy". In K.L. Reifsnider, editor, *Damage in Composite Materials.*, number 775 in ASTM STP, pages 168–183, Virginia Polytechnic Institute and State University., 1982. American Society of Testing And Materials.

[116] J. C. Williams and M. D. Rhodes. "Effect of Resin on Impact Damage Tolerance of Graphite/Epoxy Laminates". *ASTM STP 787*, pages 450–480, 1982.

[117] M. Williams. "The Stress Around a Fault Of Crack in Dissimilar Media". *Bulletin of Seismological Society of America*, 49, No. 2:199–204, 1959.

[118] M. L. Williams. "On the Stress Distribution at the Base of a Stationary Crack". *Journal of Applied Mechanics*, 24:109–114, 1957.

[119] H. Tada with the cooperation of P. Paris and G. R. Irwin. *"The Stress Analysis of Cracks Handbook"*. Paris Productions Incorporated, 226 Woodbourne Dr., St. Louis, Missouri 63105, 2nd edition, 1985.

[120] E. M. Wu. "Fracture Mechanics of Anisotropic Plates". In S. W. Tsai, J. C. Halpin, and N. J. Pagano, editors, *Composite Materials Work Shop*, volume I, pages 20 – 43. Technomic Publishing Co., Lancaster, PA., 1968.

[121] E. M. Wu. *"Strength and Fracture of Composites, Composite Materials"*, volume V, pages 191–247. Academic Press, NY, 1974.

[122] E. M. Wu and R. C. Reuter. "Crack Extension in Fiberglass Reinforced Plastics". T & AM Report 275, University of Illinois, Department of Theoretical and Applied Mechanics, Urbana, Illinoise MT and AM, February 1965.

[123] H.T. Wu and G. S. Springer. "Measurements of Matrix Cracking and Delamination Caused by Impact on Composite Plates". *Journal of Composite Materials*, 22:518–532, 1988.

[124] Y. L. Xu and K. L. Reifsnider. "A Micromechanical Analysis of Fiber Crack Propagation in Composite Materials Due to Transverse Tensile Loads". *Engineering Fracture Mechanics Journal*, 45, No. 6:813–829, 1993.

[125] Sung Yi. "Thermoviscoelastic Analysis of Delamination onset and Free Edge Response in Laminated Composites". *AIAA Journal*, 31, No. 12:2320–2327, 1993.

[126] W. L. Yin. "Axisymmetric Buckling and Growth of a Circular Delamination in a Compressed Laminate". *International Journal of Solids Structure*, 21(5):503–514, 1985.

[127] W. L. Yin and J. T. S. Wang. "The Energy-Release Rate in The Growth of a One-Dimensional Delamination". *Journal of Applied Mechanics*, 51:939–941, 1984.

Appendix A

EXPERIMENTAL RESULTS

This appendix contains some figures which show the post peak response of the different tested specimens.

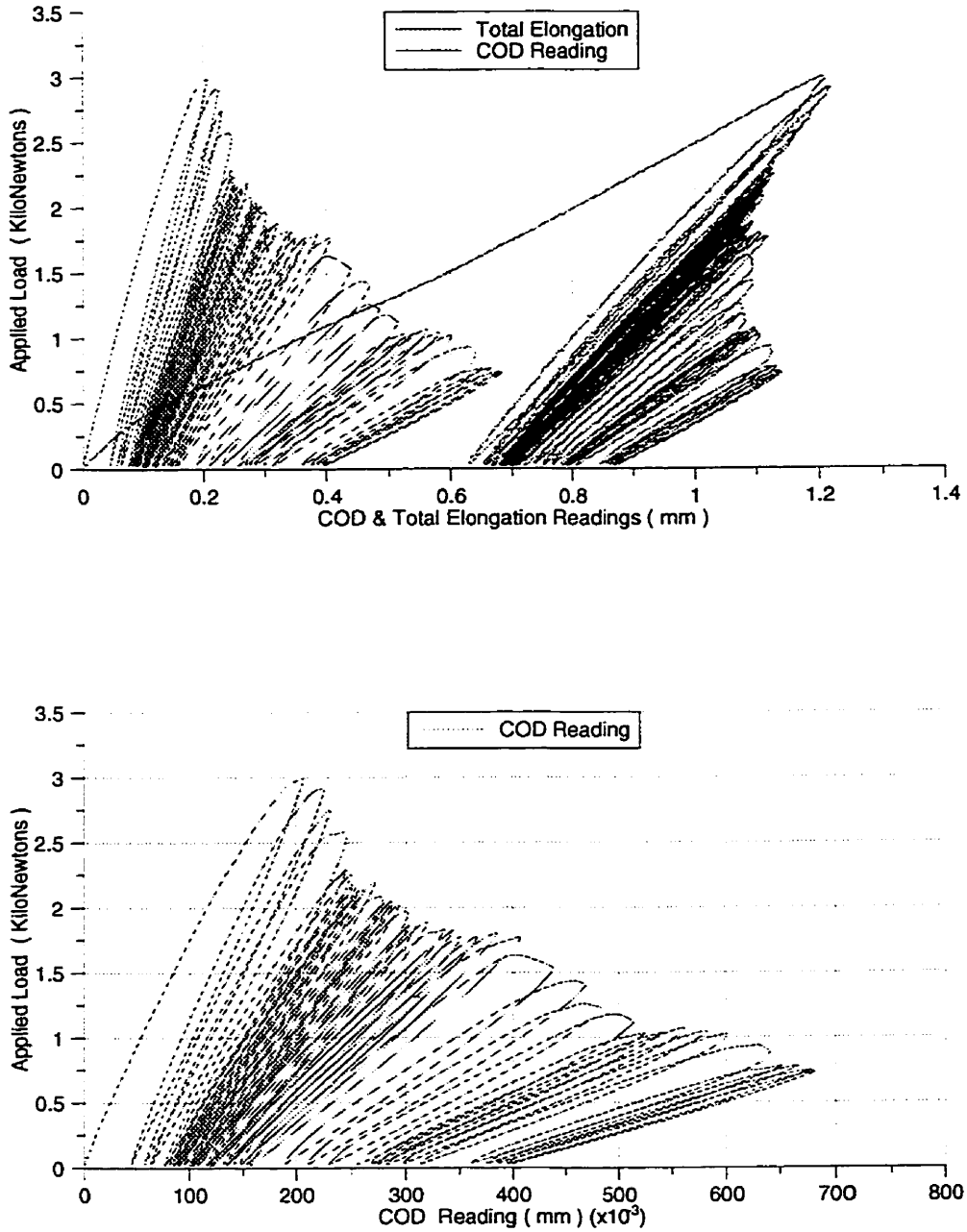

Figure A.1: Response of 12 Layers Specimen of (0/90/0) Fiber Orientation

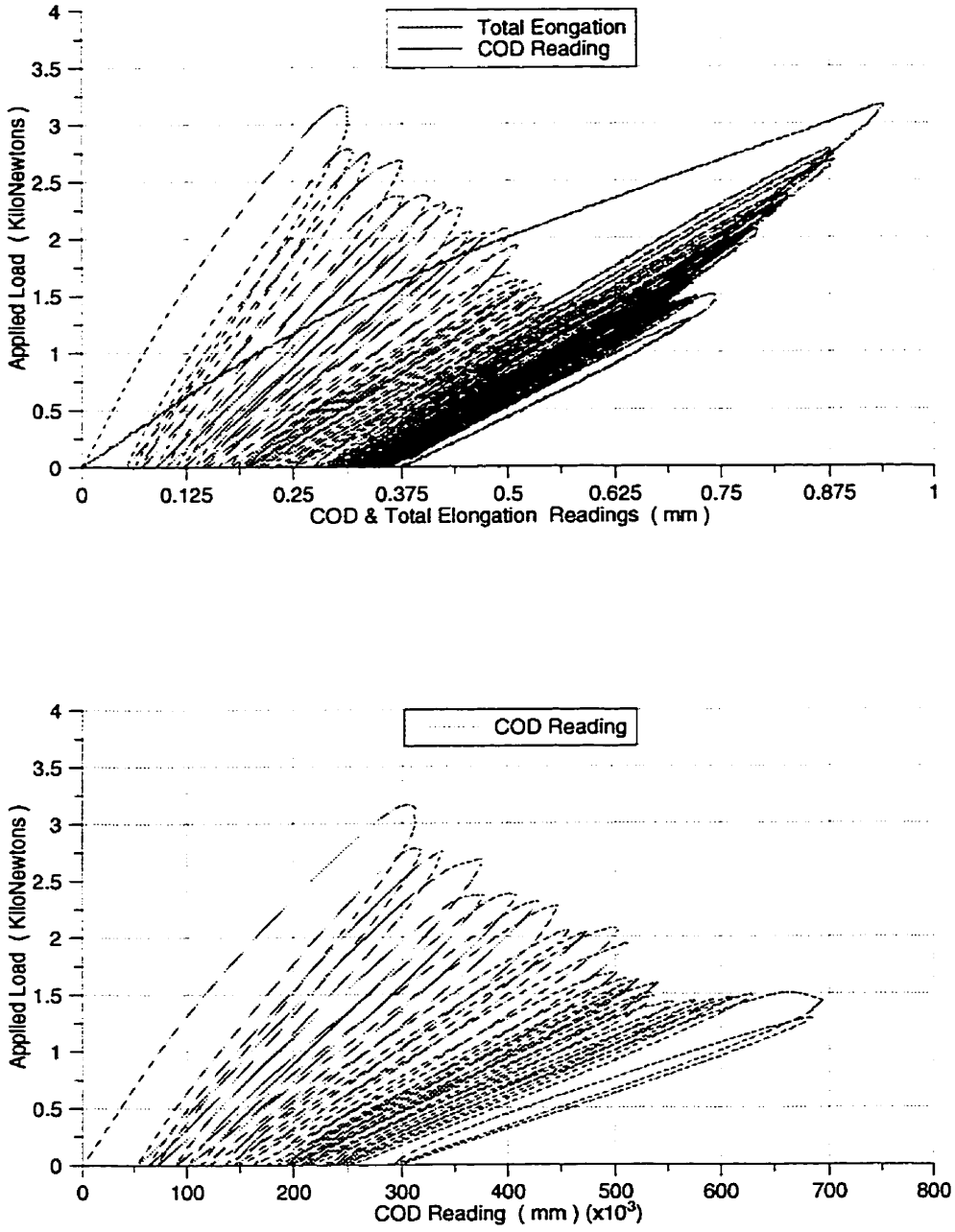

Figure A.2: Response of 12 Layers Specimen of (0/90/0) Fiber Orientation

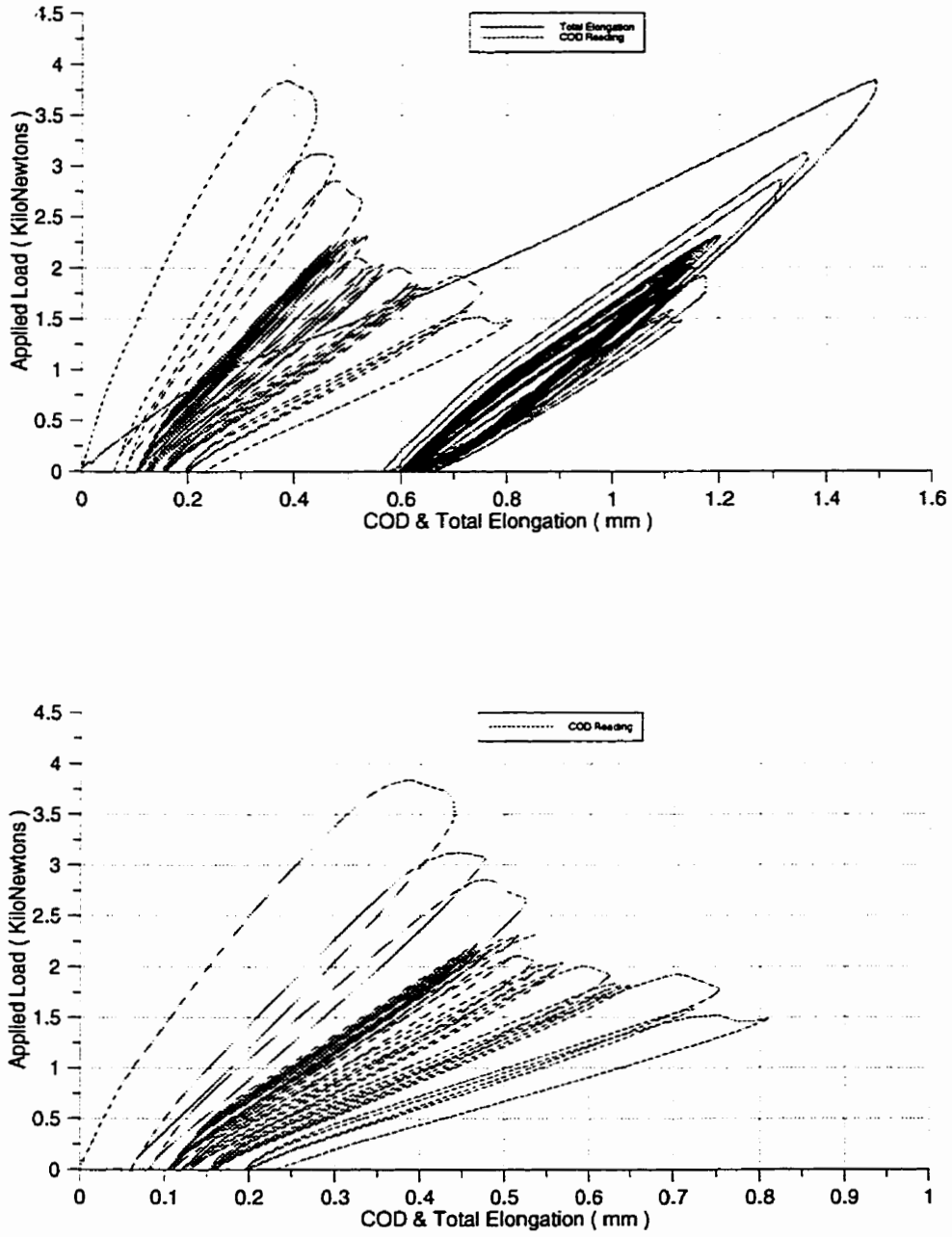

Figure A.3: Response of 12 Layers Specimen of (0/90/0) Fiber Orientation

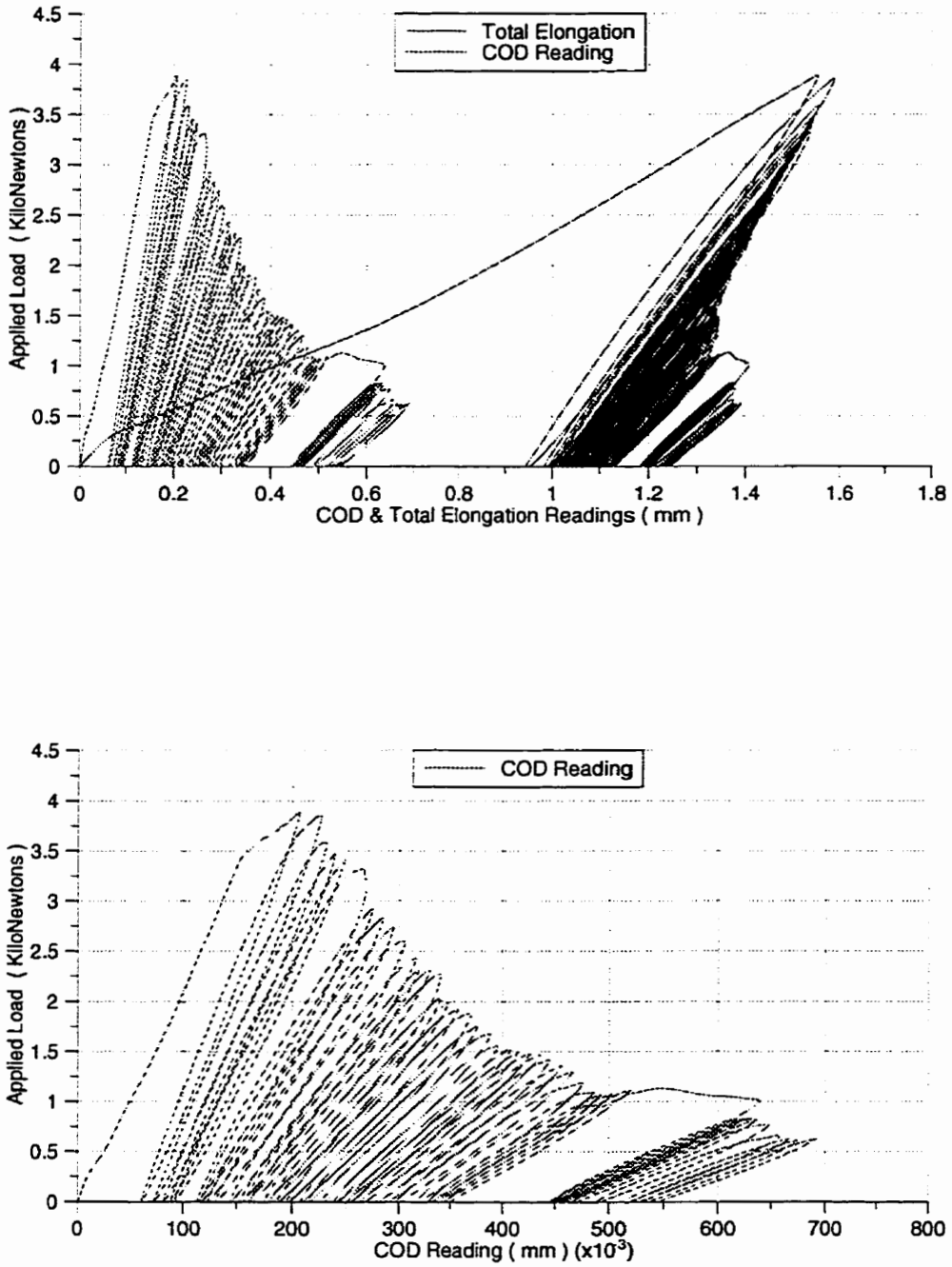

Figure A.4: Response of 16 Layers Specimen of (0/90/0) Fiber Orientation

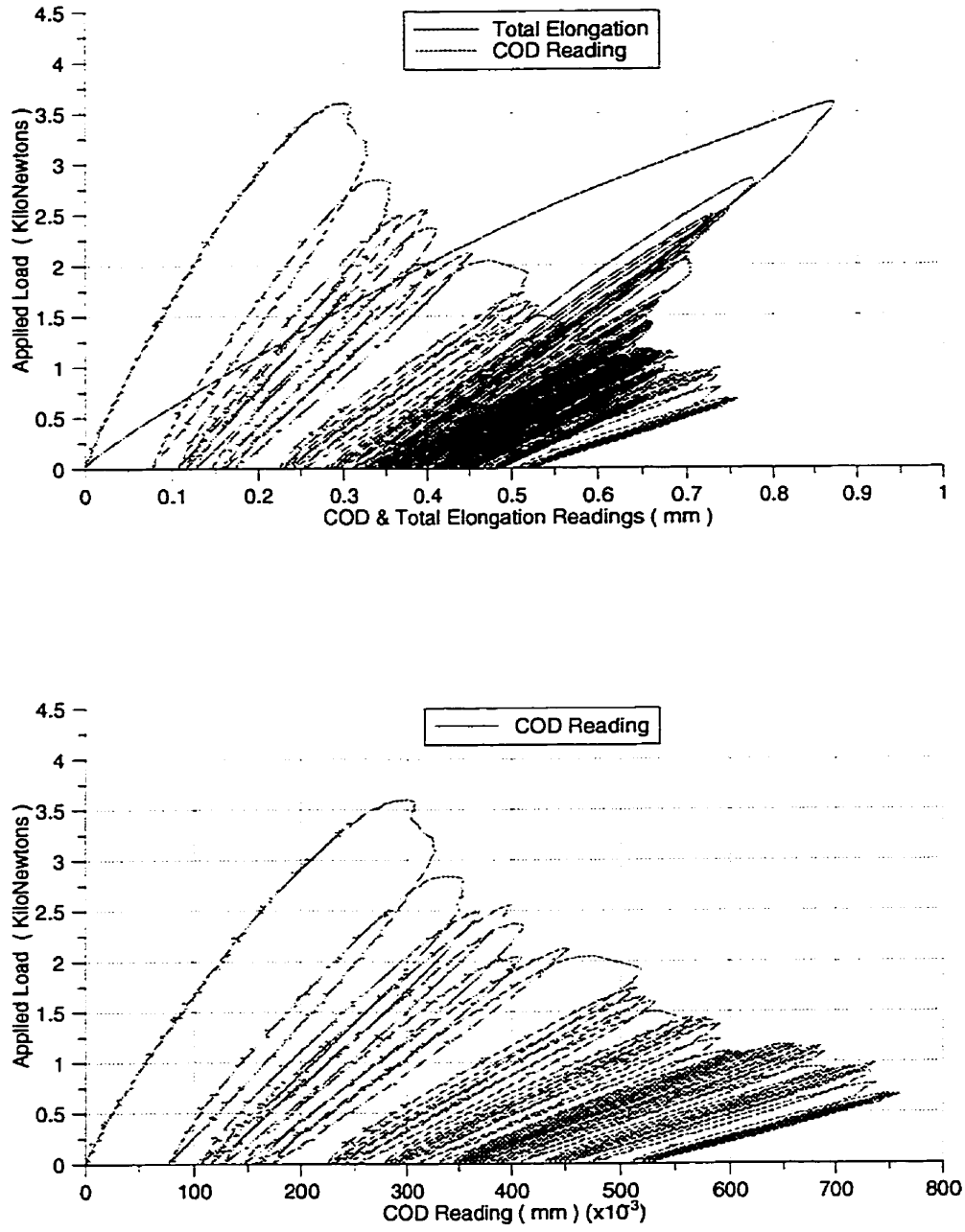

Figure A.5: Response of 16 Layers Specimen of (0/90/0) Fiber Orientation

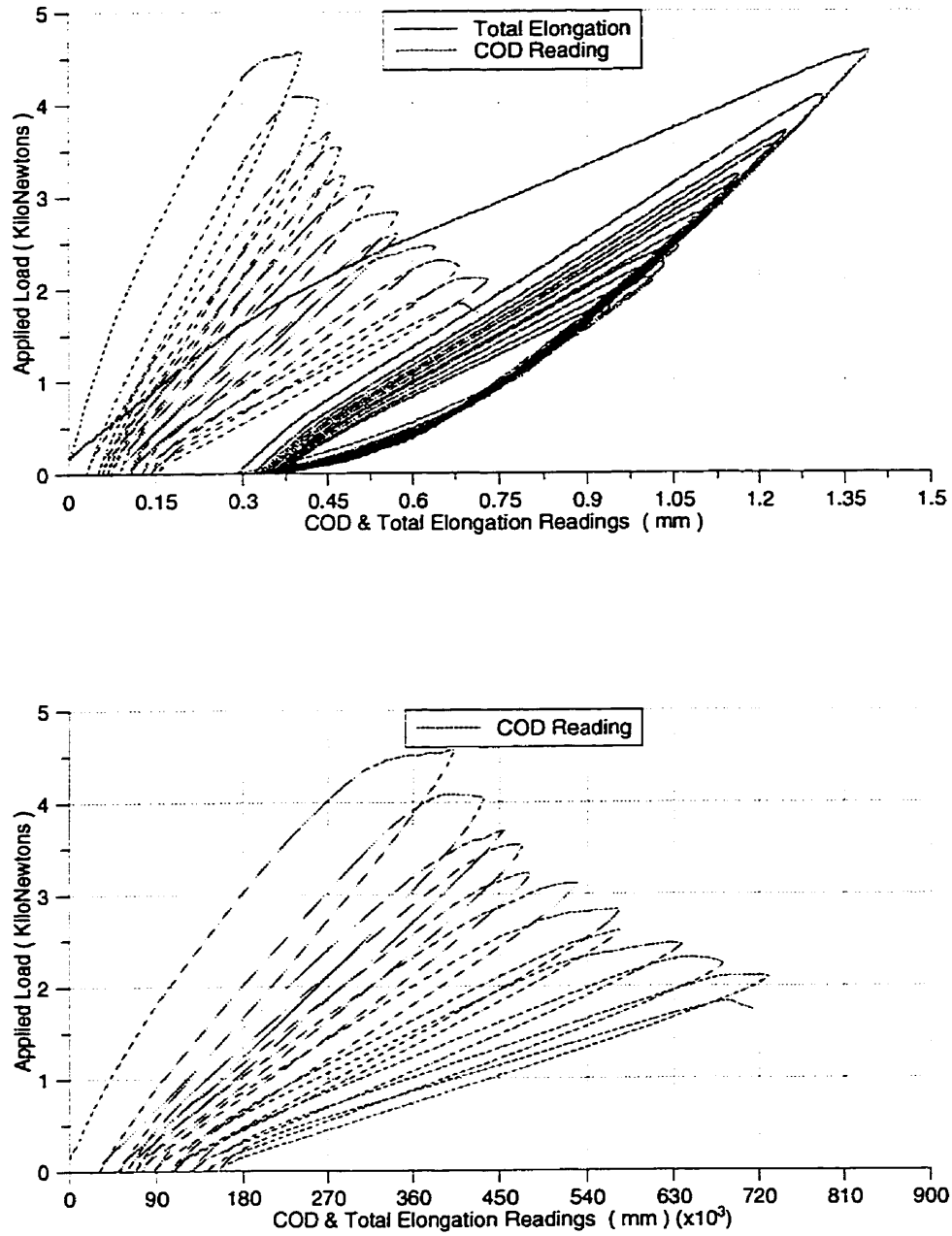

Figure A.6: Response of 16 Layers Specimen of (0/90/0) Fiber Orientation

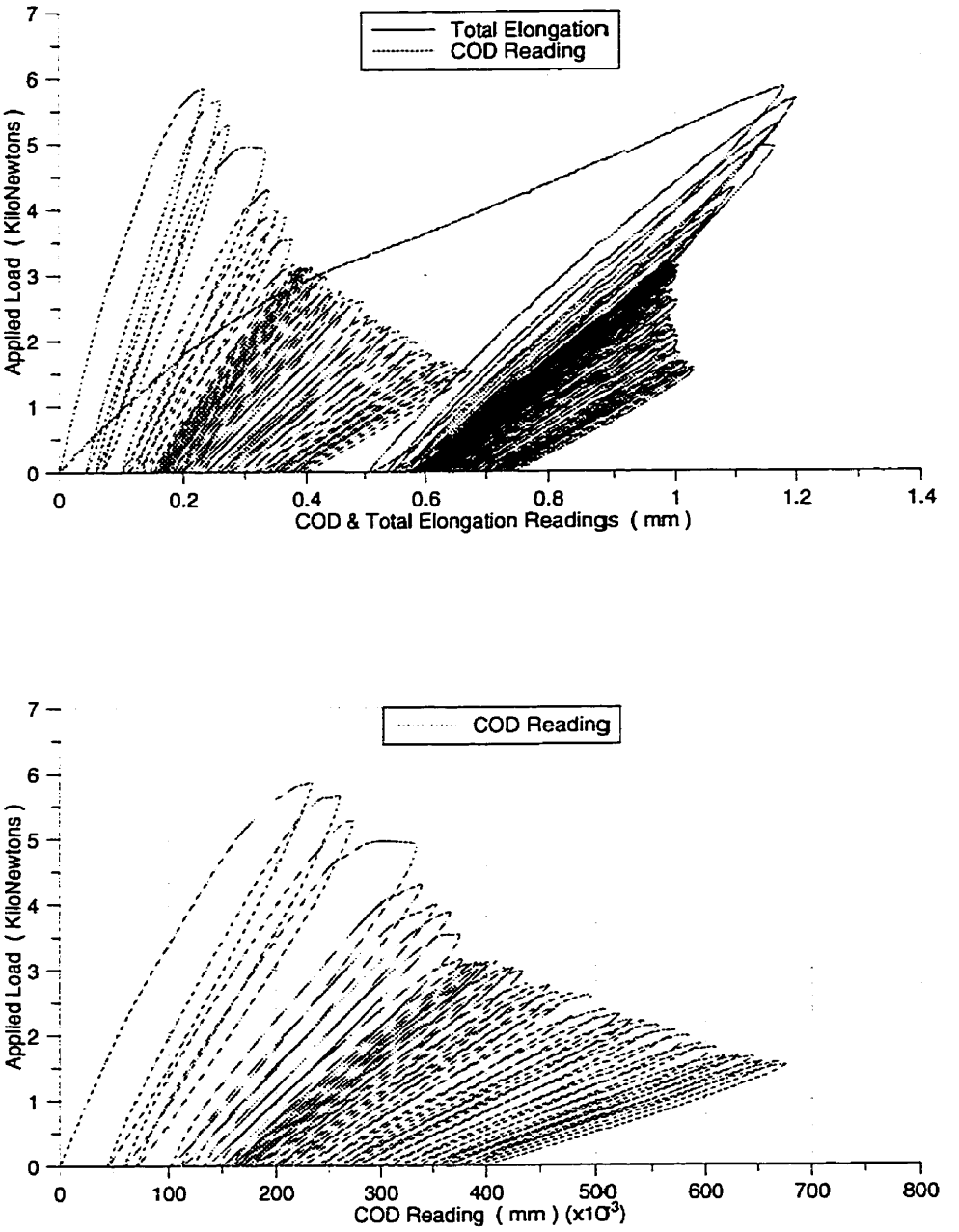

Figure A.7: Response of 20 Layers Specimen of (0/90/0) Fiber Orientation

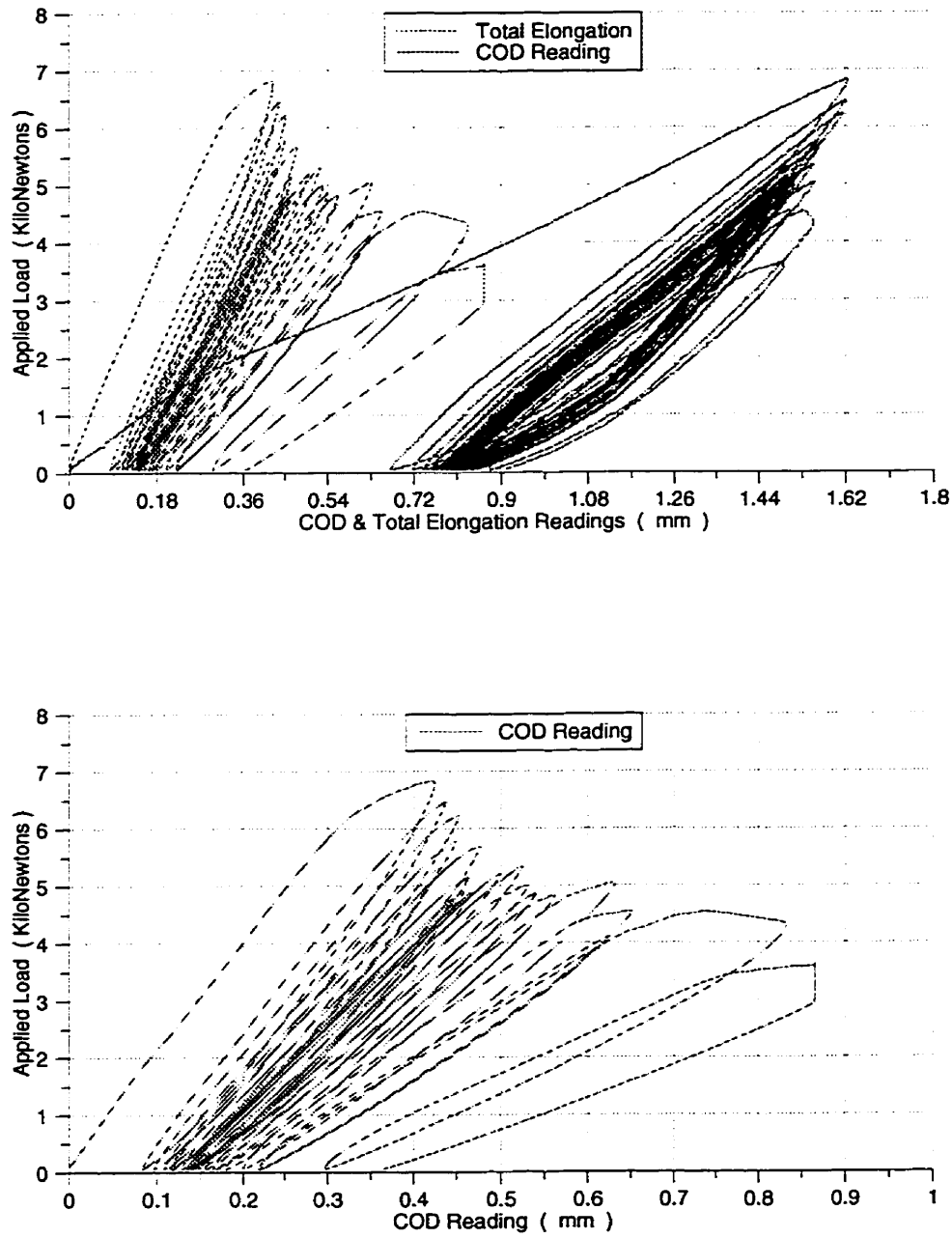

Figure A.8: Response of 20 Layers Specimen of (0/90/0) Fiber Orientation

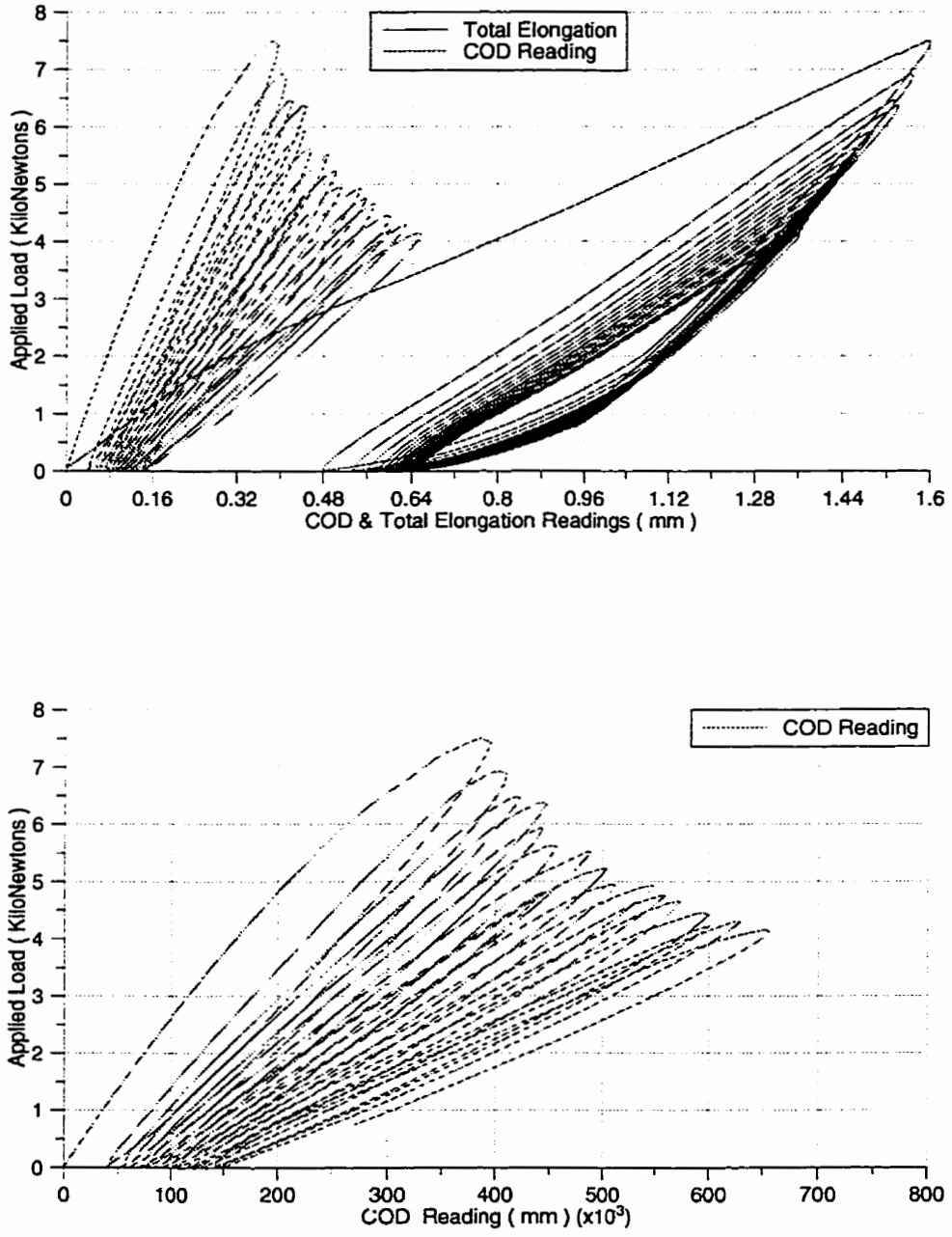

Figure A.9: Response of 20 Layers Specimen of (0/90/0) Fiber Orientation

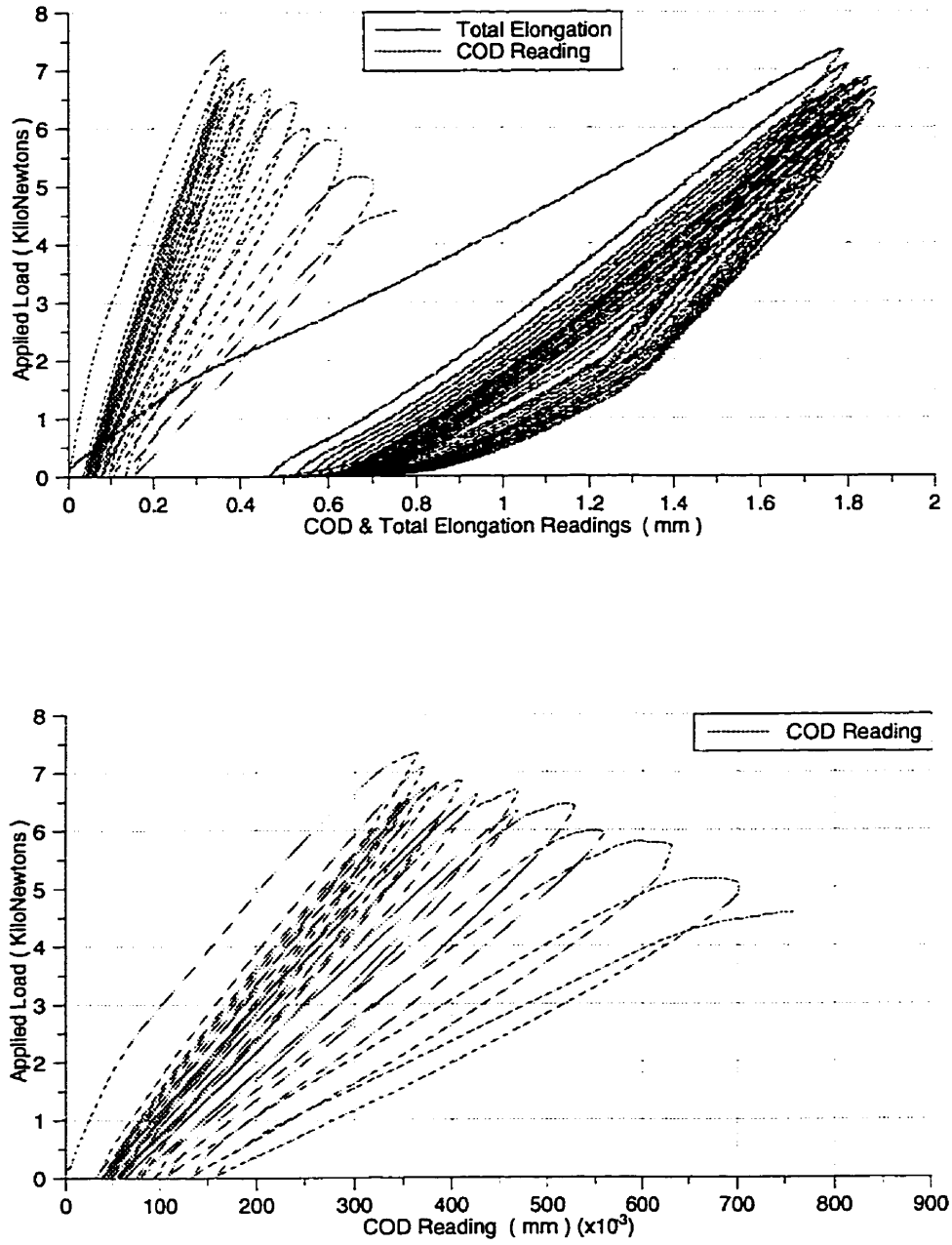

Figure A.10: Response of 20 Layers Specimen of (0/90/0) Fiber Orientation

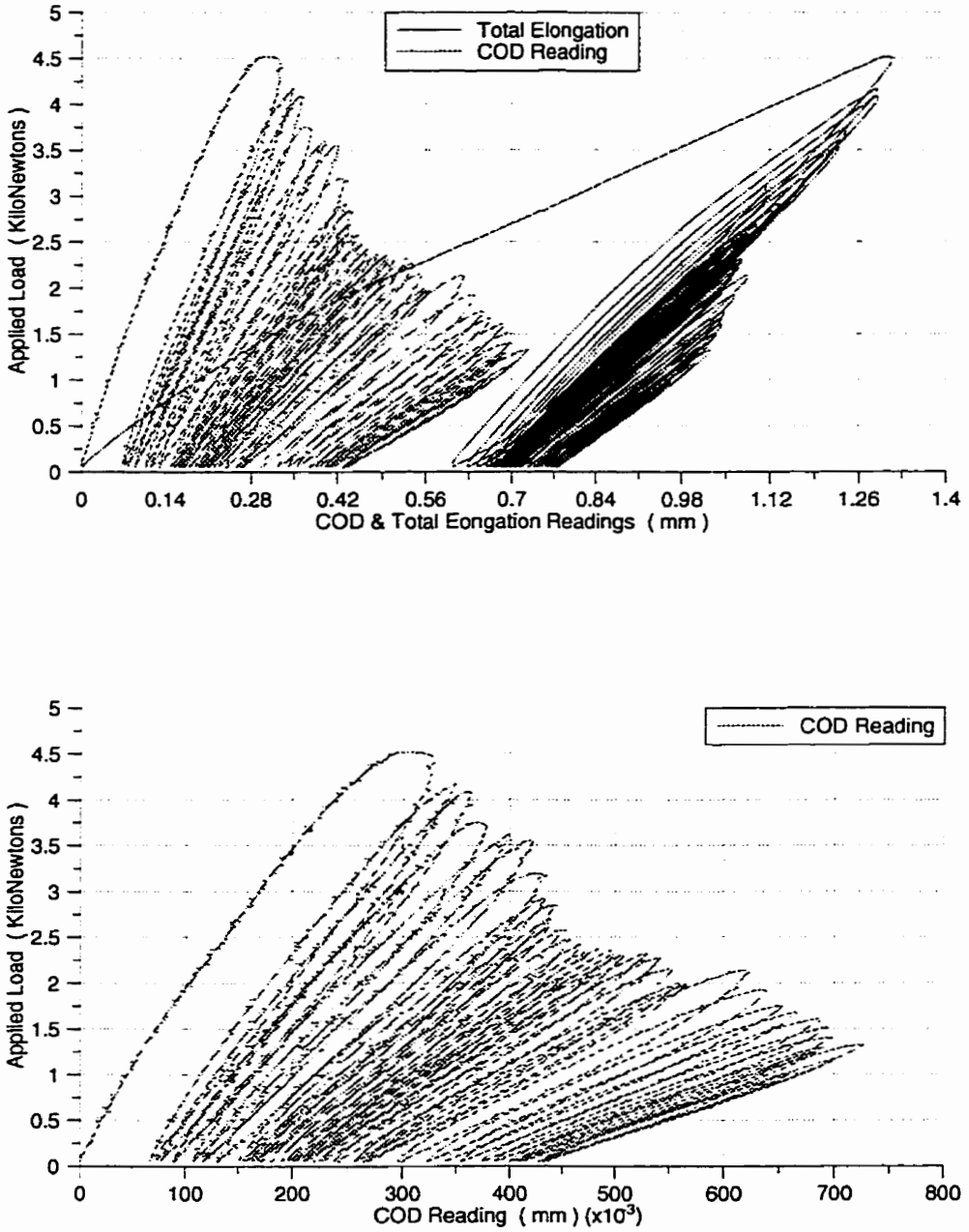

Figure A.11: Response of 16 Layers Specimen of (0/45/90) Fiber Orientation

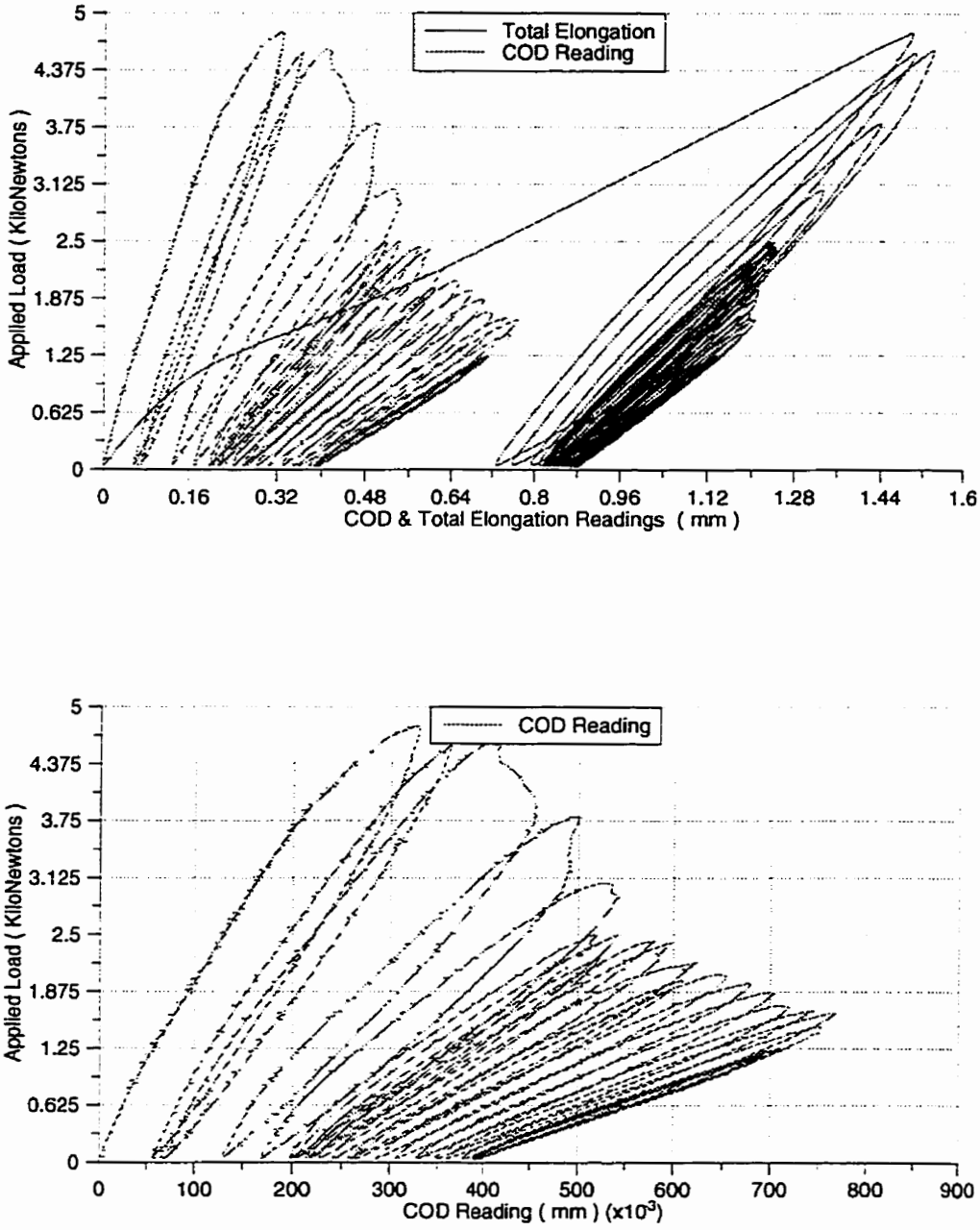

Figure A.12: Response of 16 Layers Specimen of (0/45/90) Fiber Orientation

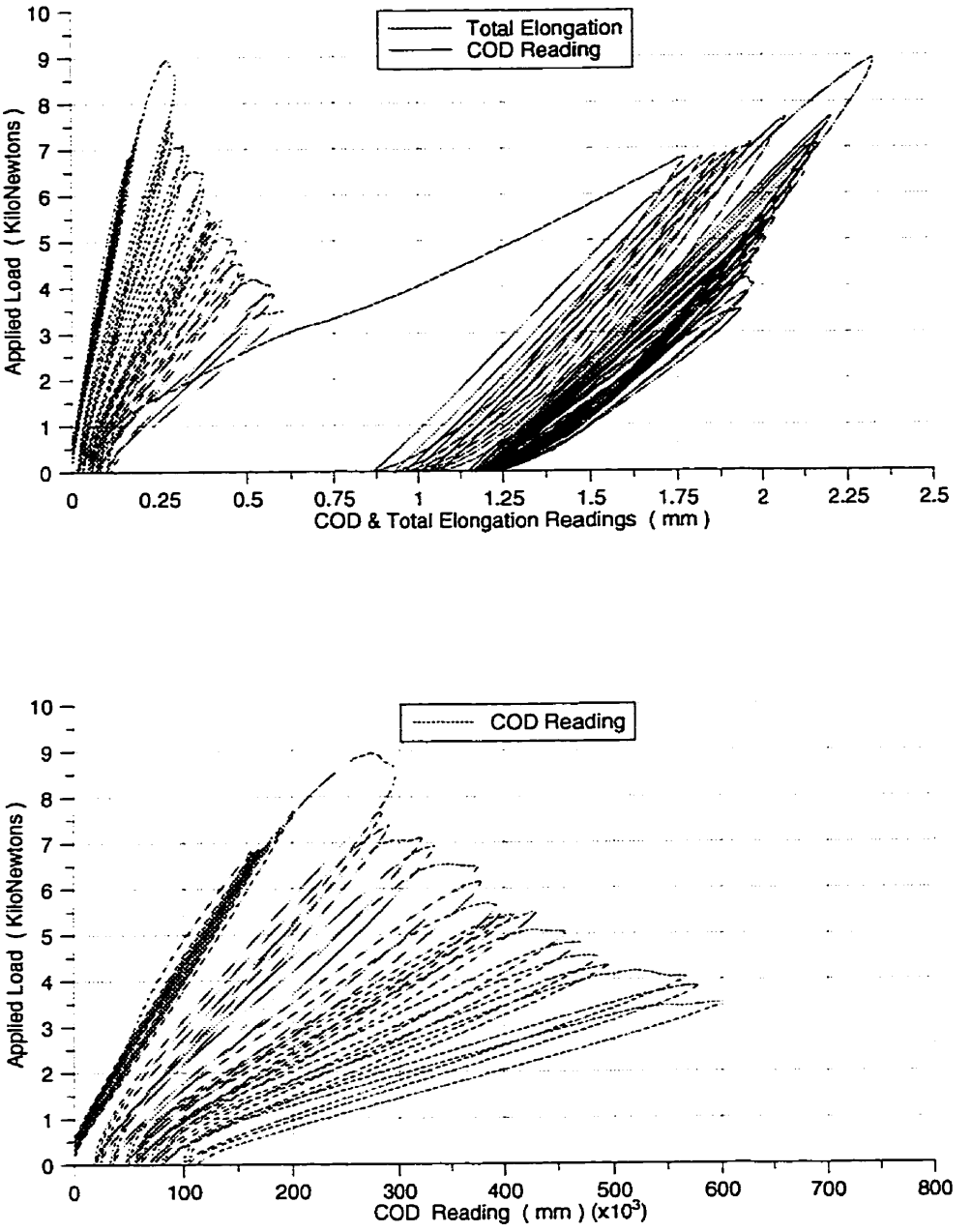

Figure A.13: Response of 20 Layers Specimen with Inclined Crack and (0/90/0) Fiber Orientation

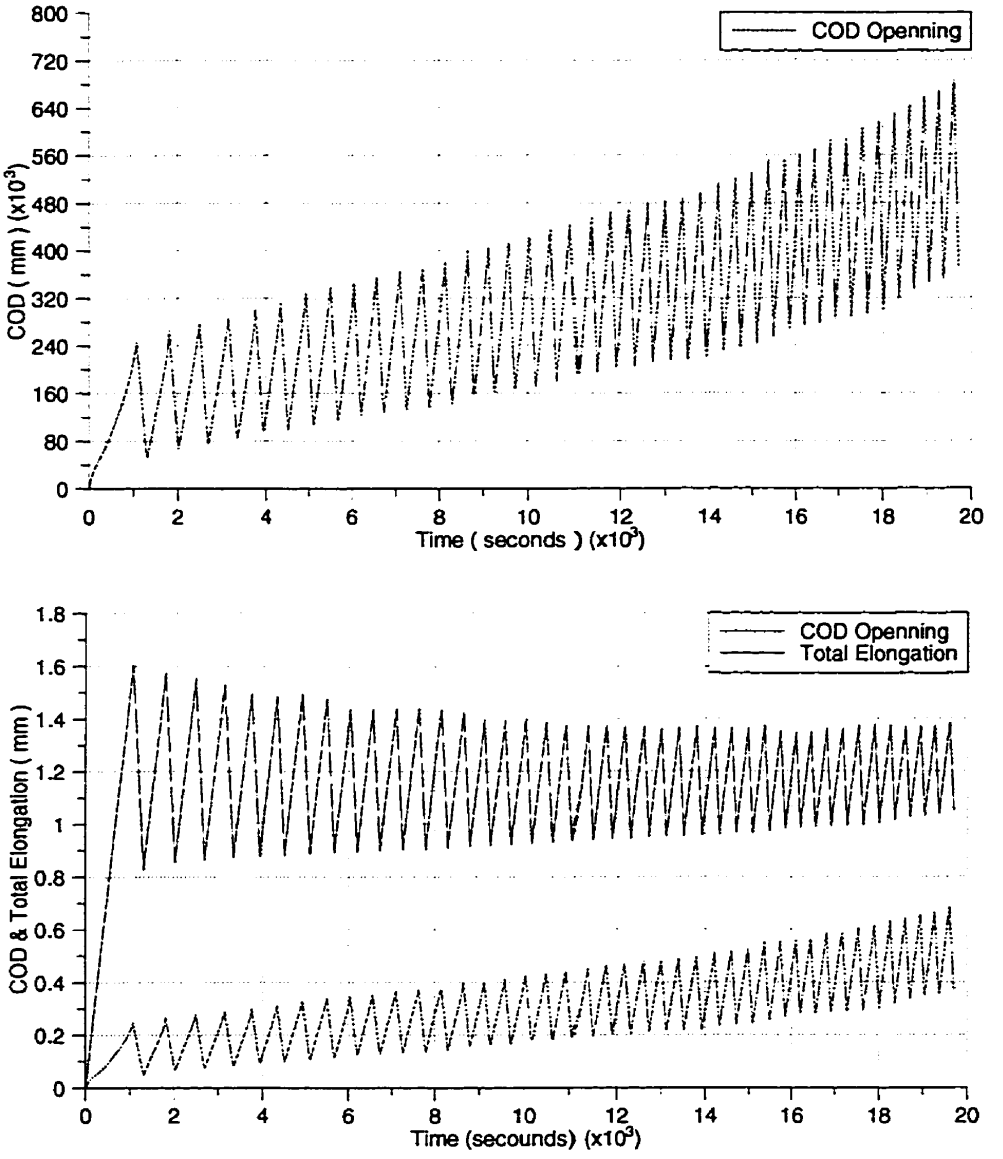

Figure A.14: Record of COD and Total Elongation Versus Time of 20 Layers Specimen of (0/90/0) Fiber Orientation

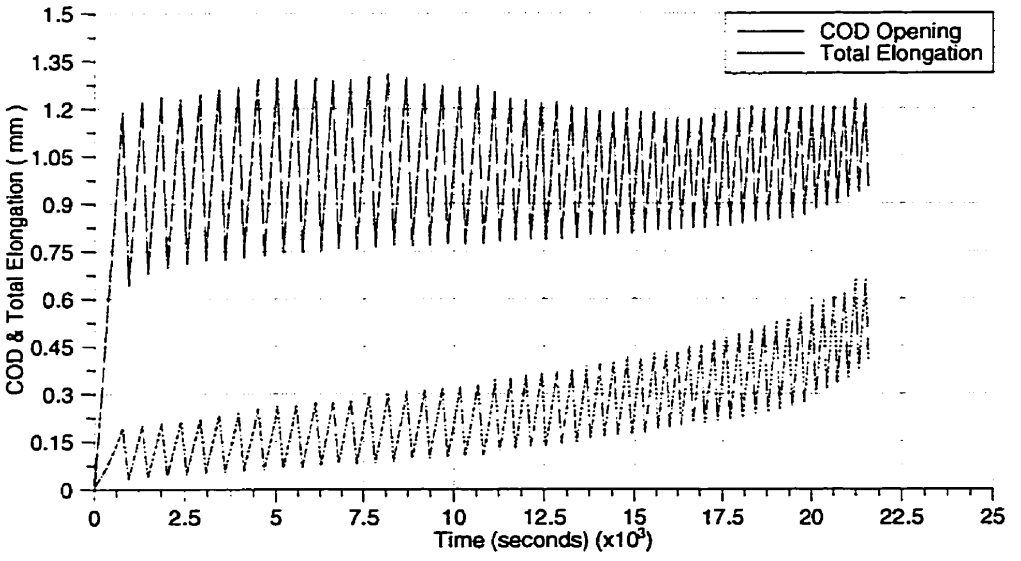

Figure A.15: Record of COD and Total Elongation Versus Time of 12 Layers Specimen of (0/90/0) Fiber Orientation

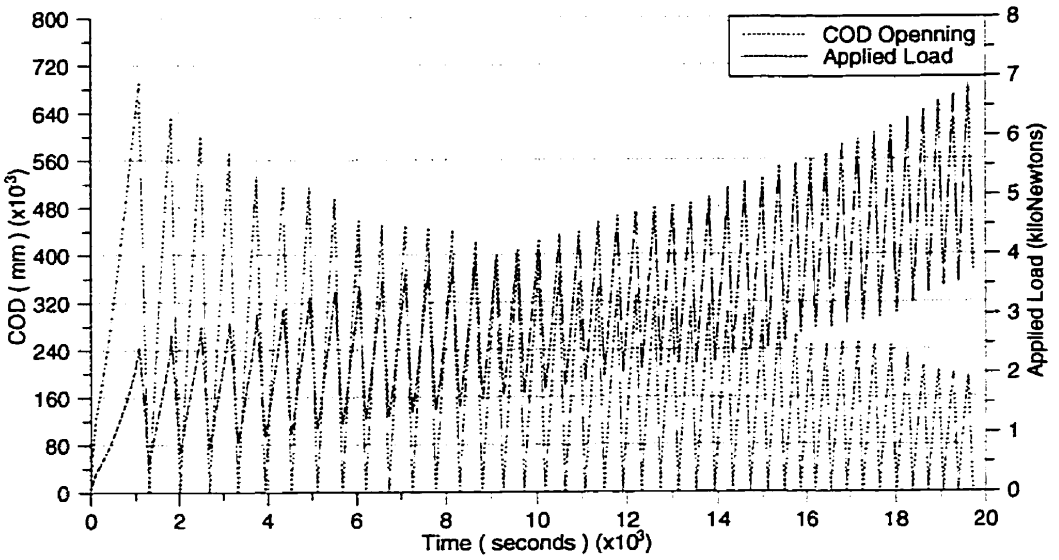

Figure A.16: Record of COD and Applied Load Versus Time of 20 Layers Specimen of (0/90/0) Fiber Orientation

Appendix B

MATERIAL PROPERTIES

This appendix contains tables showing typical properties of some metallic and composite materials.

Table B.1: Typical Properties of Some Fibers

Fibers	Typical Diameter (μ m)	Specific Gravity	Tensile Modulus GPa ($10E6psi$)	Tensile Strength GPa ($10E6psi$)	Strain to failure (%)	Poisson's Ratio
Glass						
E glass	10 (round)	2.54	72.4 (10.5)	3.45 (500)	4.8	0.20
G glass	0 (round)	2.49	68.9 (12.6)	4.30 (625)	5.0	0.22
PAN-Carbon						
T-300	7 (round)	1.76	228 (33.5)	3.2 (470)	1.4	-0.20
AS	7 (round)	1.77	220 (32)	3.1 (450)	1.2	
T-40	6 (round)	1.81	276 (40)	5.65 (820)	2.0	
Pitch-Carbon						
P-55	10	20	380 (55)	1.90 (275)	0.5	
P-100	10	2.15	690 (100)	2.2 (325)	0.31	
Kevlar 49	11.9 (round)	1.45	131 (19)	3.62 (525)	2.0	0.35 0.20
Boron	140 (round)	2.70	393 (57)	3.1 (450)	0.58	
SiC	133 (round)	3.08	400 (58)	3.44 (485)	0.38	

Table B.2: Tensile Properties of Metallic and Composite Materials

Material	Specific Gravity	Modulus GPa (Msi)	Tensile Strength $MPa(ksi)$	Yield Strength $MPa(ksi)$	Ratio of modulus to Weight $10E9m$	Ratio of Tensile Strength to Weight, $10E6m$
Metallic Materials						
SAE 1010 Steel	7.87	207	365	303	2.68	4.72
(cold-worked)		(30.0)	(53)	(44)		
AISI 4340 Steel	7.87	207	1722	1515	2.68	22.3
		(30.0)	(750)	(220)		
AL 6061-T6	2.70	68.9	310	275	2.6	11.7
		(10)	(45)	(40)		
AL 7178-T6	7 2.70	68.9	606	537	2.60	22.9
		(10.0)	(88)	(78)		
Ti-6AI-4V	4.43	110	1171	1068	2.53	26.9
Titanium Alloy		(16.0)	(170)	(155)		
17-7 PH	7.87	196	1619	1515	2.54	21.0
Stainless Steel		(28.5)	(235)	(220)		
INCO 718	8.20	207	1399	1247	2.57	14.7
Nicle Alloy		(30.0)	(203)	(181)		
Composite Materials						
High-Strength carbon	1.55	137.8	1550		9.06	101.9
Fiber-epoxy (undirec.)		(20.0)	(225)			
Hight-Modulus Carbon	1.63	215	1240		13.44	77.5
Fiber-epoxy (undirec.)		(31.2)	(180)			
E-glass Fiber-epoxy	1.85	39.3	965		2.16	53.2
(unidirectional)		(5.7)	(140)			
Kevlar 49 Fiber-epoxy	1.38	75.8	1378		5.60	101.8
(unidirectional)		(11.0)	(200)			
Boron Fiber-6061 Al	2.35	220	1109		9.54	48.1
Alloy (annealed)		(32.0)	(161)			
Carbon Fiber-epoxy	1.55	45.5	579		2.99	38.0
(quasi-isotropic)		(6.6)	(84)			

Appendix C

SPECIMEN PREPARATION AND TESTING

This appendix contains various photos of the specimens preparation using vacuum bagging technique, the experimental apparatus and test setup, and some typical specimens after testing.

Figure C.1: The Fiberglass Fabric is Cut into Equal Square Pieces

Figure C.2: Release Material is Placed on the Mold Surface and the First Two Layers of Fiberglass Fabric is Put on Top of Each Other

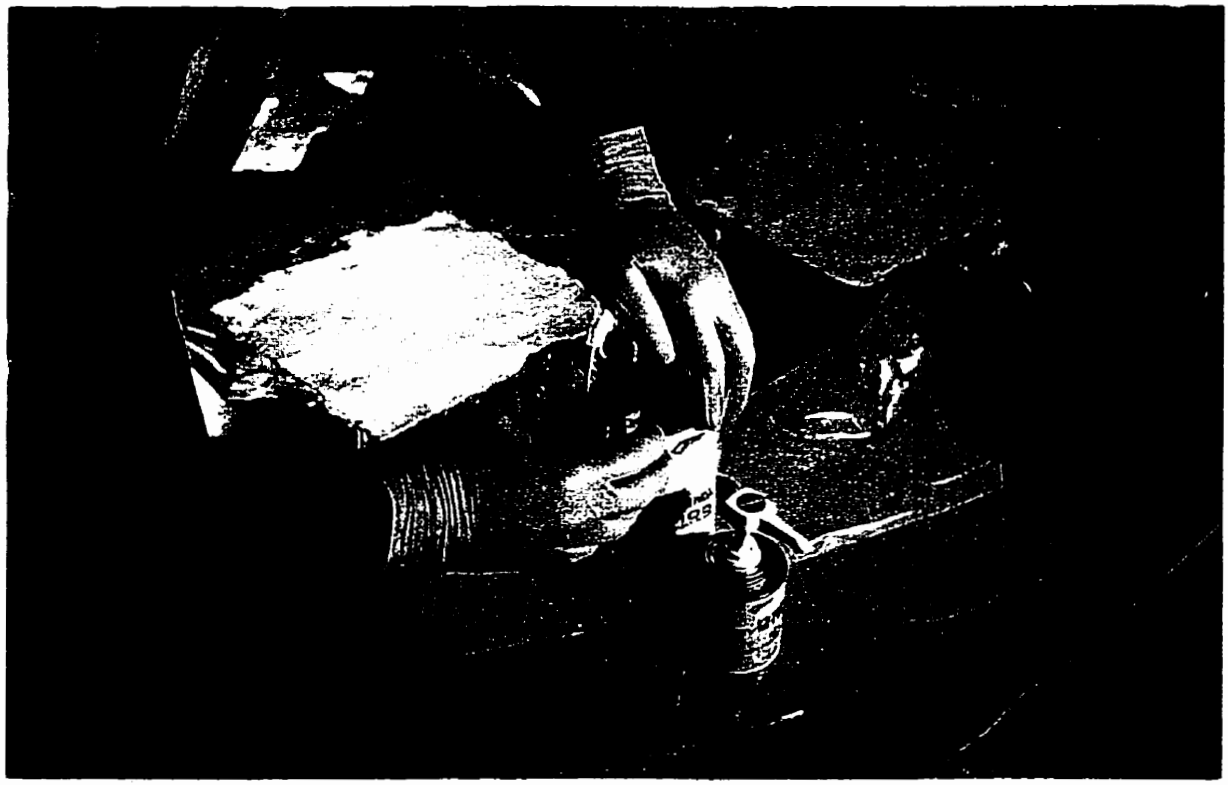

Figure C.3: Mixing Resin and Hardener Together in a Container

Figure C.4: Spreading the Resin and Hardener Mixture over the Fabric

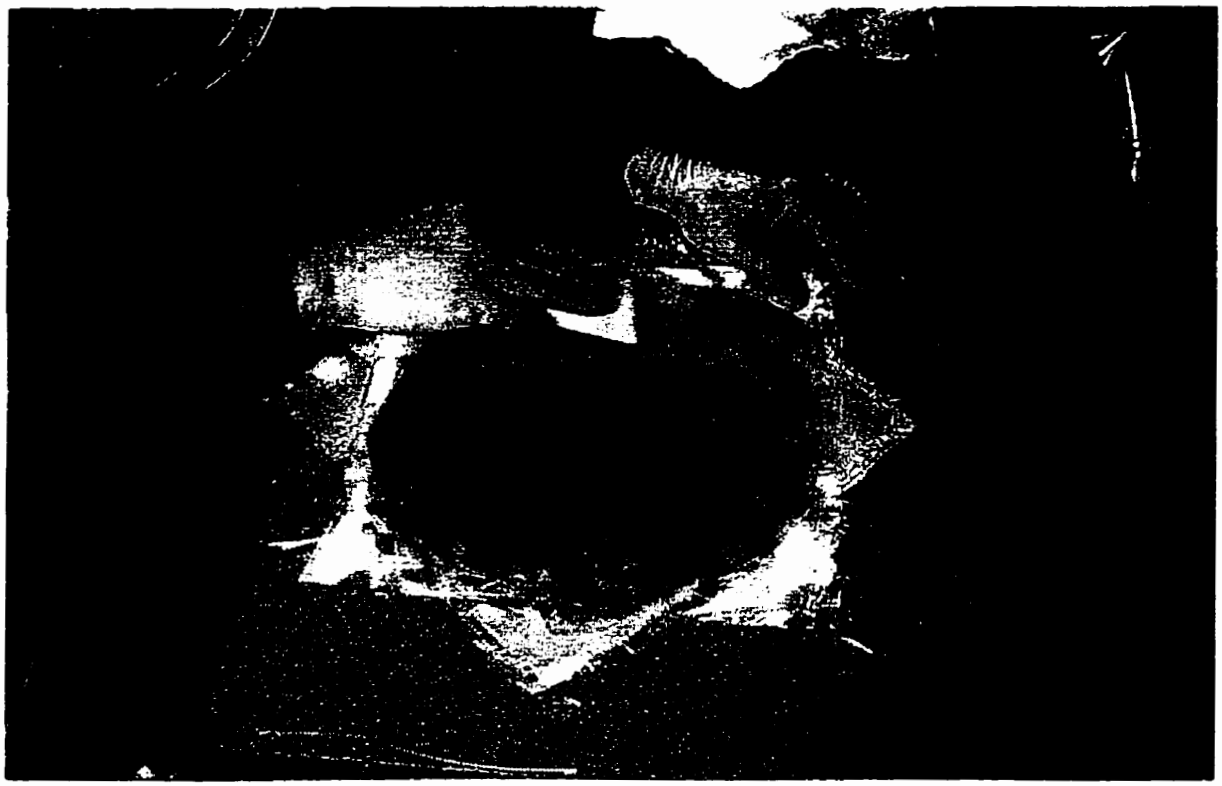

Figure C.5: More Fiberglass Fabric are Placed, Wet out, and the Excess Epoxy is Squeezed from the Surface each Time

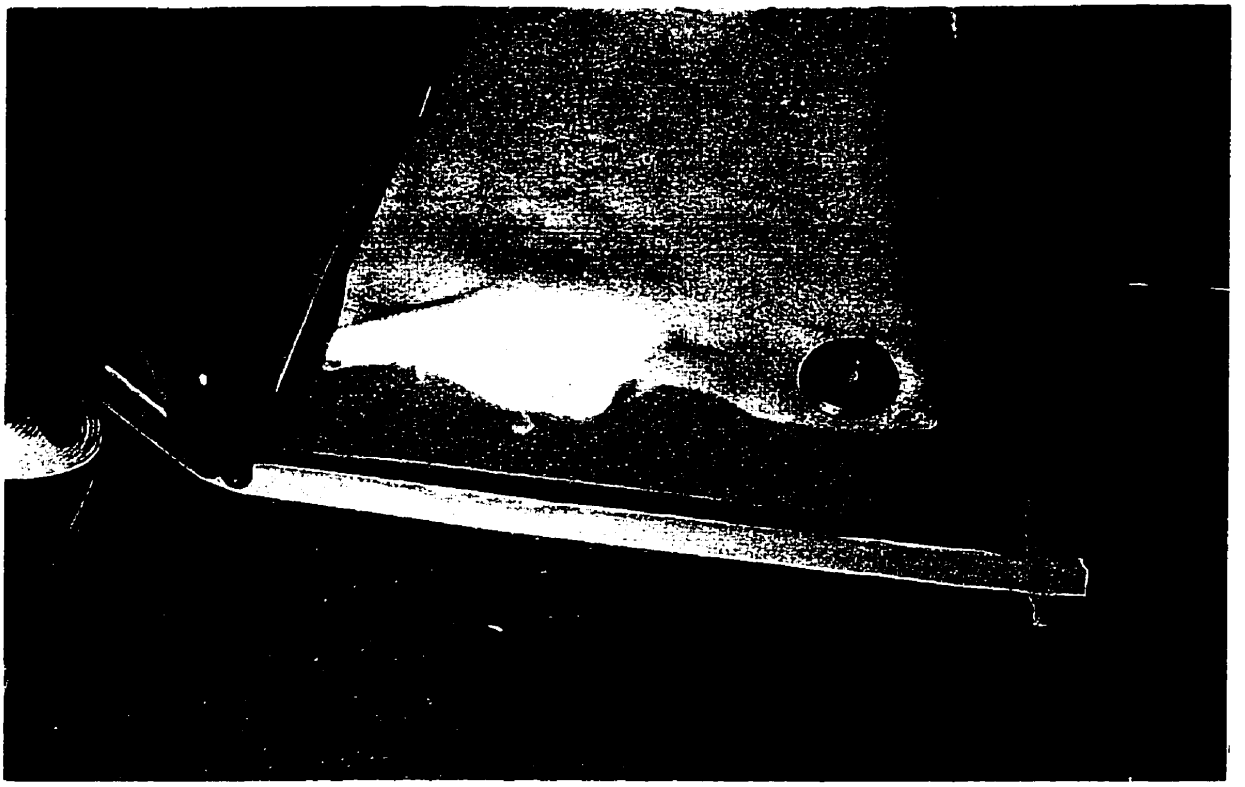

Figure C.6: A Layer of Release Fabric, Breather Fabric and the Mastic Sealant are Placed

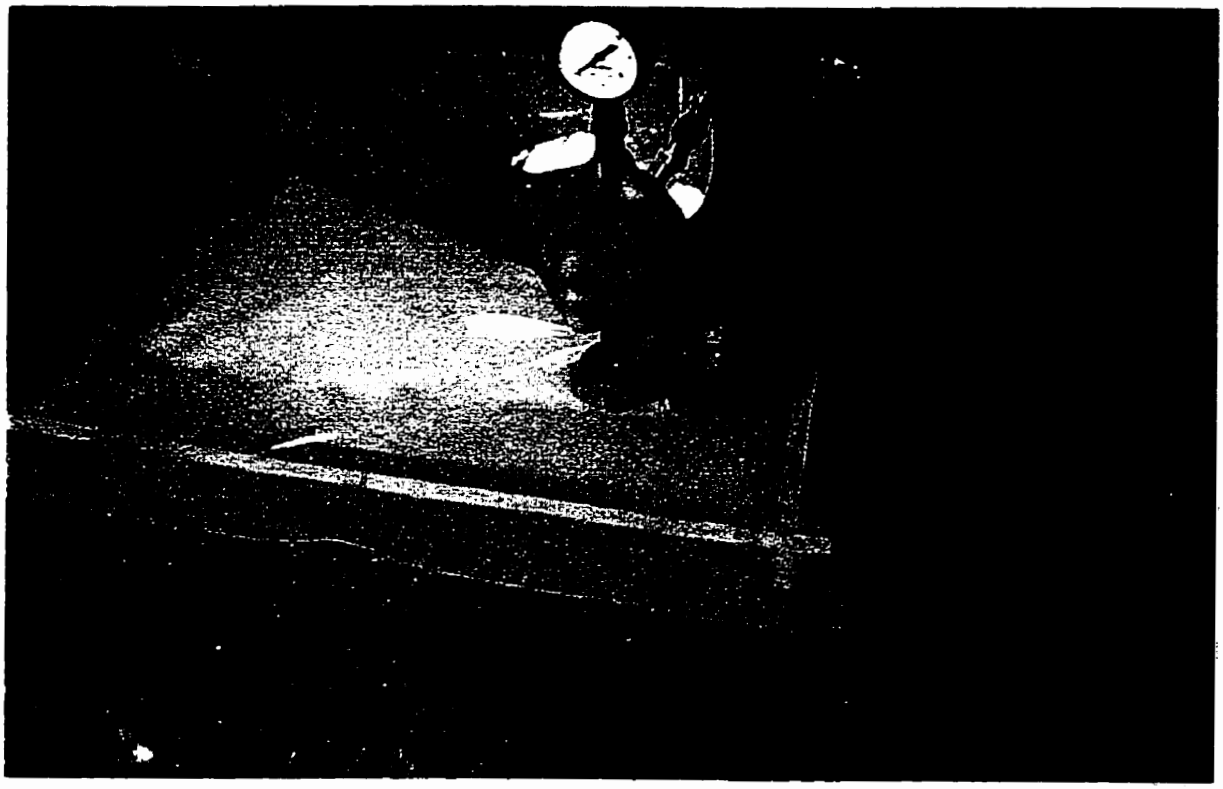

Figure C.7: The Vacuum Pump with Gage is Connected to the Bag

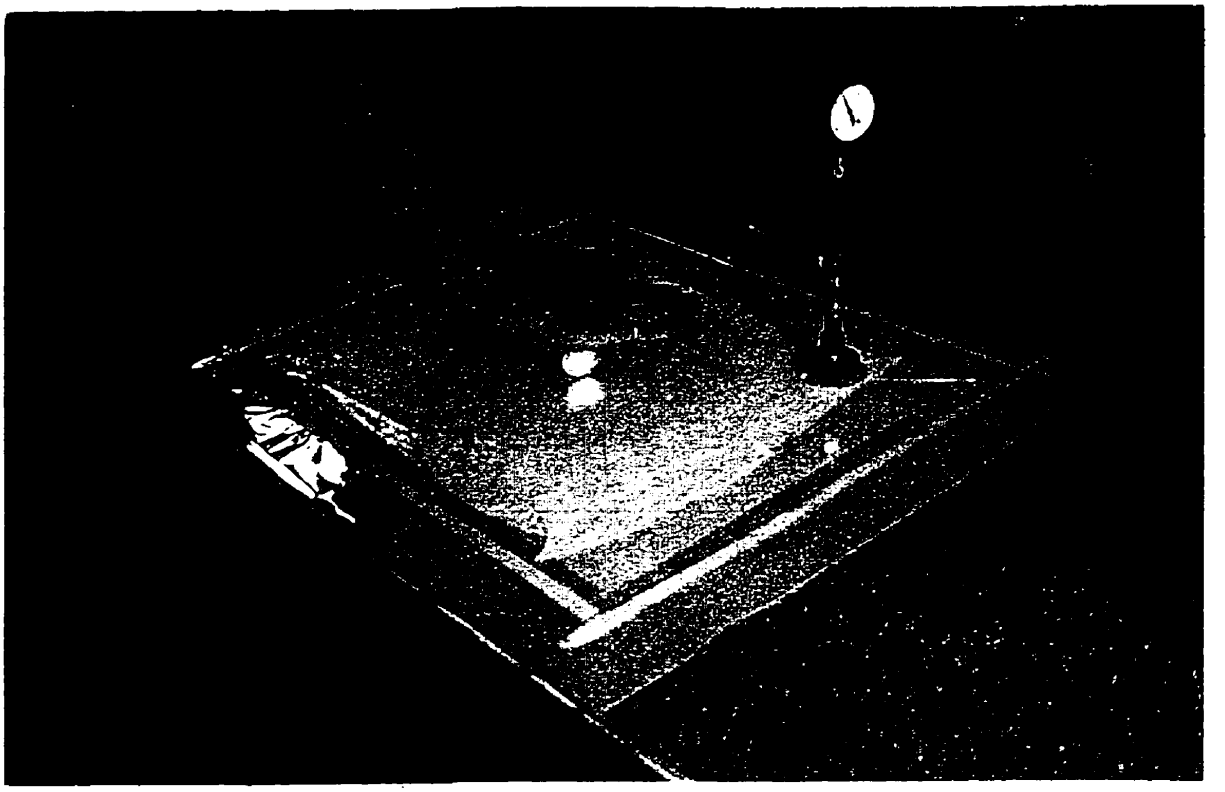

Figure C.8: Applying Manual Pressure to the Bag to Evacuate the Air and to Squeeze out the Excess Epoxy

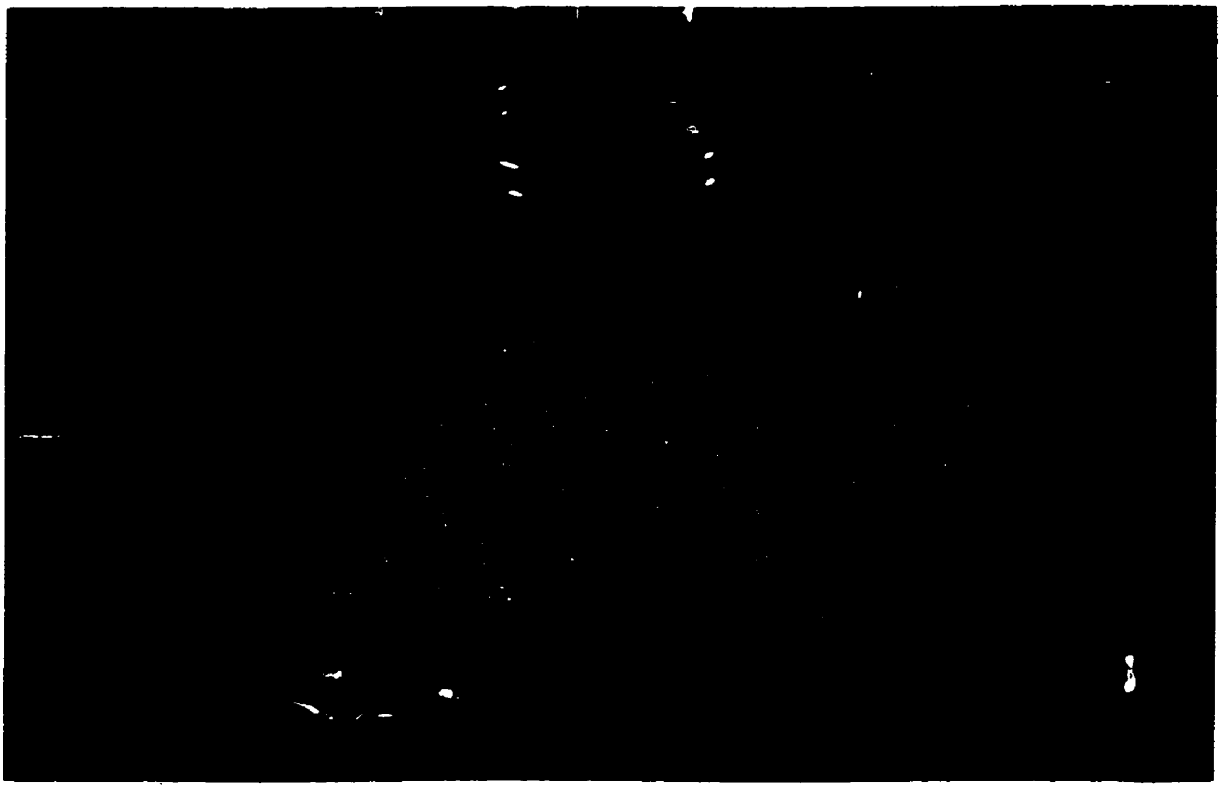

Figure C.9: The Bag Before Shutting off the Vacuum and Removing the Cover

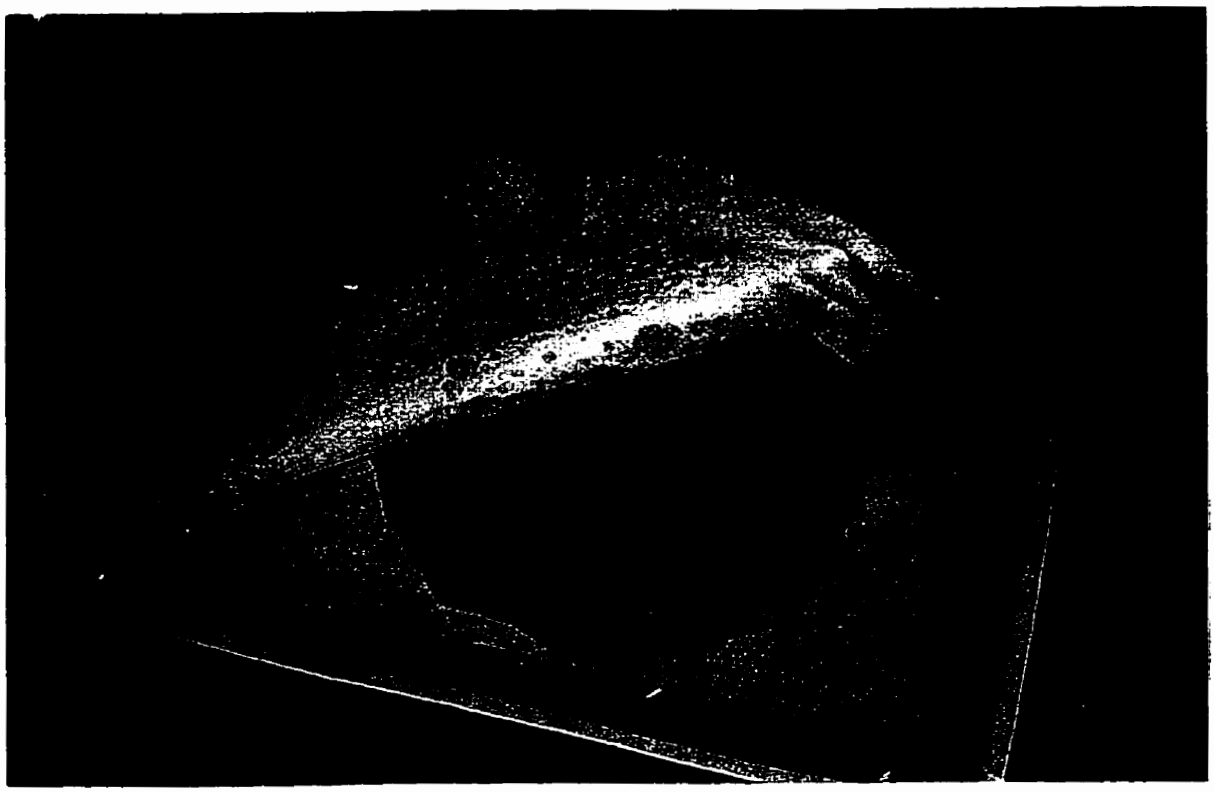

Figure C.10: The Bag after the Epoxy is Cured and the Vacuum Pump Turned off

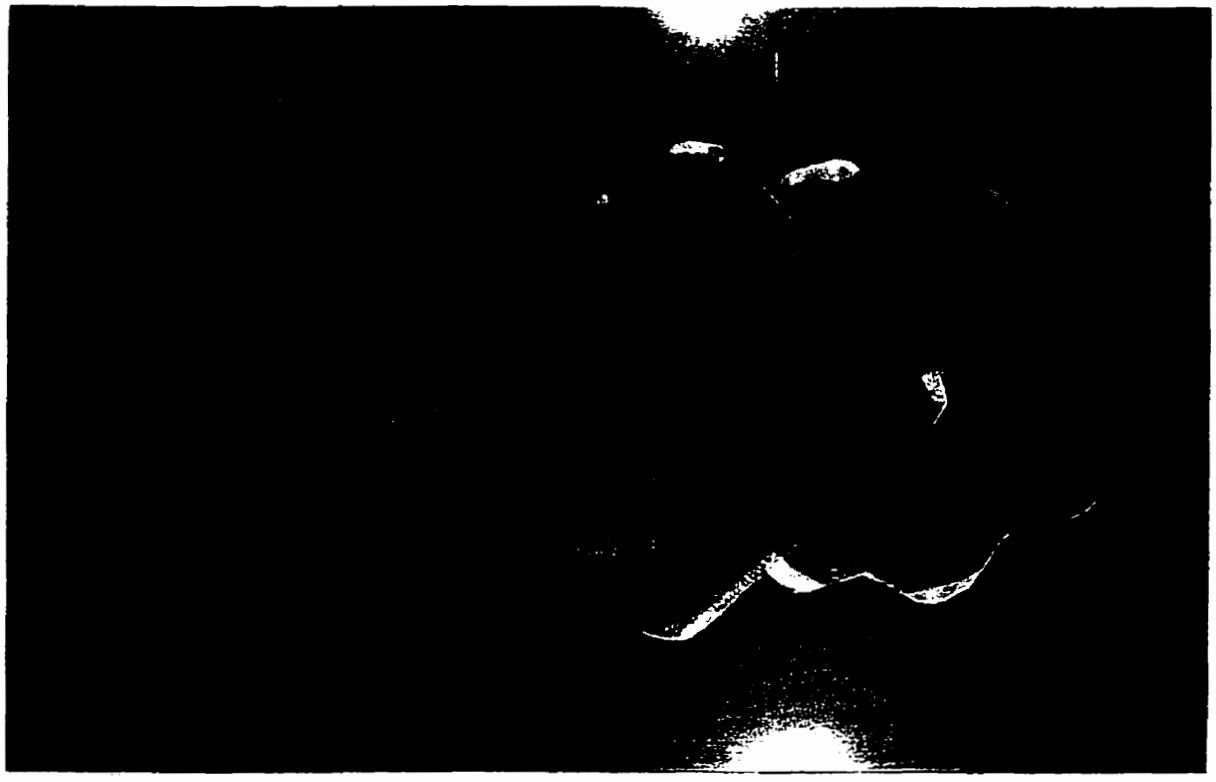

Figure C.11: Typical Panels and Specimens Made using the Vacuum Bagging Technique

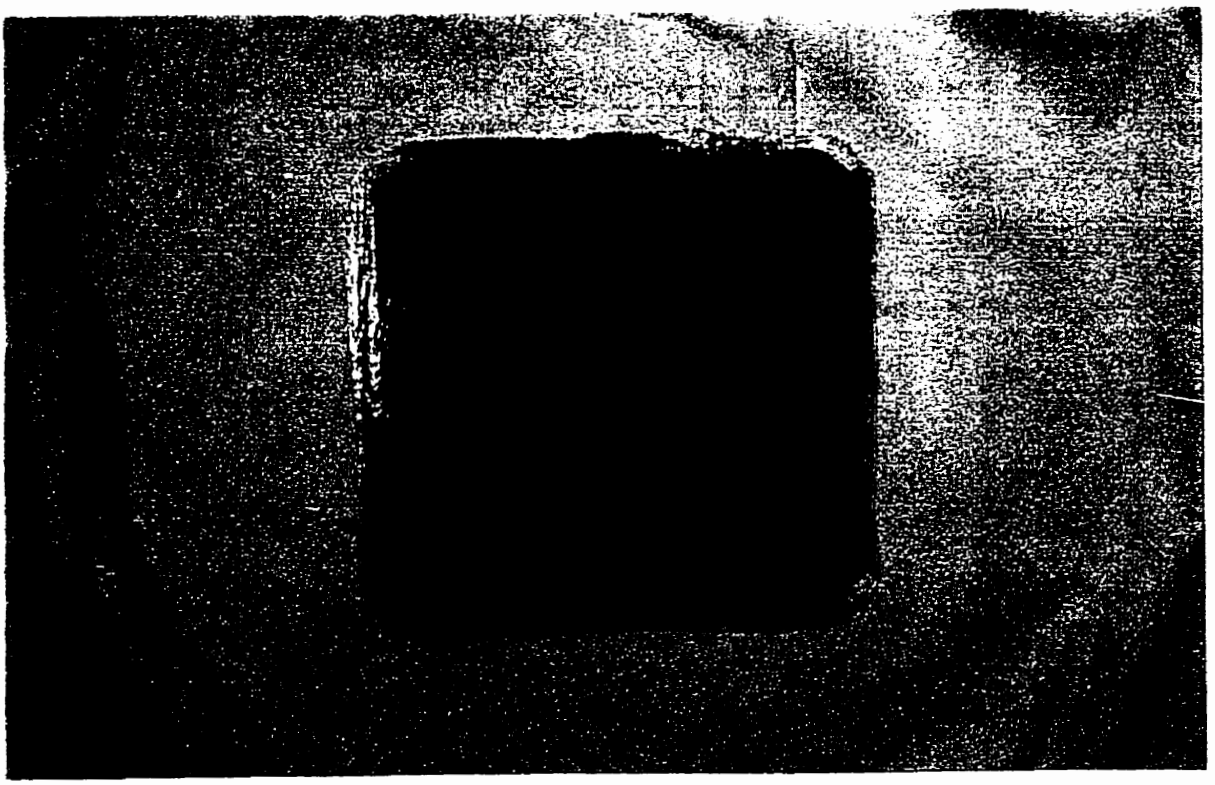

Figure C.12: Typical Panel of (0/90/0) Fiber Orientation

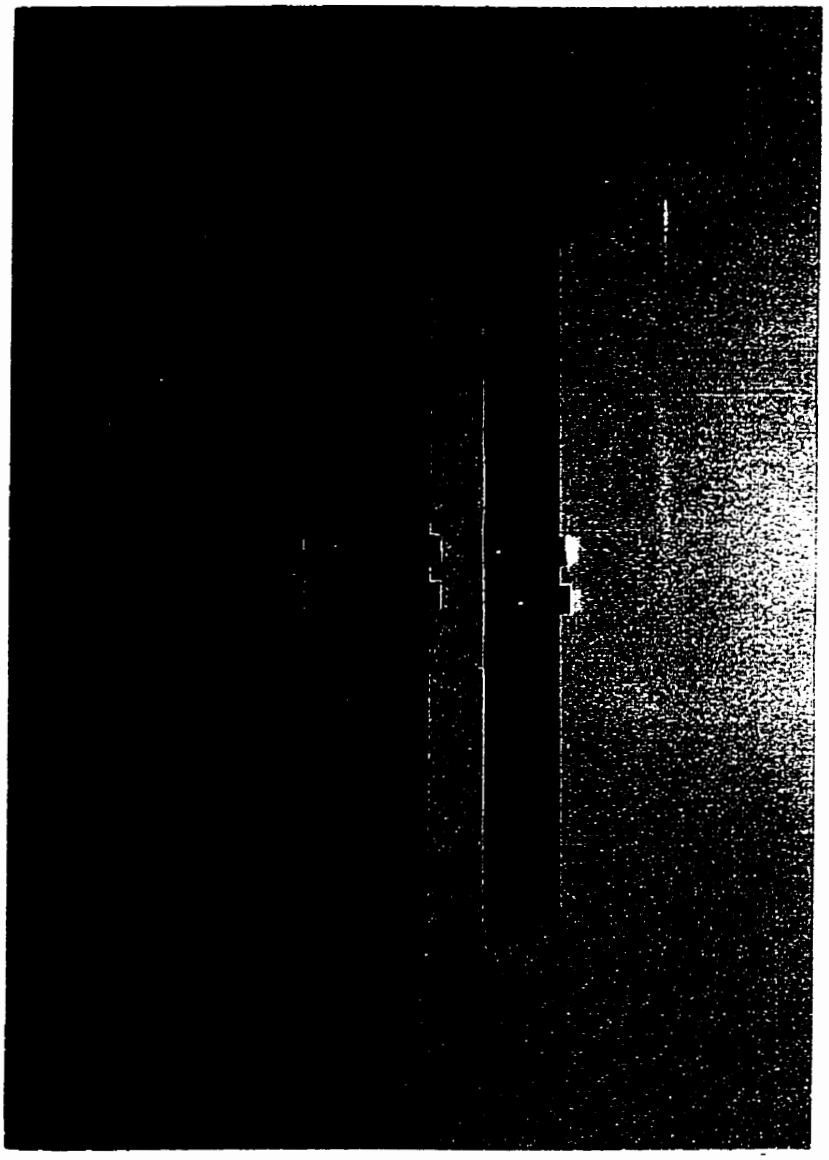

Figure C.13: Three Different Specimens with Notches and Knife Edges Placed on the Sides of the Crack.

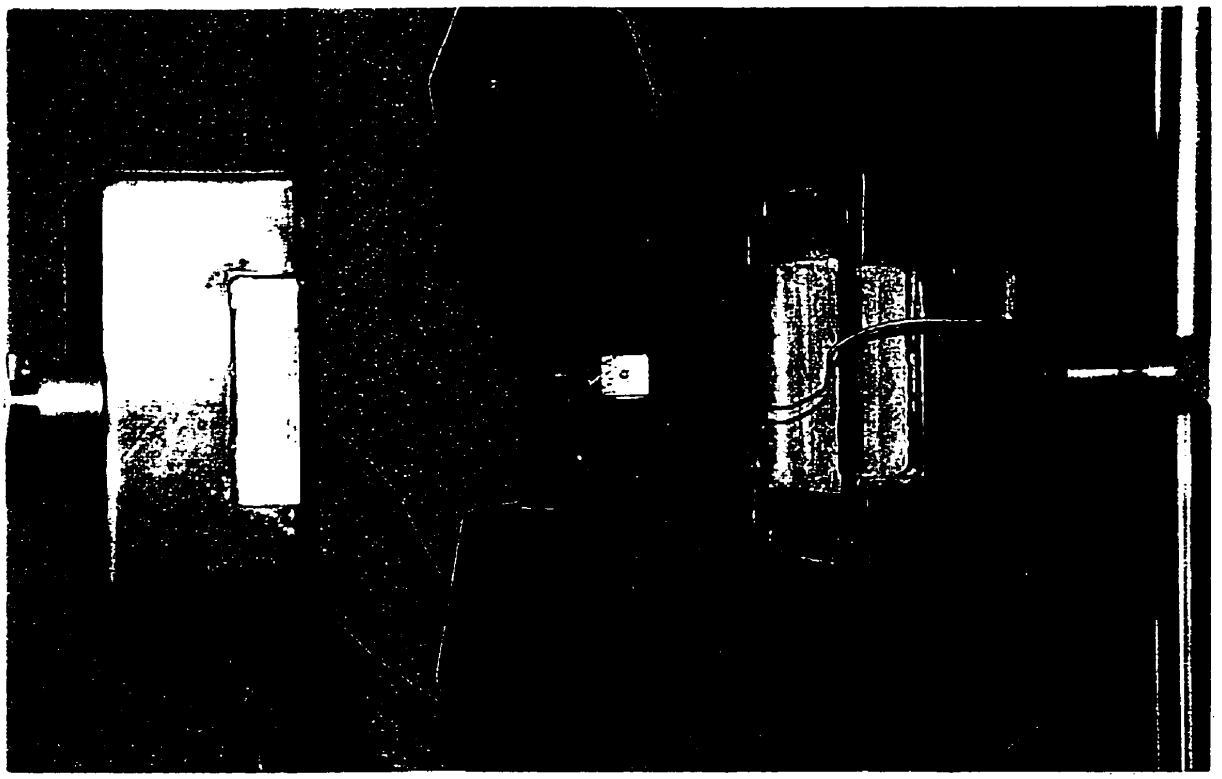

Figure C.14: The Specimen is Placed Between the Grips and the COD is Mounted to the Specimen Between the Knife Edges

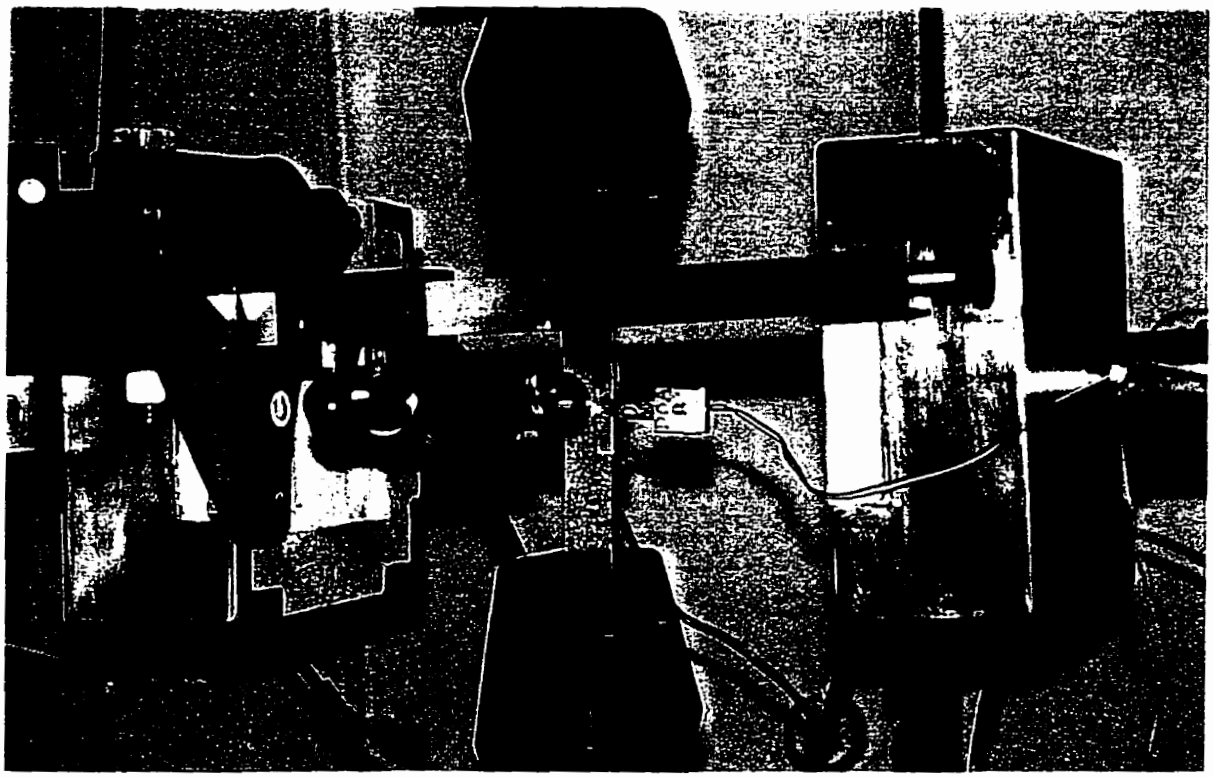

Figure C.15: The Setup Shows the Specimen, the COD, and the Microscope which is Mounted to Measure the Crack Length

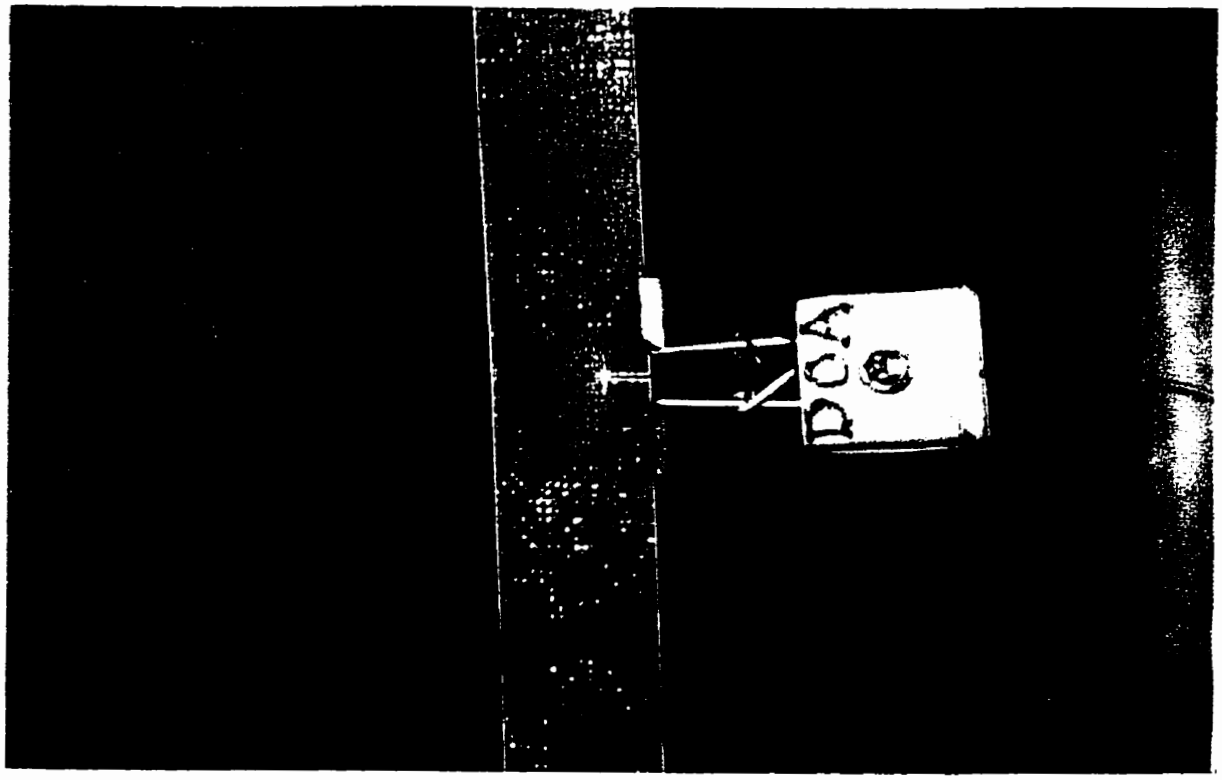

Figure C.16: Specimen of Straight Crack under Testing and the Fracture Zone Starting in Front of the Crack Tip.

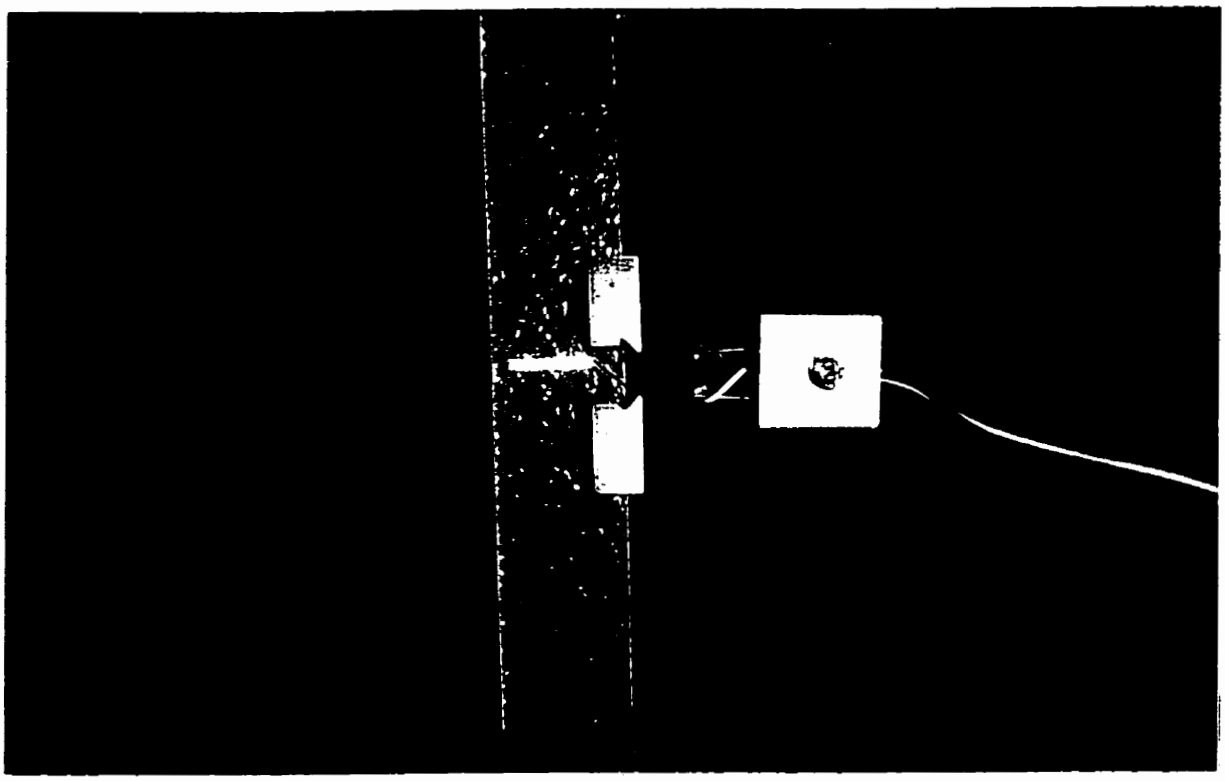

Figure C.17: Specimen of Inclined Crack under Testing where the Crack Propagation and Fracture Zone in Front of Crack Tip are Clear.

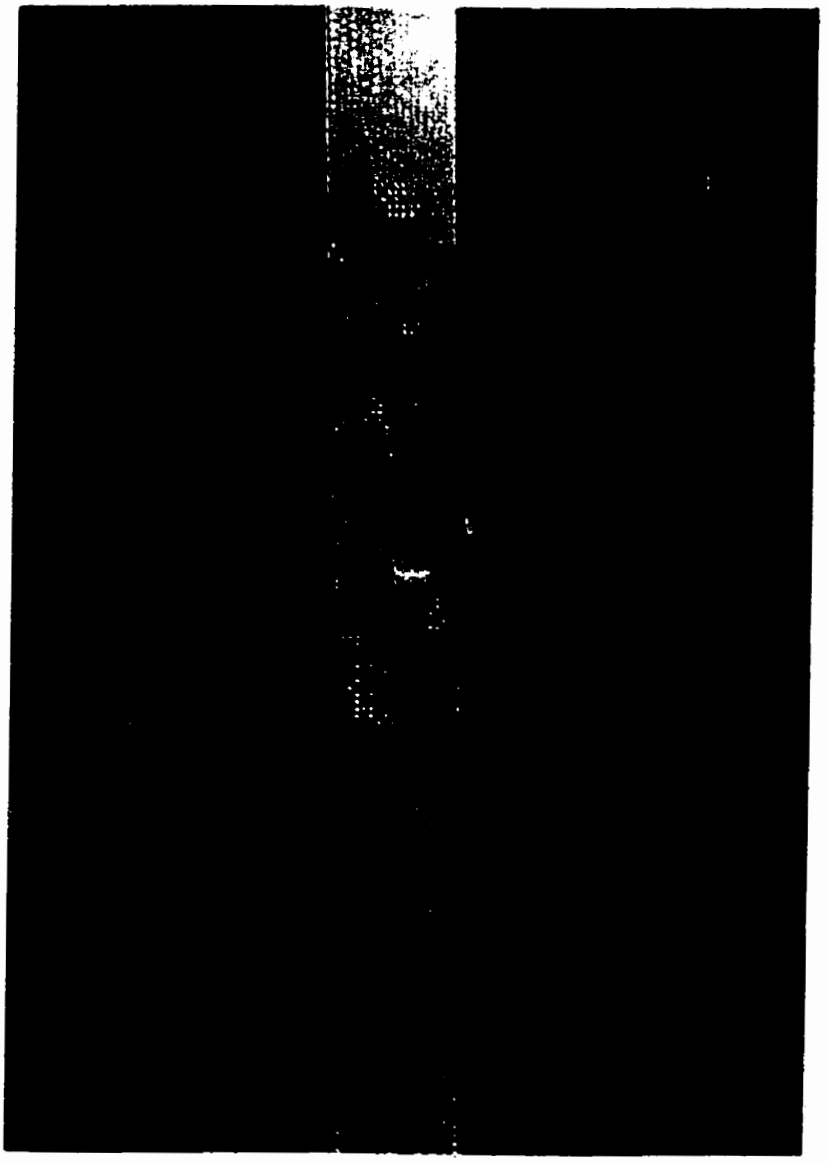

Figure C.18: Typical Specimen after 20 Cycles

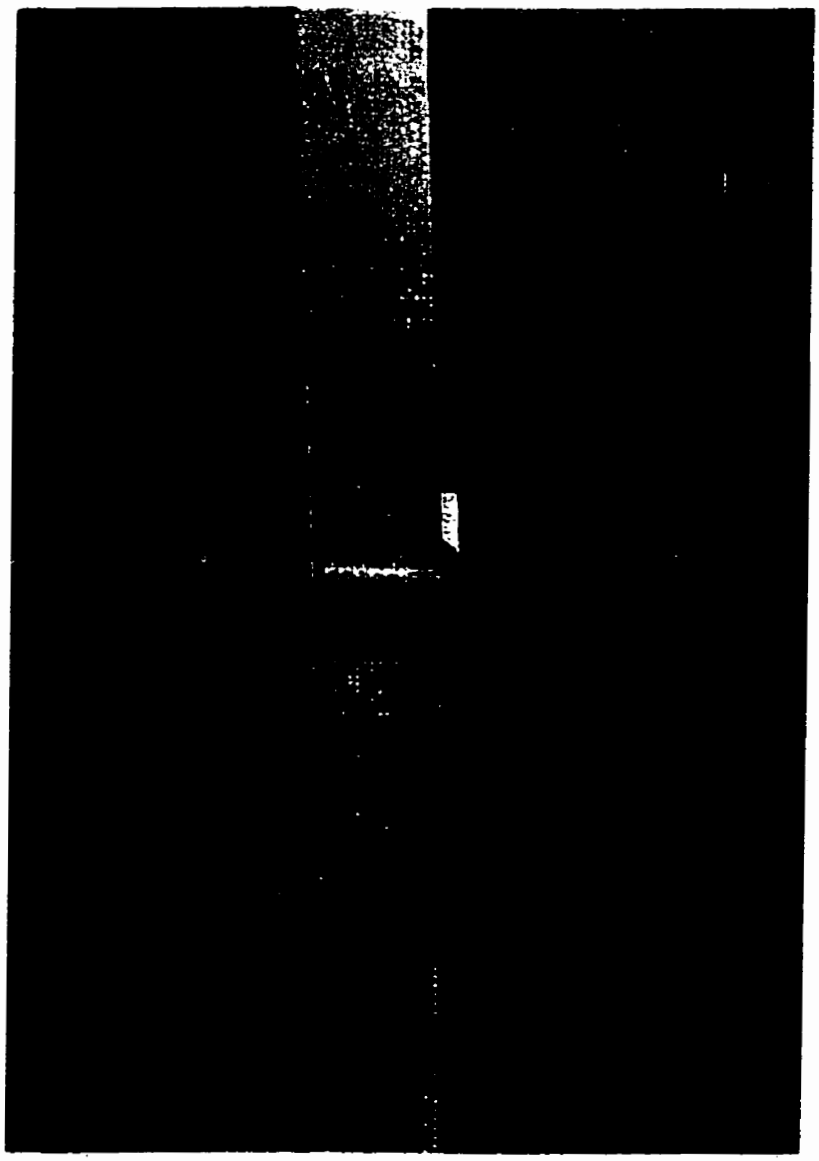

Figure C.19: Typical Specimen after 50 Cycles

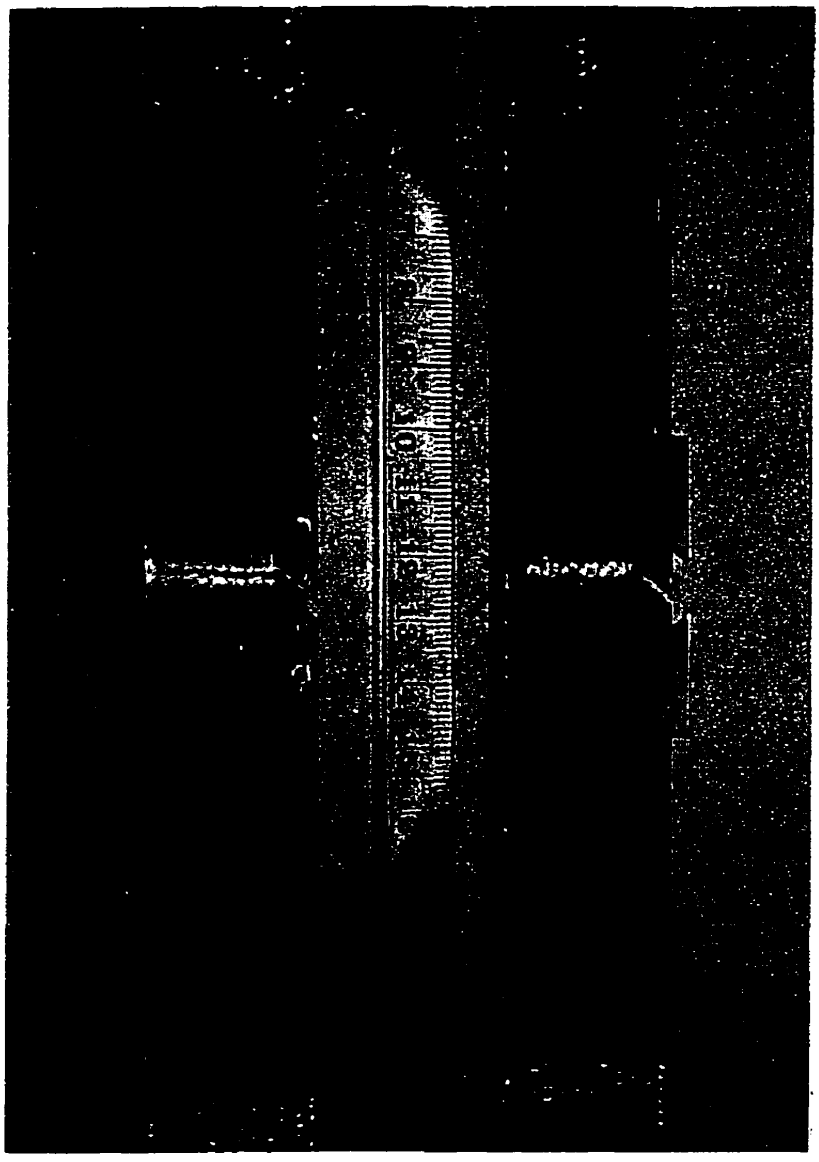

Figure C.20: Two Typical Specimens of Inclined Crack one after 50 Cycles and the other after Fracture

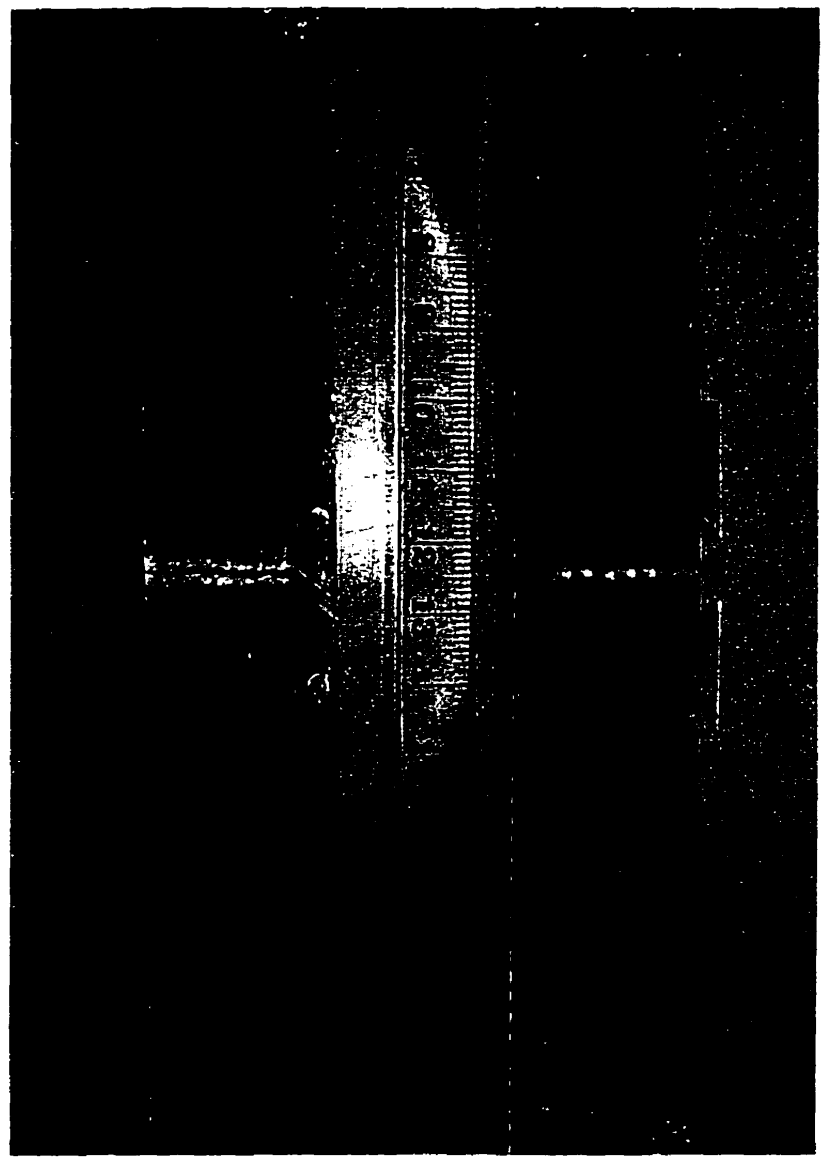

Figure C.21: Specimen with Inclined Crack after Fracture and Specimen with Straight Crack after 50 Cycles

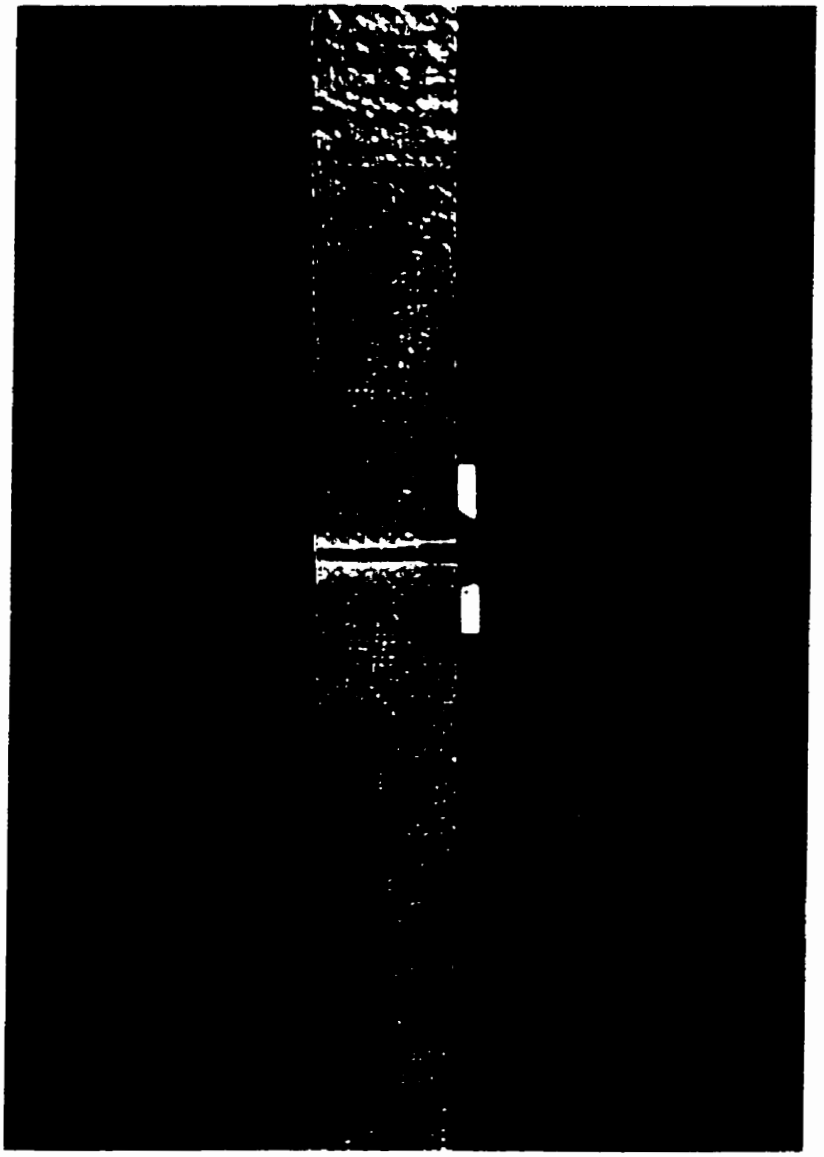

Figure C.22: Typical Specimen after Complete Fracture